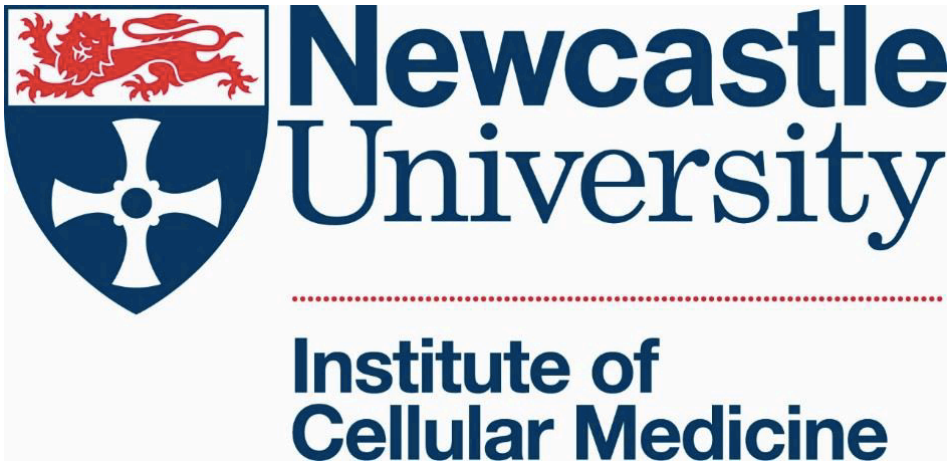


# Identification and role of microRNAs in endothelial-to-mesenchymal transition

**Nina Jordan**

Thesis submitted in partial fulfillment of the requirements for the Degree of Doctor of Philosophy

Institute of Cellular Medicine
Newcastle University

April 2019

# Abstract

Studies in fibrotic diseases demonstrate that myofibroblasts may be derived from cell types other than fibroblasts. Sources include endothelial-to-mesenchymal transition (EndMT), generating 27% to 35% of myofibroblasts in cardiac fibrosis and around 10% in kidney fibrosis.

Over the last decade, miRNAs have increasingly been described as key regulators in biologic processes but their profile remains mainly undescribed in EndMT. Therefore, we have investigated the possible role of miRNA signatures in EndMT models relevant to cardiac and kidney fibrosis.

EndMT was modelled in human umbilical vein endothelial cells (HUVEC) by treatment with TGFβ2 (10ng/mL) and IL1β (10ng/mL). Significantly decreased expression of endothelial markers such as vWF and increased levels of mesenchymal markers such as fibronectin were observed by qPCR in HUVEC after 48 hours of treatment ($p<0.05$). Similarly, immunofluorescence showed increased expression of fibronectin and decreased expression of VE-cadherin in HUVEC 6 days post-treatment.

In parallel, miRNAs were profiled with an nCounter assay in HUVEC. Profiles in untreated cells were compared to cells treated with TGFβ2 and IL1β. In these profiles, miR-126-3p was found down-regulated 24 hours' post-treatment. Over-expression of miR-126-3p in HUVEC by transfection restored the expression of CD31 and repressed the expression of fibronectin induced by TGFβ2 and IL1β treatment, protecting the cells from EndMT induction.

EndMT *in vivo* was investigated using lineage tracing with transgenic Cdh5-Cre-ERT2; Rosa26R-stop-YFP mice. Mice expressing YFP specifically in endothelial cells underwent myocardial infarction or unilateral ureteral obstruction. After sacrifice, lineage tracing showed expression of mesenchymal markers in endothelial derived cells, indicating the presence of EndMT in cardiac and kidney fibrosis. In addition, *in-situ* hybridisation revealed the presence of miR-126-3p mainly in endothelial cells in mouse heart and kidney.

We conclude that miR-126-3p may have a role in EndMT and this may have therapeutic potential in cardiac and kidney fibrosis.

# Declaration

I declare that no portion of the work compiled in this thesis has been submitted in support of any other degree or qualification at Newcastle University or any other university or institute of learning. The work has been carried out by myself unless otherwise stated. All sources of information have been acknowledged accordingly by means of reference.

# Acknowledgments

This project was funded by Marie Curie Grant from the European Commission FP7 in the framework of the POSAT ITN (Prolong Organ Survival After Transplantation, Initial Training Networks, 606979) and I am grateful for their support.

I would like to thank my supervisors Prof Simi Ali, Dr Chris Ward and Prof John Kirby for their support and their help throughout my PhD. I am grateful for their trust in the choice of my project even if my English was not always understandable. I would also like to thank you for all the opportunities you gave me which will definitely help me in my future career.
I would like to thank Prof Helen Arthur and all her team for their contribution to the *in vivo* work, for their precious advices and their collaboration on the kidney study.
I would like to extent my thanks to Prof Neil Sheerin for his collaboration and help on the kidney study.

I would like to thank Clement Larcher and Colin Dunsmore for their supervision in my secondments in QIAGEN and Almac respectively. This was a great opportunity to discover the private sector.

Special thanks go to my colleagues and friends, Laura and Shameem, this PhD would have not be the same without you. Thank you for being there in the good and in the bad moments. Shameem, thank you for teaching me all the techniques related to miRNAs. Laura, you were the French touch I needed to keep going during this PhD.
I would like to thank Katie Cooke for her active help with all the surgeries and the immunofluorescence staining (that was a real adventure). Generally I would like to thank all my colleagues from the Kirby/Ali lab for making me comfortable at work.

Massive thanks to my mom who agrees to take home her 28-years old daughter. These last months were not always easy but you made sure that I would always be in the best conditions to write this thesis. Thanks for bringing the dragon back and for encouraging me every single day.

I would like to thank my dad for his encouragements throughout my thesis and for helping moving back from Newcastle. I would to thank my sister and my family for their support over the years.

I would like to thank Clanigalu and Master soirée for their support and their unwavering friendship. A special thank you goes to Marie and Claire for sharing their experience in doing a PhD abroad.

To finish I would like to thank my love Nicolas, your move to England was the best thing that happened to me even if you started with only two English words in your vocabulary ( Hello and Thank you). Your support meant a lot to me, you always found a way to calm me down or to make me laugh. I am grateful to have you by my side.

# Table of Contents

# List of Tables

# List of Figures

# List of abbreviations

| | |
|---|---|
| αSMA | Alpha smooth muscle actin |
| 3'UTR | Three prime untranslated region |
| AcSDKP | N-acetyl-seryl-aspartyl-lysyl-proline |
| ADAM9 | Disintegrin and mettaloproteinase domain-containing protein9 |
| ALK | Activin receptor-like kinase |
| AP | Alkaline phosphatase |
| AV | Atrioventricular |
| BCIP | 5-bromo-4-chloro-3'-indolylphosphate |
| BMP | Bone morphogenetic protein |
| BRE | TFIIB recognition element |
| BSA | Bovine serum albumine |
| CDS | Coding sequences |
| CF | Cardiac fibroblast |
| COL1A1 | Collagen I alpha1 |
| Ct | Cycle treshold |
| CTGF | Connective tissue growth factor |
| CVD | Cardiovascular disease |
| DCP2 | Decapping protein 2 |
| DDX6 | DEAD-box protein 6 |
| DGCR8 | DiGeorge syndrome critical region gene 8 |
| DIG | Digoxigenin |
| DMSO | Dimethyl sulfoxide |
| DPE | Downstream promoter element |
| ECM | Extracellular matrix |
| EndMT | Endothelial-to-mesenchymal transition |
| EDC4 | Enhancer of decapping 4 |
| EGF | Epidermal growth factor |
| eIF4G | Eukaryotic initiation factor 4G |
| EMT | Epithelial-to-mesenchymal transition |
| FAM | 6-carboxyfluorescein |
| FBS | Foetal bovine serum |
| FGF | Fibroblast growth factor |
| FN | Fibronectin |
| FSP1 | Fibroblast specific protein 1 |
| GFP | Green fluorescent protein |
| GW182 | Glycin tryptophan protein of 182 KDa |
| $H_2O_2$ | Hydrogen peroxide |
| HDMEC | Human dermal microvascular endothelial cell |
| HF | Heart failure |
| HFpEF | Heart failure with preserved ejection fraction |
| HFrEF | Heart failure with reduced ejection fraction |
| HIF1α | Hypoxia-inducible factor 1 alpha |

| | |
|---|---|
| HMEC1 | Human microvascular endothelial cells |
| HSC | Heat shock cognate |
| HSP | Heat shock protein |
| HSVEC | Human saphenous vein endothelial cell |
| HUAEC | Human umbilical artery endothelial cell |
| HUVEC | Human umbilical vein endothelial cells |
| ICAM1 | Intercellular adhesion molecule type 1 |
| IL1β | Interleukin 1 beta |
| Inr | Initiator |
| IRAK4 | IL-1 receptor-activated protein kinase 4 |
| IVS | Interventricular septum |
| KD | Kawasaki disease |
| LF | Lipofectamine |
| LTBP1 | Latent transforming growth factor beta binding protein 1 |
| LV | Left ventricle |
| LVEF | Left ventricular ejection fraction |
| LVFW | Left ventricular free wall |
| LVH | Left ventricular hypertrophy |
| m7G | 7-methyl guanylate |
| MGB | Minor groove binder |
| MI | Myocardial infaction |
| miRNA | MicroRNA |
| MMP | Metalloproteinase |
| MyD88 | Myeloid differentiation primary response 88 |
| NBT | 4-nitro-blue tetrazolium |
| NFQ | Non fluorescent quencher |
| Ns miR | Non specific miRNA |
| OFT | Outflow tract |
| PAH | Pulmonary artery hypertension |
| PBS | Phosphate buffer saline |
| PCR | Polymerase chain reaction |
| PDGF | Platelet-derived growth factor |
| RanGAP | RanGTPase activating protein |
| RISC | RNA induced silencing complex |
| ROS | Reactive oxygen species |
| RT | Reverse transcription |
| SMURF2 | Smad specific E3 ubiquitin protein ligase 2 |
| snoRNA | Small nucleolar RNAs |
| snRNA | Small nuclear RNA |
| stRNA | Small temporal RNA |
| STZ | Streptozotocin |
| TAC | Transverse aortic constriction |
| TAMRA | Tetramethylrhodamine |
| TGFβ | Transforming growth factor beta |

| | |
|---|---|
| TIMP | Tissue inhibitor of metalloproteinase |
| TNFa | Tumor necrosis alpha |
| UUO | Unilateral ureteral obstruction |
| VCAM1 | Vascular cell adhesion type 1 |
| VSMC | Vascular smooth muscle cells |
| vWF | von Willebrandt Factor |

# Chapter 1. Introduction

## 1.1 Heart failure

Heart failure (HF) is a clinical manifestation of numerous cardiovascular diseases mainly represented by ischemic heart disease, valvular heart disease and hypertension (Ponikowski *et al.*, 2016). According to the European Cardiovascular Disease Statistics, cardiovascular disease (CVD) causes 45% of all deaths in Europe and 37% of all deaths in the European Union. In fact, CVD-induced heart failure results in a heart that is unable to maintain the blood flow to supply the body with oxygen. In the onset of cardiac disease, the injured heart will try to compensate its dysfunction by remodelling the tissue giving rise to a change of shape of the heart. Initially compensatory, the change of heart structure induced by the remodelling maintains normal cardiac function at first but ultimately leads to a progressive heart dysfunction (Kemp and Conte, 2012).

Historically, HF was assessed with the measurement of left ventricular ejection fraction (LVEF). As the heart function in cycle of diastole (blood filling) and systole (blood ejection), HF was distinguished between the systolic heart failure referring to a reduced ejection fraction (HFrEF) and the diastolic heart failure referring to a preserved ejection fraction (HFpEF) (Federmann *et al.*, 1994; Ponikowski *et al.*, 2016).

The main differences between HFrEF and HFpEF are the performance of contractile function and left ventricular remodelling pathways (Komamura, 2013). In patients with systolic heart failure, blood filling is normal during diastole however the failing heart is unable to eject sufficient blood during systole. Compensatory mechanism to maintain the heart function led to eccentric hypertrophy which is defined by an increased left ventricular mass and a normal relative wall thickness (Sehgal and Drazner, 2007). This hypertrophy is due to ventricular dilatation and stretching of the muscle fibers (Pearse and Cowie, 2014).

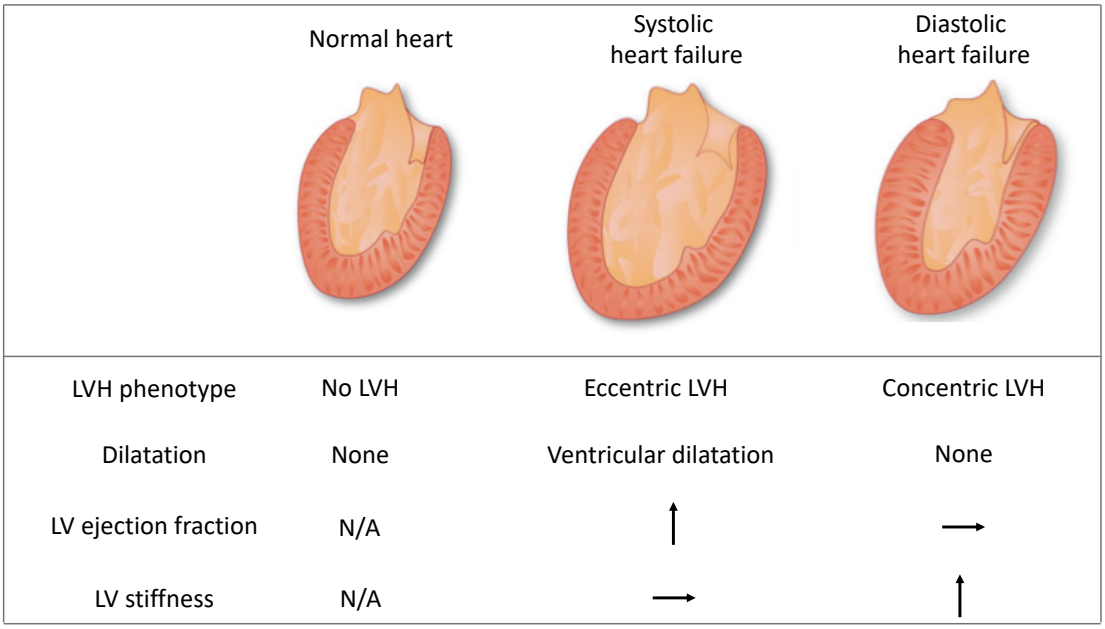


**Figure 1.1 Two types of heart failure**
Heart failure can be distinguished between the systolic heart failure (HFrEF) and the diastolic heart failure (HFpEF). HFrEF is defined by an eccentric left ventricular hypertrophy (LVH) due to ventricular dilatation. Thereafter, this dilatation induces a reduction of the ejection fraction. HFpEF is characterized by a concentric LVH where ventricular wall is thicker and myocardial stiffness is increased. (Khouri *et al.*, 2010; Komamura, 2013; Lazzeroni *et al.*, 2016)

In HFpEF patients, systolic function is preserved but filling is impaired during diastole. Impaired filling reduces cardiac output as the left ventricular (LV) is not filled enough. The decrease of cardiac output is then compensated for by an increase in myocardial stiffness which influences filling pressure. An increase in left ventricular mass and relative wall thickness is induced and gives rise to a concentric LVH (Komamura, 2013).

Cardiac remodelling is a predominant characteristic of HF and can be induced by a multitude of pathophysiological stimuli such as mechanical stress, hormonal stimuli or ischemia (Schirone *et al.*, 2017). Ventricular remodelling caused essentially an alteration in cardiomyocyte and the development of fibrosis (Unverferth *et al.*, 1986; Konstam *et al.*, 2011).

As the result of an insult, myocyte loss and therefore contractile tissue loss can be observed. Myocyte death occurs mainly through necrosis and apoptosis. Nevertheless, surviving cardiomyocytes undergo morphologic changes and become elongated or hypertrophied in order to maintain normal heart function (Segura *et al.*, 2014). In eccentric hypertrophy, lengthening of myocytes is observed while thickness of myocytes are increased in concentric hypertrophy (Gerdes, 2002).This two types of

myocyte remodelling is explained by the addition and the rearrangement of myocyte's sarcomeres (Katz and Rolett, 2016).

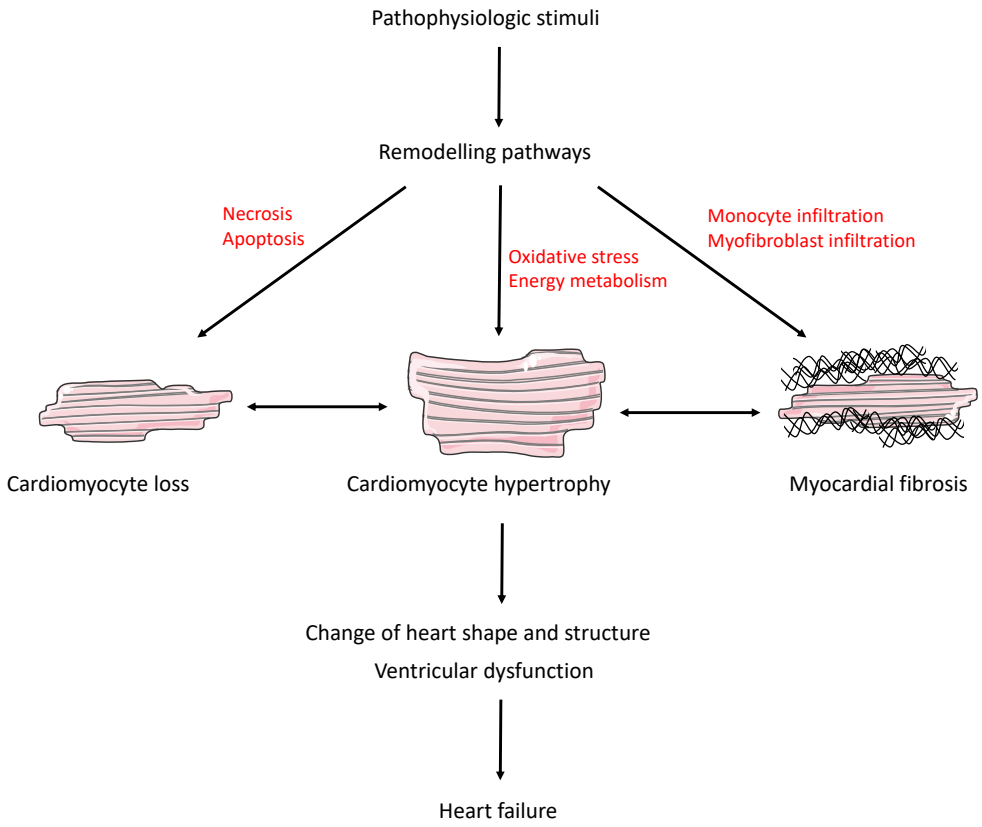


**Figure 1.2 Cardiac remodelling pathways leading to heart failure**
Remodelling of the heart occurs following pathophysiological stimuli. The remodelling affects essentially the cardiomyocyte and the extracellular matrix. Post-injury, numerous cardiomyocytes are lost through necrosis and apoptosis. In the context of oxidative stress, surviving cardiomyocytes undergo morphologic changes and became hypertrophied. Myocardial fibrosis also contributes to the remodelling via the accumulation of collagen secreted by the myofibroblasts. Altogether, the remodelling induces a change in shape and structure of the heart which can later on lead to heart failure. Reproduced from (Schirone *et al.*, 2017).

Cardiac fibrosis contributes to cardiac remodelling in both systolic and diastolic dysfunction (Brilla and Weber, 1992; Hein *et al.*, 2003). Post-injury, myofibroblasts proliferate and lead to the development of fibrosis which is defined by an accumulation of extracellular matrix (ECM). Fibrotic ECM increases myocardial stiffness and can lead to diastolic dysfunction. In systolic dysfunction, fibrosis impairs the contractility (Kong *et al.*, 2014).

## 1.2 Cardiac fibrosis

Numerous cardiovascular diseases induce a ventricular remodelling in order to preserve heart integrity and maintain heart function. This remodelling is essentially associated with the development of fibrosis. Although initially compensatory, fibrosis contributes to structure and shape changes that can later on lead to heart failure Cardiac fibrosis is defined by an accumulation of extracellular matrix and contributes to both systolic and diastolic heart failure. Several types of cells contribute to cardiac fibrosis, directly such as the myofibroblast that secrete ECM protein or indirectly such as immune cells, cardiovascular cells and endothelial cells that secrete pro-fibrogenic factors. Regardless of the etiology, fibrosis is based on common cellular effectors and common signalling pathways.

In physiological conditions, the extracellular matrix network is responsible for the laminar structure of the myocardium and prevents the sarcomeres within cardiomyocytes from stretching. In the interstitium, vascular smooth cells and the cardiac fibroblast are the most abundant cells meanwhile immune cells such as mast cells and macrophage are present in small numbers (Gersch *et al.*, 2002). CF provides a structural scaffold for cardiomyocyte, diffuse mechanical force throughout the cardiac tissue and is the mediator of electric conduction (Souders *et al.*, 2009).
In the extracellullar matrix, collagen I confers tensile strength and represents 85% of all collagen meanwhile collagen III represents only 11% and maintains elasticity of the network (Weber, 1989). In wound healing, collagen is degraded by metalloproteinase (MMP) which allows the tissue remodelling. MMP's are tightly regulated and balanced by the tissue inhibitor of metalloproteinase (TIMP). In the late phase of wound-healing, fibroblasts undergo apoptosis leaving a mature scar consisting of collagen cross-linked and other components from the matrix. (Caley *et al.*, 2015)

In response to an injury, remodelling pathways are activated and inflammation, fibroblast proliferation or scar maturation can be observed. When necrotic injury occurs, the resulting inflammation leads to recruitment of immune cells and debris removal. Immune cells release Transforming growth factor beta 1 (TGFβ1) which triggers the transdifferentiation of fibroblasts into myofibroblast. Within the cardiac tissue myofibroblasts release pro-inflammatory and prohypertrophic signals as well as TGFβ1 which regulates the deposition of extracellular matrix protein. In the absence

of cell death, fibrosis can be induced by pathophysiological stimuli such as ischemia or metabolic injury. Thereafter, cardiac fibrosis induces irreversible changes in the structure such as chamber dilatation, cardiomyocyte hypertrophy and trigger apoptosis. In addition, excess ECM and fibroblasts impair mechano-electric coupling of cardiomyocytes, thus reducing cardiac contraction.

Myofibroblasts first produce fibronectin which create a temporary scaffold for the deposition of fibrillary collagen. Fibronectin also promotes the transdifferentiation of fibroblasts in myofibroblasts through its ED-A splice variant which is well known to cooperate with TGFβ. Activated fibroblasts are the main source of collagen and a significant increase of collagen I and III can be observed in the fibrotic heart. Unlike the process of wound-healing, the MMP/TIMP balance is disturbed following a stress and this imbalance is associated with heart dysfunction. An increase of collagen in the interstitium around muscle fibers contributes to an increased ventricular stiffness and an impaired diastolic function. During fibrotic remodelling, degradation of collagen can trigger ventricular dilatation and therefore induce systolic dysfunction.

There are two types of cardiac fibrosis namely reactive interstitial fibrosis and replacement fibrosis which can be observed in different types of heart failure. The reactive interstitial fibrosis is an adaptative response to preserve cardiac structure and function .This interstitial fibrosis will ultimately progress towards the replacement fibrosis. This second type of fibrosis restores regions of cardiomyocyte death and avoids cardiac rupture.(Krenning *et al.*, 2010)

*Cardiovascular disease associated with cardiac fibrosis*

As stated before, fibrosis consists of common effectors and signalling pathways. However, the contribution of each pathway is dependent on the etiology of the ventricular remodelling.

After an acute injury such as myocardial infarction (MI), loss of cardiomyocytes triggers an inflammatory reaction which activates the reparative pathways. Infarct healing can be divided in three phases. The inflammatory phase, the proliferative phase and the formation of mature scar

During the inflammation, stimulation of cytokine and chemokine signalling results in the recruitment of immune cells into the injured area. Neutrophils and activated

macrophages remove dead cells, debris and release cytokines, growth factors leading to formation of granulation tissue. In fact, release of Interleukin-1β (IL1β) and Tumor Necrosis factor-α (TNFα) promotes MMP expression and therefore matrix degradation. Once the wound is cleared, leucocytes undergo apoptosis and pro-inflammatory mediators are inhibited which lead to the proliferative phase. During this phase, non-myocyte cells such as fibroblasts and endothelial cells proliferate. In addition, fibroblasts undergo phenotypic changes and acquire a contractile apparatus. These activated fibroblasts secrete a high level of extracellular matrix proteins in the infarct area. During the maturation phase, matrix proteins are cross-linked and form a mature scar, meanwhile fibroblast and endothelial cells within the scar undergo apoptosis (Frangogiannis, 2008). The cross-linking of collagen increases stiffness and contributes to the diastolic dysfunction

Pressure overload is a cardiac condition caused by hypertension or aortic stenosis. The remodelling includes cardiac fibrosis which is associated with increased stiffness and therefore contributes to diastolic dysfunction. If the pressure overload persists, the remodelling can lead to both, ventricular dilatation and the development of systolic dysfunction.

Volume overload can be observed in patients with valvular regurgitant lesions and contribute to systolic dysfunction. It results in a decrease of collagen due to an increase of MMP that ultimately leads to ventricular dilatation. The presence of fibrosis in volume overload heart is still debated.

## 1.3 Cardiac fibroblast

Regardless of etiology, cardiac fibroblasts (CF) are the main effectors in cardiac fibrosis. For years, fibroblasts were considered as the largest cell population in the cardiac tissue, however recent reports have suggested that cardiac fibroblast account for less than 20% of the cardiac total cells. Cardiac fibroblasts are mostly found in cardiac interstitium where they are the most abundant cell type. In addition, cardiac fibroblasts are also located in the epicardial and perivascular regions.

Their function relies on the maintenance of the cardiac extracellular matrix and the regulation of cardiac structure. Furthermore, CF contributes to mechanical, chemical and electrical functioning of the heart. In the young adult heart, cardiac fibroblasts remain quiescent and do not exhibit significant inflammatory or proliferative activity.

In general, fibroblasts are the most abundant cell type of connective tissue and are heterogeneous from one organ to the other. In physiological conditions, they do not express large amount of extracellular matrix protein and do not present any contact with cells or with the matrix.

Cells are shielded from stress by the matrix that they secrete and remodel. In wound healing, fibroblasts are able to differentiate toward a cell type close to smooth muscle cells. (Majno *et al.*, 1971) Gabbiani et al showed that fibroblasts were able to contract with the same stimuli that allow contraction of smooth muscle cells (Gabbiani *et al.*, 1971).

After cardiac injury, cytokines released by damaged cells or immune cells activate fibroblasts. Fibroblasts then migrate to the site of injury and secrete extracellular matrix. In response to alterations in ECM and cytokines within the micro-environment, fibroblast acquire their first stress fibers of cytoplasmic actin and became proto-myofibroblasts. Proto-myofibroblasts are negative for alpha smooth muscle actin ($\alpha$SMA) and are described as an intermediate step in myofibroblast differentiation. Focal adhesion connects the stress fiber to ECM proteins and N-cadherin junctions link cells to cells. During wound healing, fibroblasts secrete specific transcripts of fibronectin that later promote myofibroblast differentiation (Serini *et al.*, 1998).

Differentiation in myofibroblasts is characterised by their contractile functions and is denoted by the presence of a contractile apparatus which consists of actin filaments associated with myosin. This actin filament is a smooth muscle cell actin isoform and is called alpha smooth muscle actin (Darby *et al.*, 1990). Expression of $\alpha$SMA confers not only an increase in contractile activity but also induces a intracellular mechanical feedback loop (Hinz *et al.*, 2001). Myofibroblasts are connected to the ECM via structures called fibronexus. Fibronexus are transmembrane complexes of intracellular actin filament and extracellular fibronectin and bind to collagen from ECM.(Singer, 1979; Singer *et al.*, 1984)

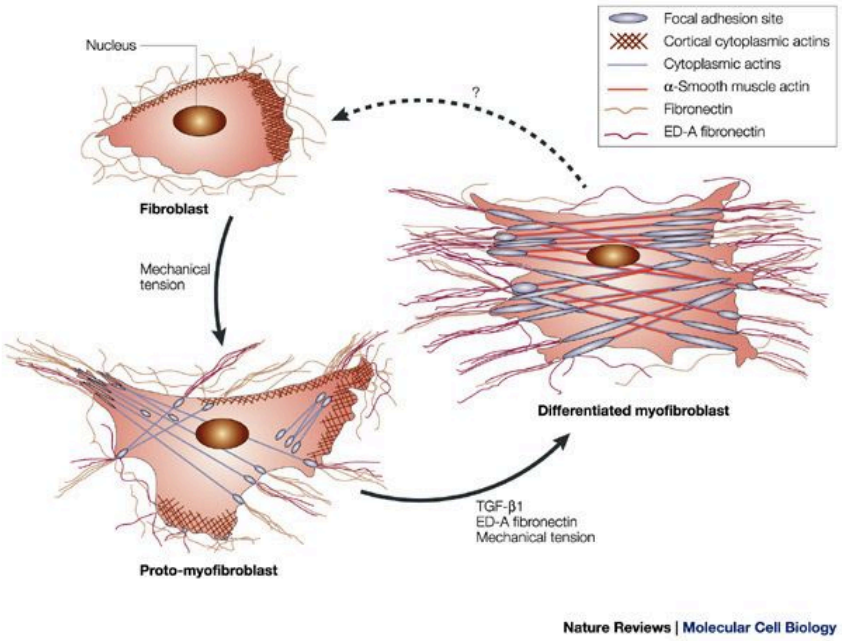


**Figure 1.3 Transdifferentiation of fibroblast**
During the transdifferentiation, fibroblasts acquire their first stress fibers of cytoplasmic actin and reach the intermediate state of proto-myofibroblast. Differentiation in myofibroblasts requires the presence of a contractile apparatus consisting in alpha smooth muscle actin filaments associated with myosin. (Tomasek *et al.*, 2002)

The complete transdifferentiation of fibroblasts into αSMA positive myofibroblasts requires three key events :

- presence of biologically active TGFβ1
- presence of ECM protein such as ED-A
- extracellular stress

Myofibroblast can efficiently contract and are essential for wound closure and structural integrity of infarct healing.

Interestingly, extracellular matrix protein deposition is not usually considered for identification of fibroblasts. Fibroblasts were first defined by their morphology. Fibroblast are flat, spindle-shaped cells and contain an oval nucleus. Fibroblasts exhibit sheet like extension and differ from other cell type by their lack of basal membrane. Despite the progress in cells identification with lineage tracing, studies of fibroblasts and activated fibroblasts remain difficult as no robust marker were identified.

Fibroblast specific protein 1 (FSP1) is considered as a reliable marker of both fibroblasts and myofibroblasts. However, recent study shows that FSP1 could be expressed by a multitude of cell line including endothelial cells. Alpha SMA reflects the activation of fibroblasts but is not specific as these actin fibers are also found in the

vascular smooth muscle cells (VSMC). Interestingly, fate mapping techniques that were normally used to study cell lineage in embryonic development, can be used to assess the relevance of fibroblast markers. A common approach of lineage tracing is the system Cre-Lox which requires 2 transgenes. The first transgene express Cre-recombinase under the promoter of a specific cell type. The second transgene is composed with a STOP cassette flanked by two sequences LoxP and a reporter gene under an ubiquitous promoter. In cells expressing the recombinase, Cre interacts with the LoxP sequence, removes the stop cassette and allows the expression of the reporter gene (Zeisberg and Kalluri, 2010). This way, cells can be traced even after a phenotypic change. In fibroblasts, the lineage tracing revealed that some markers such as periostin, fibronectin or alpha SMA were expressed by a subpopulation of fibroblasts. The transcription factors Tcf21 and Wt1 are expressed by the epicardium in embryologic development and are present in epicardium-derived cardiac fibroblasts. Thus, these two factors were used in models of lineage tracing to study the role of resident fibroblasts in cardiac fibrosis (Moore-Morris, Guimarães-Camboa, Banerjee, Alexander C Zambon, *et al.*, 2014; Kanisicak *et al.*, 2016). Furthermore, lineage tracing was performed to elucidate the origin of the fibroblast population.

| Localisation | Markers | Adult heart | Injured Adult Heart |
|---|---|---|---|
| Nuclear | WT1 | Epicardium, Endothelial cells(low) | Epicardium, Endothelial cells(low), peri-vascular |
| | Tcf21 | Fibroblast, Epicardium | Fibroblast, Epicardium |
| Cytosollic | FSP1 | Fibroblast, Pericyte,VSMC, Endothelial Cells, Immune Cells | Fibroblast, Pericyte, VSMC, Endothelial Cells, Immune Cells |
| | Prolyl-4-hydroxylase | Fibroblast, Endothelial Cells | Fibroblast, Immune Cells |
| Cytoskeletal | Vimentin | Fibroblast, Pericyte, VSMC, Endothelial Cells | Fibroblast, Pericyte, VSMC |
| | αSMA | Pericyte, VSMC | Fibroblast, Pericyte, VSMC |
| Cell membrane | PDGF alpha | Fibroblast | Fibroblast |
| | MEFSK4 | Fibroblast, Pericyte, VSMC(low) , Immune Cells | Fibroblast, Pericyte, VSMC, Endothelial Cells, Immune Cells |
| | DDR2 | Fibroblast, Pericyte, VSMC | Fibroblast, Pericyte, VSMC |
| | CD90 | Fibroblast, Pericyte, VSMC , Immune Cells, Endothelial cells | Fibroblast, Pericyte, VSMC , Immune Cells, Endothelial cells |
| | Sca1 | Fibroblast | Fibroblast |
| Extracellular | Periostin | | Fibroblast |
| | Fibronectin | Fibroblast, Endothelial Cells | Fibroblast |
| | ED-A fibronectin | | Fibroblast, Endothelial Cells |
| | Collagen type I | Fibroblast, Pericyte, VSMC | Fibroblast, Endothelial Cells, Cardiomyoctye |
| | Collagen type III | Fibroblast, Pericyte, VSMC | Fibroblast, Pericyte, VSMC |
| | FAP | | Fibroblast |

**Table 1.1 Expression of fibroblast markers**
Adapted from (Ivey and Tallquist, 2016)

## 1.4 Origin of myofibroblasts

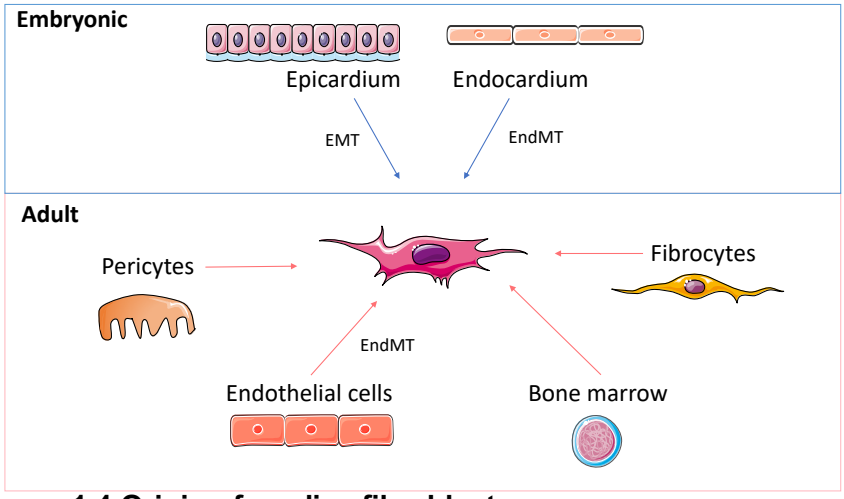


**Figure 1.4 Origin of cardiac fibroblasts**
Cardiac fibroblasts can arise from embryonic tissue through EMT and EndMT. Contribution to the pool of fibroblasts by pericytes, endothelial cells, bone marrow progenitor cells or fibrocytes was demonstrated in adult cardiac tissue in several studies.

*Resident fibroblast*

Traditionally, fibroblasts in the cardiac interstitium are thought to arise from embryonic mesenchymal cells (Norris *et al.*, 2008; Ali *et al.*, 2014). In the cardiac walls, cells from epicardium undergo epithelial-to-mesenchymal transition (EMT) (Gittenberger-De Groot *et al.*, 1998). This process is regulated by growth factors such as TGFβ, platelet-derived growth factor (PDGF) and fibroblast growth factor (FGF) (Olivey *et al.*, 2006). In addition to the development of cardiac interstitial fibroblasts, some cells from the endocardium undergo endothelial-to-mesenchymal transition and form a cushion mesenchyme that is require for the development of heart valve. (Markwald *et al.*, 1975). Furthermore, part of this fibroblast population resides in the interventricular septum (de Lange *et al.*, 2004). Recent studies revealed that resident fibroblasts derived from epicardium and endocardium are the main source of cardiac fibroblasts. Lineage tracing of epicardial derived and endocardial derived fibroblast using WT1-Cre and Tie2-Cre respectively revealed that their expression was complementary in healthy heart. In fact, 100% of fibroblast (Col1a1 +) were positive for WT1 in the right ventricle, 92% in the left ventricular free wall(LVFW) and 30 % in the interventricular septum (IVS). In addition, 12% of fibroblasts were positive for Tie2 lineage tracing in the LVFW and 60% in the IVS (Moore-Morris, Guimarães-Camboa, Banerjee, Alexander C. Zambon, *et al.*, 2014). Following an injury, cells derived from the epicardium and endocardium respectively contributed to 80-85% and 20% of fibroblast during cardiac fibrosis development.

Interestingly, these results were contradicted by recent studies suggesting the contribution of other cell type to the pool of fibroblasts in the development of cardiac fibrosis.

*Endothelial-to-mesenchymal transition origin*

After an injury, endothelial cells were suggested as a source of myofibroblasts through endothelial-to-mesenchymal transition. In order to study the contribution of endothelial cells to the fibroblast population, lineage tracing under the promoter of Tie1 (Tie1-Cre), an endothelial/hematopoietic marker was generated. This study in heart post-aortic banding revealed that cells with an endothelial origin were able to express a mesenchymal marker such as FSP1 or alpha SMA. Endothelial origin was found in 75% of alpha SMA positive cells and 15% of FSP1 positive cells (Zeisberg *et al.*, 2007). However, recent studies demonstrated that immune cells can be labeled by Tie1 and FSP1 implying that these markers were not reliable to study EndMT (Gustafsson *et al.*, 2001; Osterreicher *et al.*, 2011). Another study was performed with the Cre-Lox system under the promoter of VE-cadherin/Cdh5, to trace endothelial cells after thoracic aortic banding. No significant contribution of endothelial cells was observed, however, fibroblast identification was based on Col1A1 expression and did not overlap with mesenchymal markers expression such as FSP1(0%) and $\alpha$SMA (7%) suggesting that only a part of fibroblast population was studied. (Moore-Morris, Guimarães-Camboa, Banerjee, Alexander C. Zambon, *et al.*, 2014). Ali et al generated Tie2-Cre mice and confirmed the contribution of EndMT to the pool of fibroblast (around 20%) but did not find any difference post-injury implying that EndMT is not active after an injury (Ali *et al.*, 2014).

Interestingly, EndMT has been described as a contributor to fibrosis in other organs such as kidney and lung but remains elusive in cardiac fibrosis (LeBleu *et al.*, 2013a; Seo-Hyun Choi *et al.*, 2015).

*Bone marrow origin*

Bone marrow derived progenitor cells were described as a potential source of fibroblasts in the context of fibrosis. This has been suggested when bone marrow cells labelled with green fluorescent protein (GFP) and transplanted were found in the fibrotic cardiac tissue following myocardial infarction (van Amerongen *et al.*, 2008). Zeisberg et al show, after transplantation of Tie1-Cre bone marrow, positive cells in the heart within the vessel but none of these cells were positive to $\alpha$SMA or FSP1.

Thus, hematopoietic progenitor cell did not contribute to the pool of fibroblasts. In the same study, they performed transplantation of bone marrow cells from male mice to female mice and found that 13.4% of FSP1 positive cells and 21.1% of αSMA positive cells carried a Y chromosome, implying that these fibroblasts came from the bone marrow. Bone marrow derived cells can contribute to the fibroblast population in cardiac fibrosis but not the hematopoietic progenitor cell. (Zeisberg *et al.*, 2007).

*Fibrocytes*

Fibroblast progenitors namely fibrocytes have been observed in the circulation and present a mesenchymal-like phenotype. This population express both hematopoietic and mesenchymal marker such as CD34,CD45, vimentin and procollagen1 (Abe *et al.*, 2001). In addition, culture of fibrocytes revealed a slow decrease of CD34 expression and a progressive increase of collagen 1 production (Bucala *et al.*, 1994).

*Perivascular origin*

Cells lying in the perivascular region namely pericytes were suggested as potential contributors of the fibroblast population in fibrosis. The study of Sundberg et al. was the first to demonstrate the transformation of pericytes into fibroblast. Indeed, pericytes were developed in collagen-producing cells in the context of dermal scarring (Sundberg *et al.*, 1996). In addition, retinal pericytes were found with a similar phenotype to the mesenchymal stromal cells, suggesting their ability to transdifferentiate into mesenchymal cells (Covas *et al.*, 2008). More recently, Humphreys et al. performed lineage tracing in mice with fibrotic kidneys and observed that CD73 positive pericytes were undergoing transdifferentiation into fibroblasts in kidney fibrosis (Humphreys *et al.*, 2010).

## 1.5 Endothelial-to- mesenchymal transition

Endothelial mesenchymal transition results in the differentiation of endothelial cells to mesenchymal cells. Endothelial cells exhibit a basal apical polarity, and form a monolayer. During EndMT, the transdifferentiated cells acquire a front rear polarity, migratory properties and lose their junctions. This transition is characterized by the decrease of endothelial markers such CD31, VE -cadherin and the increase of mesenchymal markers such as alpha SMA, and secretion of components of the extracellular matrix.

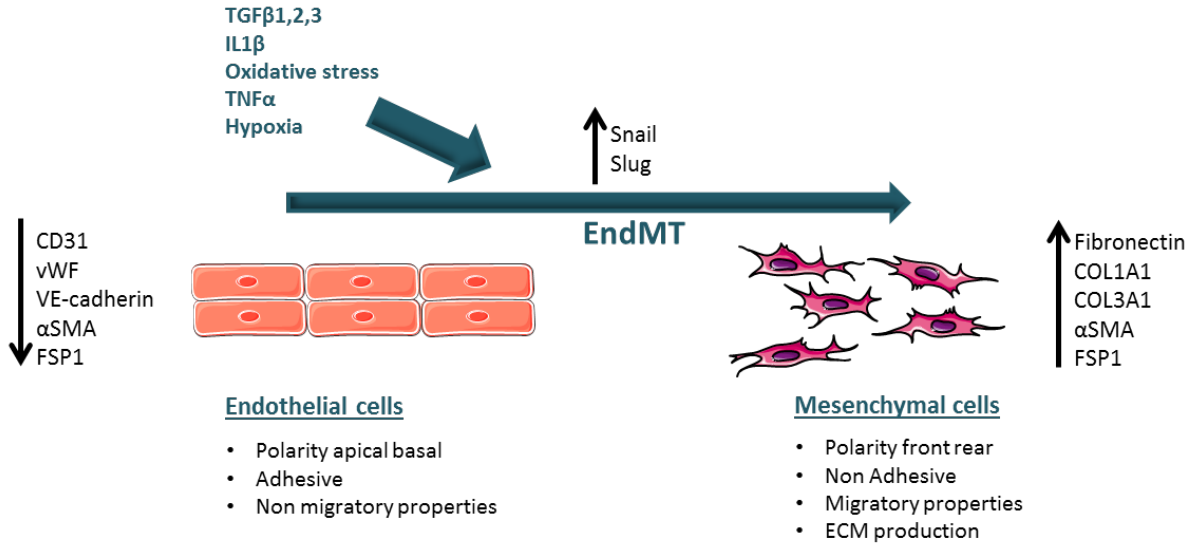


**Figure 1.5 Process of endothelial-to-mesenchymal transition**

### *1.5.1 Endothelial-to-mesenchymal transition in heart development*

EndMT was first described in embryonic development. In mouse at embryonic day 9,5, the heart consist of two layers namely the endocardium and myocardium, separated by an acellular matrix called cardiac jelly. Transmission microscopy and histologic examination during the development of embryonic hearts of rats revealed the migration of endothelial cells in the cardiac jelly and the transdifferentiation of these cells into mesenchymal cells to form the cushion tissue (Markwald *et al.*, 1975).These cells expressing Tie-1, Tie-2, VEGFRI/II and CD31 are precursors of cells forming heart valves in the outflow track (OFT) region and the atrioventricular (AV)canal. Evidence of this differentiation was confirmed in chicks *in-vitro* with the co-culture of the atrioventricular canal region and myocardium on collagen gel. Both tissues were required for the differentiation as AV canal or myocardium alone were not sufficient to induce EndMT (Runyan and Markwald, 1983). Several years later, Kinusaki et al developed a model of lineage tracing of endothelial cells Tie2-Cre;CAG-CAT-Z in mouse embryos. In this model, cells with an endothelial origin were positive for Lacz staining. LacZ staining in mouse heart embryos confirmed that mesenchymal cells forming heart valves were derived from endothelial cells (Kisanuki *et al.*, 2001). During EndMT, endocardial cells lose their cell polarity, cell–cell junctions and acquire a migratory function. Mesenchymal cells invade the ECM and populate the cardiac cushions.

Among the numerous signalling pathways involved in EndMT, three are required to complete the formation of heart valves: BMP, TGFβ and Notch signalling.

TGFβ isoforms were described in the development of multiple tissues including the heart valves. Using culture on collagen gels, Potts et al first showed that EndMT was stimulated mainly by members of the TGFβ family (Potts and Runyan, 1989). TGFβ2 and TGFβ3 were expressed in the myocardium of chick and their neutralisation by specific antibodies showed a distinct role in the process of EndMT. TGFβ2 contributed to the disruption of cell-cell contact and TGFβ3 was shown to be promoting their migration (Boyer *et al.*, 1999). Studies in various species revealed different requirement of TGFβ isoforms for the formation of heart valve. In fact, avian hearts require both TGFβ2 and TGFβ3 for the transdifferentiation whereas mouse only require TGFβ2 (Camenisch *et al.*, 2002). Additionally, inhibition of latent transforming growth factor beta binding protein 1 (LTBP1), a protein required for TGFβ1 activation prevented EndMT in mouse Av explants, arguing that TGFβ1 plays a role in EndMT (Nakajima *et al.*, 1997). Altogether, these data suggest a different role for each of the three isoforms and could be involved at different stages of EndMT. However, TGFβ2 knock-out in mouse AV explant reduced mesenchymal cells invading the collagen meanwhile, TGFβ1,3 knock-out showed invasion rates similar to the wild type, implying that EndMT was functional (Mercado-Pimentel and Runyan, 2007; Azhar *et al.*, 2009).

Bone morphogenetic proteins (BMP) proteins are essential in EndMT and particularly the protein BMP2 which is highly expressed in the myocardium before EndMT. AV canal explant stimulated with BMP2 were able to complete EndMT without the presence of myocardium explants (Sugi *et al.*, 2004). Furthermore, BMP2 deletion in the myocardium revealed its importance in the initiation of EndMT and in the cushion formation (Ma *et al.*, 2005). Signal transduction pathway of BMP proteins requires their binding to the receptors activin receptor-like kinase 2 (ALK2)/ALK3 and BMPR2. The deletion of ALK2*,* ALK3*,* or BMPR2 in endothelial cells severely impaired EndMT and reduced the expression of a transcription factor Snail1 known for its role in EndMT (Wang *et al.*, 2005). This suggests that BMP2 signals from myocardium stimulate AV canal EndMT in endocardial cells through ALK2/BMPR2 and ALK3/BMPR2 complexes.

Notch signalling lead to the expression of genes from the Hey and Hes transcription factor families (MacGrogan *et al.*, 2011). In mouse and chick heart embryos, Hey1 and

Hey2 were found in flanking atrial and ventricular chambers but not in the AV canal (Rutenberg *et al.*, 2006; Kokubo *et al.*, 2007). A gain of function of Notch, Hey1, Hey2 in the AV canal led to the repression of BMP2 which is essential for the initiation of EndMT. Thus, BMP2 expression is restricted to the AV canal due to the absence of Hey genes (Rutenberg *et al.*, 2006).

In addition, Notch signalling was found necessary for the formation of heart valves. The knockout of the RBPJK complex which is a downstream protein in Notch signalling induced the loss of Snai1 expression. This prevented EndMT by blocking the down-regulation of the cell adhesion protein VE-cadherin (Timmerman *et al.*, 2004). The gain of function of Notch in the endocardium revealed the ectopic activation of Snai1/Snail, Snai2/Slug and pro-EndMT gene. Cells became positive for mesenchymal genes and migrate to the surface of the collagen gel but fail to invade it suggesting a partial EndMT. Interestingly, addition of BMP2 to this model led to the full EndMT (Luna-Zurita *et al.*, 2010). This suggests that endocardial Notch1 interacts with myocardial Bmp2 to promote and regulate EndMT in both the AV canal and OFT. All together, these three signalling pathways are able to induce EndMT in heart development to build heart valves (Garside *et al.*, 2013).

### *1.5.2 Endothelial-to-mesenchymal transition in fibrosis*

In the last decade, the mechanism of endothelial-to-mesenchymal transition has been explored in a pathological context and more precisely in fibrotic diseases. In 2007, Zeisberg et al first described EndMT in cardiac fibrosis in adult organisms. In this work, transgenic mouse expressing a Cre-loxP recombinase under Tie-1 promoter allowed the expression of Lacz within cells of endothelial origin regardless of phenotype changes. Transgenic Mice underwent aortic banding and therefore induced cardiac fibrosis. Their results demonstrated that 27% to 35% of fibroblasts FSP1+/$\alpha$-SMA+ were positive for cells of endothelial origin in fibrotic areas (Zeisberg *et al.*, 2007). Similarly, EndMT was observed in cardiac fibrosis generated post-myocardial infarction with the ligation of the left ascending coronary artery. Lineage tracing of endothelial cells with the stem cell leukemia-Lacz system exhibited alpha SMA positive cells with an endothelial origin post-MI (Aisagbonhi *et al.*, 2011). In the study of Widyantoro et al, cardiac fibrosis induced by diabete mellitus showed FSP1 and CD31 positive cells suggesting the transdifferentiation (Widyantoro *et al.*, 2010).

EndMT was found involved in fibrotic pathologies in multiple organs such as the lung, the kidney and the gut. In mouse, bleomycin-induced pulmonary fibrosis revealed the

presence of EndMT using a lineage tracing under the promoter of the endothelial marker Tie2. Up to 16% of fibroblasts were positive to the endothelial origin. In the same work, fibroblast populations derived from endothelial cells were divided into 2 subcategories: αSMA negative, Collagen I positive fibroblasts (15%) and αSMA positive, Collagen I negative fibroblasts (85%) (Hashimoto *et al.*, 2010). EndMT was also observed in pulmonary hypertension and radiation-induced pulmonary fibrosis (Qiao *et al.*, 2014; Seo-Hyun Choi *et al.*, 2015). Ranchoux et al, combined correlative light and electron microscopy in pulmonary artery hypertensionPAH from patients to study endothelial cell behavior at an ultrastructural level. Endothelial cells from PAH patients displayed a contractile phenotype suggesting the active process of EndMT (Ranchoux *et al.*, 2015).

Zeisberg et al discovered the participation of EndMT in renal fibrosis in three different mice models: streptozotocin (STZ)-induced diabetic nephropathy, unilateral ureteral obstruction (UUO) and alpha 3 chain collagen type 4 knockout (COL4A3 KO) . In UUO mice, co-expression of CD31 and FSP1 appeared one week after ureter ligation. This co-expression was observed in COL4A3 KO mice aged 22 weeks and in STZ induced diabetic nephropathy mice aged 6 months (Zeisberg *et al.*, 2008) .These results were confirmed in STZ-induced diabetic nephropathy in early development of interstitial kidney fibrosis (Kisanuki *et al.*, 2001). Lineage tracing was performed using Tie2-cre recombinase and population of alpha SMA positive cells with an endothelial origin was identified (Li *et al.*, 2009).Tie2-cre recombinase was also used in UUO model where approximatively 10% of mesenchymal cells on site were positive for endothelial origin (LeBleu *et al.*, 2013b).

EndMT was also detected in intestinal fibrotic pathologies such as colonic fibrosis and inflammatory bowel disease. In the colonic mucosa of Crohn's disease and ulcerative colitis patients, co-expression of endothelial and mesenchymal markers was seen in endothelial cells from inflammed tissue. In mouse, chronic murine colitis was induced by administration of trinitrobenzene sulfonic acid. Using Tie2–Cre model with GFP reporter, EndMT was observed after 8 weeks of injection which was corroborated with the emergence of intestinal fibrosis (Rieder *et al.*, 2011).

## 1.6 Inducers of EndMT in fibrosis

### *1.6.1 TGFβ*

TGFβ is a pleiotropic growth factor that belongs to the TGFβ-superfamily and is characterized as the main EndMT inducer. The TGF-β superfamily is divided in two major categories including BMPs and TGFβ/activin A subfamilies. TGFβ can be found in 3 isoforms in human, TGFβ1, TGFβ2 and TGFβ3 which share high homology but are coded by three individual genes (Massague and Chen, 2000). These three isoforms are unequally distributed across various tissues and exhibit distinct roles. TGFβ is released in a latent form and requires series of proteolytic steps in order to convert into mature TGFβ . Thereafter, bioactive TGFβ acts as a ligand and binds to a TGFβ transmembrane receptor 1 which activates the TGFβ transmembrane receptor 2 and subsequently transduces the signal via Smad-dependent and independent pathways. In endothelial cells, TGF-β binds two distinct type I receptors, ALK1 and ALK5 which activate respectively Smad1/5/8 and Smad2/3. In both pathways, activated Smads form with Smad 4, a heteromeric complex which is able to translocate in the nucleus and interact with DNA. ALK1 And ALK5 pathways regulate different genes and have opposite biological functions in these cells (Goumans *et al.*, 2002).

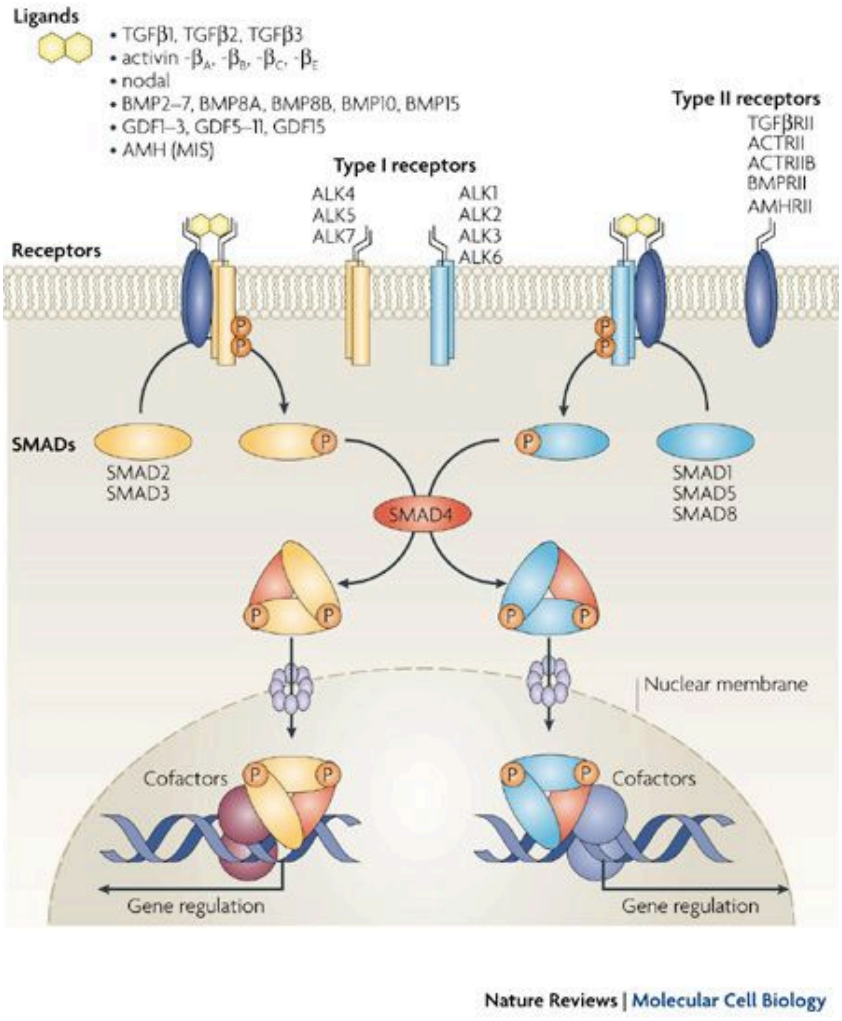


**Figure 1.6 TGFβ superfamily signalling (Schmierer and Hill, 2007)**

In endothelial cells, three TGFβ isoforms are expressed and each of them have the potential to induce activated fibroblasts via a phenotypic conversion. In fact, TGF-β efficiently induces EndMT in different types of endothelial cells both *in vitro* and *in vivo*. Arcienegas et al first promoted the transition in bovine aortic endothelial cell with TGFβ1 treatment. Post-treatment, factor VIII was significantly decreased and alpha SMA increased suggesting the transdifferentiation(Arciniegas *et al.*, 1992). Similarly, TGFβ1 treatment induced alpha SMA expression in ovine aortic valve endothelial cell (Paranya *et al.*, 2001).

Likewise, TGFβ2 treatment in endothelial cells induced a decrease of cell adhesion markers such as VE cadherin and PECAM1 and were positive to alpha-SMA. Treated cells acquired a spindle shape morphology similar to mesenchymal cells.(Medici *et al.*, 2011; Mihira *et al.*, 2012; R Kumarswamy *et al.*, 2012).

Studies for TGFB3-induced EndMT in fibrosis are quite sparse. The role of TGFβ3 in EndMT was mostly described in heart development where its inhibition resulted in the

inhibition of cell invasion (Boyer *et al.*, 1999). However, TGFβ3 treatment was able to increase α-SMA expression at the same level as TGFβ2 and TGFβ1 in mouse pancreatic microvascular endothelial cells suggesting a proper role in EndMT.
Similarly, TGFβ3 induced EndMT in mouse embryonic endothelial cells. Surprisingly, the effect of TGFβ3 treatment in human endothelial cells is lacking.
The downstream mechanism of TGFβ in EndMT involves the transcription factors Snail and Slug, known as suppressors of cell adhesion. In fact, Snail was found up-regulated in endothelial cells post-treatment with TGFβ2 (Medici *et al.*, 2011). The repression of Snail by siRNA prevented the down-regulation of claudin 5 and the up-regulation of α-SMA, thus reducing EndMT.

### *1.6.2 TNFα*

Tumor necrosis factor-alpha is a pro-inflammatory cytokine involved in endothelial activation. TNFα signalling is initiated by its binding to one of two receptors, TNF receptor type 1 or TNF receptor type 2, downstream molecules are recruited and lead to transcription factors activation such as NF-κB (MacEwan, 2002). In endothelial cells, TNF-α activity induces various cell adhesion molecules such as E-selectin, intercellular adhesion molecule type 1 (ICAM-1) and vascular cell adhesion molecule type 1 (VCAM-1) and increase permeability, suggesting that TNFα is involved in adhesion and extravasation of leucocytes during inflammation (Mackay *et al.*, 1993). Besides endothelial activation, evidence showed that TNFα could induce EndMT by activating NF-κB. In fact, TNFα treatment in porcine aortic valve endothelial cells stimulated Akt/ NF-κB signalling which in turn resulted in the up-regulation of α-SMA and meanwhile endothelial markers such as VE-cadherin were reduced(Mahler *et al.*, 2013). Similarly, EndMT was induced by TNFα in lymphatic endothelium.(Chakraborty *et al.*, 2015).

### *1.6.3 IL1β*

IL1β is a pro-inflammatory cytokine which is mainly secreted by immune cells such as macrophage and monocyte. IL1β is synthesized in an inactive form namely pro-IL1β whose cleavage by the protease caspase 1 releases the mature IL1β (Lopez-Castejon and Brough, 2011). Transduction of IL1β signalling is via the binding to IL1R1 receptor. IL-1RacP is recruited and stimulates the recruitment of the adaptor protein MyD88 (myeloid differentiation factor 88) and IRAK4 (IL-1 receptor-activated protein kinase 4). Downstream signalling stimulates several pathways including NFκB and MAP kinase

(Turner, 2014). In human dermal microvascular endothelial cells, IL1β treatment induces phenotypic changes, including the change from cobblestone to spindle shape. Moreover, PECAM and vWF were largely decreased implying that endothelial cells undergo a dedifferentiation and acquire a fibroblast-like phenotype. The same results were obtained in human intestinal microvascular endothelial cells and in human epithelioid dermal microvascular endothelial cells (Chaudhuri *et al.*, 2007; Rieder *et al.*, 2011). Interestingly, combination of TGFβ2 and IL1β treatment revealed an additive effect on EndMT. Using different conditions of treatment, evidence showed that IL1β treatment was only required for the initiation of EndMT and that TGFβ2 could sustain it (Maleszewska *et al.*, 2013).

### *1.6.4 Hypoxia*

Evidence has shown that EndMT could be induced under hypoxic conditions. The effect of hypoxia on cells is mainly due to the increased expression of the transcription factor hypoxia-inducible factor 1 alpha (HIF1α). Under hypoxic conditions, this transcription factor stabilize and dimerises with HIF1β. Thereafter, the newly formed dimer translocates into the nucleus, binds to hypoxia response element and can regulate gene expression. In the study of Xu et al, human cardiac endothelial cells were exposed to 1% oxygen for 4 days and an increase of HIF1α was observed. In addition, endothelial cells under hypoxic conditions lose their endothelial markers such as VE-cadherin and CD31 and gain mesenchymal markers such as α-SMA and COL1A1. Snail and Slug transcription factors were also up-regulated during hypoxia implying that hypoxic conditions are sufficient to induce EndMT (Xu *et al.*, 2016). Interestingly, HIF1α was described as inducer of Snail expression due to its binding to the promoter region of Snail (Xu *et al.*, 2015). Similarly, the hypoxic damage due to radiation stimulated EndMT through HIF1α up-regulation (S.-H. Choi *et al.*, 2015).

### *1.6.5 Oxidative stress*

Reactive oxygen species (ROS) derive from multiple sources and are the main mediator of oxidative stress. Under normal conditions, a low concentration of ROS is observed and is related to cellular processes in healthy cells. However, an increase of ROS during oxidative stress can cause DNA damage and cell death. ROS include the superoxide anion ($O_2^-$), hydroxyl radical($OH^\bullet$) and hydrogen peroxide ($H_2O_2$) (Schieber and Chandel, 2014). Montorfano et al showed that treatment with $H_2O_2$ triggers the transdifferentiation of endothelial cells in mesenchymal cells. Interestingly, oxidative stress-induced EndMT lead to secretion of TGFβ1 and TGFβ2 implying the

role of TGFβ signalling in oxidative stress. Indeed, $H_2O_2$-induced EndMT was prevented by silencing of the receptor ALK5 or the transcription factor Smad3 both involved in TGFβ signalling (Montorfano *et al.*, 2014). In a study from the same group, $H_2O_2$ treatment enhanced the migration of endothelial cells undergoing EndMT(Sarmiento *et al.*, 2015).

### *1.6.6 MiRNAs*

Recently, MicroRNAs (miRNAs) appear as a potential inducer of EndMT (R. Kumarswamy *et al.*, 2012; Li *et al.*, 2017). Due to their capacity to target and silence numerous mRNA, miRNA are able to regulate signalling pathway in various biological processes. Certain miRNAs were described as regulator of the signalling pathway of previously described inducers of EndMT. Thus, the identification of miRNA involved in EndMT could define new therapeutic targets for fibrosis.

## 1.7 MicroRNA biogenesis and function

MicroRNAs are defined as non-coding small RNA around 17-22 nucleotides and were discovered in *C elegans*. A small RNA lin-4 was found not coding for a protein but was necessary to regulate lin-14 protein. In addition, lin-4 was complementary to 3 prime untranslated region (3'UTR) of lin14 suggesting a direct RNA-RNA interaction (Lee *et al.*, 1993). Seven years later, Reinhart et al discovered a second small RNA let-7 also regulating lin14 in *C.elegans* (Reinhart *et al.*, 2000). As both small RNAs were involved in timing of development, these miRNAs were first called small temporal RNA (stRNAs). Identification of 21 new human small RNAs showed evidence of large class of small RNAs nominated microRNAs (Lagos-Quintana *et al.*, 2001). Large discovery of miRNAs was then supported by deep-sequencing technologies and use of computational prediction tools. In 2018, the database miRBase enumerated 48885 mature microRNA from 271 species such as plants, invertebrate and vertebrate.

### *1.7.1 Genomic organisation*

After the discovery of numerous miRNAs in multiple species, the origin of miRNAs was addressed. In parallel to the identification of 21 new human miRNAs , Lagos-Quitana et al highlighted the presence of miRNA cluster which refers to group of miRNA genes located at short distance on a chromosome.(Lagos-Quintana *et al.*, 2001, 2003) Lee et al showed that these clusters were transcribed polycistronically and therefore as a single transcript.(Lee *et al.*, 2002) They also demonstrated that long primary transcripts

derived from the cluster could be processed into to medium length precursor and to mature miRNAs cluster consisting in miR-35,-36,-37,-38,-39,-40,-41 (Lau *et al.*, 2001) Furthermore, study on the miR-23a, miR-27a and miR24-2 cluster revealed that miRNAs could have cluster-specific promoters (Lee *et al.*, 2004). The related miRNAs are not always clustered however; miRNAs involved in a genomic cluster are often related to each other.

Regarding the genomic location, miRNAs can either be intergenic or can be derived from a pre-mRNA. Intergenic miRNAs are localised in regions distinct from annotated transcription units and are transcribed with their own promoter.(Lagos-Quintana *et al.*, 2003)Their transcription can be monocistronic or polycistronic where a group of miRNA genes is transcribed in a single primary transcript with a common promoter. MiRNAs derived from pre-mRNA can arise from intron or exon. In 2004, half of the 232 mammalian miRNas repertoire were found within intron of either non coding TU or protein coding TU (Antony Rodriguez *et al.*, 2004). Similar to intergenic miRNAs, intronic and exonic miRNAs can be present as single or as group of miRNAs gene. The cluster miR-25,-93,-106b and the single miR-190 are located in protein-coding introns of the gene MCM7 and TLN2 respectively. In long non-coding RNA DLEU2 and NCMRS, miR-15a,-16-1 cluster and miR135a-2 were localized in intron respectively (Calin *et al.*, 2002; A. Rodriguez *et al.*, 2004). These miRNAs are defined by a shared single primary transcript with the gene in which they reside and a proportional expression to the host gene expression.

Another class of miRNAs deriving from pre-mRNA, originate from exons. These miRNAs are mainly found in non-coding TU such as miR-155 in BIC gene. BIC is composed of 3 exons with a miRNA stem loop of miR-155 within the third exon (Tam, 2001; Lagos-Quintana *et al.*, 2002).

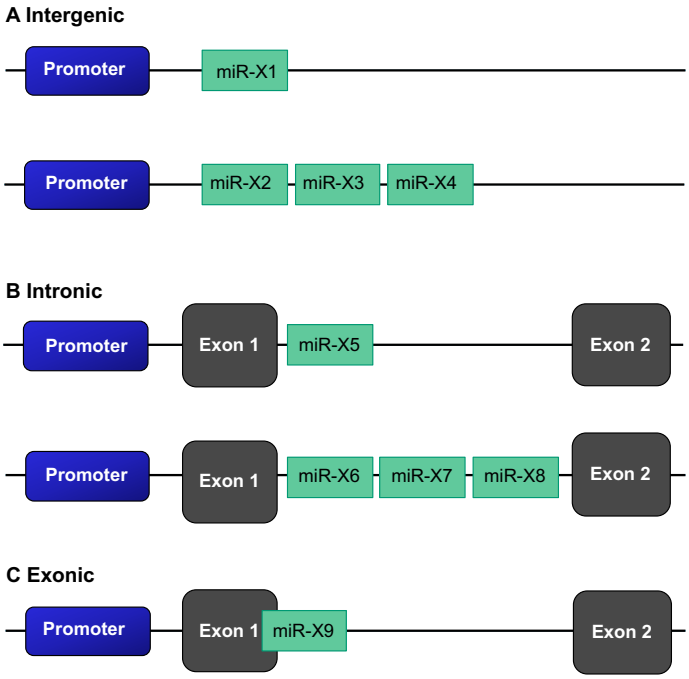


**Figure 1.7 Genomic location of miRNA genes**
MiRNA genes can be found as a single miRNA gene or clustered. A cluster of miRNA is defined by several miRNA genes at short distance on a chromosome that share a same primary transcript. In addition, multiple genomic location were observed for both organization. A) In a region distinct from transcription unit. Intergenic miRNA are transcribed with their own promoter B) In an intronic region non-coding or coding for a protein. In most intronic miRNA, host gene promoter is shared with miRNA gene C) In an exonic region overlapping on an intronic region non-coding for a protein. In most exonic miRNA, host gene promoter is shared with miRNA gene. Adapted from(Olena and Patton, 2010)

### *1.7.2 MiRNA transcription*

MiRNAs are generated from a first long single transcript called primary miRNA (pri-miRNA) and containing a stem loop structure. Both RNA polymerases II and III were considered for the transcription machinery of miRNAs. RNA polymerase III is well known for the transcription of short and non-coding RNA including tRNAs, U6 small nuclear RNA(snRNA) whereas RNA polymerase II generates mRNAs and some non-coding RNAs such as four snRNA of the spliceosome and small nucleolar RNAs (snoRNAS) (Dieci *et al.*, 2013). First observations of miRNA transcription suggested that RNA pol II was responsible for the transcription of miRNAs. In fact, the pri-miRNA transcript can be longer than basic transcripts of RNA polymerase II. Furthermore, pri-miRNA often contain repetitive uridine residues which would terminate the transcription of RNA polymerase III (Bartel, 2004). Cai et al showed that mature miRNA were derived from capped and polyadenylated pri-miRNA. The 5′ end of the pri-miRNA consists in 7-methyl guanylate (m7G) cap and the 3′ end in poly(A) tail (CAI *et al.*, 2004). These modifications were observed on most eukaryotic mRNAs implying that

miRNAs transcription was RNA polymerase II dependant. Meanwhile, Lee et al proved experimentally that miRNAs were mostly transcribed by the RNA polymerase II. In fact, HeLa cells treated with α-amanitin, an inhibitor of RNA polymerase II showed a significant decrease of all the pri-miRNAs tested (Lee *et al.*, 2004). A detailed study on miRNA promoters revealed similarities with mRNA promoter. As promoter encoding from RNA pol II transcripts, miRNA promoters were found with Cpg islands, TATA box, TFIIB recognition element (BRE), an Initiator (Inr) or even downstream promoter element (DPE).

In the same work, part of intronic miRNas were found with an initiation transcription site independent on the gene in which they reside. In this case, miRNAs can be co-transcribed with the host gene and have its own transcripts (Ozsolak *et al.*, 2008).

Therefore, RNA polymerase II transcribed most miRNAs gene in pri-miRNA with some exceptions such as the cluster found on the human chromosome 19 which is transcribed by RNA polymerase III (Borchert *et al.*, 2006).

### *1.7.3 miRNA maturation*

*Nuclear maturation*

Once transcribed by RNA polymerase II, pri-miRNAs are cleaved in the nucleus by an RNAse III protein called Drosha. This enzyme require the presence of a cofactor, DiGeorge syndrome critical region gene 8 (DGCR8)(Han *et al.*, 2006). DGCR8 and Drosha form a complex called microprocessor where DGCR8 interact with pri-miRNA and Drosha cleaves at 11nt away from the stem loop. Interestingly, Morlando et al found that cleavage of pri-miRNA occurred co-transcriptionally and that Drosha did not impair the splicing (Morlando *et al.*, 2008). The complex releases a hairpin RNA around 70 nucleotides long called pre-miRNA and generate one end of the mature miRNA (Denli *et al.*, 2004).

A drosha-DCGR8 independent pathway was discovered where intronic miRNA are generated from the splicing of a small intron. These miRNA entitled miRtrons have been first described in *C. elegans* and Drosophilia (Okamura *et al.*, 2007; Ruby *et al.*, 2007). Ruby et al showed that the initial spliced intron was not linear and gave rise to a lariat where the intron 5' end was connected to a 3' end branch point (Ruby *et al.*, 2007). A lariat debranching enzyme linearises the intron which can thereafter fold into pre-miRNA. Both miRNAs Drosha-DGCR8-dependent and miRtrons are then submitted to the canonical biogenesis pathway (Westholm and Lai, 2011).

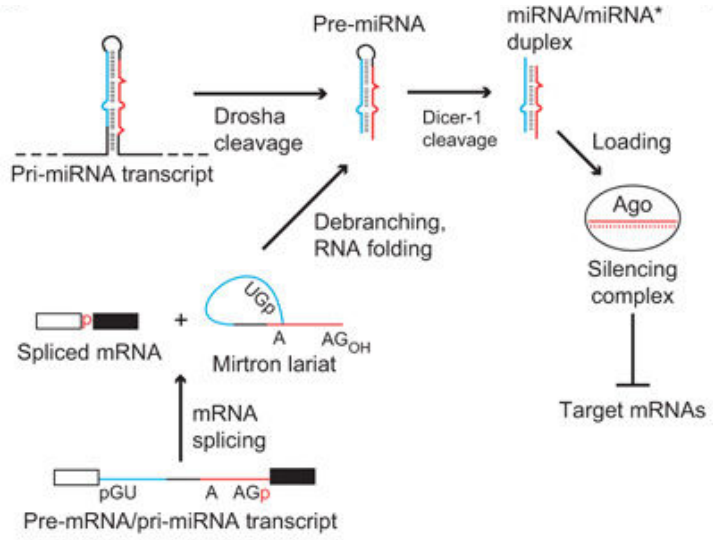


**Figure 1.8 miRtrons biogenesis**
miRtron comes from intronic miRNA gene whose transcript is not linear and form a lariat. After splicing, the 5'end is connected to a 3'branchpoint. A debranching lariat enzyme linearise the miRtron lariat which can then fold into pre-miRNA. Thereafter, pre-miRNA of miRtrons follows the canonical biogenesis pathway

Thereafter, Exportin 5 a nuclear protein transport , is associated with the cofactor Ran-GTP and translocates pre-miRNA in the cytoplasm (Bohnsack *et al.*, 2004; Lund *et al.*, 2004). Exportin5:RanGTP recognizes double-stranded stem and the 2 nucleotides 3′ overhang of the pre-miRNA. This interaction forms a hetero ternary complex Exp-5:RanGTP:pre-miRNA. Once in the cytoplasm, hydrolysis of RanGTP in RanGDP by RanGTPase activating protein (RanGAP) allows the release of the pre-miRNA and the return of exportin 5 in the nucleus (Okada *et al.*, 2009).

*Cytoplasmic maturation*

In the cytoplasm, pre-miRNa released from Exportin 5 are cleaved by a second RNAse III protein Dicer. Dicer is highly conserved between species and have been found in worms, flies, plants, fungi and mammals. This nuclease cleaves double stranded RNA and was first described in the RNA interference pathway (Bernstein *et al.*, 2001). Indeed, Dicer was required to produce small RNAs which are homologous to the target gene and repress their expression.

In *C.elegans*, Grishok et al observed that Dicer was not only involved in the RNAi pathway but was also necessary for the maturation of the miRNAs lin-4 and let-7 (Grishok *et al.*, 2001; Ketting *et al.*, 2001). Evidence of the role of Dicer in miRNA biogenesis was further confirmed in Drosophila where the inactivation of Dicer led to a precursor accumulation of the miRNA let-7 (Hutvágner *et al.*, 2001). Regarding

the structure of *Giardia* Dicer and Human Dicer, the RNase III protein consists in a processing center with two RNase III domains that are connected to the PAZ domain by a long, positively charged helix. PAZ domain contain a 3'two-nucleotide RNA binding pocket that allow the binding of miRNA duplex 3' end generated previously by Drosha (MacRae *et al.*, 2006; Liu *et al.*, 2018). Furthermore, evidence showed that human Dicer was interacting with two related protein TRBP and PACT that seem to contribute to the stabilisation of Dicer (Chendrimada *et al.*, 2005; Ha and Kim, 2014). Thereafter, Dicer acts as molecular ruler and cleaves at 25 nucleotides of the dsRNA end. This length correspond to the distance between the RNA binding pocket and the active site of the RNase IIIa. Cleavage of pre-miRNAs give rise to a mature double stranded miRNA (Svobodova *et al.*, 2016). The mature miRNA sequence was determined on one end by Drosha and the second end by Dicer .

Interestingly, some miRNAs bypass the Dicer cleavage such as the miR-451 whose maturation depends on the argonaute protein Ago2 (Herrera-Carrillo and Berkhout, 2017).

The double stranded miRNA is loaded into Argonaut protein to form a RNA induced silencing complex (RISC). Argonaut proteins are ubiquitous and can be divided in two sub-families: the PIWI subfamily and the AGO subfamily. Four copies of AGO proteins were found in humans and Ago1,Ago3 and Ago4 genes were clustered on the chromosome 1 whereas Ago2 was found on chromosome 8 (Sasaki *et al.*, 2003). Ago protein consists in two domain interacting with the duplex RNA (PAZ and MID) and one catalytic slicer domain PIWI that is functional only with Ago2 (Meister *et al.*, 2004). The PAZ domain bound to the 3'end of the duplex meanwhile the 5' end is anchored to the interface of MID and PIWI. Although, only Ago2 possess a target cleavage activity, copies of Ago proteins can still repress translation and conduct to exonucleolytic mRNA degradation through interaction with other protein factors.

The formation of the RISC complex can be separated into two steps, the loading of the double stranded miRNA into the Argonaut protein and the unwinding of the miRNA duplex (Ha and Kim, 2014). After the processing of the pre-miRNA, Argonaut protein is recruited by the protein TRBP associated to Dicer. The formation of RISC complex is an active process and requires consumption of ATP to induce the loading of miRNA (Yoda *et al.*, 2010). Iwasaki et al found out that the heat shock cognate 70 (HSC70)–heat shock protein 90 (HSP90) machinery hydrolysed ATP that mediates the conformational opening of Ago and therefore allows the loading of the duplex into the

Ago protein (Iwasaki *et al.*, 2010). The Ago opening conformation was compared to a stretched rubber band which contains structural tension. It has been suggested that the release of this tension supports the ATP-independent unwinding. In some species, the association of the duplex to Argonaut protein is controlled by the structure of the precursor unlike in human where the four Argonaut proteins bound similarly to miRNAs.

After the loading of the miRNA duplex, one strand is selected to generate a mature RISC. The strand selected remains in the complex as mature miRNAs, whereas the other strand is considered as a passenger strand and is degraded. The unwinding of the miRNA duplex can be induced by cleavage. However, the cleavage requires base-paired at the centre and an Argonaut protein with an endonuclease activity. In humans, only Ago2 possess a slicer activity and is able to remove the passenger strand by cleavage. This mechanism is not often used as central mismatches are common and that human Ago1, Ago3, Ago 4 lack the slicer activity. In both cases, the passenger strand is removed by a bypass mechanism where seed and central mismatch could facilitate the dissociation of the passenger strand (Yoda *et al.*, 2010).The selection of the guide strand is based on the thermodynamic stability of both ends of the miRNA duplex. The less stably paired at the 5´ side is usually the strand selected as guide (Khvorova *et al.*, 2003). Study on the expression and the sequence of human miRNAs revealed a sequence bias in the strand selection. In fact, miRNA strand with a uracil in the 5' end were highly expressed unlike strand with a cytosine in the 5' end that were lowly expressed. A high expression was also observed in strands composed with an excess of purine. Strand selection is not a stringent process and sometimes allows the production of both microRNA strands, sometimes at the same frequency (Ro *et al.*, 2007).

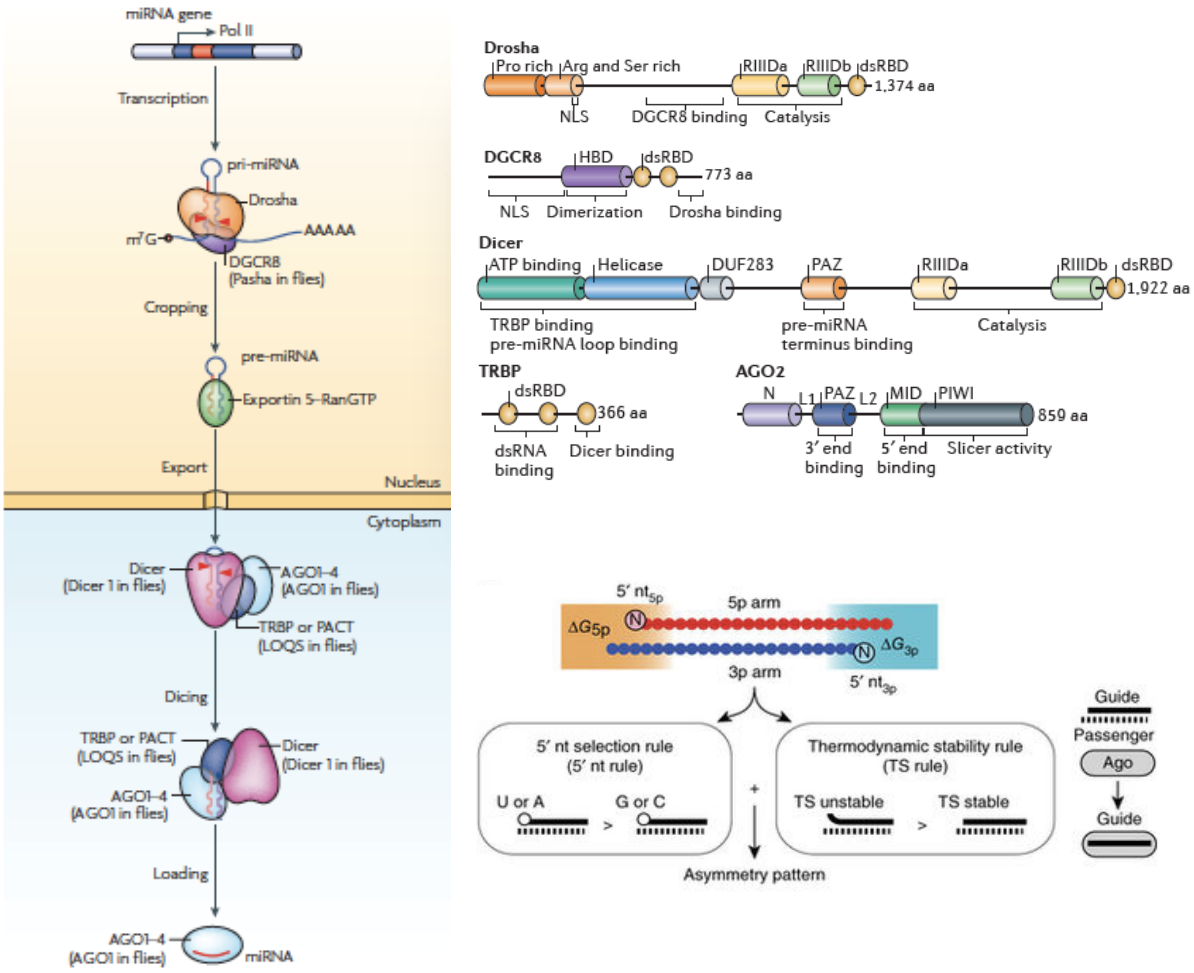


**Figure 1.9 Biogenesis of miRNAs**
In the nucleus, RNA polymerase II first transcribed miRNA gene and gave rise to a pri-miRNA with stem loop structure. Drosha, a RNAse III protein, is binding to cofactor DGCR8 to form the microprocessor complex which cleaves 11 nucleotides away from the stem loop. Pre-miRNA is released with 2 nucleotide 3' overhang which is recognized by Exportin 5 coupled to RanGTP. After the translocation of the pre-miRNA to the cytoplasm by Exportin5, Ran GTP is hydrolysed and set free the pre-miRNA. Dicer, another RNAse III protein, is associated with TBRP and cleaves at 22 nucleotides of the pre-miRNA end. A miRNA duplex is generated meanwhile TRBP recruit an Argonaute protein. MiRNA duplex interact at the 3'end with the PAZ domain and is anchored on the 5' end at the interface between the domains MID and PIWI. The miRNA duplex is loaded into the argonaute protein, and the duplex is dissociated. One strand remain in the complex as guide strand and the other passenger strand is degraded. The selection of the guide strand is based on thermodynamic stability and on the sequence. Once the guide strand is selected, the miRISC (Argonaute+ miRNA) can then repress translation and induce mRNA decay.(Kim *et al.*, 2009; Ha and Kim, 2014; Suzuki *et al.*, 2015)

### *1.7.4 Target mRNA recognition*

A few years after the discovery of miRNAs , Reinhardt et al observed that miRNA can regulate mRNA translation by interacting with their 3'UTR (Reinhart *et al.*, 2000). These results were confirmed and showed that the interaction of miRNA-mRNA could disturb mRNA stability or regulate translation (Valencia-Sanchez *et al.*, 2006; Standart and Jackson, 2007). In animals, extensive complementarity, is a rare phenomenon. In the few cases with a perfect complementarity, mRNA target is cleaved by the miRISC

including the protein Ago2 which is the only human Ago protein with a slicer activity (Meister *et al.*, 2004; Yekta *et al.*, 2004). In order to predict miRNA targets, algorithms were developed to search segments of the UTR with a perfect Watson-Crick complementarity to the seed region of the miRNA. The seed sequence consists in the nucleotide 2 to nucleotide 8 on 5' end of the miRNA and is very well conserved between species (Lewis *et al.*, 2003). The importance of the seed sequence was corroborated in Drosophila where the miRNA 5' end was complementary of the 3'UTR of known mRNA target (Stark *et al.*, 2003). In many instances, mRNA target can be recognized only with a matching seed (Lewis *et al.*, 2005). However, studies revealed that 3'end of the miRNA also contributed to the binding (Grimson *et al.*, 2007). Wiktos et al reviewed the interaction between the miRNA and 3'UTR mRNA target (Witkos *et al.*, 2011)(**Figure 1.10**). Three of these interactions were called canonical sites, and represent the majority of validated conserved targets :

*7mer-A1 site*: A perfect seed match and a Watson-Crick match with an adenine in the first position. Evidence showed that an adenine as anchor in the first position could increase the specificity of target prediction. Among prediction target tool, adenine in position 1 was not rewarded except for the target tool Target Scan.

*7mer-m8 site* : A perfect seed match and a Watson-Crick match at the position 8

*8-mer site* : 8 nucleotides with a perfect Watson-Crick complementarity at the seed region along with the position 1 and 8.

Some other target sites are non-canonical. The conformation 6-mer requires the 6 nucleotide matching in the seed region but its specificity in target recognition is reduced. The 3' supplementary and the 3' compensatory site are based on additional Watson-Crick pairing in 3' of the miRNA to respectively contribute to the specificity and compensate a mismatch in the seed region (Bartel, 2009; Witkos *et al.*, 2011).

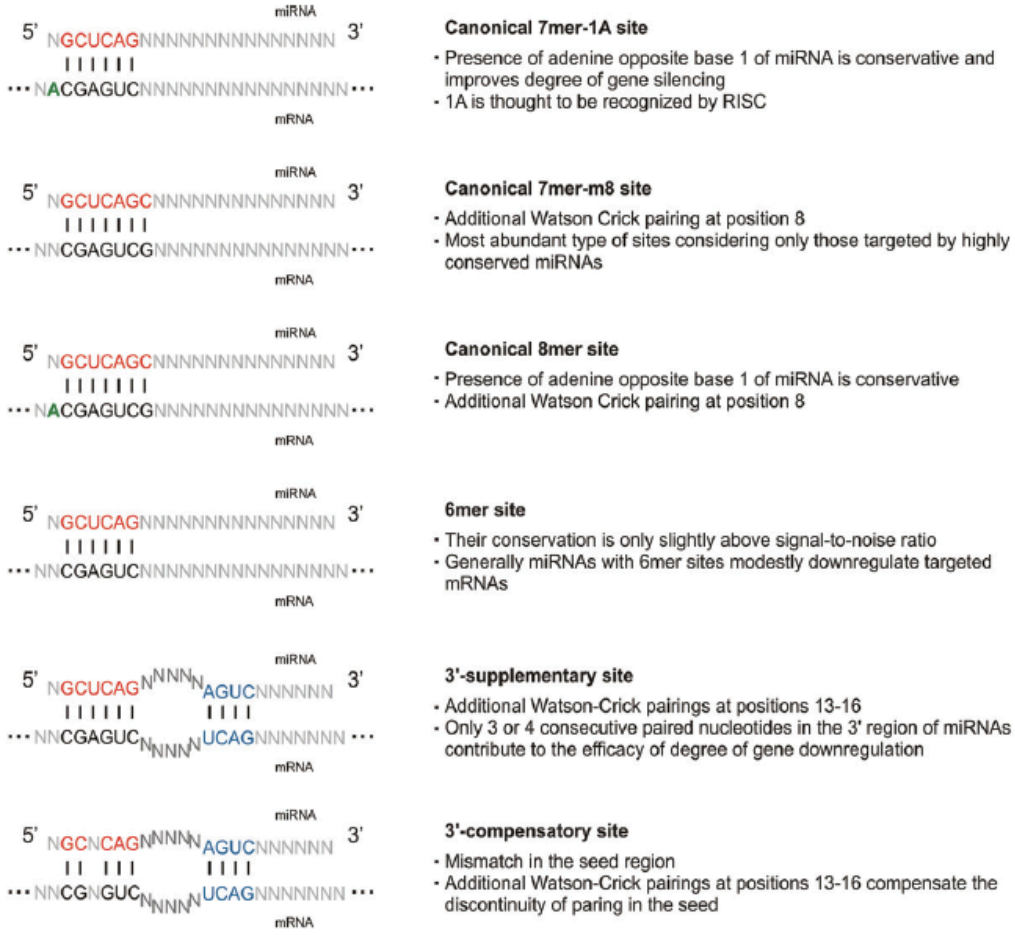


**Figure 1.10 MiRNA target sites**
Three types of miRNA target sites are considered as canonical sites with a perfect seed match. 6-mer site require 6 matched nucleotides in the seed region but is less specific than the canonical sites. 3'supplementary and 3' compensatory site are additional pairing that support the specificity of target recognition. In this figure, the seed region is represented in red, the adenine in first position in green and additional pairing in blue.(Witkos *et al.*, 2011)

Multiple tools were developed in order to predict miRNA targets. Each algorithm was based on a selection of criteria such as the pairing in the seed region, the conservation between species, the thermodynamic and others. The analysis beyond these prediction tools will be addressed in Chapter 4, Materials and Methods.

### *1.7.5 Regulation of gene expression*

In order to accomplish their regulatory functions, miRNA incorporated in the miRISC complex can initiate the decay or the translation repression on its mRNA targets (Filipowicz *et al.*, 2008). The degradation of mRNA by the endonucleotic activity of AGO2 is not frequently adopted by mammalian RISCs as most miRNAs are partially complementary of their targets. In this case, silencing of mRNA targets is mediated by the interaction of Ago protein with the GW182 protein family (Tritschler *et al.*, 2010).

Glycine tryptophane protein of 182KDa (GW182) can bind with its silencing domain to PABPC1 and compete with eukaryotic initiation factor 4G (eIF4G). Interaction between PABPC1 and eIF4G is known to be essential for the circularisation of mRNA which stimulates translation. Due to the interaction GW182-PABPC1, silenced mRNAs are not circularised anymore and this represses the recruitment of initiation factors and reduces translation efficiency.(Zekri *et al.*, 2009) GW182 proteins also participate to the recruitment of the CCR4-CAF1-NOT and PAN2-PAN3 deadenylase complexes.(Braun *et al.*, 2011; Huntzinger *et al.*, 2013). Deadenylation is followed by the decapping with a protein recruited by miRISC decapping protein 2 (DCP2).(Nishihara *et al.*, 2013) DCP2 requires additional proteins including DCP1, enhancer of decapping 4 (EDC4) and the putative RNA helicase DEAD-box protein 6 (DDX6). (Ling *et al.*, 2011) Post-deadenylation and decapping, mRNA is exposed to 5′-to-3′ exonucleolytic degradation by XRN1. A direct interaction of DCP1 and XRN1 was observed suggesting the mRNA decay (Braun *et al.*, 2012).

Regarding the localisation of the translation repression, argonaute proteins, miRNAs, and miRNA targets were found colocalised in cytoplasmic foci called P-bodies. Accumulation of protein involved in mRNA degradation such the decapping DCP1:DCP2 complex and exonuclease XRN1 or the presence of GW182were observed in P-bodies. This suggests that the silencing of the mRNAs translation and the mRNA decay might occurs in P-bodies (Liu *et al.*, 2005; Filipowicz *et al.*, 2008).

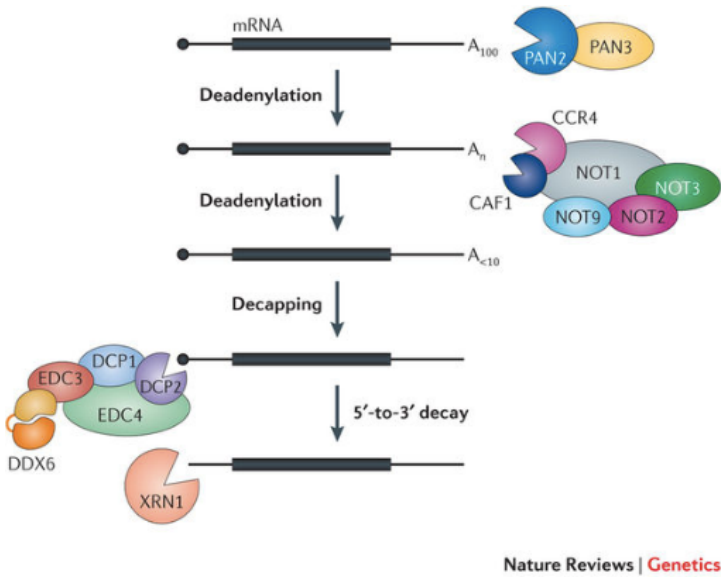


**Figure 1.11 Summary of mRNA degradation regulated by miRNA**
Once miRISC binds specifically to its mRNA target, the proteins GW182 are recruited and interact with deadenylation complexes Pan2-Pan3 and CCR4-NOT. Following deadenylation, decapping complex DCP2 associated with a multitude of decapping proteins remove the cap from the 5' end. Deadenylated and decapped miRNA is then exposed to the XRN1 exoribonuclease and is degraded from 5'end to the 3'end (Jonas and Izaurralde, 2015).

## 1.8 MicroRNA and myocardial infarction

Myocardial infarction (MI), commonly known as heart attack, results from a prolonged ischemia that lead to an irreversible death of cardiomyocytes. In this pathological context, several studies demonstrated the up-regulation and down-regulation of specific miRNAs in MI tissue.

MiR-1 was demonstrated as a key miRNA in cardiovascular diseases and in cardiac development. Following ischemia/reperfusion injury, miR1 transgenic mice showed an increased infarct area whereas the knockdown of miR-1 by antagomir led to an attenuation of cardiac injury (Pan *et al.*, 2012).

MiR-15 family is composed with several miRNAs miR-15a, miR-15b, miR-16-1, miR-16-2, miR-195, and miR-497 and was found up-regulated in porcine and murine infarct tissue. The use of antagomir against miR-15 family members effectively decreased infarct size and reduce cardiac remodeling (Hullinger *et al.*, 2012)

During MI, cardiomyocytes underwent apoptosis and this was correlated with an increase of miR-34 family (Bernardo *et al.*, 2012). Inhibition of miR-34 family led to an improvement of cardiomyocyte survival. MiR-499, miR-24 are down-regulated in MI and the restoration of their expression has a protective effect against apoptosis (Wang *et al.*, 2011; Chen *et al.*, 2017). MiR-24 targets the pro-apoptotic protein Bim and therefore over-expression of miR-24 inhibits apoptosis (Qian *et al.*, 2011). Post-ischemia reperfusion injury, miR-320 was found down-regulated. This miRNA directly

targets the cardioprotective proteins IGF1 and HSP20 and the silencing of miR-320 by antagomir allowed the reduction of the infarct size (Ren *et al.*, 2009; Song *et al.*, 2016). Expression of miR-214 was found up-regulated after acute myocardial infarction or ischemic cardiac injury. Deletion of miR-214 led to an increased apoptosis post-MI suggesting that miR-214 has a cardioprotective role (Aurora *et al.*, 2012; Yang *et al.*, 2016).Decrease of miR-873 and miR-2861 expression was observed post ischemia-reperfusion injury. Both miRNAs were found involved in the process of cardiomyocyte necrosis and their inhibition led to an improvement of cardiomyocyte survival (K Wang *et al.*, 2016; Kun Wang *et al.*, 2016).

All together, these miRNAs are suggested as regulator of cardiomyocytes death/survival in the context of MI. Interestingly, miR92-a was found up-regulated after acute myocardial infarction and was correlated with the increase of endothelial injury markers. In fact, the inhibition of miR-92a reduced the expression of endothelial injury markers and promoted endothelial activation which show an improvement of the cardiac tissue post-MI (Liu *et al.*, 2016).

## 1.9 MicroRNA related to endothelial-to- mesenchymal transition

To date very few studies have identified miRNAs and have shown evidence of their role of miRNAs in EndMT.

*In vitro studies*

Some miRNAs were described as negative regulators of endothelial-to-mesenchymal transition which means that their down-regulation is required to allow EndMT and their over-expression is preventing it.

In healthy endothelial cells, the inhibition of let-7 family by LIN28, a well-known regulator of let-7, increased the expression of TGFBR1 receptor which in turn activated TGFβ signalling. This activation resulted in an increase of mesenchymal markers and a decrease of endothelial markers (Chen *et al.*, 2012).

Over-expression of miR-29 family (miR-29a, miR-29b and miR-29c) in endothelial cells treated with TGFβ2 attenuated EndMT. Indeed, transfection of miR-29 induced a marked decrease in cell migration(Kanasaki *et al.*, 2014).

Endothelial cells treated with glucose (25-30nM) undergo EnDMT and display a fibroblast-like phenotype. In this model, miR-18a-5p and miR320 were both down-regulated post-treatment (Feng and Chakrabarti, 2012; Geng and Guan, 2017). In

addition, mimic transfection of miR-18a-5p prevented EndMT in high glucose conditions. In the same study, a Notch2 receptor, known to initiate EndMT, was predicted and validated as a direct target of miR-18a-5p, implying that the down-regulation of miR-18a-5p could allow EndMT(Geng and Guan, 2017).

Interestingly, serum from patients with Kawasaki disease has been shown to promote EndMT by increasing connective tissue growth factor (CTGF) expression, a key factor in EndMT. Kawasaki disease is an inflammatory disease which affects the vasculature and cells implicated in the arterial wall damage could originate from EndMT. With the use of prediction target tool, CTGF appeared to be a direct target of miR-483 which was found down-regulated in KD sera. Its over-expression reduced EndMT by silencing the factor CTGF(He *et al.*, 2017).

Certain miRNAs are defined as positive regulators of EndMT including miR-21-5p. Increased expression of mir-21-5p was detected in an ionizing radiation and TGFβ model of EndMT but contradictory results were also observed about the role of miR-21-5p. In fact, post-treatment with TGFβ2, inhibition of miR-21-5p was shown to prevent the transition. Meanwhile in ionizing radiation-induced EndMT, miR-21-5p was found to be dispensable factor in the initiation of EndMT (R. Kumarswamy *et al.*, 2012; Guo *et al.*, 2015; Kwon *et al.*, 2016). Therefore, miR-21-5p is up-regulated in EndMT but its precise role remains elusive.

*Preclinical studies*

As EndMT is described as an active process during fibrosis, profiles of miRNA were assessed in tissue from animals with fibrotic disease. Differential expression suggests implication of miRNAs in fibrosis but does not directly indicate that these miRNAs are involved in EndMT. However, once the correlation made between miRNA expression, extent of fibrosis and amplitude of EndMT, implication of specific miRNAs in EndMT was suggested.

Studies in diabetic mouse showed a negative correlation between kidney fibrosis and the expression of miR-29. In addition, restoration of miR-29 expression led to reduced fibrosis. Evidence demonstrated the presence of EndMT in diabetic kidneys but the relation between EndMT and miR-29 was not directly studied. Interestingly, the miR-29 family was found down-regulated in EndMT *in vitro* suggesting that miR-29 could have a role in EndMT *in vivo* (Kanasaki *et al.*, 2014).

Another study on diabetic mice demonstrated that miR-200b-3p was down-regulated in cardiac fibrosis. Interestingly, miR-200-3p was markedly down-regulated in

endothelial cells and its expression was unchanged in myocytes. Transgenic mice overexpressing miR-200b-3p only in endothelial cells attenuated cardiac fibrosis and was able to prevent EndMT (Feng *et al.*, 2016a).

As previously stated, miR-18a-5p inhibits EndMT by silencing Notch2. In cardiac fibrosis induced by high glucose conditions, over-expression of miR-18a-5p reduced cardiac fibrosis and prevented EndMT.

*In vitro*, inhibition of let-7 by a miRNA sponge induced EndMT. Interestingly, administration of a let-7 antagomir promoted EndMT by increasing mesenchymal markers in endothelial cells in healthy mouse liver. Its role was then investigated with a transplant rejection model of aorta in transgenic mice with lineage tracing of endothelial cells under the promoter of VE-cadherin (Cdh5). Analysis of tissue was proceeded two weeks post-transplantation, and mice treated with let-7 antagomirs revealed an increase proportion of luminal endothelial cells undergoing EndMT had increased from (61% to 80-90%). On the contrary, a let-7 mimic reduced the proportion of endothelial cells undergoing EndMT(33.7%) and inhibited collagen deposition (Chen *et al.*, 2012).

Consistent with *in vitro* data, up-regulation of miR-21-5p was observed in two fibrotic models: radiation-induced pulmonary fibrosis and transverse aortic constriction (TAC) which generates cardiac fibrosis. Interestingly, antagomiR-21 treatment in TAC mouse reduced the number of cells co-stained for a mesenchymal marker and endothelial marker, thus attenuated EndMT.

Altogether these data suggest that miRNA expression can be modulated *in vivo* and affect EndMT.

*Therapeutic applications of miRNA*

Some studies have demonstrated that treatments for fibrotic disease could have an impact on miRNA expression that are involved in EndMT. In Kawasaki's disease, atorvastatin was able to prevent EndMT by targeting the KLF4-miR-483-CTGF axis. In diabetic mice, treatment with linagliptin restored miR-29 level which reduced DDP4 expression and finally lead to reduced kidney fibrosis (Kanasaki *et al.*, 2014). N-acetyl-seryl-aspartyl-lysyl-proline (AcSDKP) treatment was shown to inhibit EndMT and to reduce kidney fibrosis in diabetic mouse. In addition, AcSDKP prevented the down-regulation of let-7 which can inhibit EndMT.

In order to stimulate or block a signalling pathway that could lead to an amelioration of the disease stage, miRNA can be targeted and their expression can be modified *in*

*vivo*. The use of synthetic miRNA mimics or pre-miRNA sequence can be used to increase the miRNA expression meanwhile miRNA sponge or miRNA mask can block the interaction miRNA-mRNA.

Therapy based on miRNA have entered into the clinic for the first time in 2013 with MRX34. MRX34 was able to replace the lost expression of miR-34 and was involved in the silencing of 24 oncogenes in liver cancer. This clinical study was stopped in 2016 due to adverse effects (Bouchie, 2013).Progress has been made with the miR-122 inhibitor (Miravirsen) in the field of hepatitis C virus. In fact, miR-122 is miRNA mostly found in the liver and is involved in the life cycle of HCV. Miravirsen, specifically antisense oligonucleotide of miR-122, hybridizes with the mature miR-122 and consequently reduces HCV RNA expression (Gebert *et al.*, 2014).

Last year, another miRNA-based therapy RG-012 entered into a phase II clinical trial. RG-012 is an inhibitor of miR-21 that could prevent Alport syndrome. Alport syndrome is a genetic disorder which is characterized by a renal dysfunction. This disease is progressive with a glomerular and tubulointerstitial fibrosis that can lead to an end-stage renal disease. MiR-21 was largely studied in fibrotic disease and contributed to kidney fibrosis, its inhibition has an important therapeutic potential against the Alport Syndrome (Gomez *et al.*, 2015).

Numerous studies demonstrate the alteration of miRNA expression in disease. The interpretation of these changes could improve the diagnosis and the monitoring in various human diseases. Furthermore, selective modulation of miRNA could have an impact on a disease prognosis. In conclusion, targeting miRNA involved in EndMT may offer the possibility to reduce the progression of fibrotic diseases.

## 1.10 Aim of the study

Endothelial-to-mesenchymal transition contributes to the pool of myofibroblasts in fibrosis of various organs. Targeting EndMT might therefore be effective as a therapeutic treatment in fibrotic diseases. Over the last decade, miRNAs were described as regulator of key biological processes by modulating gene expression. This study hypothesised that miRNA could play a role in endothelial-to-mesenchymal transition and might be useful for diagnostic or therapy of fibrotic diseases.

## 1.11 Objectives

1. To establish a model of EndMT *in vitro*
2. To explore the miRNAs profile in EndMT *in vitro*.
3. To investigate the role of miR-126-3p in EndMT both *in vitro* and *in vivo*

# Chapter 2. Materials and methods

## 2.1 Cells line and primary cells

### *2.1.1 Human microvascular endothelial cell line (HMEC-1)*

The human microvascular endothelial cell line (HMEC-1) was purchased from ATCC and was immortalized through transfection with the PBR-322-based plasmid containing the sequences encoding the protein Simian virus SV40 Large T. The HMEC-1 cells express von Willebrand factor(vWF), CD31, CD36 but also adhesion molecules such as CD44 or ICAM1.

HMEC-1 cells were grown in reconstituted MCDB 131. Powdered MCDB- 131 and 15,7mL of sodium bicarbonate was added to 900mL of sterile water. Medium was filtered through sterile 0.2µm filters using a vacuum pump and supplemented with 10% Fœtal bovine serum (FBS),100U/mL penicillin, 100µg/ml streptomycin, 10ng/mL of epidermal growth factor (EGF) (Prepotech) and 1µg/ml of hydrocortisone (Sigma). HMEC-1 cells were also cultured in MCDB 131 media (Thermofisher scientific) with the same supplements and L-glutamine.

### *2.1.2 Human saphenous vein endothelial cells*

Primary endothelial cells from saphenous vein were obtained from Dr Lash. Cells were maintained in cell vascular basal medium (ATCC) supplemented with 50ug/mL ascorbic acid, 5ng/mL EGF, 5% FBS, 0.75U/mL heparin sulphate, 10mM L- glutamine, 1ug/mL hydrocortisone and 0.2%bovine brain extract (ATCC). As primary endothelial cells became senescent after passage 7-8, cells were only cultured until passage 7.

### *2.1.3 Human umbilical vein endothelial cells (HUVEC)*

Human umbilical vein endothelial cells were purchased from Promocell. These cells originated from pooled tissue from up to 4 different umbilical cords and have a doubling population of over 15 times. HUVECs are positive for CD31, vWF and negative for Alpha-SMA. These cells were chosen to establish a model of endothelial-to-mesenchymal transition as they were negative to alpha SMA, and therefore did not present any signs of stress or baseline levels of endothelial-to-mesenchymal transition.

.

## 2.2 Cell culture

All laboratory work was performed in a containment level II laboratory in accordance with University Health and Safety policy. COSHH and BIOCOSH forms were reviewed and signed post-induction and before the work has started. Cell culture was carried out in Class II biosafety cabinets which were cleaned with 70% ethanol before use. During culture, all cell types were grown in 75cm$^2$ plastic tissue culture flasks placed horizontally (Corning) and were incubated in a humidified atmosphere of 5% $CO_2$ at 37°C. Every cell types were sub- cultured every 2-3 days in order to prevent high confluence and stress of the cells

### *2.2.1 Cell passaging for sub-culturing*

In a 90% confluent 75cm$^2$ flask, media was carefully removed. Cells were washed with sterile phosphate buffer saline (PBS) and then with HEPES buffered saline solution in order to remove proteins that could inactivate trypsin. Trypsin EDTA was used to detach adherent cells from the flask and was incubated for 5min at 37°C. Once cells were detached and transferred to a 50mL falcon tube, complete media was added to inactivate the trypsin. Tubes were spun at 300G for 5 min and the supernatant was discarded. Pellets containing cells were then resuspended in an appropriate volume of media and split into 75cm$^2$ flasks containing 10-15mL of media. Cells were routinely split to a ratio of 1:2 to 1: 4 depending on the cell types.

### *2.2.2 Counting*

Cells were counted when necessary using an improved Neubauer chamber haemocytometer. After resuspension of cells, 20µl was added to the chamber, cells were counted in one diagonal in each corner square of the counting area. Cells number was multiplied by $10^4$ to obtain the relative number of cells per mL.

### *2.2.3 Cryopreservation*

Cells were cryopreserved in liquid nitrogen in order to maintain a stock of cells. Once cells were pelleted, they were resuspended in 500µl of freezing media and transferred in a Cryo Vial, Freezing media consisting in 20% dimethyl sulfoxide (DMSO) in FBS was directly added to the cells in 1:1 ratio. A different freezing method was used for HUVEC cells. CryoSFM (Promocell), a freezing media optimised for HUVEC was added to the pellet of cells. Cryovials were then placed at -80°C in a freezing container “Mr Frosty” (Thermofisher) filled with isopropanol which allow a cooling rate of -

1°C/minute. Cells were removed from the container 24 hours later and placed in -80°C or in liquid nitrogen.

For cell recovery following cryopreservation, cells were quickly warmed up in the water bath at 37°C and were added to pre-warmed media in a T75 flask. Media was changed the next day to prevent any cell death due to the presence of traces of DMSO.

### *2.2.4 Mycoplasma testing*

Mycoplasma are one of the major potential contaminants in cell culture and compete with cells for media nutrients altering cellular responses. Mycoplasma are prokaryote\ lacking a cell wall, making antibiotics such as penicillin ineffective. Mycoplasma infection is undetectable under the microscope and can only be suggested by a slow growth rate. Detection testing for mycoplasma was performed using the MycoAlertTM mycoplasma detection kit (Lonza) to ensure healthy cell proliferation. This kit is based on mycoplasmal enzyme activity, measured by luminescence, where mycoplasma are lysed to release enzymes and enzyme substrate is added. To perform the test, supernatant from cell cultures was collected, mycoAlert reagent was added in a 1:1 ratio and luminescence was read five minutes later (Reading A). The same volume of MycoAlert substrate was incubated 10 minutes before a second reading (Reading B). A ratio of Reading B to Reading A greater than 1,2 was considered as positive for mycoplasma infection. Only cells negative for mycoplasma were used in this project.

## 2.3 Molecular biology

Reagents were designed for molecular biology and were RNAse free. Autoclaved Eppendorf tubes and sterile filter tips were used for each experiment. RNA samples were stored in first instance at -20°C and then at -80°C.

### *2.3.1 Total RNA extraction*

Pellets were collected as described in 2.2.1 and an extra wash was performed with cold PBS followed by 5 min centrifugation at 300G. Supernatant was carefully removed and RNA extraction was processed using QIAGEN RNeasy kit. Pellets were dissolved in Buffer RLT plus (volume according to the cells number). After 30 seconds of vortexing, lysates were placed through a gDNA eliminator column and centrifuged progressively to 10 000G for 1 minute. Columns were discarded and the flow through was mixed with the same volume of ethanol 70%. The mix was placed into RNeasy spin columns and centrifuged 15 seconds at 10,000G. Flow through was discarded

and the column was washed with RW1 buffer for 15 seconds at 10,000G. Three washes were performed with RPE buffer. Columns were then placed in a new collection tube and spun at 10,000G for 2 minutes in order to dry the membrane of the column. RNA free water was added and tubes were spun progressively for 2 minutes at 10,000g. RNA concentrations were quantified according to absorbance at 260nm with a Nanodrop and samples were stored at -80°C.

### *2.3.2 Total RNA extraction enriched in small RNAs*

The recovery of miRNAs from total RNA extraction was performed with the mirVana Paris kit. Pellets were collected as described in 2.2.1 and an extra wash was performed with cold PBS followed by 5 min centrifugation at 300G. Cell disruption buffer was added to the pellet on ice followed by the same volume of 2X denaturation buffer. A volume of Acid: phenol chloroform equal to the volume of the lysate and denaturing solution was added and mixed vigorously. The sample was spun 5 min at 10,000G to dissociate the sample into two phases: aqueous (upper phase) and organic (lower phase). The upper phase containing RNA was carefully collected without disturbing the lower phase. The upper, aqueous phase was gently mixed with 1.25X 100% ethanol and was placed in the column and spun at 10,000G for 30 seconds. The column was washed with miRNA wash solution 1 and centrifuged for 30 seconds at 10,000G. The flow-through was discarded and washing steps were repeated twice with wash solution 2/3. The empty column was then spun 1 for minute in order to dry the membrane. The column was transferred to a new collection tube, pre-heated nuclease free water at 95°C was applied to the center of the column and centrifuged for 1 min at 10,000G. RNA concentrations were quantified at 260nm with Nanodrop and samples were stored to -80°C.

### *2.3.3 Determination of RNA concentration and purity*

RNA concentration and purity was assessed by Nanodrop spectrophotometer. The RNA concentration was determined by measuring absorbance at 260nm. To evaluate RNA purity, absorbance was also measured at 280nm to estimate the amount of protein and 230nm to detect other contaminants such as phenol or residual guanidine thiocyanate. Samples with ratios 260/230 and 260/280 superior to1,8 were considered free of contaminants.

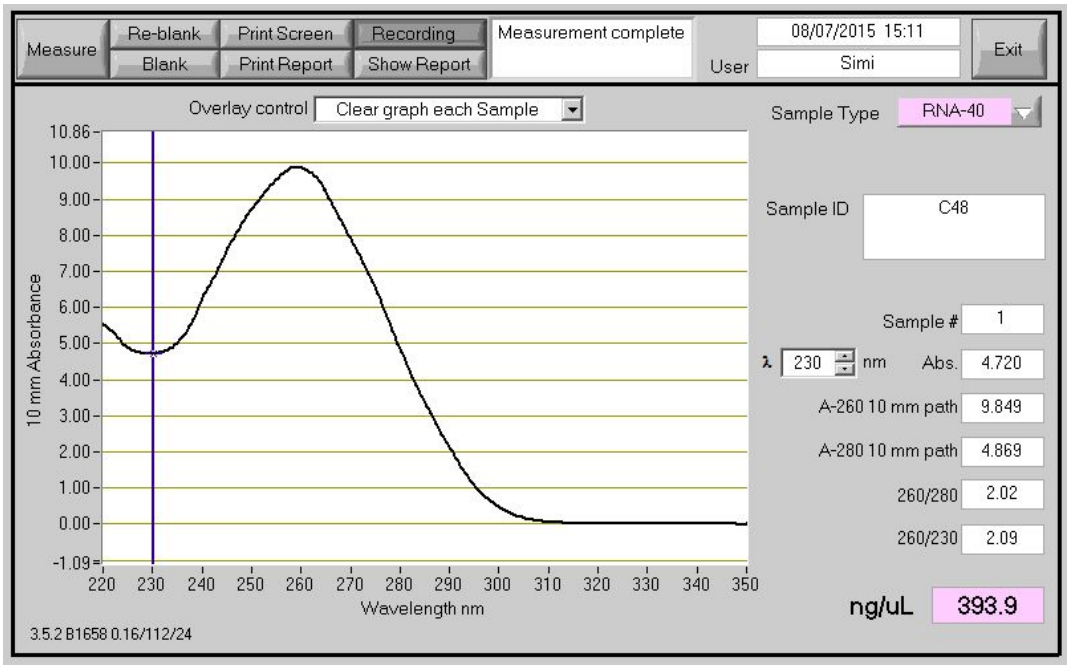


**Figure 2.1 RNA measurement using a Nanodrop spectrophotometer**

### *2.3.4 Messenger RNA reverse transcription*

To convert mRNA into cDNA, reverse transcription was carried out with the Tetro cDNA synthesis kit (Bioline). Each reagent was vortexed and quickly spun before use. The reverse transcription(RT) was performed with oligo dT primers that bind to the poly-A tail representing most of mRNAs. Up to 5ug of RNA was mixed to 10µM oligo dT, 10mM dNTP mix, 200U of tetro reverse transcriptase, RNAse inhibitor and reverse transcriptase buffer. Samples were made up to a final volume of 20µl with DEPC treated water and were incubated at 45°C for 30 minutes, 85°C for 5 minutes using a T100™ Thermal Cycler (BioRad). cDNA samples were stored at -20°C.

### *2.3.5 MiRNA reverse transcription*

Reverse transcription of specific miRNAs was performed with TaqMan™ MicroRNA Reverse Transcription Kit (Thermofisher). First, an RT mix was prepared with 100mM dNTPs, 50U of multiscribe reverse transcriptase, 10x reverse transcriptase buffer, $9.10^{-3}$U RNAse inhibitor and nuclease free water up to 15µL for each reaction.
Total RNA sample concentration was diluted to 20ng/µL and 100ng was used for each reaction. A specific RT primer was then added and the mix was spun and left on ice for 5 minutes. Samples were loaded into the T100™ Thermal Cycler and incubated 30 minutes at 16°C, 30 minutes at 42°C and 5 minutes at 85°C. Samples were stored at -20°C.

## 2.4 Real time polymerase chain reaction

### *2.4.1 General principle*

The Polymerase chain reaction (PCR) is a reaction which amplifies specific sequences of DNA. This method is based on repeating cycles of amplification of DNA. Each cycle is composed of three steps: denaturation, annealing and elongation. During denaturation, the sample is heated to around 95°C and double stranded DNA is denatured to single strand. Annealing is characterized by the binding of primers to complementary single strand DNA at a lower temperature. For the last step of elongation, a polymerase extends the DNA sequence from 5' to 3' by adding bases on 3' of primers. The amplification is exponential and each cycle produce $2^{(\text{Number of cycle } +1)}$ copies of the amplicon. In conventional PCR, only the detection of the amplicon is analysed. In real time PCR, the amplification is measured at each cycle due to the presence of a fluorescent reporter in each reaction and gene expression can be analysed. An internal reference dye can be included to normalise the fluorescence between reactions.

Real time PCR plots show two phases:

- Exponential phase: Increased number of cycles generate accumulation of the amplicon necessary to increase fluorescence above background signal and give rise to the amplification curve. The cycle threshold (CT) is then defined as the intersection between the threshold and the amplification curve
- Non-exponential phase: As reagents are limited, amplification slows down and amplification plot results show a plateau

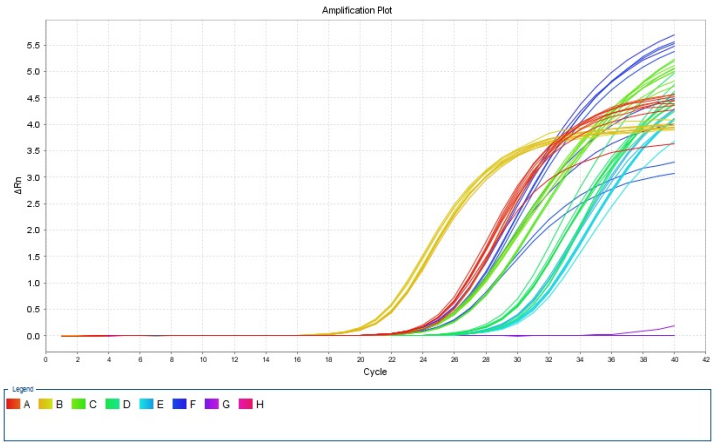


**Figure 2.2 Amplification plot of real time PCR**

### 2.4.2 *Taqman probe-based assays*

PCRs were carried out with Taqman assay probes or with Taqman miRNA assay (Thermofisher). Both assays contains probes 250nM, with 900nM of forward and reverse primers.

Probes are labelled with a FAM dye on the 5' end and a non fluorescent quencher (NFQ) with minor groove binder (MGB) on the 3' end. When the PCR starts, fluorescence is repressed by the proximity of the quencher. The probe binds to the template during annealing and the MGB increases the melting temperature to stabilize probe target complex. In the course of elongation, the probe is cleaved and the fluorescent dye is freed from the quencher. Fluorescent intensity increases at each cycle due to the cleavage of the probe.

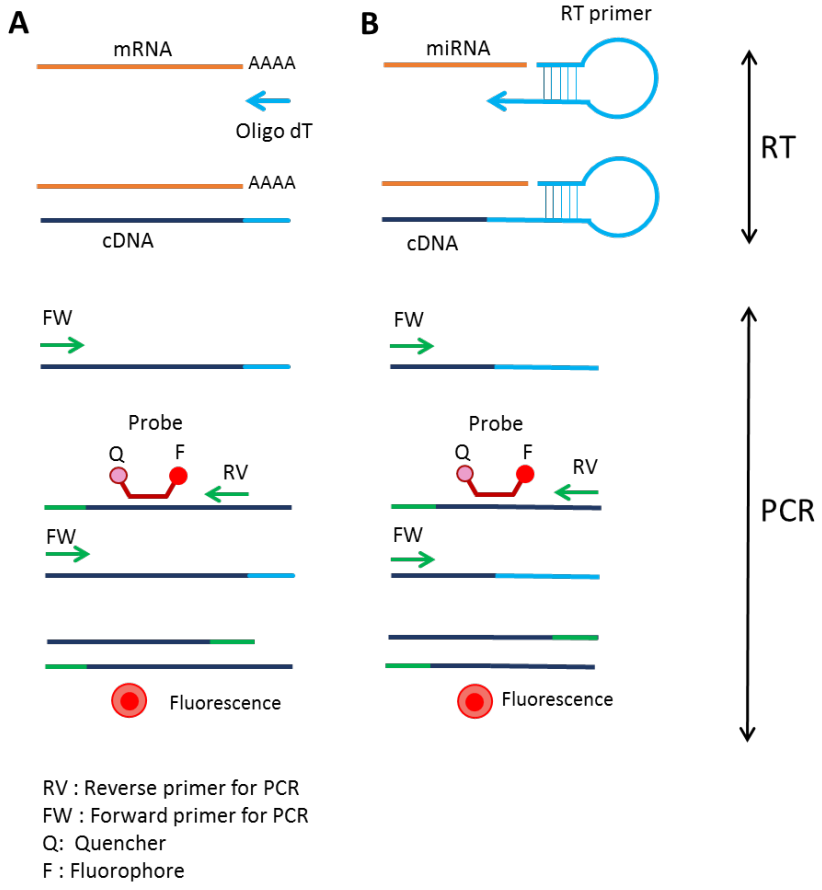


**Figure 2.3 Reverse transcription and real time PCR using Taqman technologies for mRNA or miRNA.**
Reverse transcription of mRNA is based on Oligo dT primers that bind to the poly-A tail whether RT of miRNA requires a specific stem-loop primer. Taqman technologies for PCR consists of a forward primer, reverse primer and probe. The probe contains a fluorophore and a quencher which inhibits the fluorescence. During annealing the probe binds to the cDNA and the polymerase cleaves the probe in the course of elongation. The fluorophore is released from the quencher and emits fluorescence.(Chen *et al.*, 2005)

PCR reactions were performed with the SensiFAST Probe Hi-ROX Mix (Bioline). First, a PCR mastermix was created with 20x Taqman assay probe, 2x SensiFAST Probe Hi-ROX Mix made up to 18 µL with nuclease free water. Each reaction was executed in triplicate. The mastermix was first placed into 96 well plates and cDNA template (25-100ng) were added directly into the well for a final reaction volume of 20µl. The plate was spun and placed into the Step one plus Real time PCR system (thermofisher). For Taqman probe assays, reactions were incubated 5 minutes at 95°C to activate the polymerase and then by a 40 x cycle of 10 seconds at 95°C for denaturation, 20 seconds at 60°C for annealing and extension.

### *2.4.3 Primer efficiency*

PCR efficiency is defined by the rate of template amplification. If the amplicon doubles in every cycle during exponential phase, PCR efficiency is equal to 100%. This value is calculated from PCR with serial dilutions of cDNA plotted on a standard curve. The standard curve represents the log of cDNA factor dilution on log axis and the Ct value obtained for each dilution on the Y axis. Amplification efficiency is defined by the slope of the standard curve: *Efficiency (E) = 10^ (-1/slope)* and *%Efficiency = (E-1)x100*
The optimal slope for the standard curve is -3.32 as it represents 100% efficiency. Efficiency should be between 90-100%, lower efficiency can relate to poor primer design and higher efficiency can be explained by presence of PCR inhibitors or by amplification of non-specific products such as primer dimers. Figure 2.2 shows the efficiency curves for miRNA taqman primers.

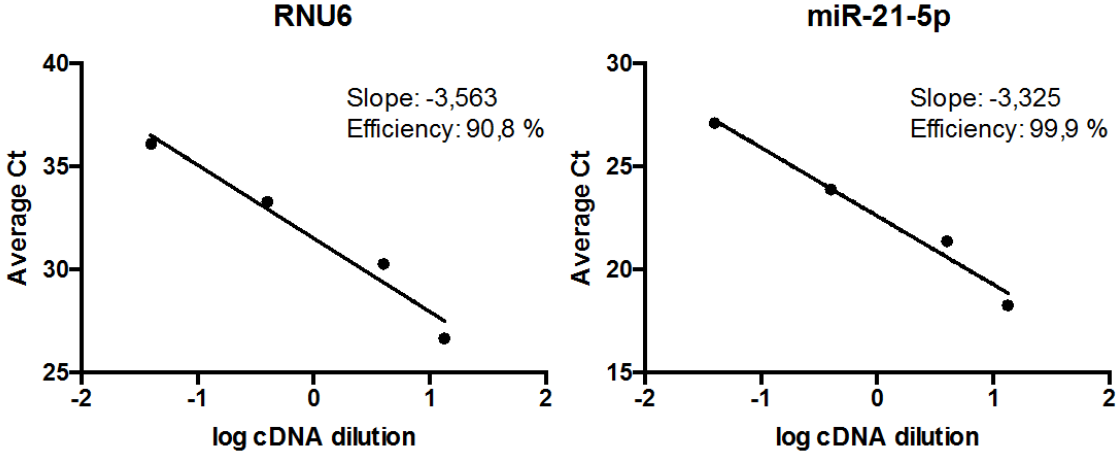


**Figure 2.4 Primers efficiency of Taqman microRNA assay.**
Primer efficiency was evaluated by PCR with different dilutions of cDNA. The log of cDNA dilution were plotted against the average of cycle threshold. Efficiency was calculated from the slope of the standard curve. RNU6 and miR-21-5p were within the range of 90-100% of primer efficiency.

### 2.4.4 Gene expression analysis

For gene expression analysis, the ΔΔCt method was performed for each PCR as the procedure states below:

a) ΔCt treated = Average Ct target gene (treated) – Average Ct reference gene (treated)

*This step was carried out for each sample.*

b) ΔCt control= Average Ct target gene (control) – Average Ct reference gene (control)

c) ΔΔCT = ΔCt treated - ΔCt control

*ΔΔCT is then converted to relative expression or fold change*

d) Fold change= $2^{-\Delta\Delta Ct}$

### 2.4.5 List of Taqman Assay

Taqman assays for this project had 6-carboxyfluorescein (FAM) as a fluorophore and tetramethylrhodamine (TAMRA) as the quencher. (Table 2.1)

| Gene | ID |
|---|---|
| HPRT1 | Hs02800695_m1 |
| S100A4 | Hs00243202_m1 |
| vWF | Hs01109446_m1 |
| FN1 | Hs01549976_m |
| PECAM1 | Hs01065279_m1 |
| PCDH12 | Hs00170986_m1 |
| ADAM9 | Hs00177638_m1 |
| SMURF2 | Hs00224203_m1 |
| ACTA2 | Hs00426835_g1 |
| COL1 | Hs00164004_m1 |
| TWIST1 | Hs01675818_s1 |
| SNAI1 | Hs00195591_m1 |
| SNAI2 | Hs00161904_m1 |
| IL1β | Mm00434228_m1 |
| TGFβ2 | Mm00436955_m1 |

| miRNA | ID |
|---|---|
| RNU48 | 1006 |
| RNU6B | 1093 |
| hsa-miR-146a-5p | 468 |
| hsa-miR-21-5p | 397 |
| hsa-miR-195-3p | 2117 |
| hsa-miR-103a-3p | 439 |
| hsa-miR-494-3p | 2365 |
| hsa-miR-548a-5p | 2412 |
| hsa-miR-944 | 2189 |
| hsa-miR-519c-3p | 1163 |
| hsa-miR-199b-5p | 500 |
| hsa-miR-126-3p | 2228 |
| hsa-miR-30b-3p | 2129 |
| hsa-miR-200b-3p | 2251 |

**Table 2.1 List of Taqman assays.**
Both Taqman assay probes and the Taqman microRNA assay was used in this project. Hs is designed for human Taqman assay and Mm for mouse Taqman assay.

## 2.5 Immunofluorescence

### *2.5.1 Immunofluorescence on cells*

Cells were grown in a chamber in a humidified atmosphere of 5% $CO_2$ at 37°C. Post-incubation, media was removed and cells were gently washed with PBS and fixed with cold methanol (-20°C) for 10 minutes at room temperature. Methanol was carefully removed and chamber slides were left to dry at room temperature for 5 minutes. Slides were then quickly washed with PBS, and were blocked with PBS 1% bovine serum albumin (BSA) (Sigma) for one hour on rocker at room temperature. Primary Antibodies were diluted in PBS 1%BSA according to manufacturer's protocol and placed into each well overnight at 4°C

The next day, chamber slides were washed once for 5 minutes with PBS 0,1% Tween20 and once for 5 minutes with PBS. Fluorescent conjugated secondary antibodies diluted in PBS 1%BSA were added and incubated during one hour on the rocker. Chamber slides were washed once 5 minutes with PBS 0,1% Tween20 and once 5 minutes with PBS. To counterstain nuclei, DAPI (Biolegend) was diluted in PBS and added to each well, with incubation for 30min on the rocker at room temperature. After one wash with PBS 0,1% Tween and one wash PBS, wells were removed from the slides. Slides were mounted with Fluoromount (Sigma) and analysed by a fluorescence microscope Leica TC SP2 UV laser or Zeiss axioimager. Slides were stored at 4°C in the dark.

### *2.5.2 Immunofluorescence on tissue*

Immunofluorescence was performed on frozen sections. Sections were fixed in acetone and stored at -20°C prior to the staining. Immediately before the staining, slides were soaked in PBS and the tissue was delimited with a hydrophobic barrier pen in order to keep reagents on tissue. Blocking buffer consisting in PBS 0,5% Tween 1% BSA 5% goat serum (Sigma) was added to the tissue for 2 hours at room temperature. Excess of liquid was removed and primary antibody diluted in blocking solution were applied overnight at 4°C in humidified chamber. Slides were washed twice for 5 minutes with PBS 0,1% Tween20 and once 5 minutes with PBS. Fluorescent conjugated secondary antibodies diluted in PBS 0,5% Tween 1% BSA 5% goat serum were added and incubated during 2 hours. Slides were washed twice 5 minutes with PBS 0,1% Tween20 and a final wash of 5 minutes with PBS. Slides were mounted into mountant containing DAPI Prolong Gold (Thermofisher). Stained slides was stored in

4°C and were visualised at least 24 hours later on a fluorescence microscope Zeiss Axioimager or Nikon A1R confocal microscope.

### 2.5.3 Antibodies

Antibodies in the table 2.2 were used for immunofluorescence of cells or tissue.

| Primary Antibody Unconjugated | Specie | Dilution | Company | Product number | |
|---|---|---|---|---|---|
| Anti-VE-cadherin | Rabbit | 1/200 | Abcam | ab33168 | |
| Anti-GFP | Chicken | 1/400 | Abcam | ab13970 | |
| Anti-Fibronectin | Rabbit | 1/200 | Abcam | ab2413 | |
| Anti-CD31 | Mouse | 1/100 | BD Pharmingen | 550389 | |
| Anti-CD31 | Rat | 1/200 | BD Pharmingen | 550274 | |
| Anti-Cytokeratin | Mouse | 1/200 | DAKO | M7018 | |
| Primary antibody conjugated | Specie | Dilution | Company | Product number | Dye |
| Anti-Actin, Smooth Muscle | Mouse | 1/200 | Sigma | C6198 | Cy3 |
| Secondary Antibody conjugated | Specie | Dilution | Company | Product number | Dye |
| Goat anti-Chicken IgY (H+L) | Goat | 1/200 | Thermofisher | A-11039 | Alexa Fluor®488 |
| Goat anti-Rat IgY (H+L) | Goat | 1/200 | Thermofisher | A-11007 | Alexa Fluor®4594 |
| Goat anti-Mouse IgG (H+L) | Goat | 1/200 | Thermofisher | A-11029 | Alexa Fluor®488 |
| Goat anti-Mouse IgG (H+L) | Goat | 1/200 | Thermofisher | A-11001 | Alexa Fluor®489 |
| Goat anti-Rabbit IgG (H+L) | Goat | 1/200 | Thermofisher | A-11008 | Alexa Fluor®490 |
| Goat anti-Rabbit IgG (H+L) | Goat | 1/200 | Immunoreagent | GtxRb-003 | DyLight® 550 |

**Table 2.2 List of primary and secondary antibodies used in this project.**
Each antibody was diluted according to manufacturer protocol.

### 2.5.4 Quantification

Immunofluorescence was quantified using image J software. Intensity and area of fluorescence were measured for each dye. Cells were automatically counted for each picture and the ratio intensity of fluorescence on number of cells was calculated.
For each condition, a least three pictures from different areas of the slide were quantified.

## 2.6 In-situ hybridisation

### 2.6.1 In-situ hybridisation for miRNAs

Detection of endogenous miR-126-3p was performed by in-situ hybridisation with the

microRNA ISH Optimization Kit (FFPE) (Exiqon). This kit is based on a colorimetric antibody system with miRCURY LNA miRNA detection probes which are double labelled anti-Digoxigenin(DIG) (5'and 3'). Probes are complementary and bind to the miRNA, Digoxigenin on the probe is then detected by an anti-DIG conjugated with alkaline phosphatase. Alkaline phosphatase reacts with the substrates 4-nitro-blue tetrazolium (NBT) and 5-bromo-4-chloro-3'-indolylphosphate (BCIP) to result in dark-blue NBT-BCIP precipitate. The precipitate can be easily visualised and defines the localisation of miRNAs.

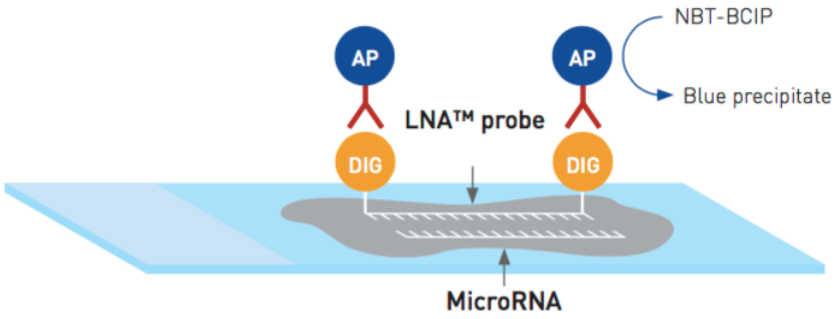


**Figure 2.5 Mechanism of in-situ hybridisation for miRNA.**
A probe double labelled with digoxigenin binds to the miRNAs in the tissue. Digoxigenin is detected by an antibody anti-DIG coupled with alkaline phosphatase. The substrate NBT–BCIP is applied onto the tissue and alkaline phosphatase transform it in blue precipitate.

| | |
|---|---|
| SSC solutions from 20x SSC | 5xSSC (1 L=250 mL 20xSSC + 750 mL water) |
| | 1xSSC (1 L=50 mL 20xSSC + 950 mL water) |
| | 0.2xSSC (1 L=10 mL 20xSSC + 990 mL water) |
| PBS 1 %Tween | Add 1 mL of Tween-20 to 1 L of PBS. |
| KTBT (AP stop solution) | Tris-HCl (50mM) + NaCl (150mM), KCl (10mM) + up to 1L of RNAse free water |
| BSA 30% | 15g BSA in 50mL of RNAse free water |

**Table 2.3 Buffers for in-situ hybridisation.**
Buffers were prepared and autoclaved before the one day experiment of in-situ hybridisation. 30% BSA solution was aliquoted and stored at -20°C. Other buffers were stored at room temperature.

Prior to hybridisation, buffers described in table 2.3 were prepared and autoclaved. In situ-hybridisation was performed on frozen sections. Out of the freezer, slides are quickly dipped into sterile PBS and sections delimited using a hydrophobic barrier pen.

A hybridisation mix was prepared with microRNA ISH buffer at a 1 :1 ratio of nuclease free water and 40nM of miRNA detection probe. Tissue sections were hybridised at 30˚C lower than the probe Tm for an hour in an oven. Slides were washed at hybridization temperature with pre-warmed SSC buffer with decreasing concentration. Blocking solution (PBS 0.1% Tween 1% BSA 2% Sheep serum) and diluent solution (PBS 0.05% Tween1% BSA 1% Sheep serum) were prepared. Slides were blocked 15 minutes with the blocking solution followed by an incubation with 1: 800 anti-DIG (Roche) in diluent solution for 1 hour at room temperature. Sections were washed twice with PBS-Tween and NBT-BCIP substrate was applied for a minimum of an hour at 30°C. The reaction was stopped with the KTBP buffer and sections were washed with water. For counterstaining Nuclear Fast Red (Vector Laboratories) was applied and slides went through dehydration steps in ethanol solutions. Slides were mounted with permanent aqueous mounting medium (DAKO) and were dried overnight. Sections were analysed with an Olympus microscope equipped with an SC50, 5-megapixel color camera.

### *2.6.2 Probes and control*

Probes specifically target miRNAs in tissue and their hybridisation temperature is defined 30°C below the RNA melting temperature. Scramble is a unique sequence of bases which have low sequence identity with mouse. Scramble miR is therefore a negative control and sets the background of the in-situ hybridisation.

As the kit was optimised with miR-126-3p as positive control, we did not use any other positive control.

| Probe | Sequence | RNA Tm °C | Company | Product number |
|---|---|---|---|---|
| Scramble miR | /5DigN/GTGTAACACGTCTATACGCCCA/3DigN/ | 87 | Exiqon | 699-004-360 |
| hsa-miR-126-3p | /5DigN/GCATTATTACTCACGGTACGA/3DigN/ | 84 | Exiqon | 619-866-360 |

**Table 2.4 In situ hybridisation probes used in this project.**
These probes were compatible with the microRNA ISH Optimization Kit (FFPE) (Exiqon).

## 2.7 Statistics

Data were plotted with GraphPad prism software version 5 or 6. Comparison between different groups was assessed by one-way analysis of variance (ANOVA) with a Tukey test as a post hoc test. This post hoc test examines for significant differences between groups, with a p-value P <0.05. In this project, significance is defined as follows:

* p<0.05, ** p<0.01 and *** p<0.001.

Comparisons between two groups were performed by Student's t-test, with the same thresholds for significance.

# Chapter 3. In-vitro model of endothelial-to-mesenchymal transition

## 3.1 Introduction

Endothelial-to-mesenchymal transition has been first observed in heart development where endothelial cells from the endocardium migrate to the cardiac jelly and transdifferentiate into mesenchymal cells with the support of the myocardium. EndMT is essential to build heart valves in the outflow track (OFT) region and the atrioventricular (AV) canal (Markwald *et al.*, 1975). Culture of AV canal endothelial cells with explant of myocardium showed that EndMT was stimulated mainly by members of the TGFβ family (Potts and Runyan, 1989). During cardiogenesis in chick, TGFβ2 and TGFβ3 were the main isoforms expressed in the myocardium and their inhibition exhibit a distinct role in EndMT. TGFβ2 seems to mediate the disruption of cell-cell contact and TGFβ3 to promote their migration (Boyer *et al.*, 1999). However, Camenisch et al revealed that each TGFβ isoforms play a different role in EndMT according to the species. In fact, mouse only requires TGFβ2 for the transdifferentiation, whereas avian heart requires both TGFβ2 and TGFβ3 (Camenisch *et al.*, 2002). In mouse AV explant, EndMT was prevented with the inhibition of LBTP1, a protein required for TGFβ1 activation, arguing that TGFβ1 plays a role in EndMT (Nakajima *et al.*, 1997). All together, these data suggest that the three isoforms play a role and could be involved at different stages of EndMT.

Nevertheless, in mouse Av explant, mesenchymal cells invading the collagen were reduced in TGFβ2 knock-out mouse compared to TGFβ1,3 knock-out where invasion was similar to the wild type and therefore EndMT was functional (Mercado-Pimentel and Runyan, 2007; Azhar *et al.*, 2009).
Recently, the transition of endothelial cells in mesenchymal cells was described also in the context of fibrosis as a source of myofibroblasts (Zeisberg *et al.*, 2007, 2008).
To better understand EndMT mechanism, models of endothelial-to-mesenchymal transition were developed in-vitro. Arcienegas et al first promoted the transition in bovine aortic endothelial cell where cells were treated with TGFβ1. Factor VIII was significantly decreased and alpha SMA increased suggesting the transdifferentiation (Arciniegas *et al.*, 1992). Similar results were obtained with the absence of cell to cell contact (Frid *et al.*, 2002). In ovine aortic valve endothelial cell, TGFβ1 treatment induced alpha SMA expression and stimulation with PDGF increased their migration.

EndMT was also observed in culture with deprivation of fibroblast growth factor meanwhile Krenning et al combined both treatment in HUVEC to give rise to mesenchymal cells (Frid *et al.*, 2002; Ishisaki *et al.*, 2003; Krenning *et al.*, 2008).

As different isoform of TGFβ could be involved in EndMT, Montorfano et al showed that oxidative stress-induced EndMT lead to secretion of TGFβ1 and TGFβ2. These two factors seemed to play a pivotal role as their inhibition abolished the transdifferentiation (Montorfano *et al.*, 2014). In several endothelial cell types, TGFβ2 treatment reduced endothelial junction markers such as VE cadherin and PECAM1 and were positive for alpha-SMA. Treated cells acquired a spindle shape morphology similar to mesenchymal cells (Medici *et al.*, 2011; Mihira *et al.*, 2012; R. Kumarswamy *et al.*, 2012). Increased expression of Snail, a transcription factor related to suppression of cell adhesion was observed in endothelial cells post-treatment with TGFβ2 (Medici *et al.*, 2011).

Interestingly, a model only based on the inflammatory cytokine IL1β treatment could permanently transdifferentiate human dermal microvascular endothelial cells (HDMEC) in mesenchymal cells (Chaudhuri *et al.*, 2007).

In recent publications, new model of EndMT was developed by treating endothelial cells with TGFβ2 and an inflammatory cytokine IL1β. Malesweska et al showed that treating endothelial cells during 3 days with TGFβ2 and IL1β followed by 2 days of TGFβ2 treatment induced EndMT at the same level than 5 days of treatment with IL1β and TGFβ2. This suggests that TGFβ2 and IL1β treatment induce EndMT and that IL1β is only required for the induction of EndMT.(Maleszewska *et al.*, 2013; Nie *et al.*, 2014)

## 3.2 Specific aims

In this chapter, in-vitro model of EndMT was established in two different cell types HMEC1 and HUVEC. We aimed to :

- To investigate the effect of TGFβ2 and IL1β treatment in endothelial cells
- To examine the expression at RNA level of endothelial markers and mesenchymal markers in endothelial cells post-treatment with TGFβ2 and IL1β
- To examine the expression at protein level of endothelial markers and mesenchymal markers in endothelial cells post-treatment with TGFβ2 and IL1β
- To assess the expression of the transcription factors Snail and Slug in endothelial cells post-treatment with TGFβ2 and IL1β

## 3.3 Specific material and methods

*Cell treatment*

Cells were treated with 10ng/mL of TGFβ2 (Prepotech) or TGFβ2 and IL1β (Prepotech) both at the concentration of 10ng/mL (Maleszewska *et al.*, 2013). For treatment equal or less than 3 days, cells were seeded at 30% confluence and 15% confluence for treatment longer than 3 days. Treatment was added at least few hours after the seeding to allow the cells to settle down. Media and treatment were changed every three days.

## 3.4 Results

### *3.4.1 Effect of TGFβ2 and IL1β on endothelial cells morphology*

The endothelial cell line HMEC1 was used to prevent the limitations of isolation of microvascular endothelial cells. The immortalized cells present endothelial features such as the secretion of vWF or the expression of the cell adhesion marker CD31. In culture, HMEC1 form a monolayer with a cobblestone appearance and grow to a higher density than primary endothelial cells. HMEC1 were stimulated with TGFβ2 and IL1β for 72 hours. A change in the morphology is observed post- treatment on endothelial cells. HMEC1 monolayer is disrupted post-treatment and cells acquire a spindle shape (**Figure 3.1**).

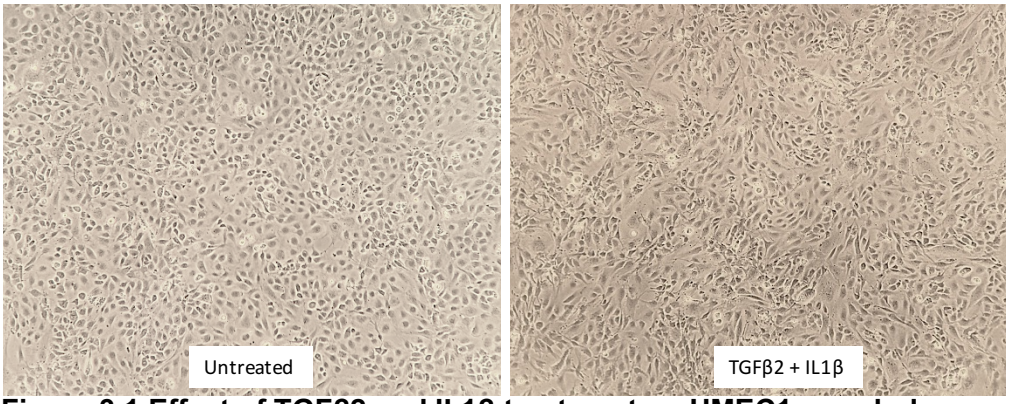


**Figure 3.1 Effect of TGFβ2 and IL1β treatment on HMEC1 morphology.**
Cells were stimulated with TGFβ2 (10ng/mL) and IL1β (10ng/mL) for 72 hours. Untreated cells grow round with an appearance of cobblestone and form a continuous monolayer. HMEC1 post-treatment acquire a spindle shape and a disruption of the monolayer.

HUVECs are primary endothelial cells from large vessel and represent a classic model to study endothelial phenotype. HUVECs grew as a monolayer with intercellular junctions. Once the confluence is reached, these polygonal cells acquired a cobblestone morphology. HUVECs morphology was changed only 24 hours post-treatment with TGFβ2 and IL1β. The monolayer was disrupted and the phenotype was similar to fibroblast in culture. Cells acquired a spindle shape and grew in parallel clusters (**Figure 3.2**).

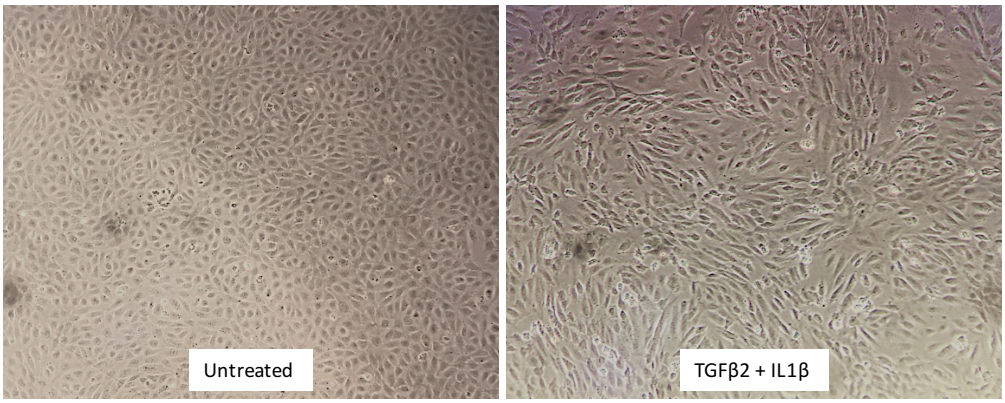


**Figure 3.2 Effect of TGFβ2 and IL1β treatment on HUVEC morphology.**
Cells were treated with TGFβ2 (10ng/mL) and IL1β (10ng/mL) for 24 hours. HUVECs develop as a monolayer with a cobblestone appearance. Post-treatment, morphology of HUVECs changes with a disruption of the monolayer and cells acquire a spindle shape.

### *3.4.2 Effect of TGFβ2 and IL1β on fibronectin expression in endothelial cells*

In order to develop a model of endothelial to mesenchymal transition in-vitro, fibronectin expression by endothelial cells was studied.

Fibronectin is an extracellular matrix glycoprotein that serve as cell adhesion and guide cellular interaction into the extracellular matrix. Fibroblasts synthesised fibronectin dimers and interact with them via an integrin-dependent process to assemble into fibrillar matrix. An increase in fibronectin expression is correlated with fibroblast differentiation.

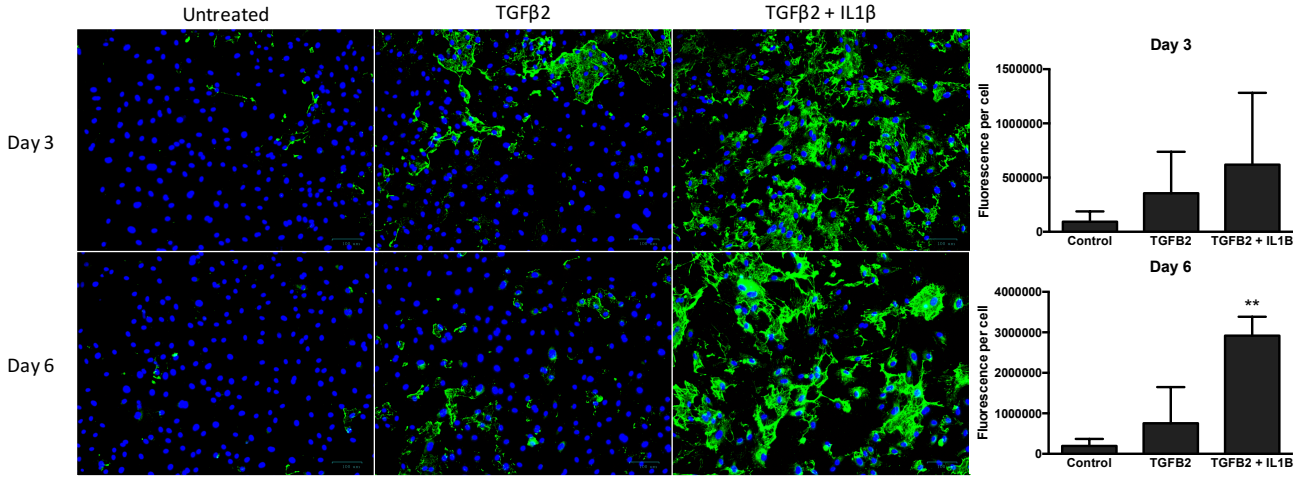


**Figure 3.3 Fibronectin staining in endothelial cells from saphenous vein treated with TGFβ2 or TGFβ2 and IL1β.**
HSVEC were treated during 3 or 6 days with TGFβ2 (10ng/ml) or TGFβ2 and IL1β (10ng/ml). Immunofluorescence was performed for fibronectin followed by a secondary antibody Alexa fluor 488 conjugate and nuclei were counterstained with DAPI. Pictures were taken with Bio-rad microscope (Original magnification ×20). Fluorescence was quantified using image J. Values are mean +/- SD of three pictures for each condition. (n=2) Statistical significance was assessed by One-way ANOVA followed by Tukey test *(**, p<0.01)*

For this experiment, primary endothelial cells from saphenous vein (HSVEC) were treated with TGFβ2 (10ng/mL) and IL1β (10ng/mL) for three and six days. Media was replaced every three days. After fixation, staining for fibronectin was performed. No significant change in fibronectin expression was observed between untreated cells and cells post-treatment with TGFβ2. However, fibronectin was significantly increased only 6 days post-treatment with TGFβ2 and IL1β suggesting that a longer treatment with TGFβ2 and IL1β could induce the expression of fibronectin by endothelial cells.

Fibronectin expression was also assessed in HMEC1 and HUVEC to confirm the results in **Figure 3.3**. Cells were treated for 6 days with TGFβ2 (10ng/mL) and IL1β (10ng/mL) and immunofluorescence for fibronectin was performed. As shown in **Figure 3.4**, no significant change of fibronectin expression was observed in cells treated with TGFβ2 compared to untreated cells.
After 6 days of treatment with TGFβ2 and IL1β fibronectin was significantly increased in the endothelial cell line as well as primary cells from both the sources.(**Figure 3.4**)

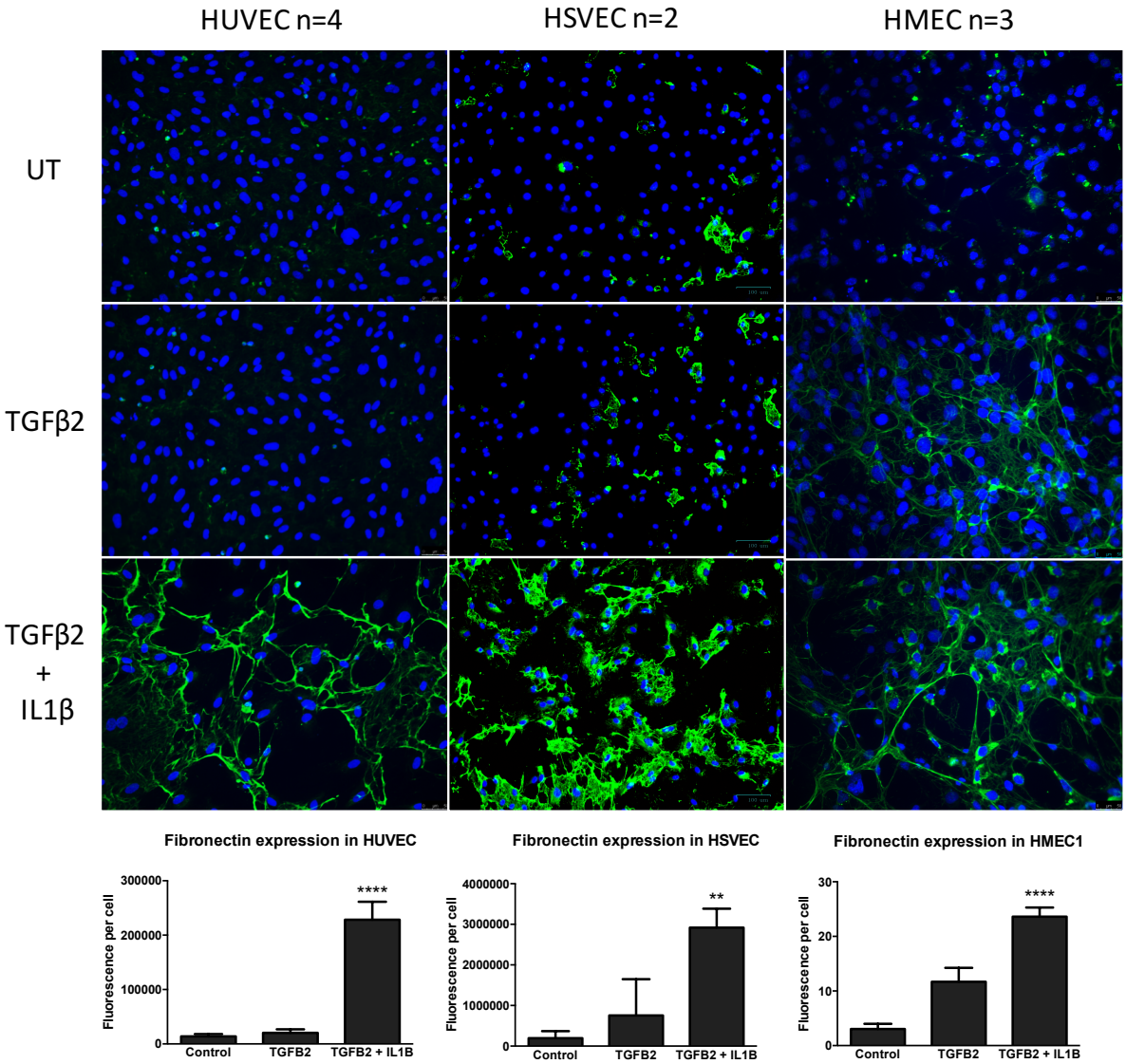


**Figure 3.4 Fibronectin staining in endothelial cells treated with TGFβ2 or TGFβ2 and IL1β.**

Endothelial cells were treated during 6 days with TGFβ2 (10ng/ml) or TGFβ2 and IL1β (10ng/ml) and were stained for fibronectin followed by a secondary antibody Alexa fluor 488 conjugate. DAPI counterstaining was performed for nuclei. Pictures were taken with Zeiss axioimager II upright (HUVEC), Bio-Rad microscope (Primary EC) and Leica (HMEC) (Original magnification ×20). Fluorescence was quantified using image J. Values are mean +/- SD of three pictures for each condition. All data is representative of at least two independent experiments and one-way ANOVA with Tukey test was performed for multiple comparison *(**, p<0.01; ****, p <0.0001)*

### *3.4.3 Induction of EndMT in HMEC1*

EndMT is defined by the decrease of endothelial markers and the increase of mesenchymal markers. In order to validate previous studies suggesting that TGFβ2 and IL1β can induce EndMT *in vitro*, endothelial marker such as von Willebrandt Factor, a glycoprotein produced in endothelial cells or CD31 a cell surface marker encoded by PECAM1 were studied at gene expression level. To characterize the

transition in mesenchymal cells, alpha SMA a marker of activated fibroblast and fibronectin expression levels were analysed.

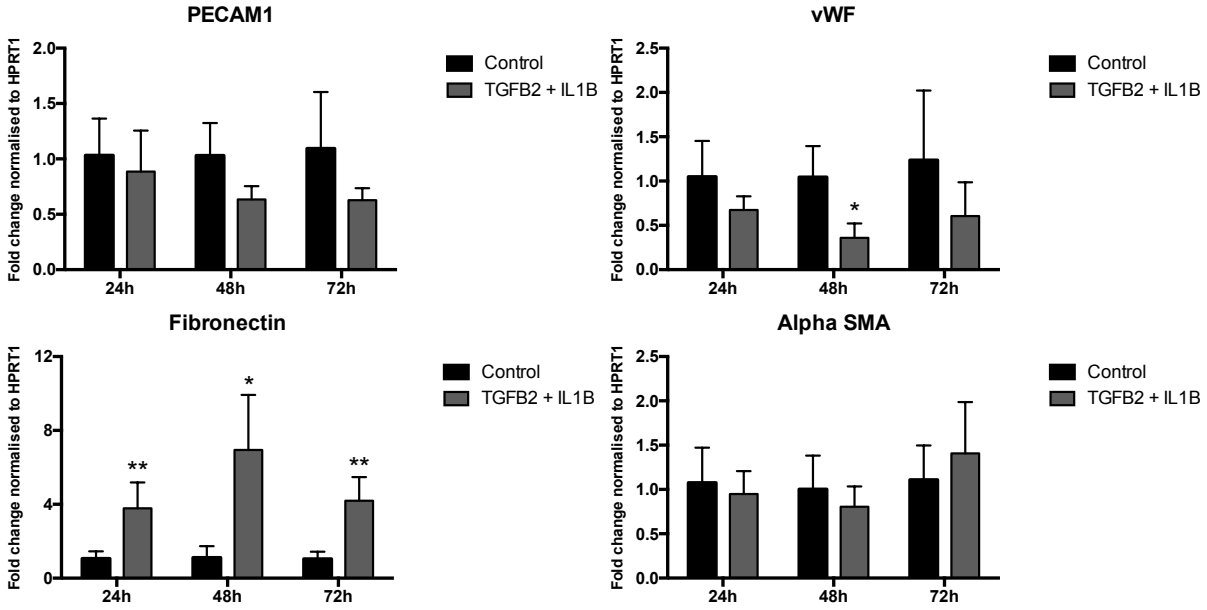


**Figure 3.5 Effect of TGFβ2 and IL1β treatment on genes expression in HMEC1**
Cells were treated from 24 hours to 72 hours with TGFβ2 and IL1β (10ng/ml). RNA was extracted, cDNA was synthesised by reverse transcription and a qRT-PCR was performed to study genes expression. Each gene expression was normalised to the housekeeping gene Hprt1 expression and compared to the control. Errors bars are representative of standard deviations. All data is representative of at least three independent experiments and statistical significance was assessed by multiple unpaired Student's *t* test. *(*, p <0.05; **, p<0.01)*

HMEC1 cells were treated for 24, 48 & 72 hours with TGFβ2 (10ng/mL) and IL1β (10ng/mL) respectively. From the RNA of HMEC1 cells, gene expression was studied by RT-qPCR with Taqman technologies. An endogenous control gene Hprt1 was quantified for normalisation and data were analysed with the delta delta Ct method ($2^{-\Delta\Delta CT}$ method). Each gene expression in treated cells was compared to the untreated cells. PECAM1 expression was non significantly reduced after 48 and 72 hours of treatment, whereas, vWF expression was significantly decreased 48 hours post treatment with p=0,037. As previously observed at protein level in **Figure 3.4**, fibronectin gene expression was significantly up-regulated post-treatment. This increase was detected at each timepoint suggesting a continuous overexpression of fibronectin with TGFβ2 and IL1β treatment. However, the treatment did not affect the expression of alpha SMA **(Figure 3.5)**.

The treatment induced a decrease of endothelial markers expression such as PECAM1 and vWF and an increase of fibronectin. Alpha SMA was not affected by the treatment.

### 3.4.4 Induction of EndMT in HUVEC

As the serial passaging of cell line can alter their phenotype, the use of human primary endothelial cells appears as the most relevant model to study the differentiation of endothelial cells in mesenchymal cells. The effect of TGFβ2 and IL1β treatment was investigated on human umbilical vein endothelial cells.

Adherens junctions in HUVEC are mediated by VE-cadherin which plays a role in the maintenance of vascular integrity. Cytoplamic domain of VE-cadherin is linked to p120-catenin, β-catenin and plakoglobin and these complexes form the cell-cell adherens junctions. Due to the restriction of VE-cadherin to endothelial cells, this marker was relevant to the study of EndMT.

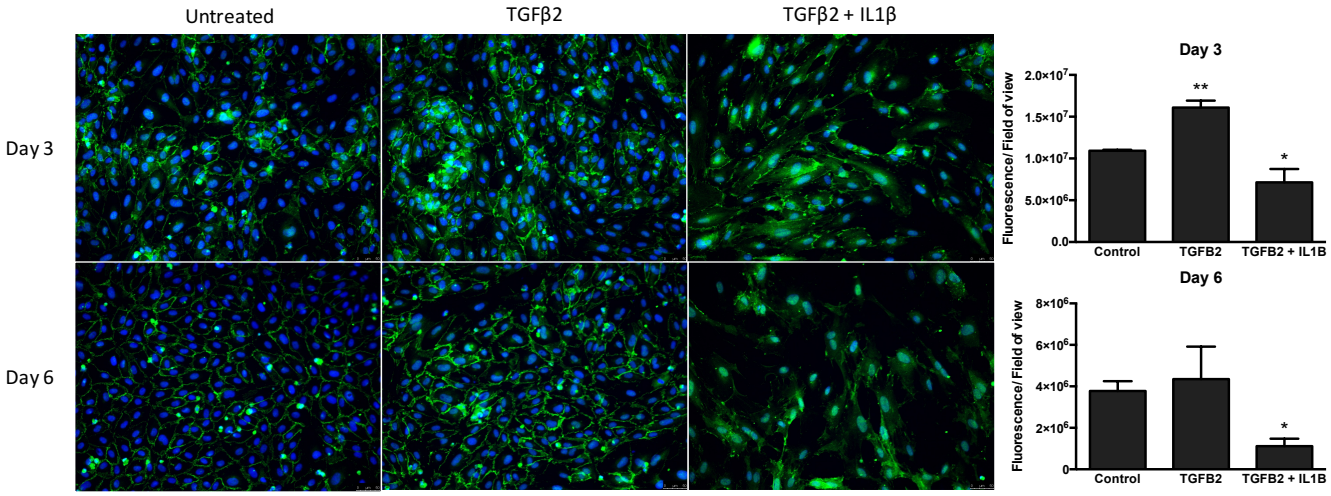


**Figure 3.6 VE-cadherin staining in HUVECs treated with TGFβ2 or TGFβ2 and IL1β.** HUVEC were treated during 3 or 6 days with TGFβ2 (10ng/ml) or TGFβ2 and IL1β (10ng/ml). Immunofluorescence was performed for VE-cadherin followed by a secondary antibody Alexa fluor 488 conjugate and nuclei were counterstained with DAPI. Pictures were taken with Bio-rad microscope (Original magnification ×20). Fluorescence was quantified using image J. Values are mean +/- SD of three pictures for each condition. (n=3) Statistical significance was assessed by One-way ANOVA followed by Tukey test *(*, p<0,05; **, p<0.01)*

HUVECs were treated for 3 and 6 days with TGFβ2 (10ng/mL) or TGFβ2 and IL1β (10ng/mL). After fixation in cold methanol, cells were stained for VE-cadherin coupled to a secondary antibody Alexa fluor 488 conjugate.

In untreated HUVECs, VE-cadherin staining displayed the distribution of adherens junctions in endothelial cells and a similar staining pattern was observed in TGFβ2 treated cells with an increased expression after three days of treatment. Post-treatment with TGFβ2 and IL1β, VE-cadherin staining pattern was disorganised and not localised to the cell junctions. Quantification of VE-cadherin showed that the protein was significantly down-regulated after 3 days and 6 days of treatment (**Figure 3.6**).

As seen previously with HMEC1 cells, HUVECs express CD31, a cell adhesion molecule at the cell surface. HUVECs were treated for 6 days with TGFβ2 (10ng/mL) or TGFβ2 and IL1β (10ng/mL). A double immunofluorescence with primary antibodies from different species was performed for an endothelial marker CD31 (green) and an extracellular matrix marker fibronectin(red). CD31 antibody was raised in mouse and fibronectin antibody was raised in rabbit. An antibody anti-mouse coupled with Alexa fluor 488 and an antibody anti-rabbit Dylight 550 were used for an indirect immunofluorescence.

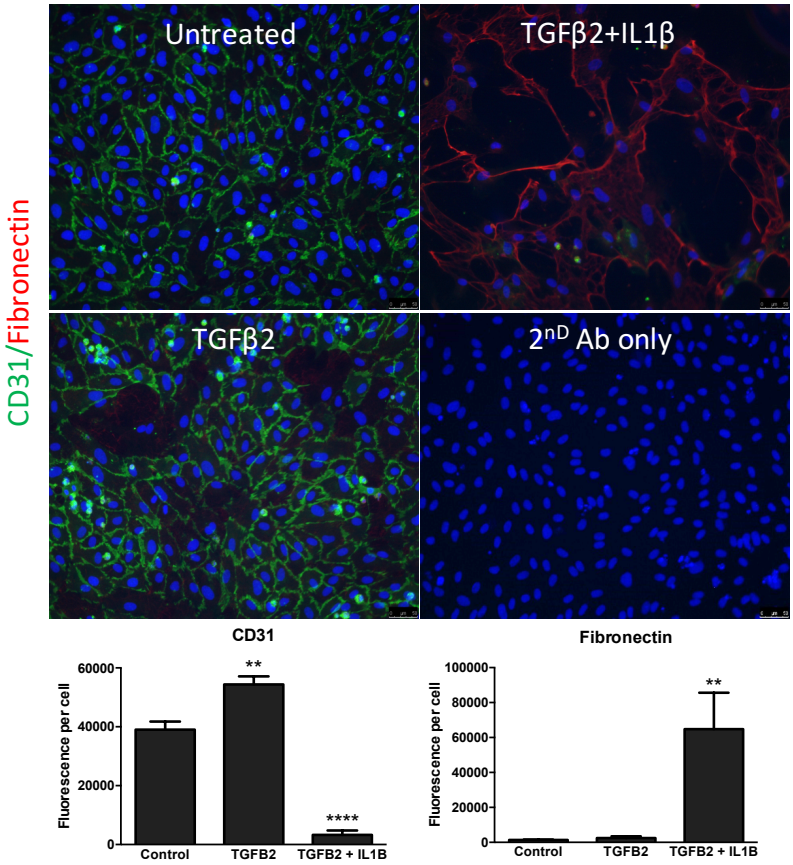


**Figure 3.7 Fibronectin and CD31 staining in HUVECs treated with TGFβ2 or TGFβ2 and ILβ1.**

HUVECs were treated for 6 days with TGFβ2 (10ng/ml) or TGFβ2 and ILβ1 (10ng/ml). Double immunofluorescence was performed for CD31 followed by a secondary antibody Alexa fluor 488 and fibronectin followed by a secondary antibody DyLight 550 conjugate. Nuclei were counterstained with DAPI. Pictures were taken with Zeiss axioimager II upright (original magnification ×20) Fluorescence was quantified using image J. Values are mean +/- SD of three pictures for each condition. *(*n =3) Statistical significance was assessed by One-way ANOVA followed by Tukey test *(**, p<0.01; ****, p<0.0001).*

As previously observed with the junction marker VE-cadherin, CD31 was displayed at the cell membrane in untreated cells and TGFβ2 treated cells. Furthermore,TGFβ2 treatment increased significantly the expression of CD31. In these two conditions , no significant change of fibronectin expression was observed. However, cells treated with TGFβ2 and IL1β showed a 46 fold increase expression of fibronectin and a 12 fold

decrease of CD31. At protein level, TGB2 and IL1b treatment was able to reduce the expression of VE cadherin and CD31 meanwhile fibronectin expression was increased. Similar to the experiments performed with HMEC1, gene expression of endothelial and mesenchymal markers were assessed in HUVEC. Cells were treated for 24 , 48 & 72 hours respectively with TGFβ2 (10ng/mL) and IL1β (10ng/mL) in order to study gene expression by qRT-PCR. Ct values obtained for each gene and each treatment condition were normalised to the Ct values of an endogenous control Hprt1. Then, fold change was calculated using $2^{-\Delta\Delta CT}$ method.

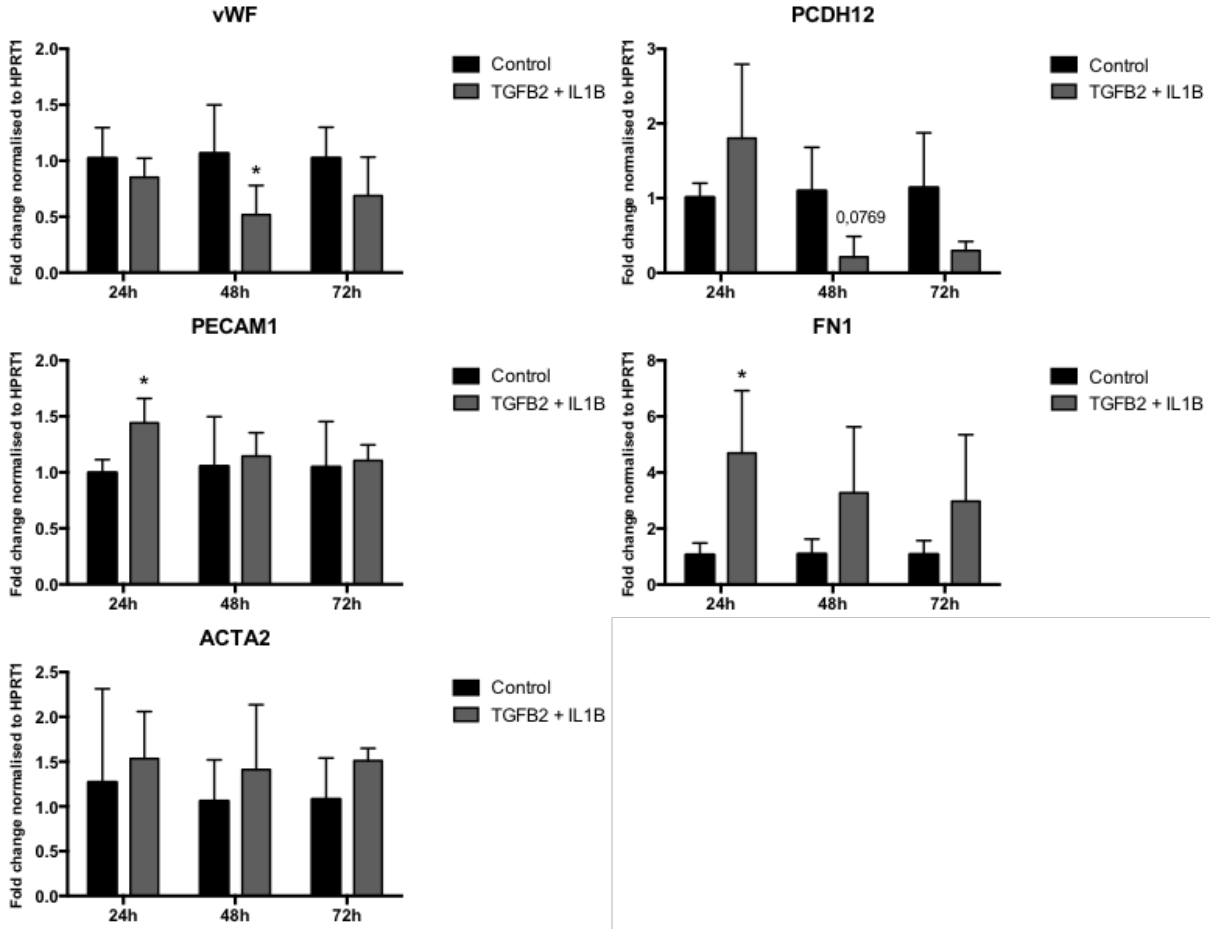


**Figure 3.8 Effect of TGFβ2 and IL1β treatment on genes expression in HUVEC**
Cells were treated from 24 hours to 72 hours with TGFβ2 and IL1β (10ng/ml). RNA was extracted, cDNA was synthesised by reverse transcription and a qRT-PCR was performed to study genes expression. Each gene expression was normalised to expression of the housekeeping gene Hprt1 and compared to the control. Errors bars are representative of standard deviations. All data is representative of three independent experiments and statistical significance was calculated by multiple unpaired Student's *t* test. *(*, p <0.05)*

In the **figure 3.8**, VE-cadherin encoded by PCDH12 tends to increase in the first 24 hours post-treatment but was down-regulated at 48 hours (p=0,077) and 72 hours (p=0,121). These results are correlated with the results obtained in **figure 3.6** where

the protein VE-cadherin expression was significantly decreased at 3 and 6 days post treatment.

Regarding CD31(PECAM1) expression, the treatment did not contribute to any change in expression. Interestingly, these results do not correspond to the results obtained at protein level as the treatment induced a significant decrease of CD31 6 days post-treatment. As observed in HMEC1 cells, vWF was significantly decreased 48 hours post treatment.

In conclusion, the TGFβ2 and IL1β induce decrease of PCDH12( VE-cadherin) and vWF gene expression but did not affect PECAM1 expression.

Fibronectin gene expression (FN1) was significantly increased 24 hours post treatment and the fibronectin protein (**Figure 3.7**) was also found up-regulated 6 days post-treatment. The treatment did not change the expression of alpha SMA and the same results were observed in HMEC1 cells.

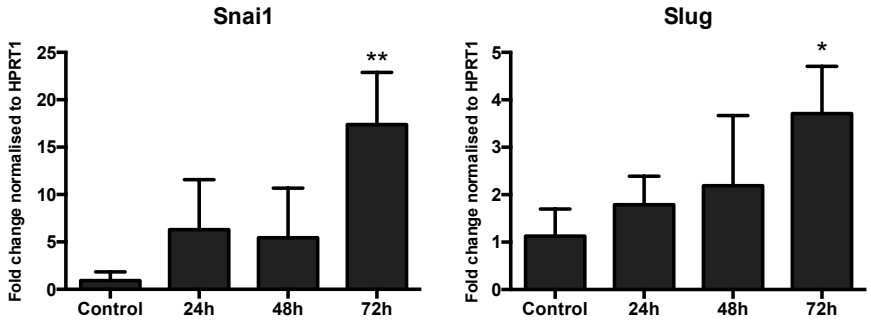


**Figure 3.9 Effect of TGFβ2 and IL1β treatment on transcription factors expression in HUVEC**

Cells were treated from 24 hours to 72 hours with TGFβ2 and IL1β (10ng/ml). RNA was extracted, cDNA was synthesised by reverse transcription and a qRT-PCR was performed to study transcription factors expression. Each gene expression was normalised to expression of the housekeeping gene Hprt1 and compared to the control. Errors bars are representative of standard deviations. All data is representative of three independent experiments and statistical significance was calculated by One-way ANOVA followed by Tukey test. *(*, p <0.05; **, p<0,01)*

Snai1 (Snail) and Snai2 (Slug) are transcription factors from the transcriptional repressor family and are implicated in loss of cell adhesion by suppressing gene encoding protein involved in cell-cell junctions. Mostly described in epithelial-to-mesenchymal transition, both factors were found involved in endothelial-to mesenchymal transition.(Kokudo *et al.*, 2008; Medici *et al.*, 2011; Cooley *et al.*, 2014) Their expression was assessed in HUVEC post-treatment with TGFβ2 and IL1β(10ng/ml). Cells were treated from 24 hours to 72 hours. Both Snail and Slug were significantly up-regulated 72 hours post-treatment (17.4 fold $\pm$ 5.5 and 3.7 fold $\pm$ 1.0 respectively)(**Figure 3.9**).

## 3.5 Discussion

Endothelial-to-mesenchymal transition is required for building valve in heart development meanwhile in fibrosis, this transition increases the number of fibroblasts and therefore contributes to the pathologic tissue repair. *In vitro* model of EndMT were developed to understand the mechanism behind the transition. In this study, *in vitro* model of EndMT based on the treatment with TGFβ2 and IL1β was investigated and optimised in endothelial cell line and primary endothelial cells.

During EndMT, endothelial cells lose their basal apical polarity and a monolayer disruption is observed. They start acquiring a front rear polarity, develop some migratory and invasive properties. This transition is characterized by the decrease of endothelial markers such CD31, VE-cadherin and the increase of mesenchymal markers such as alpha SMA, and the secretion of components of the ECM.

| Endothelial markers Down-regulated in EndMT | Mesenchymal markers Up-regulated in EndMT | Transcription Factors Up-regulated in EndMT |
|---|---|---|
| CD31/PECAM1 | α-SMA/ACTA2 | Snail |
| vWF | FSP1 | Slug |
| VE-cadherin/ PCDH12 | SM22α | Twist1 |
| eNOS | N-cadherin | |
| Claudin-5 | Collagen I and III | |
| | Fibronectin | |
| | Calponin | |

**Table 3.1 General markers studied in EndMT**

In this project, TGFβ2 was not able to induce fibronectin expression by endothelial cells on its own at protein level. However, expression of fibronectin was significantly increased when endothelial cells were treated with TGFβ2 combined to a pro-inflammatory cytokine IL1β. Increased expression of fibronectin was also described in a model of EndMT where HUVECs were exposed to oxidative stress. In this model, the RNA silencing of TGFβ1 or TGFβ2 led to a decrease of fibronectin expression confirming the important role of TGFβ family in EndMT (Montorfano *et al.*, 2014). Interestingly, in-vivo studies showed that TGFβ2 was the most expressed isoform in EndMT in mouse and avian heart (Camenisch *et al.*, 2002). In mouse model TGFβ1 $^{-/-}$ and TGFβ3 $^{-/-}$, endothelial-to-mesenchymal transition was functional whereas TGFβ2 $^{-/-}$ exhibited cardiac phenotype defect. These results point out that TGFβ2 might be the

most relevant isoform in EndMT. In human umbilical vein endothelial cells, co-stimulation with TGFβ2 and IL1β synergistically promoted EndMT. In the same study, the role of TGFβ1 and TGFβ2 in the initiation of EndMT was assessed. Co-stimulation of TGFβ1 and IL1β induced only a 6 fold increase of the mesenchymal marker SM22α whereas TGFβ2 and IL1β treatment induced a 17 fold increase of the same marker (Maleszewska *et al.*, 2013). Thus, the co-treatment TGFβ2 and IL1β seemed the most efficient treatment to generate EndMT

Post-treatment with TGFβ2 and IL1β , HMEC1 cells showed an significant up-regulation of fibronectin and down-regulation of VWF at gene expression level. CD31 expression was non significantly decreased after 48 hours and 72 hours of treatment. Unexpectedly ,VE cadherin gene expression presented very low Ct value and the results were not included as VE cadherin expression could not be differentiated from background expression. In the study of Kryczka et al, EndMT was induced in HMEC1 with TGFβ2 treatment, EndMT was observed with the decrease of VE cadherin and PAI and the increase of fibronectin and FSP-1 (Kryczka *et al.*, 2017). The low expression of VE cadherin in our model might be due to the high passage of the cells that can cause phenotypic changes and disturb the expression of endothelial markers.

The potentiality of TGFβ2 or TGFβ2 and IL1β treatment to induce EndMT in primary endothelial cells HUVEC was examined at protein and RNA level. At protein level, fibronectin was significantly increased and endothelial markers such as VE- cadherin and CD31 were significantly decreased after 6 days of treatment with TGFβ2 and IL1β. However, TGFβ2 alone was not sufficient to induce the decrease of endothelial markers neither the increase of fibronectin in our experiments. To investigate EndMT at RNA level, cells were treated up to 3 days and gene expression was studied at 24 hours, 48 hours and 72 hours. vWF was significantly down-regulated 48 hours post-treatment and fibronectin was significantly increased in the first 24 hours. VE cadherin was upregulated in the first 24 hours and then non significantly down-regulated at 48 and 72 hours. Unexpectedly, alpha SMA expression, the marker for activated fibroblast, was unchanged.

Several models of EndMT have been developed with HUVEC, cells were subjected to oxidative stress, treatment with TGFβ2 alone or combined with IL1β (R Kumarswamy *et al.*, 2012; Maleszewska *et al.*, 2013; Montorfano *et al.*, 2014). In the study of Kumarswamy et al, HUVECs were treated daily with TGFβ2 and evidence showed that this treatment decreased VE-cadherin and increased FSP1 protein expression.

Furthermore, the combination of TGFβ2 and IL1β lead to a synergistic induction of EndMT where IL1β is necessary to induce EndMT and not to maintain it. Thus, TGFβ2 have the potential to generate EndMT in HUVEC, however a daily renewal or a longer treatment might be required to observe the first sign of the transition of endothelial cells in mesenchymal cells.

At gene expression level, our results were comparable to the study of Maleszewska et al where HUVECs were treated with TGFβ2 and IL1β for 15 days. Each gene expression was analysed at day 1, 3, 5, 7 10 and 14. They showed that vWF was significantly down-regulated 3 days post-treatment and fibronectin significantly up-regulated 24 hours post-treatment. In correlation, with our results, TGFβ2 and IL1β treatment did not induce an increase of alpha SMA before the day 7. However, VE-cadherin expression displayed different results as its expression was up-regulated until day 7 post-treatment and non-significantly down-regulated at 15 days post treatment (Maleszewska *et al.*, 2013). Difference in VE-cadherin expression could be explained by a difference of confluence of the cells.

In our model, both Snai1 and Slug were significantly up-regulated 72 hours post treatment with TGFβ2 and IL1β which was in concordance with the literature. Indeed, Snail and Slug ( respectively Snai1 and Snai2) are zinc finger transcription factor and are involved in the repression of E-cadherin in the context of EMT. Several studies shows that both factors might be involved in EndMT (Kokudo *et al.*, 2008; Li and Jimenez, 2011; Medici *et al.*, 2011; Cooley *et al.*, 2014; Seo-Hyun Choi *et al.*, 2015; Xu *et al.*, 2015). On mouse pulmonary endothelial cells, TGFβ1 treatment induced up-regulation of alpha SMA and Snai1. Li et Jimenez showed that the silencing of Snai1 repress TGFβ1-induced alpha SMA expression (Li and Jimenez, 2011). Furthermore in TGFβ1 treated HUVEC, both Snai1 and Slug were found up-regulated post-treatment (Cooley *et al.*, 2014). Increased expression of Snai1 was also observed in hypoxia-induced EndMT in human coronary endothelial cells (Xu *et al.*, 2015). The silencing of Snai1 in endothelial cells treated with TGFβ2 prevented the TGFβ2-induced EndMT as well as observed in TGFβ1-induced EndMT model (Medici *et al.*, 2011) .

In this chapter, model of EndMT was successfully established with TGFβ2 and IL1β treatment in HMEC1 and HUVEC. HMEC-1 cells were considered as a suitable model of endothelial cells for EndMT research as it bears most of the endothelial cell features. Furthermore, the use of a cell line allows less variability for data acquisition. Post-treatment in HMEC1 , vWF and CD31 were down-regulated and fibronectin was up-

regulated suggesting an induction of the transdifferentiation. However, HMEC1 were not expressing VE-cadherin unlike the primary endothelial cells HUVEC. In HUVEC, the endothelial markers such as vWF, VE cadherin and CD31 were down-regulated post-treatment meanwhile fibronectin was increased. Marker of activated fibroblast, alpha SMA was not up-regulated post-treatment in both cell type which correspond to previous observations. In addition, analysis of transcription factors Snail and Slug in HUVEC showed an increased expression post-treatment. Therefore, the use of primary endothelial cells seemed more appropriate to establish a model of EndMT in vitro.

# Chapter 4. MicroRNA profile in endothelial-to-mesenchymal transition in-vitro

## 4.1 Introduction

In Chapter 3, an *in vitro* model of endothelial-to-mesenchymal transition was developed. EndMT was shown to have occurred in a pro-fibrotic environment, following treatment of endothelial cells with TGFβ2 and IL1β. To date very few studies have demonstrated that miRNAs may regulate signalling pathways involved in EndMT. In order to study associated miRNA expression profiles a miRNA array was therefore performed in Chapter 4.

Two *in vitro* studies reported the implication of miRNAs in EndMT. In the TGFβ2-induced EndMT model, the miR-29 family was found to be significantly down-regulated. Mimic transfection of miR-29a, miR-29b and miR-29c independently inhibited EndMT. Indeed, cell migration and mesenchymal markers were decreased meanwhile endothelial markers were increased (Kanasaki *et al.*, 2014).
In HUVEC and human umbilical artery endothelial cells (HUAEC), inhibition of the let-7 family lead to an increase in TGFBR1 receptor and an activation of TGFβ signalling pathway. This activation resulted in transdifferentiation of endothelial cells in mesenchymal cells (Chen *et al.*, 2012).

Most studies have focussed on one miRNA and its targets. In high-glucose-induced EndMT, miR-18a-5p and miR-320 were found to be down-regulated (Feng and Chakrabarti, 2012; Geng and Guan, 2017). Over-expression of miR-18a-5p in high glucose conditions prevented EndMT by decreasing levels of mesenchymal markers and by increasing endothelial marker expression. In the same study, a target prediction tool and experimental validation showed that the Notch2 receptor, known to induce EndMT, was a direct target of miR-18a-5p, implying that the down-regulation of miR-18a-5p could trigger EndMT (Geng and Guan, 2017).
In the study of He et al, HUVEC cells were treated with serum from Kawasaki disease patients. Kawasaki disease is an inflammatory disease which affects the vasculature and cells implicated in the arterial wall damage could originate from EndMT. When endothelial cells were treated with the serum, EndMT was induced and expression of CTGF,a key factor in EndMT, was markedly increased. Prediction target tools and

experimental validation revealed that CTGF was a direct target of miR-483. In fact, miR-483 was found down-regulated in KD sera, and its over-expression attenuated the process of EndMT, via the silencing of CTGF (He *et al.*, 2017).

| Cells | miRNAs | Ref. |
|---|---|---|
| Endothelial progenitor cells | ↓126-5p | (Zhang *et al.*, 2013) |
| Human aortic endothelial cells | ↓200a | (Zhang *et al.*, 2017) |
| Human aortic valve endothelial cells | ↓18a-5p | (Geng and Guan, 2017) |
| Human coronary artery endothelial cells | ↑155 | (Sun *et al.*, 2017) |
| Human dermal microvascular endothelial cells | ↓let-7,29 | (Srivastava *et al.*, 2013; Kanasaki *et al.*, 2014) |
| Human pulmonary endothelial cells | ↑21-5p | (Kwon *et al.*, 2016) |
| Human umbilical artery endothelial cells | ↓let-7 | (Chen *et al.*, 2012) |
| Human umbilical vascular endothelial cells | ↓let-7,20a,320,483<br>↑21-5p,216a | (Chen *et al.*, 2012; Feng and Chakrabarti, 2012; R. Kumarswamy *et al.*, 2012; Correia *et al.*, 2016; He *et al.*, 2017) |
| Lung microvascular endothelial cells | ↑130a | (Li *et al.*, 2017) |
| Mouse cardiac endothelial cells | ↓122a,127,196,375<br>↑let-7, 21-5p, 30b, 125b, 195 | (Ghosh *et al.*, 2012) |
| Mouse embryonic endothelial cells | ↑155 | (Bijkerk *et al.*, 2012) |

**Table 4.1 MiRNAs expression profile according to the type of endothelial cells undergoing EndMT in vitro.**
Down-regulated miRNAs in EndMT model are represented in green and up-regulated miRNAs in red.

Some miRNAs have been found to be up-regulated in TGFβ-induced EndMT including miR-21-5p, miR- 216a, miR-155 and miR-130a. .
Regarding miR-155, miR-216a and miR-130a, their expression was elevated post-treatment with TGFβ isoforms TGFβ1, TGFβ2 and TGFβ3 respectively. Each TGFβ isoform therefore seems able to induce EndMT, and each displays a differential miRNAs expression (Bijkerk *et al.*, 2012; R. Kumarswamy *et al.*, 2012; Li *et al.*, 2017).

Few studies have demonstrated a differential expression of EndMT in several cell types. In fact, miR-21-5p was studied in 3 different cell types and 4 different models of EndMT. Increased expression of mir-21-5p was observed in ionizing radiation-induced

EndMT and TGFβ-induced EndMT but contradictory results were also observed about the role of miR21-5p in EndMT. In fact, in ionizing radiation-induced EndMT, miR-21-5p was found to be dispensable factor in the induction of EndMT. Meanwhile post-treatment with TGFβ2, inhibition of miR-21-5p was shown to prevent the transition (R. Kumarswamy *et al.*, 2012; Guo *et al.*, 2015; Kwon *et al.*, 2016). Therefore, up-regulation of miR-21-5p in EndMT is implicated but its precise role remains elusive.

Given the sparse and ambiguous literature regarding EndMT and miRNA my working hypothesis for Chapter 4 was that in the model of EndMT based on treatment with TGFβ2 and IL1β, profiling associated miRNAs involvement could consolidate data from previous studies or identify new miRNAs potentially involved in EndMT.

## 4.2 Specific aims

- To assess the expression profile of miRNAs in the validated EndMT model
- To identify miRNAs potentially involved in EndMT
- To investigate the predicted target of the miRNAs selected

## 4.3 Specific material and methods

### *4.3.1 nCounter miRNA assay*

nCounter technologies are based on color-coded barcodes that allow the multiplexing of hundreds of targets in a single reaction. In miRNA assays, up to 800 miRNAs can be simultaneously assayed from 100ng of total RNA. In addition, the counting of miRNAs is direct as the detection does not require any amplification. All samples were prepared according to manufacturer's protocol. The first step involved the ligation of a miRtag sequence to miRNAs to allow a greater sensitivity and specificity. Thereafter, hybridization was performed overnight at 65˚C where excess of probe pairs target the miRNAs. The probe pair is composed of a capture probe with a biotin at the 3' end and a reporter probe with color coded barcode at the 5' end. During hybridisation, both probes form a complex with their targets (**Figure 4.1**).

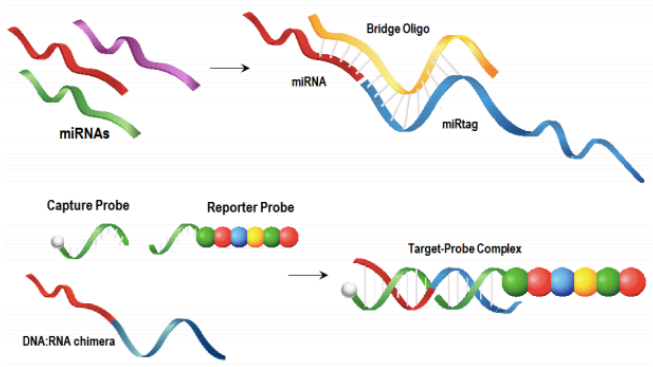


**Figure 4.1 miRtag ligation and probe annealing in nCounter assay**
(*nCounter® Technology | NanoString Technologies*, no date)**.**

After hybridisation, samples are transferred into the Prep station (Nanostring) where the complex target-probes are purified and immobilised on the nCounter cartridge (**Figure 4.2**). The cartridge is then loaded in Digital Analyzer (Nanostring) for detection and analysis. Acquired raw data were normalised against negative control to confirm specificity of the ligation reaction and estimate background hybridization counts. A second normalisation based on the positive control assessed the sample preparation step such as the ligation and the annealing. The last step includes the normalisation to the first 100 highest expressed miRNAS. Normalised data were then analysed with nSolver software.

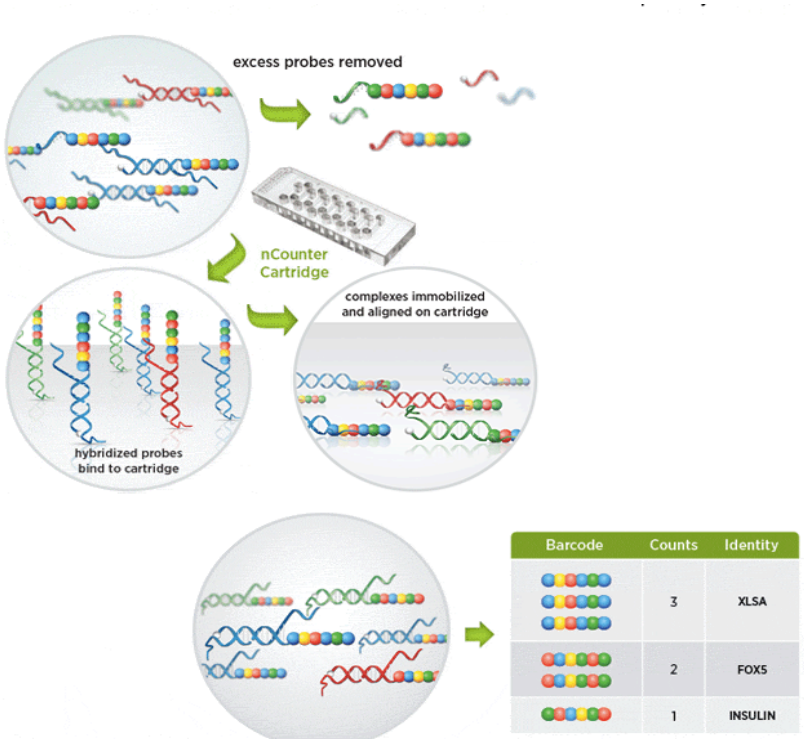


**Figure 4.2 Purification and immobilization of the complex target probe in nCounter assay**
(*nCounter® Technology | NanoString Technologies,* no date).

### *4.3.2 Prediction target tools*

Prediction target tools were developed to facilitate the search of miRNAs potential targets. The algorithm of these tools is based on the conserved Watson Crick pairing between the seed region at the 5'end of the miRNA and 3'UTR within the whole-genome alignments. The conserved Watson Crick pairing is sufficient to predict miRNAs targets and decrease the false positive predictions. In addition, a perfect seed pairing improves the target recognition. In most tools, the thermodynamic properties of the miRNA–mRNA duplex formation was considered as a criteria for target recognition (Bartel, 2009). Prediction target tools generate a table of potential targets which are sorted by a prediction score related to the specificity of the interaction. Most of these were developed to reduce false positives, however important variation was observed between tools as the predicted targets do not overlap.

Some of the common tools are:

- *TargetScan*

TargetScan is an algorithm developed in 2003 to predict miRNA target in vertebrate The last release TargetScan7 use the context++ model to identify miRNA targets and is more predictive than other tools(Agarwal *et al.*, 2015). In fact the context ++ is based on multiple features including:

- Site type (8mer> 7mer-m8> 7mer-A1)
- 3′-supplementary pairing
- Local AU content
- Distance from the closest 3′-UTR end
- Target site abundance
- Seed-pairing stability
- Predicted structural accessibility
- Probability of conserved targeting (PCT)
- 3'UTR length
- ORF length
- Offset-6mer sites in the 3′ UTR
- 8 mer in ORF
- Nucleotide in position 8 of the target
- Nucleotide in positions 1 and 8 of the sRNA

- *DIANA tool*

The DIANA tool combines a target prediction algorithm (DIANA microT-CDS), a database for experimentally verified target (Tarbase 7.0), a miRNA pathway prediction interface (miRpath) and an algorithm for the prediction of miRNA function (DIANA-mirExTra).

DIANA microT was created in 2009 and provides information on miRNA-mRNA interaction. The latest version of DIANA microT, microT-CDS, identifies miRNA targets both in the 3′UTR and in coding sequences (CDS). In this way targets with multiple sites in both regions will be ranked higher in predictions. Several features are considered such as the binding category weight, distance from the closest 3'UTR end, distance to a closest binding site, thermodynamic properties, conservation, the local AU content and the site accessibility (Paraskevopoulou *et al.*, 2013). This tool was used to study experimental verified target and to predict the pathways of miRNA targets

- *miRwalk*

MiRwalk can predict miRNAs target in the 5'UTR, CDS and 3'UTR. For 3'UTR targets, this interface allows the cross-referencing of 8 prediction target tools. For each miRNA, a table of suggested targets is generated where the ranking is based on the overlapping prediction between the online tools. Dweep *et al.*, 2011).

## 4.4 Results

### *4.4.1 Expression of miRNAs in EndMT in-vitro model*

In Chapter 3, we demonstrated that TGFβ2 and IL1β treatment was able to induce EndMT in HMEC1 and HUVEC cells. Prior to using an array to profile miRNAs involved in EndMT, initial experiments were carried out to determine the optimum cell line and time points for the experiment using miRNAs already identified as a regulator of EndMT.

*Expression of miRNAs in HMEC1*

Two candidate miRNAs were chosen to compare their expression in TGFβ2 and IL1β EndMT model based on the available literature. A multitude of studies suggest a role for miR-21-5p in fibrosis. MiR-21 was found highly expressed in failing myocardium in comparison to normal myocardium and its expression mainly came from the fibroblast population (Thum *et al.*, 2008). *In vitro*, miR-21-5p was able to partially mediate TGFβ-induced EndMT (R. Kumarswamy *et al.*, 2012). MiR-200b-3p is a member of the miR200 family and is recognised as an important regulator of EMT. In fact, miR200 targets ZEB1 and ZEB2 which are transcriptional repressors of E-cadherin, thus preventing EMT (Korpal *et al.*, 2008). In transgenic miR-200b mice, EndMT induced by diabetic conditions is reduced, implying the role of miR200b (Feng *et al.*, 2016b).

HMEC1 cells were treated with TGFβ2(10ng/mL) and IL1β(10ng/mL) for 18 and 24 hours. From the total RNA, miRNA-21-5p and miR200-3p were converted in cDNA using specific reverse transcriptase primer and qPCR was performed. An endogenous control rnU6 was quantified for normalisation and data were analysed with the delta Ct method ($2^{-\Delta\Delta CT}$ method). Each miRNA expression in treated cells was compared to the untreated cells.

After 18 hours of treatment, both expression of miR-21-5p and miR-200-3p seemed unchanged. However, miR-21-5p expression was non-significantly increased 24 hours post-treatment. (2,2 fold±0,3) (**Figure 4.3**). Similarly, an elevated expression of miR-200-3p was observed 24 hours post-treatment (1,7 fold±0,2). Up-regulation of miR-21-5p was predictable from previous studies, whereas the up-regulation of miR-200b-3p, a miRNA known to prevent EndMT, differed from literature data.

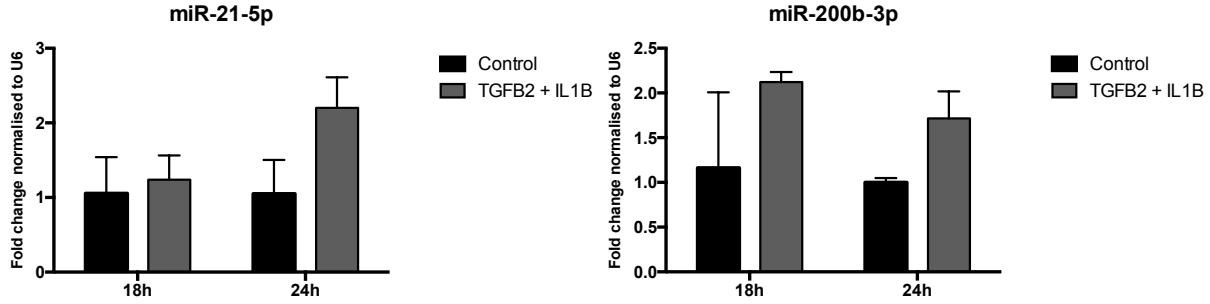


**Figure 4.3 Effect of TGFβ2 and IL1β treatment on miRNAs expression in HMEC1**
Cells were treated for 18 and 24 hours with TGFβ2 and IL1β (10ng/ml). Total RNA enriched in miRNAs was extracted, cDNA was synthesised by reverse transcription with specific miRNA primer and a RT-qPCR was performed to study miRNA expression. Each miRNA expression was normalised to expression of the endogenous control U6 and compared to the control. Errors bars are representative of standard deviations. All data is representative of two independent experiments carried out in triplicate.

*Expression of miRNAs in HUVEC*

The candidate miRNAs studied in HMEC1, were assessed in HUVECs undergoing EndMT. In addition, another miRNA miR-195-3p was chosen for assessment. MiR-195-3p was previously found up-regulated in EndMT, along with miR-21-5p and miR-125-5p. In this study, cardiac endothelial cells were treated for 7 days with TGFβ2 to induce the transition and miRNA profile was assessed with a mouse miRNA array.(Ghosh *et al.*, 2012)The magnitude of the difference in expression of miR-195-5p after EndMT makes it a promising candidate.

TGFβ2(10ng/mL) and IL1β(10ng/mL) were added to HUVEC cultures for 18 hours and 24 hours respectively.

MiR-21-5p was found to be significantly up-regulated at both 18 and 24 hours of treatment with 1,8 fold$\pm$0,3 and 3,6 fold$\pm$1,5 respectively (p=0,002 and p=0,012). The expression of miR-200b-3p seemed unchanged at 18 hours and tended to increase after 24 hours of treatment 3,9 fold$\pm$3,4 and 3,0 fold$\pm$1,9 respectively (p=0,37 and p=0,15). These results correlate with the miRNA expression observed in HMEC1. Regarding miR-195-3p, its expression was significantly increased only 18 hours post-treatment (p=0,048) and correlate with published results obtained in cardiac endothelial cells treated with TGFβ2 (**Figure 4.3**).

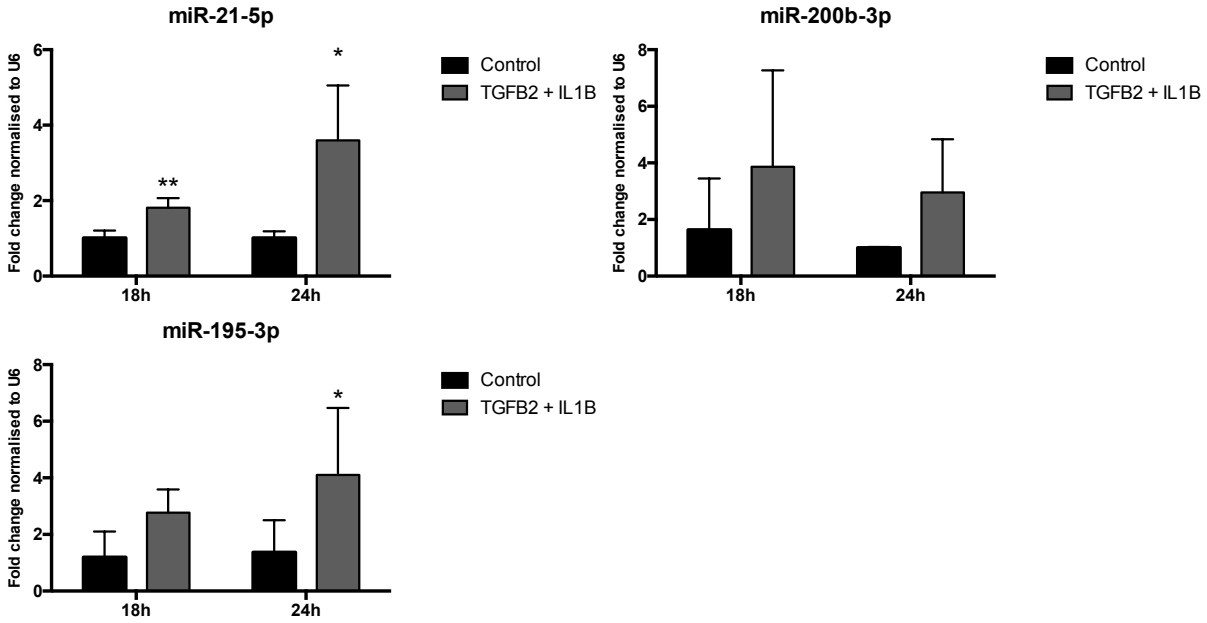


**Figure 4.4 Effect of TGFβ2 and IL1β treatment on miRNAs expression in HUVEC**
HUVECs were treated for 18 and 24 hours with TGFβ2 and IL1β (10ng/ml). Total RNA enriched in miRNAs was extracted, cDNA was synthesised by reverse transcription with specific miRNA primer and a qRT-PCR was performed to study miRNA expression. Each miRNA expression was normalised to expression of the endogenous control U6 and compared to the control. Errors bars are representative of standard deviations. All data is representative of three independent experiments carried out in triplicate. Statistical significance was calculated by multiple unpaired Student's *t* test. *(*, p <0.05; **, p<0,01)*

### *4.4.2 MiRNA profile in an in vitro model of EndMT*

*Up-regulated miRNAs expression*

In order to define a miRNA signature in EndMT, a nCounter miRNA assay( Nanostring) was performed. Nanostring technologies requires only 100ng of total RNA and allows the quantification of up to 800 miRNAs without amplification in a single condition.
Primary cells HUVECs were preferred to the endothelial cell line HMEC1 for this assay as HUVECs were more responsive to the treatment with TGFβ2 and IL1β and markedly underwent EndMT.

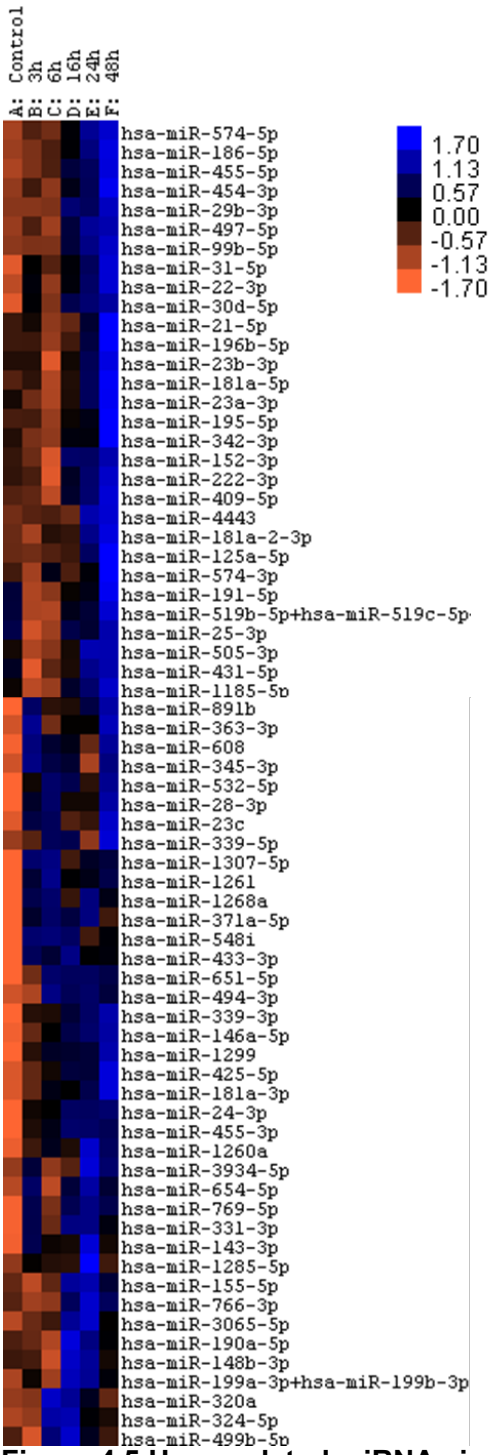


**Figure 4.5 Up-regulated miRNAs in HUVEC post-treatment with TGFβ2 and IL1β**
Cells were treated from 3 to 48 hours with TGFβ2 and IL1β(10ng/mL). Total RNA was isolated and miRNAs expression was assessed with nCounter miRNAs expression panel. MiRNAs were ligated to specific probes with color-coded barcode and quantification was performed by imaging. MiRNA expression was normalised to positive and negative control. The heatmap illustrates the relative expression of up-regulated miRNA expression. Orange and blue colours represent decreased and increased expression of miRNAs, respectively. (n=2)

HUVECs were treated with TGFβ2 and IL1β from 3h to 48h and total RNA including small RNAs was extracted. As the cartridge contain 12 wells, each condition was performed in duplicate. To the 100 ng of total RNA, a miRtag sequence was first added to the miRNAs. Thereafter probes were hybridised to the miRNAs targeted and went

through purification steps. Then, the complex probe-miRNAs were immobilised in the cartridge and analysed in the Digital analyser (Nanostring). Raw data was normalised in three steps (1) Against the negative control (2) with the positive controls (3) with the top 100 highest expressed miRNAs. As each condition was performed in duplicate, data were grouped by time point. A heatmap was generated on nSolver Analysis software with normalised grouped data summarised the up-regulated miRNAs post-treatment with TGFβ2/IL1β and therefore up-regulated in EndMT. In the **Figure 4.5**, blue pixels correspond to an elevated abundance of the miRNA whereas orange pixels indicate low miRNA levels. The heatmap revealed a differential of expression within the up-regulated miRNAs. In fact, some miRNAs with low expression level in the untreated cells (control) were found to be up-regulated at the earliest time point; miR-494-3p and miR-146a-5p after 6 hours of treatment or miR-433-3p after 3 hours. For other miRNAs, the level of expression was increased at 24 hours post-treatment, which was the case for miR-21-5p and miR-195-5p. Their expression profile correlated with results obtained by RT-qPCR in the **Figure 4.4**.

*Down-regulated miRNAs expression*

Similarly to the figure 4.5, a heatmap was generated summarising miRNAs down-regulated post-treatment with TGFβ2 and IL1β. The colour coding of the heatmap is blue for elevated abundance and orange for low miRNA expression. As in **Figure 4.5**, expression profile was variable within the down-regulated miRNAs. Expression of miR-126-3p was decreased with time of treatment. Some miRNAs expression was decreased at the earliest time point such as miR-151a-5p and some at the latest time point such as miR-125b-3p.

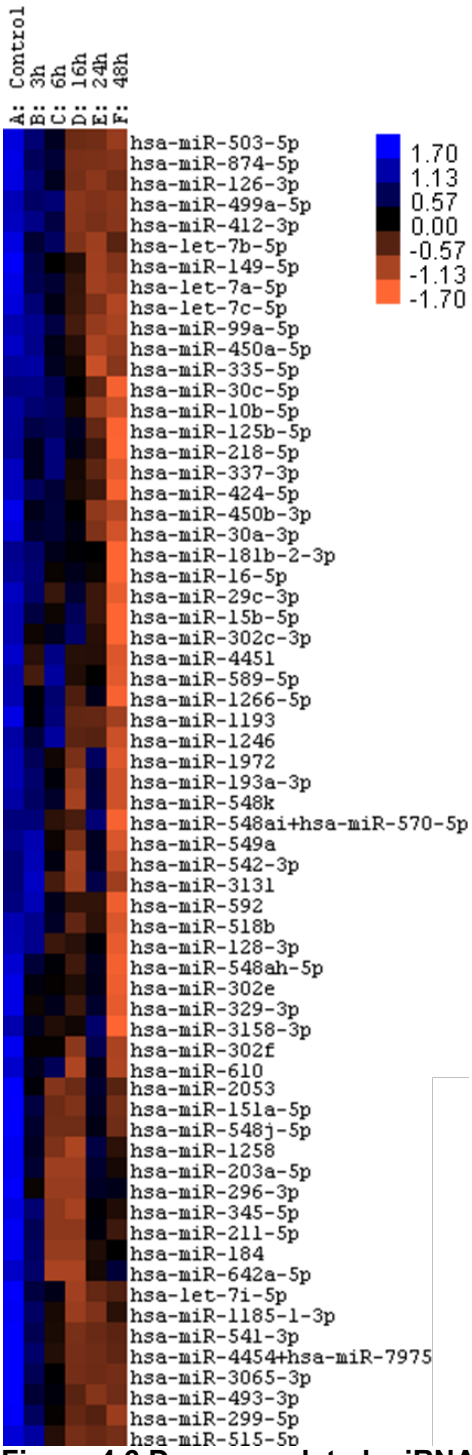


**Figure 4.6 Down-regulated miRNAs in HUVEC post-treatment with TGFβ2 and IL1β**
Cells were treated from 3 to 48 hours with TGFβ2 and IL1β(10ng/mL). Total RNA was isolated and miRNAs expression was assessed with nCounter MiRNAs expression panels. MiRNAs were ligated to specific probes with color-coded barcode and quantification was performed by imaging. MiRNA expression was normalised to positive and negative control. The heatmap illustrates the relative expression of down-regulated miRNA. Orange and blue colours represent decreased and increased expression of miRNAs, respectively. (n=2)

### 4.4.3 First selection of miRNA candidates

Potential markers of EndMT were initially selected depending on their fold change in comparison to the control, a list of the most-upregulated miRNAs and most down-regulated miRNAs was generated. Each microRNA was then run into miRpath from the Diana tool. MiRNAs were chosen depending on signalling pathways of their predicted targets. Pathways that could plausibly be involved in EndMT such as adherens junction, ECM receptor interaction or TGFβ signalling were prioritised and reduced the number of potential candidates. As algorithms are different for each prediction target tool, predicted targets were compared with each prediction target tool. Six miRNAs were selected including 3 up-regulated and 3 down-regulated post-treatment with TGFβ2 and IL1β.

| | | Fold change | | | | |
|---|---|---|---|---|---|---|
| miRNA | Accession number | 3h | 6h | 16h | 24h | 48h |
| hsa-miR-146a-5p | MIMAT0000449 | 4.05 | 10.87 | 22.31 | 31.10 | 54.00 |
| hsa-miR-494-3p | MIMAT0002816 | 1.42 | 30.80 | 19.46 | 22.86 | 15.00 |
| hsa-miR-548a-5p | MIMAT0004803 | 2.02 | 2.13 | -1.40 | 2.00 | 1.24 |
| hsa-miR-199b-5p | MIMAT0000263 | -4.77 | -2.72 | -5.29 | -3.18 | 1.52 |
| hsa-miR-200b-3p | MIMAT0000318 | 1.07 | -4.85 | -2.19 | -3.72 | -3.76 |
| hsa-miR-944 | MIMAT0004987 | -2.48 | -6.39 | -2.38 | -5.45 | -3.96 |

**Table 4.2 First selection of miRNAs potentially involved in EndMT**

*Validation of miRNA candidates*

MiRNAs selected as potential markers of EndMT were studied further by RT-qPCR in order to confirm the expression profile obtained with the nCounter assay. HUVEC cells were treated with TGFβ2 (10 ng/mL) and IL1β (10ng/mL) for 24 hours. Total RNA including small RNAs was extracted and RT-qPCR was performed using Taqman technologies.

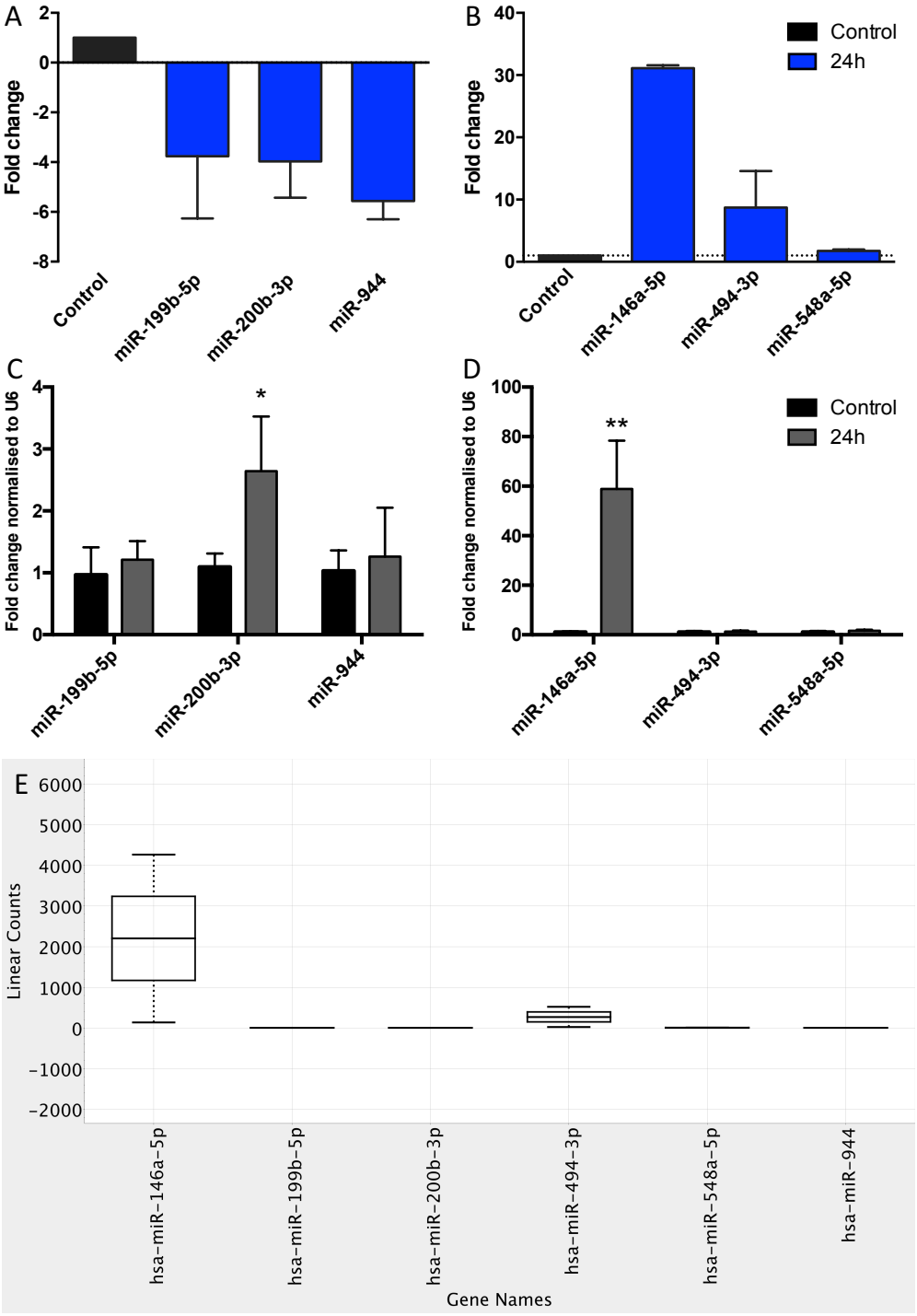


**Figure 4.7 Validation of miRNAs expression in HUVEC post-treatment with TGFβ2 and IL1β**

Cells were treated for 24 hours with TGFβ2 and IL1β(10ng/mL), total RNA was isolated and miRNAs expression was studied. **A-B** Down-regulated (A) and up-regulated (B) miRNAs expression quantified with nCounter assay (n=2). **C-D** Validation of down-regulated (C) and up-regulated (D) selected miRNAs by qRT-PCR. Statistical significance was calculated by multiple unpaired Student's *t* test. (n=3) *(*, p <0.05; **, p<0,01)* **E** Box plot of selected miRNAs count (n=2). Errors bars are representative of standard deviations.

In **Figure 4.7**, results previously obtained with the nCounter assay are represented by (A) and (B). In the same figure, (C) and (D) show the analysis of the RT-qPCR data. Unexpectedly, results were not correlated between the two methods. In fact, 24 hours

post-treatment, expression of down-regulated miRNA in the nCounter assay was unchanged for miR-199b-5p and miR-944 or significantly up-regulated for miR-200b-3p with the RT-qPCR. In a similar way, for the up-regulated miRNAs from the nCounter assay, miR-494-3p and miR-548a-5p expression was unchanged when analysed by RT-qPCR.

Only one miRNA miR-146a-5p showed similar expression profile with the nCounter assay and the RT-qPCR. After 24 hours of treatment with TGFβ2 and IL1β, miR-146a-5p was up-regulated with 31-fold increase from the nCounter assay and 59-fold increase from RT-qPCR data.

In order to understand the difference between the two methods, the quantification from the nCounter assay was studied. Each miRNA count was plotted in a box plot where the vertical axis shows the linear count and demonstrates the difference of expression between untreated cells and 24 hours post-treatment. Interestingly, only miR-146a-5p was abundant and showed a difference of 4000 counts between the treated and untreated cells. This suggests that the other miRNAs selected were low in abundance and might be part of the background.

### *4.4.4 Second selection of miRNA candidates*

A second selection of potential miRNAs involved in EndMT was initiated. Abundance of miRNA was one of the criteria of this selection and all miRNAs counts from the nCounter assay were plotted into a scatter plot. The scatter plot displayed the difference of expression in treated cells to the control with the count for treated cells on the y-axis and the count for untreated cells on the x-axis. In figure 4.8, the pink line represents the expression of miRNAs in untreated cells. Differentially expressed miRNAs were found by looking for miRNA with a large change between control. Dots below the control line are considered as down-regulated and dots above as up-regulated. As previously observed in **Figure 4.7** , counts of miR-146a-5p was elevated in treated cells and progressively increased depending on the time of treatment. MiR-494-3p was in the first selection and was found up-regulated post-treatment. However, results from PCR were not correlated to the nCounter results.

Two miRNAs with highest abundance than miR-146a-5p were down-regulated post-treatment with TGFβ2 and IL1β : miR-126-3p and miR-4454.

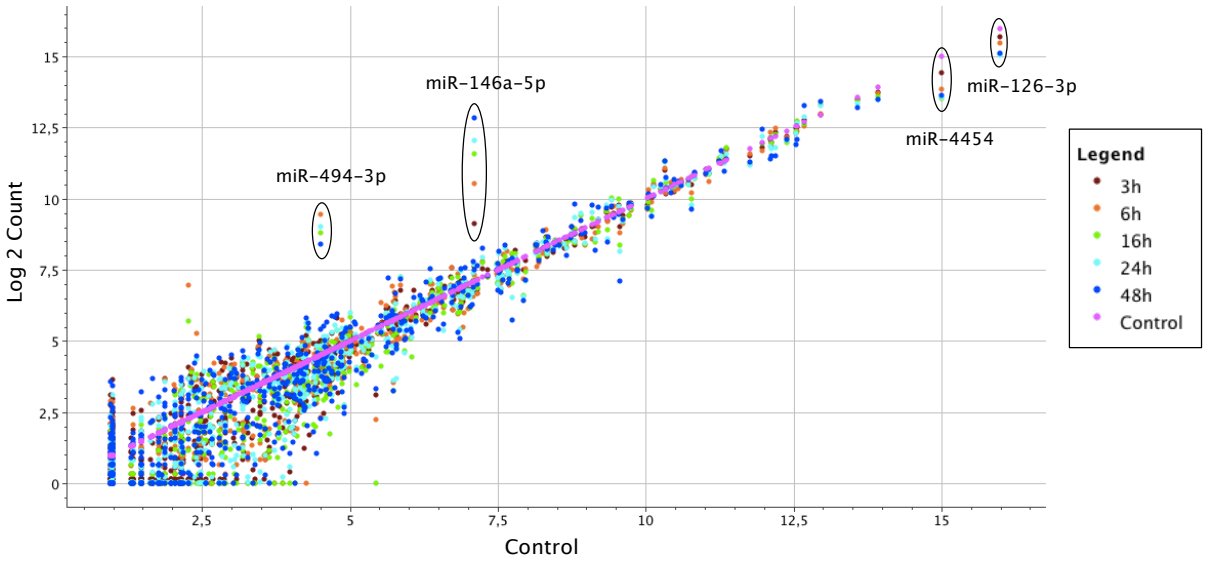


**Figure 4.8 Differential expression of miRNAs in HUVEC post-treatment TGFβ2 and IL1β**

Cells were treated from 3 to 48 hours with TGFβ2 and IL1β(10ng/mL). Total RNA was isolated and miRNAs expression was assessed with nCounter MiRNAs expression panel. MiRNAs were ligated to specific tag with color-coded barcode and quantified by imaging. MiRNA expression was normalised to positive and negative control. The scatter plot displays the variation of miRNAs counts between the control and the treated cells. (n=2) The pink dots illustrate the control. Dots above and under the control represent up-regulated and down regulated miRNAs respectively.

In order to confirm the second selection, data from nCounter assay were plotted in a volcano plot.The volcano plot shows the relationship between the fold change and the p-values. On the y-axis log2 fold change were plotted and -$\log_{10}$ p-values were plotted on the x axis. A vertical line was traced at X=0 which represent unchanged expression of miRNAs and a horizontal line at Y= 1,30 which represent the threshold for statistical significance p=0,05. In figure 4.9, the plot is based on data from 24 hours treated versus untreated cells. As expected, miR-146-5p was found in the upper right quadrant meaning that this miRNA was significantly up regulated post-treatment. The potential candidate miR-126-3p was located in the upper left quadrant and thus was significantly down-regulated post-treatment. In conclusion, miR-126-3p down regulation and miR-146a-5p up regulation might be potential markers for EndMT.

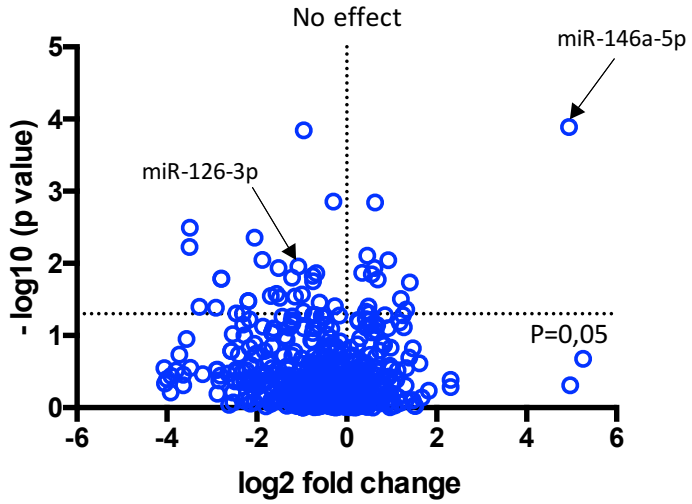


**Figure 4.9 Significant variation of miRNAs expression in HUVEC post-treatment TGFβ2 and IL1β**

Cells were treated for 24 hours with TGFβ2 and IL1β(10ng/mL). Total RNA was isolated and miRNAs expression was assessed with nCounter MiRNAs expression panel. MiRNAs were ligated to specific tag with color-coded barcode and quantified by imaging. MiRNA expression was normalised to positive and negative control. Volcano plot displays significantly up-regulated and down-regulated miRNAs. Statistical significance was calculated by multiple unpaired Student's *t* test (n=2).

*Validation of miRNA 126-3p and 146a-5p*

Expression of miR-126-3p and miR-146a-5p were analysed by RT-qPCR to validate the expression profile obtained with the nCounter assay. HUVEC cells were treated with TGFβ2 (10 ng/mL) and IL1β (10ng/mL) for 24 hours. Total RNA including small RNAs was extracted and RT-qPCR was performed using Taqman technologies. An endogenous control RnU6 for miR-146a-5p and RnU48 for miR-126-3p were quantified for normalisation and data were analysed with the delta delta Ct method ($2^{-\Delta\Delta CT}$ method). In **Figure 4.10**, expression of miR-146a-5p and miR-126-3p from nCounter assay are displayed in (A) and (B) respectively. In addition, results from RT-qPCR are represented in (C) (D) and abundance of these miRNAs in (E) (F). As previously observed in **Figure 4.7**, miR-146a-5p showed similar expression profile with the nCounter assay and the RT-qPCR. From the nCounter assay, miR-126-3p was down regulated post-treatment with a 2,9 fold decrease. The same expression profile was observed with the qPCR results as miR-126-3p was down-regulated post-treatment with 2,4 fold decrease. Both miR-126-3p and miR-146a-5p were abundant in endothelial cells and their expression profile was significantly changed post-treatment with TGFβ2 and IL1β.

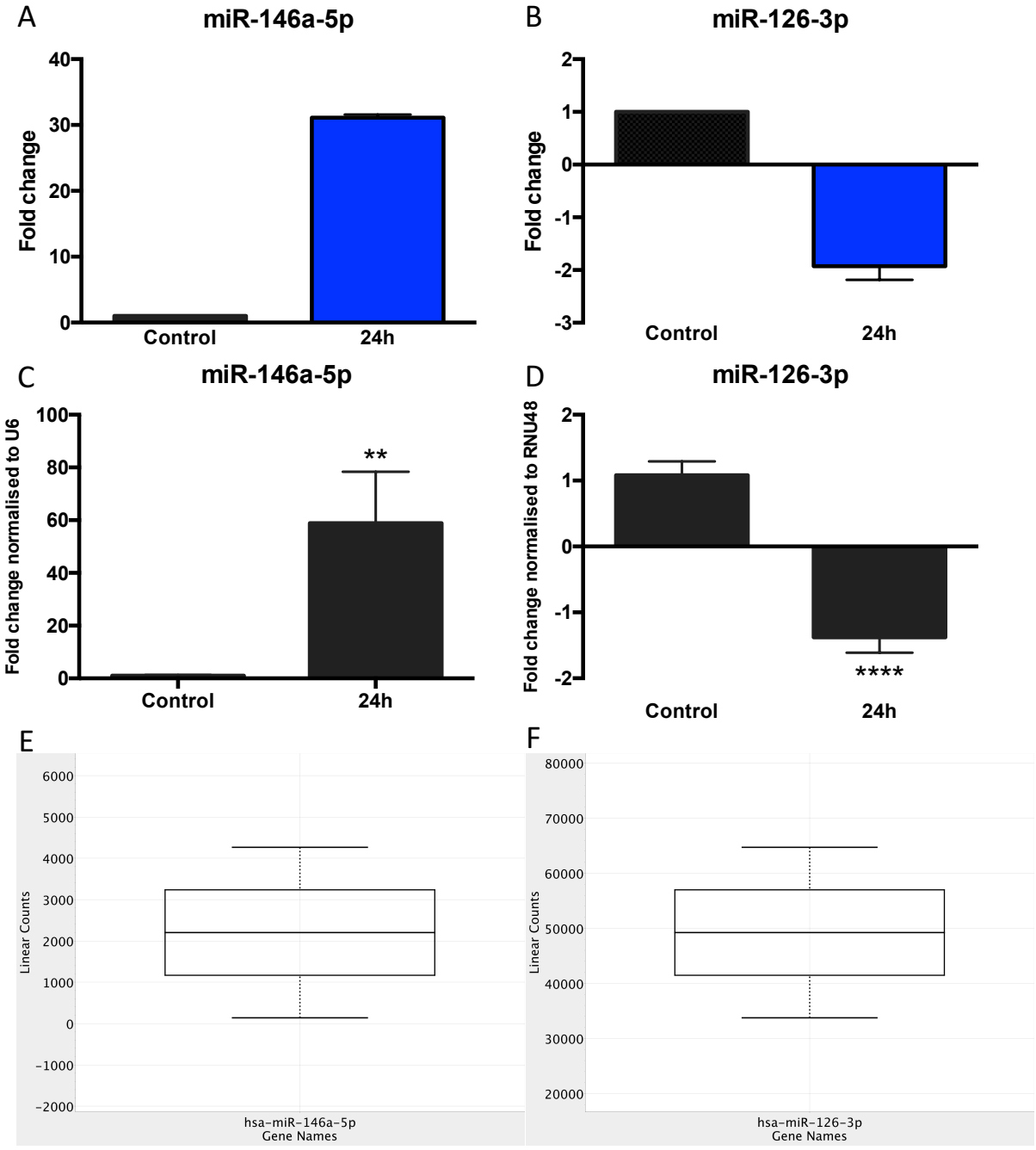


**Figure 4.10 Effect of TGFβ2 and IL1β treatment on miR-146a-5p and miR-126-3p expression in HUVEC**

Cells were treated for 24 hours with TGFβ2 and IL1β(10ng/mL). Total RNA was isolated and miRNAs expression was studied. **A-B** miRNAs expression quantified with nCounter assay. (n=2) **C-D** Validation of miRNAs by qRT-PCR. Statistical significance was calculated by multiple unpaired Student's *t* test. *(**, p <0.01; ****, p<0,0001)* (n=3) **E** miRNAs Abundance (n=2). Errors bars are representative of standard deviations.

### 4.4.5 Target prediction

Multiple studies report the role of mir-146a-5p in different biological processes. This miRNA seems to act as an oncogene in several cancers (Lu *et al.*, 2017; Zhou *et al.*, 2017), as a mediator of EMT (C. Wang *et al.*, 2016). In endothelial cells, miR-146a-5p mediates inflammation by regulating IRAK-1, an receptor for IL1β (Lo *et al.*, 2017). As the proposed EndMT model is based on IL1β treatment that triggers the TGFβ2-induced EndMT, variation of expression of miR-146a-5p might be induced by IL1β treatment and therefore does not have a role in EndMT

Interestingly, miR-126-3p was described to increase migration of endothelial cells and knockdown of this miRNA in endothelial cells impacts on the formation of tubes on matrigel (Fish *et al.*, 2008). This suggests that miR-126-3p plays a specific role in endothelial cells. The down-regulation of this miRNA post-treatment with TGFβ2 and IL1β might be due to the transition of endothelial cells in mesenchymal cells. From published data, miR-126-3p have a greater potential to be involved in EndMT than miR-146a-5p. Thus, target prediction was only performed for miR-126-3p.

As algorithm from TargetScan was the most predictive model, miR-126-3p was first run though this prediction target tool. In TargetScan, miRNA repertoire is based on mature miRNA sequences from miRbase. For some miRNAs, a difference in the 5'end can be observed after analysis which leads to the addition of miRNAs such as miR-126-3p. To distinguish the modification, a suffix .1 or .2 is added to these miRNAs and target identification is performed for each miRNA (Agarwal *et al.*, 2015). Multiple target genes were reported and were ranked according to the feature of the context++ model( see methods). From the list of potential target of miR-126-3p, two genes were identified for potential involvement in EndMT:

- ADAM9 as predicted target of miR-126-3p.1 with a 8-mer conserved site
- SMURF2 as predicted target of miR-126-3p.2 with a 7-merA1 conserved site

| Target gene | Representative transcript | Gene name | Number of 3P-seq tags supporting UTR + 5 | Link to sites in UTRs | Conserved sites | | | |
|---|---|---|---|---|---|---|---|---|
| | | | | | total | 8mer | 7mer-m8 | 7mer-A1 |
| PLXNB2 | ENST00000449103.1 | plexin B2 | 82 | Sites in UTR | 1 | 1 | 0 | 0 |
| RGS3 | ENST00000374140.2 | regulator of G-protein signaling 3 | 2735 | Sites in UTR | 1 | 1 | 0 | 0 |
| ADAM9 | ENST00000487273.2 | ADAM metallopeptidase domain 9 | 6435 | Sites in UTR | 1 | 0 | 0 | 1 |
| HERPUD1 | ENST00000379792.2 | homocysteine-inducible, endoplasmic reticulum stress-inducible, ubiquitin-like domain member 1 | 804 | Sites in UTR | 1 | 0 | 0 | 1 |
| KANK2 | ENST00000586659.1 | KN motif and ankyrin repeat domains 2 | 1735 | Sites in UTR | 1 | 0 | 1 | 0 |
| SLC7A5 | ENST00000565644.1 | solute carrier family 7 (amino acid transporter light chain, L system), member 5 | 155 | Sites in UTR | 1 | 0 | 0 | 1 |
| FBXO33 | ENST00000298097.7 | F-box protein 33 | 306 | Sites in UTR | 1 | 0 | 0 | 1 |
| PLK2 | ENST00000274289.3 | polo-like kinase 2 | 689 | Sites in UTR | 1 | 0 | 0 | 1 |
| EGFL7 | ENST00000371699.1 | EGF-like-domain, multiple 7 | 29 | Sites in UTR | 1 | 0 | 0 | 1 |
| CRK | ENST00000398970.5 | v-crk avian sarcoma virus CT10 oncogene homolog | 1841 | Sites in UTR | 1 | 0 | 0 | 1 |
| CAMSAP1 | ENST00000389532.4 | calmodulin regulated spectrin-associated protein 1 | 966 | Sites in UTR | 1 | 0 | 0 | 1 |
| IRS1 | ENST00000305123.5 | insulin receptor substrate 1 | 804 | Sites in UTR | 1 | 0 | 0 | 1 |
| BAK1 | ENST00000442998.2 | BCL2-antagonist/killer 1 | 15 | Sites in UTR | 1 | 0 | 0 | 1 |
| DIP2C | ENST00000280886.6 | DIP2 disco-interacting protein 2 homolog C (Drosophila) | 359 | Sites in UTR | 1 | 0 | 0 | 1 |
| ITGA6 | ENST00000375221.2 | integrin, alpha 6 | 1328 | Sites in UTR | 1 | 0 | 0 | 1 |
| EFHD2 | ENST00000375980.4 | EF-hand domain family, member D2 | 1411 | Sites in UTR | 1 | 0 | 0 | 1 |
| GNA13 | ENST00000439174.2 | guanine nucleotide binding protein (G protein), alpha 13 | 190 | Sites in UTR | 1 | 0 | 0 | 1 |
| TRIM46 | ENST00000392451.2 | tripartite motif containing 46 | 69 | Sites in UTR | 1 | 0 | 0 | 1 |
| PCDH7 | ENST00000543491.1 | protocadherin 7 | 95 | Sites in UTR | 1 | 0 | 0 | 1 |
| GBP2 | ENST00000370466.3 | guanylate binding protein 2, interferon-inducible | 1309 | Sites in UTR | 1 | 0 | 0 | 1 |
| AKAP13 | ENST00000394518.2 | A kinase (PRKA) anchor protein 13 | 53 | Sites in UTR | 1 | 0 | 0 | 1 |
| TRAF7 | ENST00000326181.6 | TNF receptor-associated factor 7, E3 ubiquitin protein ligase | 1505 | Sites in UTR | 1 | 0 | 0 | 1 |
| LRP6 | ENST00000261349.4 | low density lipoprotein receptor-related protein 6 | 157 | Sites in UTR | 1 | 0 | 0 | 1 |
| PTPN9 | ENST00000306726.2 | protein tyrosine phosphatase, non-receptor type 9 | 644 | Sites in UTR | 1 | 1 | 0 | 0 |
| SAMD14 | ENST00000330175.4 | sterile alpha motif domain containing 14 | 88 | Sites in UTR | 1 | 0 | 1 | 0 |

**Table 4.3 Target prediction of miR-126-3p.1 from TargetScan Release 7.2**

ADAM9 is a type I transmembrane protein with disintegrin and metalloprotease domain-containing protein 9. The metalloproteinase domain allows the cleavage and the release of cell surface proteins. This includes cytokines, growth factors or cell adhesion molecules. *In vitro*, over-expression of ADAM9 and membrane protein in Cos7 cells showed an increase in level of shedding for endothelial markers such as VE-cadherin or VCAM1 (Guaiquil *et al.*, 2009). In addition, evidence showed that ADAM9 over-expression enhance the recycling of E-cadherin in colon cancer cell, thus promoting EMT (HIRAO *et al.*, 2005). Considering that ADAM9 promotes EMT and is able to cleave cell adhesion molecule in endothelial cells, this protein might have a role in EndMT

| Target gene | Representative transcript | Gene name | Number of 3P-seq tags supporting UTR + 5 | Link to sites in UTRs | Conserved sites | | | |
|---|---|---|---|---|---|---|---|---|
| | | | | | total | 8mer | 7mer-m8 | 7mer-A1 |
| S1PR2 | ENST00000590320.1 | sphingosine-1-phosphate receptor 2 | 10 | Sites in UTR | 1 | 1 | 0 | 0 |
| PCNXL4 | ENST00000535349.1 | pecanex-like 4 (Drosophila) | 268 | Sites in UTR | 1 | 1 | 0 | 0 |
| KLF10 | ENST00000285407.6 | Kruppel-like factor 10 | 320 | Sites in UTR | 1 | 1 | 0 | 0 |
| ANKRD44 | ENST00000282272.8 | ankyrin repeat domain 44 | 187 | Sites in UTR | 1 | 1 | 0 | 0 |
| AKT2 | ENST00000392038.2 | v-akt murine thymoma viral oncogene homolog 2 | 525 | Sites in UTR | 1 | 1 | 0 | 0 |
| ADAMTS9 | ENST00000295903.4 | ADAM metallopeptidase with thrombospondin type 1 motif, 9 | 5 | Sites in UTR | 1 | 1 | 0 | 0 |
| CD97 | ENST00000357355.3 | CD97 molecule | 1041 | Sites in UTR | 1 | 1 | 0 | 0 |
| KANK2 | ENST00000586659.1 | KN motif and ankyrin repeat domains 2 | 1735 | Sites in UTR | 1 | 0 | 1 | 0 |
| TLN2 | ENST00000561311.1 | talin 2 | 371 | Sites in UTR | 1 | 1 | 0 | 0 |
| RER1 | ENST00000378512.1 | RER1 retention in endoplasmic reticulum 1 homolog (S. cerevisiae) | 2954 | Sites in UTR | 1 | 0 | 0 | 1 |
| LGALSL | ENST00000409537.2 | lectin, galactoside-binding-like | 334 | Sites in UTR | 1 | 1 | 0 | 0 |
| LRRC1 | ENST00000370888.1 | leucine rich repeat containing 1 | 343 | Sites in UTR | 1 | 1 | 0 | 0 |
| SMURF2 | ENST00000262435.9 | SMAD specific E3 ubiquitin protein ligase 2 | 978 | Sites in UTR | 1 | 0 | 0 | 1 |
| PDGFRB | ENST00000261799.4 | platelet-derived growth factor receptor, beta polypeptide | 320 | Sites in UTR | 1 | 0 | 1 | 0 |
| PIK3R1 | ENST00000521381.1 | phosphoinositide-3-kinase, regulatory subunit 1 (alpha) | 217 | Sites in UTR | 1 | 0 | 1 | 0 |
| PLAGL2 | ENST00000246229.4 | pleiomorphic adenoma gene-like 2 | 254 | Sites in UTR | 1 | 0 | 1 | 0 |
| PSD3 | ENST00000327040.8 | pleckstrin and Sec7 domain containing 3 | 133 | Sites in UTR | 1 | 1 | 0 | 0 |
| PLXNA4 | ENST00000321063.4 | plexin A4 | 9 | Sites in UTR | 1 | 0 | 0 | 1 |
| TADA2B | ENST00000310074.7 | transcriptional adaptor 2B | 38 | Sites in UTR | 1 | 0 | 1 | 0 |
| GPR39 | ENST00000329321.3 | G protein-coupled receptor 39 | 151 | Sites in UTR | 1 | 0 | 0 | 1 |
| ST5 | ENST00000526757.1 | suppression of tumorigenicity 5 | 139 | Sites in UTR | 1 | 0 | 0 | 1 |
| APMAP | ENST00000447138.1 | adipocyte plasma membrane associated protein | 186 | Sites in UTR | 1 | 0 | 0 | 1 |
| TEAD1 | ENST00000361905.4 | TEA domain family member 1 (SV40 transcriptional enhancer factor) | 740 | Sites in UTR | 1 | 0 | 0 | 1 |
| OTOF | ENST00000338581.6 | otoferlin | 5 | Sites in UTR | 1 | 0 | 0 | 1 |
| PDE4A | ENST00000380702.2 | phosphodiesterase 4A, cAMP-specific | 48 | Sites in UTR | 1 | 0 | 1 | 0 |
| FBXO33 | ENST00000298097.7 | F-box protein 33 | 306 | Sites in UTR | 1 | 0 | 0 | 1 |
| LPP | ENST00000312675.4 | LIM domain containing preferred translocation partner in lipoma | 1894 | Sites in UTR | 1 | 0 | 1 | 0 |
| SMEK1 | ENST00000554684.1 | SMEK homolog 1, suppressor of mek1 (Dictyostelium) | 713 | Sites in UTR | 1 | 1 | 0 | 0 |
| CISD3 | ENST00000439660.2 | CDGSH iron sulfur domain 3 | 3508 | Sites in UTR | 1 | 0 | 1 | 0 |

**Table 4.4 Target prediction of miR-126-3p.2 from TargetScan Release 7.2**

Smad ubiquitin regulatory factor 2 (SMURF2) is an E3 ubiquitin ligase that regulates TGFβ signalling. SMURF2 interacts with R-Smad(Smad1/2) and with I-Smad (Smad7) which lead to ubiquitin-dependant degradation of both Smad protein type (Inoue and Imamura, 2008). In addition, over-expression of SMURF2 reduces TGFβ-induced EMT in mammary epithelial cells (Chandhoke *et al.*, 2016). SMURF2 might have a role in EndMT as negative regulator of TGFβ signalling.

MiR-126-3p was then processed in miRwalk which allowed the comparison of predicted targets between the different prediction target tools. ADAM9 was found in the predicted target in 5 different tools including miRwalk, miRmap, Pictar2, RNA hybrid and TargetScan. Furthermore, ADAM9 is a target of miR-126-3p that is experimentally verified. Direct interaction of miR-126-3p with ADAM9 was demonstrated with a luciferase 3'UTR assay in pancreatic cancer cells. The knockdown of ADAM9 by the miRNA restored expression of E-cadherin and prevented EMT (Hamada *et al.*, 2012). Therefore, ADAM9 might be regulated by miR-126-3p during EndMT.

SMURF2 was only predicted in RNA hybrid and TargetScan. However, SMURF2 interaction with miR-126-3p was not confirmed by experiments. SMURF2 was only recognised in prediction target tool suggesting that this target might be a false positive from TargetScan.

## 4.5 Discussion

There are some miRNAs that contribute to the regulation of EndMT including positive and negative regulation. In our study, miRNAs profiles were investigated in the TGFβ2/IL1β-induced EndMT model.

Expression of miRNAs known for their implication in EndMT were studied in our model. In 24 hours treated cells with TGFβ2 and IL1β, miR-21-5p was significantly up-regulated in HUVEC and tended to increase in HMEC1. In the same way, expression of miR-195-5p was significantly increased in HUVEC 24 hours post-treatment Unexpectedly miR-200b-3p tended to increase in HMEC1 and HUVEC cells but the variation of expression did not allow conclusions to be made.

Increased miR-21-5p was previously reported in two studies where HUVEC cells were treated with TGFβ for 24 hours (R. Kumarswamy *et al.*, 2012; Guo *et al.*, 2015). In the study from Ghosh et al, EndMT was induced in mouse cardiac endothelial cells with TGFβ2, and miRNAs were screened 7 days post-treatment. Interestingly, miR-21-5p was found up-regulated along with miR-195-5p and a multitude of other miRNAs (see **Table 4.1**) (Ghosh *et al.*, 2012). The correlation of the expression of these two miRNAs corroborated our EndMT model, thus miRNAs profile could be assessed.

MiR-200b-3p was recognised as a miRNA regulating EMT by silencing co-transcriptional repressor of genes such as Cdh1 encoding for E-cadherin protein. In our lab, miR-200b-3p was found to be significantly down-regulated in human bronchial epithelial cells undergoing EMT (Ladak *et al.*, 2016) In addition, overexpression of miR-200-3p in mouse cardiac cells where EndMT was induced with high glucose, lead to an inhibition of EndMT(Feng *et al.*, 2016a). This suggests that miR-200b-3p might be down-regulated during EndMT. However, our results did not confirm this hypothesis as expression of miR-200b-3p was not significantly increased. A repeat of this

experiment would reduce the variation of expression and would have further clarified the profile of expression.

MiRNA profiling was addressed with the nCounter miRNA assay from Nanostring technologies. MicroRNA assay was performed with total RNA isolated from HUVEC and HUVEC undergoing EndMT with TGFβ2 and IL1β treatment. Each condition was duplicated and up to 800 miRNAs were quantified without amplification and identified using a color-coded barcode. MiRNA profiling showed an alteration of miRNA expression between the untreated and treated cells. Some miRNAs were found up-regulated and some others were down-regulated in EndMT. Six miRNAs were first selected and considered for validation with RT-qPCR. Selection was based on the fold change and their predicted target. MiRNA targeting mRNA that encoded for a protein that could have a role in EndMT were chosen. Unexpected results were observed during the validation by RT-qPCR. Only one miRNA, miR-146a-5p, showed concordant data for expression by RT-qPCR and miRNA obtained in the nCounter assay. Among these six candidates, miR200b-3p was selected as miRNA assay showed a 3,72 fold decrease 24 hours post-treatment and previous results obtained by RT-qPCR needed confirmation.(**Figure 4.4**) Interestingly, miR-200b-3p was found significantly up-regulated 24 hours post-treatment which was opposite to the down-regulation observed in the miRNA assay.

In order to explain the disparity of miRNA between the two methods, raw data from nCounter were analysed. The count of miRNA revealed that only miR-146a-5p was abundant in the control and treated cells which lead us to the conclusion that the 5 other miRNAs were part of the assay background and were very lowly expressed. In addition, a study from Camarillo et al demonstrated the low correlation between microarray and qPCR. In adult mesenchymal stromal cells undifferentiated and differentiated, miRNA profile was performed with a microarray from Invitrogen and qPCR using Taqman technologies. Out of 454 miRNAs, an alteration of expression was observed for only 93 miRNAs in differentiated cells. Among these 93 miRNAs, 70 miRNAs were found in both assay with poor correlation. Interestingly, the highest expressed miRNAs gave a better correlation than low expressed miRNAs.(Camarillo *et al.*, 2011) This might explain why only miR-146a-5p expression was correlated in both assay.

A second selection of miRNAs was performed by analysing the abundance and the difference in the counting. Then, fold change and p-value of selected miRNAs were taken into account. In addition to miR-146a-5p, miR-126-3p was selected due to its high abundance and its down-regulation post-treatment with TGFβ2 and IL1β. Down-regulation was confirmed by RT-qPCR where miR-126-3p was significantly decreased 24 hours post-treatment. (P<0,0001). These data are consistent with results from Zhang et al., a study where miR-126 was down-regulated in endothelial progenitor undergoing EndMT (Zhang *et al.*, 2013). In addition, miR-126-3p appeared in the literature as a miRNA restricted to endothelial cell and implicated in the regulation of angiogenesis and vascular integrity. In mouse, deletion of miR-126 lead to vascular leakage and hemorrhaging (Fish *et al.*, 2008; Wang *et al.*, 2008). Interestingly, over-expression of miR-126-3p increase the migration and the proliferation in human saphenous vein endothelial cells mediated through the target SPRED1 and PiK3R2 (Qu *et al.*, 2017). These two targets of miR-126-3p were experimentally validated and are found in the VEGF signalling pathway which regulates angiogenesis and vascular integrity (Fish *et al.*, 2008).This suggests the role of miR-126-3p in the regulation of endothelial-to-mesenchymal transition.

Using bioinformatics prediction tools, a list of potential targets of miR-126-3p was generated. We determined two targets from this list that could potentially be involved in EndMT: ADAM9 and SMURF2. ADAM9 is a type I transmembrane protein with disintegrin and metalloprotease domain-containing protein 9 which can cleave adhesion molecule. Over-expression of ADAM9 promotes EMT and might have a similar role in EndMT. SMURF2 is an E3 ubiquitin ligase that can regulate TGFβ signalling. As TGFβ is a key factor to induce EndMT, miR-126-3p down-regulation could increase SMURF2 and negatively regulate TGFβ signalling.

In conclusion, both the nCounter assay and RT-qPCR showed the up-regulation of miR-146a-5p and the down-regulation of miR-126-3p in our EndMT model. As miR-126-3p seemed restricted to endothelial cells, further experiments should study its role in EndMT and investigate the interaction of this miRNA with its supposed targets ADAM9 and SMURF2. Such data may have translational significance, suggesting new treatment strategies for pathophysiologies where EndMT is implicated.

# Chapter 5. Role of miRNA 126-3p in endothelial-to-mesenchymal transition in-vitro

## 5.1 Introduction

In Chapter 4, miRNA profile was assayed in the *in vitro* model of EndMT developed in Chapter 3 and the down-regulation of an endothelial-specific miRNA miR-126-3p was observed. To further study miR-126-3p, its role in EndMT *in vitro* and *in vivo* was questioned in this chapter. EndMT was suggested as contributor of the pool of fibroblast in fibrotic diseases and was examined in a multitude of pathological context. Zeisberg et al were the first to describe the presence of EndMT in cardiac fibrosis. In this work, lineage tracing under the promoter of Tie1 (Tie1-Cre), an endothelial/hematopoietic marker was generated using the system Cre-loxP.(Zeisberg *et al.*, 2007) Cre-loxP is based on the expression of Cre under a specific cell type promoter and a second transgene containing loxP sequence followed by a reporter under a ubiquitous promoter. Cre recombines loxP sequences and allows the expression of the reporter in the specific cell type (Zeisberg and Kalluri, 2010). In this study, LacZ was expressed within cells of endothelial origin regardless of phenotype changes. In the model of aortic banding-induced fibrosis, lineage tracing of endothelial cells revealed that 27% to 35% of fibroblasts FSP1+/$\alpha$-SMA+ in fibrotic areas were positive for endothelial origin (Zeisberg *et al.*, 2007). Post-myocardial infarction, lineage tracing of endothelial cells in cardiac fibrosis with the stem cell leukemia-Lacz system displayed alpha SMA positive cells with an endothelial origin post-MI (Aisagbonhi *et al.*, 2011). However, contribution of EndMT in cardiac fibrosis was contradicted in studies using lineage tracing under VE-cadherin or Tie-2 promoter (Ali *et al.*, 2014; Moore-Morris, Guimarães-Camboa, Banerjee, Alexander C. Zambon, *et al.*, 2014).

Interestingly, EndMT contribution in cardiac fibrosis remains elusive whereas strong evidence demonstrated the implication of EndMT in kidney fibrosis (LeBleu *et al.*, 2013a). EndMT was observed in three different mice models: streptozotocin (STZ)-induced diabetic nephropathy, unilateral ureteral obstruction (UUO) and alpha 3 chain collagen type 4 knockout (COL4A3 KO). In this study, EndMT was illustrated by the co-expression of CD31 and FSP1. Using Tie2-cre system (Kisanuki *et al.*, 2001), EndMT was observed in STZ-induced diabetic nephropathy in early development of

interstitial kidney fibrosis as cells positive for endothelial origin were also positive for the marker of activated fibroblast αSMA (Li *et al.*, 2009). Based on the same model of lineage tracing, 10% of cells positive to αSMA were also positive to an endothelial origin in UUO mice. This suggests the important role of EndMT in kidney fibrosis.

Interestingly, few studies *in vivo* showed a link between EndMT and miRNA in the context of cardiac and kidney fibrosis. In cardiac fibrosis induced by TAC, miR-21-5p was found increased and the treatment with antagomiR-21 lead to an attenuation of EndMT suggesting the role of miR-21 in EndMT *in vivo* (R. Kumarswamy *et al.*, 2012). In transplant rejection model of aorta, the role of let-7 was analysed in EndMT through treatment with antagomir or mimic. Lineage tracing under VE-cadherin promoter revealed that antagomir treatment increased EndMT (61% to 80-90%) meanwhile mimic transfection lead to a decrease (33,7%) (Chen *et al.*, 2012). In diabetic-induced cardiac fibrosis, expression of miR-200b-3p was found down-regulated and more specifically was down-regulated in endothelial cells. The use of transgenic miR-200b mouse, over-expression of miR-200b was able to prevent EndMT(Feng *et al.*, 2016a). In kidney fibrosis, miR-29 was suggested as a regulator of EndMT. MiR-29 down-regulation was correlated to the increase of kidney fibrosis and the restoration of miR-29 reduced fibrosis. However, the association of miR-29 to EndMT *in vivo* was not directly studied (Kanasaki *et al.*, 2014).

As none of this study linked miR-126-3p to the EndMT process identified in Chapter 4 as down-regulated miRNA during the transdifferentiation, my working hypothesis for Chapter 5 was to investigate the role miR-126-3p in EndMT. Due to the controversial studies on EndMT *in vivo*, lineage tracing of endothelial cells was essential to assess the presence of EndMT in the context of cardiac and kidney fibrosis before studying miRNA expression.

## 5.2 Specific aims

In this chapter, we aimed to:

- To investigate the role of miR-126-3p in EndMT *in vitro*
- To examine the regulation of miR-126-3p predicted targets
- To determine the presence of EndMT in cardiac fibrosis
- To confirm the presence of EndMT in kidney fibrosis
- To localise miR-126-3p in both cardiac and kidney fibrosis

## 5.3 Specific material and methods

### *5.3.1 MiRNAs mimic Transfection*

*Lipid-based transfection*

MiRNAs mimic delivery into cells is facilitated with lipid-based transfection. Reagents such as Lipofectamine® RNAimax (Thermofisher) consists of cationic lipids that interact with miRNA mimics and results in a one-layer liposomal structure with a positive surface charge when in water. Positive liposomes allow the fusion of the miRNA mimics-liposome complex with the negatively charged cell membrane. The complexes enter through endocytosis and diffuse into the cytoplasm.

MiRIDIAN miRNA mimics (Dharmacon) are synthetic duplexes of mature miRNAs. Mimics are transfected to increase endogenous miRNA activity in cells. These mimics are chemically modified in order to incorporate a preferential strand into a RISC complex that is able to regulate its targets by binding to their 3'UTR.

Transfection of specific miRNAs needs a negative control in order to detect any effect from the transfection reagent. Cells were transfected with a mimic negative control cel-miR-67. This miRNA from C. elegans has very low sequence identity in human and should not have any biological effects on the cells. Transfection optimisation was performed using miRIDIAN MiRNA Mimic Transfection Control with Dy547 (Dharmacon) and analysed with different volumes of lipofectamine or different concentration of mimics.

*Volume of lipofectamine optimisation*

HUVECs were seeded in chamber slides 24 hours prior to the transfection. Lipofectamine RNAimax volume from 0,5µL to 1µL was first diluted in 32µL final volume of OPTI-MEM media. From a stock solution of 1µM, 1 µL of mimic transfection control with Dy547 was diluted into 32µL final volume of OPTI-MEM. After 5 minutes of incubation at room temperature, lipofectamine (LF) and mimic were mixed and left at room temperature for 20 minutes. In the meantime, media was removed from the well, cells were washed once with PBS and 234µL of OPTI-MEM media was added. An extra 32µL of OPTI-MEM was added into the well without any mimics. Complexes lipofectamine-mimic were then mixed up and down into the well. The final concentration of mimics was equal to 3,3nM. Chamber slides were incubated 24hours to 48 hours in a humidified atmosphere of 5% $CO_2$ at 37°C. Post-incubation, media

was removed and cells were washed with PBS and fixed with cold methanol (-20°C) during 10 minutes at room temperature. Methanol was carefully removed and slide was mounted using a mountant containing DAPI (Vectashield). Transfection efficiency was then visualised using a fluorescent microscope (**Figure 5.1)**

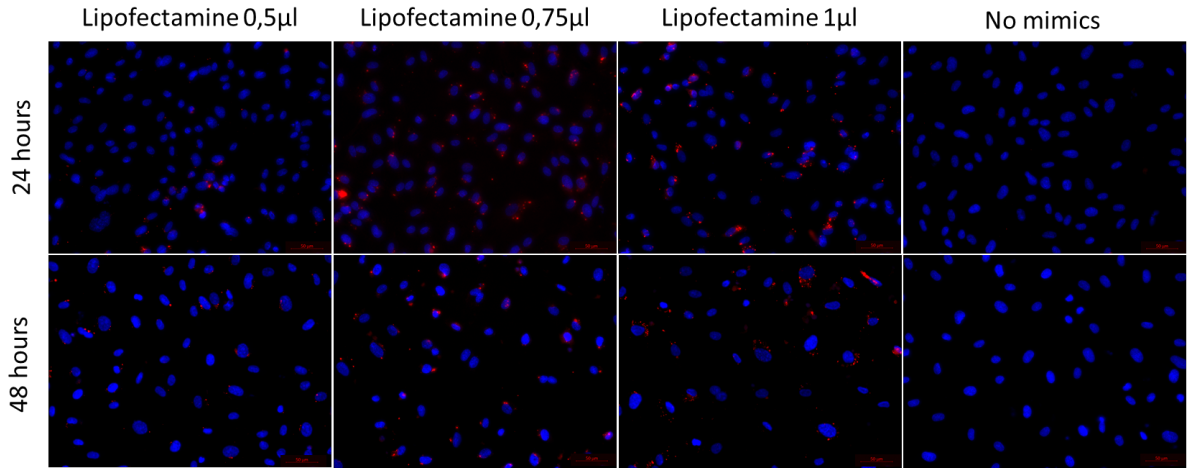


**Figure 5.1 Optimisation of lipofectamine volume for miRNAs transfection in HUVEC.** Transfection of mimic transfection control with Dy547 (3,3 nM) was optimised with a range of 0,5µl to 1µL of lipofectamine. HUVECs were transfected for 24 hours or 48 hours. Volumes of 0,75µl and 1µL showed transfected mimics control. Transfection was less efficient at 48 hours.

Results showed that transfection could be realised with 0,75µl or 1µL of lipofectamine but could be improved with higher concentrations of mimics as miRIDIAN can be used up to 200nM. In the first instance, 1µL of lipofectamine was chosen to perform further experiments

*Mimic concentration optimisation*

Cells were seeded in chamber slides 24 hours prior to the transfection. Lipofectamine RNAimax volume of 1µL was first diluted in 32µl final volume of OPTI-MEM media. A volume of 1 µL, 1,65 µL or 3,3 µL of mimic transfection control with Dy547 from 1 µM stock was diluted into 32µl final volume of OPTI-MEM to obtain respectively 3,3nM, 5,5nM or 11nM of mimics in the well. The same protocol described above was then performed. (**Figure 5.2**)

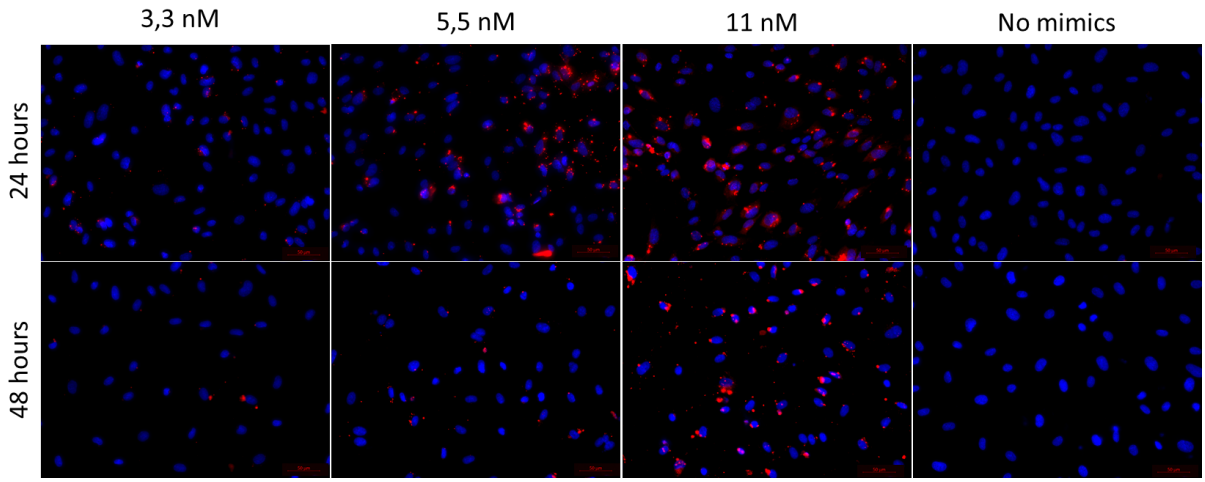


**Figure 5.2 Optimisation of mimic concentration for miRNAs transfection in HUVEC.** Transfection was optimised with different concentrations of mimic transfection control with Dy547. HUVECs were transfected for 24 hours or 48 hours and a constant volume of 1µL of lipofectamine RNAimax was used. Increased concentration of mimics showed increased transfection efficiency. Transfection was less efficient at 48 hours for concentrations of 3,3 nM and 5,5nM. With a mimic concentration of 11nM, transfection efficiency was similar at 24 hours and 48 hours.

The concentration of mimics was directly correlated with the transfection efficiency 24 hours post-transfection. More miRNAs mimics were transfected into the cells with a higher concentration. After 48 hours of transfection, miRNAs were not detectable with an initial concentration of 3,3nM and 5,5nM. Therefore, the combination of 1µL of lipofectamine and 11nM of mimics were used for the experiments.

With these conditions, transfection for miR-126-3p was performed for 24 hours in HUVEC but a high level of cell mortality was observed. Thereafter, transfection was performed for 18 hours and total RNA including small RNA was extracted. Transfection of miR-126-3p increased the level of the miRNA in untreated (19 fold increase) and treated (23 fold increase) cells. Non-specific miRNA (Ns miR) transfection did not affect the level of miR-126-3p in both untreated and treated cells (**Figure 5.3**). This suggests the correct execution of the transfection.

*MiR-126-3p transfection optimisation*

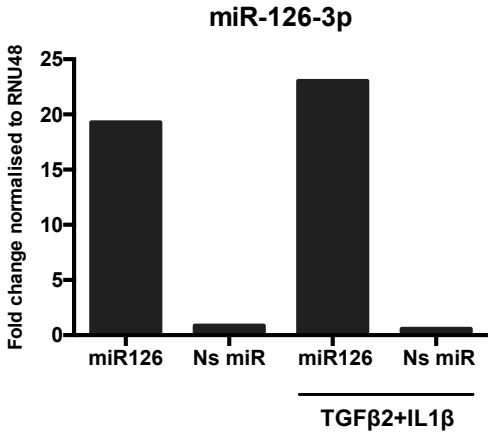


**Figure 5.3 Expression of miR-126-3p after transfection**
HUVEC were transfected for 18 hours with 1μl of lipofectamine and 11nM of mimics (miR-126-3p or NS miR). Post-transfection, cells were treated for 48 hours with TGFβ2 and IL1β (10ng/mL). Total RNA enriched in miRNAs was extracted, cDNA was synthesised by reverse transcription with specific miRNA primer and a RT-qPCR was performed to study miR-126-3p expression. Each miRNA expression was normalised to expression of the endogenous control RNU48 and compared to the control (n=1).

The transfection reagent lipofectamine RNaimax is known to be toxic to the cells. Therefore its effect 18 hours post-transfection was assessed in HUVEC by immunofluorescence. HUVEC were cultured in presence or absence of lipofectamine (1μl) for 18 hours. After fixation in cold methanol, cells were stained for CD31 coupled to a secondary antibody Alexa fluor 488 conjugate. In cells cultured without lipofectamine, CD31 was stained at the cell membrane and displayed the cell-cell contact. Interestingly, CD31 expression was visually decreased and no cell-cell contact were observed in cells cultured with LF implying that LF is toxic to HUVEC cells.

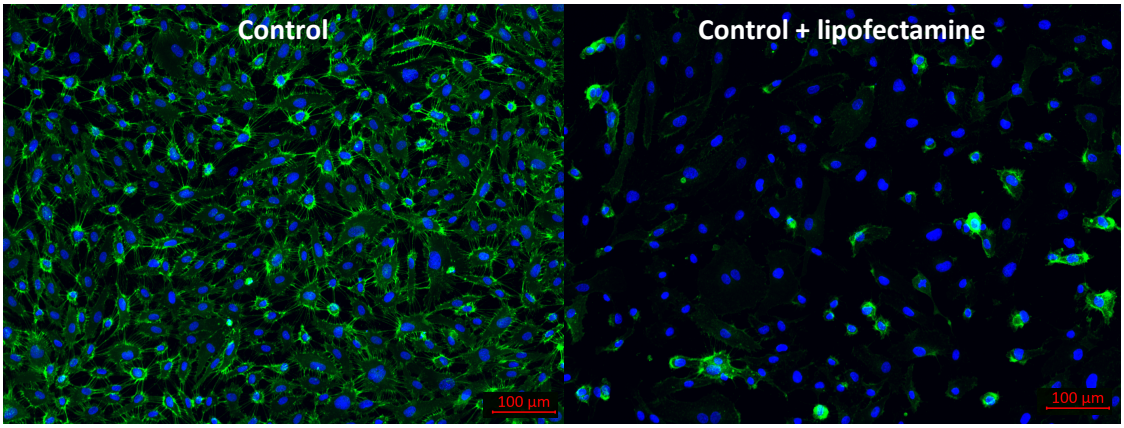


**Figure 5.4 Effect of lipofectamine on CD31 expression in HUVEC**
Confluent HUVEC were treated with or without LF (1μl) for 18 hours. Immunofluorescence was performed for CD31 followed by a secondary antibody Alexa fluor 488 conjugate and nuclei were counterstained with DAPI. Pictures were taken with Zeiss axioimager II upright microscope (Original magnification ×20)(n=1).

In order to reduce the lipofectamine-related toxicity, culture with lipofectamine was reduced to 6 hours. Furthermore, two conditions of transfection were tested. The first condition was the same than **Figure 5.2** with 1µl of lipofectamine in 65µl of OPTI-MEM media and 11nM of mimics. In the second condition, the volume of lipofectamine was reduced to 0,5µl and concentration of mimics was increased to 30nM. Transfection with miR-126-3p and Ns miR were performed during 6 hours and non-transfected cells were cultured with lipofectamine for the same time. After fixation, staining for CD31 was performed. In HUVEC cultured with lipofectamine for 6 hours, CD31 staining showed a high expression at the cell membrane. In addition , HUVEC cells were forming a monolayer whereas in **Figure 5.4** cells treated 18 hours with lipofectamine lead to the disruption of the monolayer and to a low expression of CD31.

The transfection with 1µl of lipofectamine and 11nM of mimics leads to the disruption of the monolayer and confluency was different from the non-transfected cells. In transfected cells with 0,5µl of lipofectamine and 30nM of mimics, cells were more confluent and the culture was more similar to the non-transfected cells. In conclusion, cells seemed healthier with a 6 hours transfection and a reduced volume of lipofectamine 0,5µl (**Figure 5.5**).

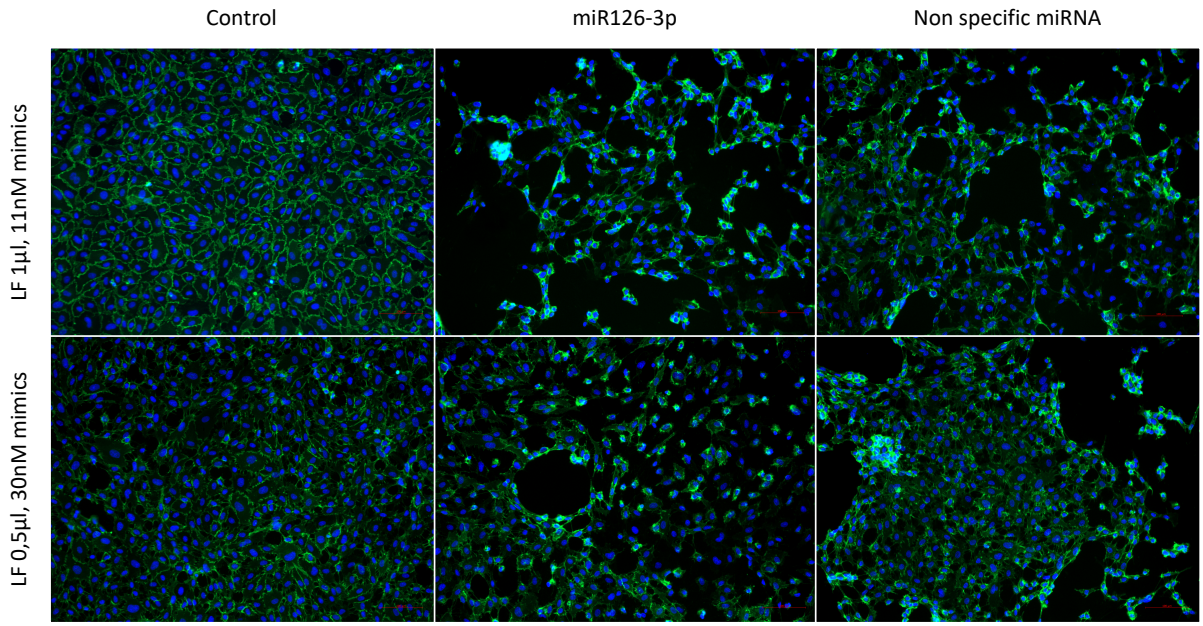


**Figure 5.5 Optimisation of lipofectamine volume and mimics concentration in HUVEC transfection**

HUVEC were transfected with miR-126-3p and Ns miR for 6 hours. LF was added for 6 hours to the non-transfected cells. Two conditions of transfection were tested: (1) LF 1µl, 11nM mimics (2) LF 0,5µl, 30nM mimics. Cells were stained for CD31 followed by a secondary antibody Alexa fluor 488 conjugate. DAPI counterstaining was performed for nuclei. Pictures were taken with Zeiss axioimager II upright microscope (Original magnification ×20)(n=1).

The condition of transfection (LF 0,5µl, 30nM mimics) was tested for 3 hours in order to evaluate if transfected cells monolayer could be comparable to the non-transfected cells. In the non-transfected cells, lipofectamine was added to the media. Similarly to previous optimisations, indirect immunofluorescence for CD31 was performed. Interestingly, 3 hours transfection showed a disruption of the monolayer and a low expression of CD31 in both transfected and non-transfected cells. (**Figure 5.6**). This suggests that 6 hours was the most relevant time point for transfection.

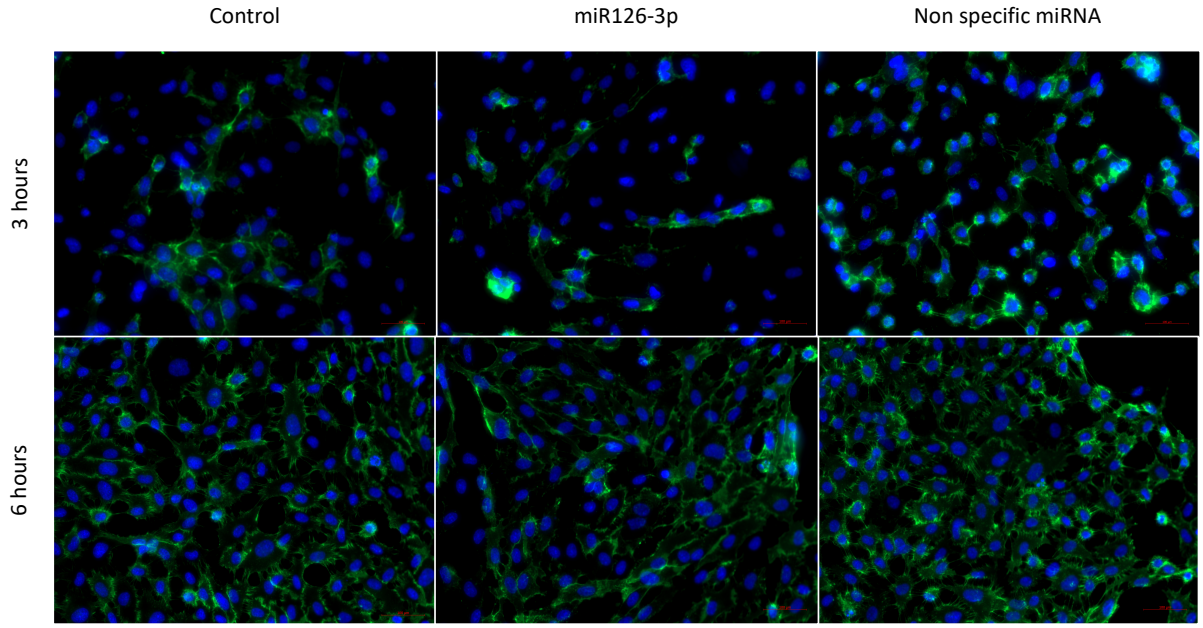


**Figure 5.6 Optimisation of transfection time point in HUVEC**
HUVEC were transfected with 0,5µl of LF and 30nM of miR-126-3p mimics or Ns miR . Transfection were performed for two time points 3h and 6h and non-transfected cells were cultured in presence of lipofectamine for the same time points.Cells were stained for CD31 with a secondary antibody Alexa fluor 488 conjugate. Counterstaining was performed with DAPI. Pictures were taken with Zeiss axioimager II upright microscope (Original magnification ×20)(n=1).

Effect of miR-126-3p in EndMT was studied by transfection of mimic in HUVEC undergoing EndMT with TGFβ2 and IL1β treatment. Transfections were first carried out with 0,5µl of LF and 30nM of miR-126-3p mimics or Ns miR. Control and TGFβ2/IL1β treated cells were cultured in presence of 0,5µl of lipofectamine. Six hours post-transfection, cells were treated with TGFβ2 and IL1β for 48 hours to induce EndMT. Cells were then stained for CD31 followed by a secondary antibody Alexa fluor 488 conjugate. CD31 expression was decreased in TGFβ2 and IL1β treated cells compared to the untreated cells. However, no change in CD31 expression was observed between the treated cells and the treated cells transfected with miR-126-3p (data not shown). Thereafter, concentration of mimics was increased to 50nM and

100nM to elucidate the possible effect of miR-126-3p over-expression in HUVEC undergoing EndMT. Using the same protocol, transfection of 50nM and 100nM miR-126-3p was carried out (**Figure 5.7**). A decrease of CD31 expression was observed in TGFβ2 and IL1β treated cells. In addition, over-expression of miR-126-3p with 50nM and 100nM seems to restore the level of CD31 in TGFβ2/IL1β treated cells. In cells transfected with non-specific miR, expression of CD31 was similar to the TGFβ2/IL1β non transfected cells. The 50nM and 100nM concentrations of mimics allow the partial restoration of CD31 in cells undergoing EndMT ,thus 50nM concentration was used for further experiments.

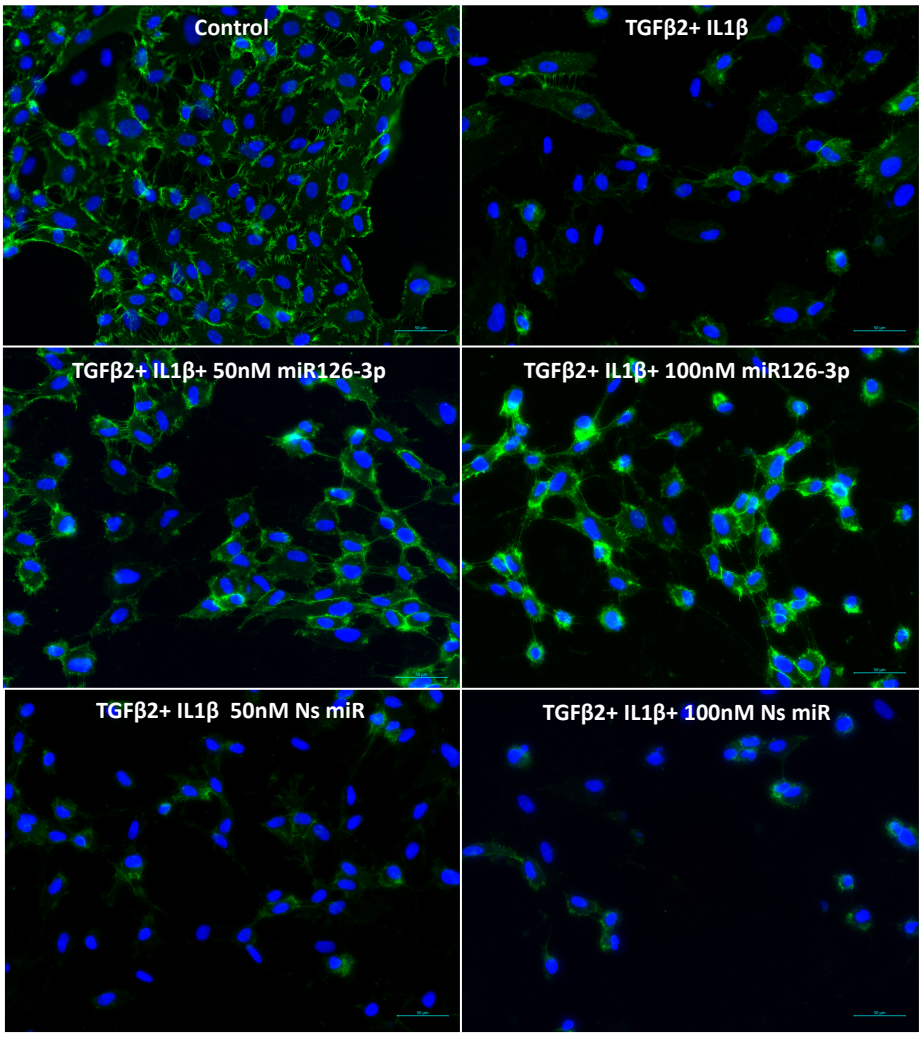


**Figure 5.7 Effect of 50nM and 100nM mimic concentrations on CD31 expression in HUVEC undergoing EndMT**

HUVEC were transfected for 6 hours with 0,5µl of LF and 50nM or 100nM of mimics. Non-transfected cells were cultured in presence of lipofectamine for 6 hours. Transfections were performed with miR-126-3p and NsmiR followed by 48 hours of treatment with TGFβ2 and IL1β (10ng/mL). Immunofluorescence was performed for CD31 with a secondary antibody Alexa fluor 488 conjugate and nuclei with DAPI. Pictures were taken with Zeiss axioimager II upright microscope (Original magnification ×20)(n=1).

### 5.3.2 Mouse strains

All experiments were carried out under UK Home Office Licence and were performed in accordance with the Animals (Scientific Procedures) Act 1986. *Cdh5(PAC)-CreER$^{T2}$* mice express a tamoxifen inducible Cre recombinase under the promoter of VE-cadherin. *Cdh5(PAC)-CreER$^{T2}$* mice crossed with Rosa-YFP mice resulting in the expression of YFP only in endothelial cells. Hearts from VE-Cre-Rosa-YFP T/T mice were directly obtained from Professor Helen Arthur (Institute of genetic medicine). In order to activate Cre recombinase, 2 mg of tamoxifen was injected via intraperitoneal route for 5 consecutive days. Surgery took place at least 7 days after the last injection of tamoxifen in order to get tamoxifen-free mice. Genotyping of these mice was carried out by Esha Singh.

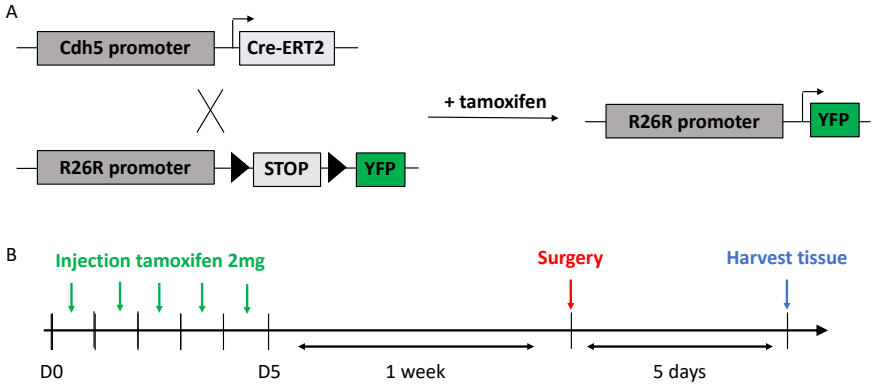


**Figure 5.8 Mouse strain**
A**.** Cdh5-CreERT2 mouse model allows the expression of the tamoxifen-inducible Cre recombinase under VE-cadherin promoter Cdh5. Rosa26R-YFP mice were crossed with inducible Cdh5-CreERT2 to generate lineage tracing of endothelial cells. B. Timeline for transgenic mouse experiments.

### 5.3.3 Mouse model of myocardial infarction

Myocardial infarction was generated by permanent coronary artery ligation. First, mice were anesthetised with isoflurane followed by an intubation and ventilation to maintain anesthesia. A left thoracotomy was performed to expose the heart and the left anterior descending (LAD) artery which was permanently ligated using 7-0 prolene suture. Post suture changes of color of the artery was used as an indication of MI. Wound and incision for intubation were then stitched with 5-0 vicryl suture. Anesthesia was turned off and subcutaneous injection of buprenorphine was performed for analgesia. For recovery mice were placed into pre-warmed cage at 33°C and underwent a soaked diet. All surgeries were performed by Dr Rachael Redgrave (Institute of genetic medicine).

### 5.3.4 Mouse model of unilateral ureteral obstruction

Kidney fibrosis was induced with unilateral ureteral obstruction. Mice were first anesthetised with isoflurane. Thereafter, buprenorphine was injected for pain relief and laparotomy was performed to expose the kidney. On the left kidney, ureter was isolated and three knots were executed (2 on the top and 1 at the bottom) with Mersil 6.0. Thereafter, left ureter was cut between the second and the third knot. Wound closure was performed by stitching with 5-0 vicryl suture and mice recovery did not require special care. All surgeries were performed by Katie Cooke (ICM)

### 5.3.5 Tissue processing and sectioning

After dissection, hearts or kidneys were incubated in 0,2% or 1% paraformaldehyde (PFA) respectively on a shaker at 4°C overnight. Next day, organs were placed in 30% sucrose with gentle agitation at 4°C overnight. Organs were disposed in plastic dispomould with OCT and were frozen on dry ice. After freezing, samples were stored at -80°C.

## 5.4 Results

### *5.4.1 Impact of miR-126-3p transfection on EndMT in HUVEC*

The induction of EndMT with the TGFβ2 and IL1β treatment significantly decreases the endothelial specific miRNA miR-126-3p. In order to investigate the potential role of miR-126-3p, over-expression of the miRNA was realised by transfection of mimics. Mimic delivery into cells was facilitated with lipid-based transfection. Transfections were performed for 6 hours with 0,5µl of LF and 50nM followed by 48 hours of treatment with TGFβ2 and IL1β. Immunofluorescence for CD31 was performed and quantified using imageJ. CD31 expression was significantly decreased in TGFβ2/IL1β treated cells, non-transfected and transfected with NS miR (p=0,030 and p=0,045). In TGFβ2 and IL1β treated cells, level of CD31 was restored in cells transfected with miR-126-3p compared to non-transfected and transfected with NS miR (p=0,0003 and p=0,0004).

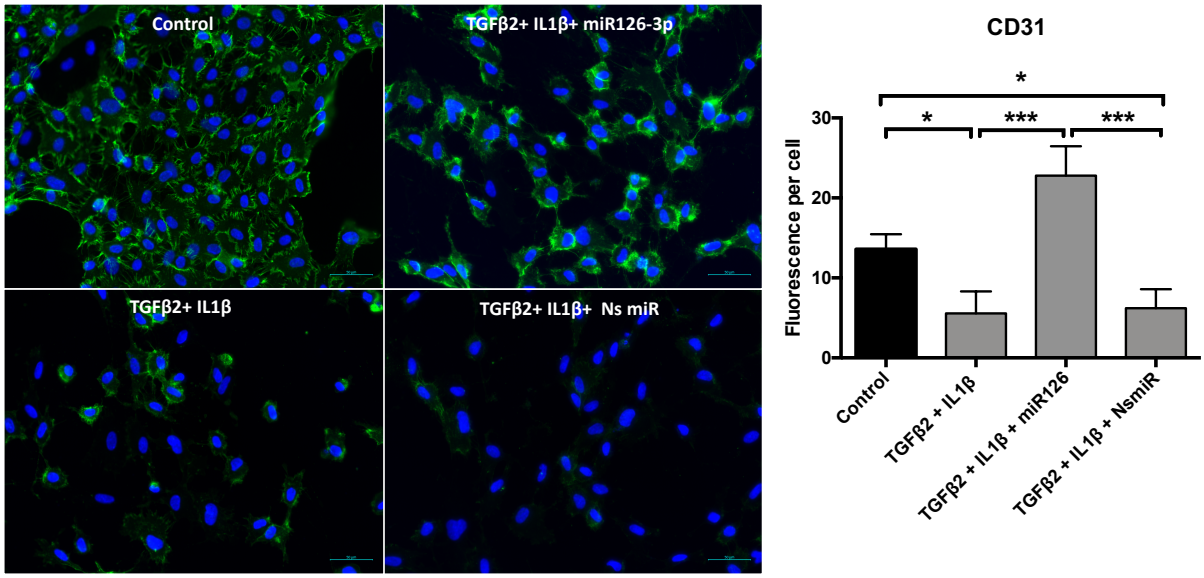


**Figure 5.9 Expression of CD31 after miR-126-3p transfection in HUVEC undergoing EndMT**

HUVEC were transfected for 6 hours with 0,5µl of LF and 50nM miR-126-3p or NsmiR. LF was added for 6 hours to the non-transfected cells. Cells were then treated 48 hours with TGFβ2 and IL1β (10ng/mL). Immunofluorescence was performed for CD31 followed by a secondary antibody Alexa fluor 488 conjugate and nuclei were counterstained with DAPI. Pictures were taken with Zeiss axioimager II upright microscope (Original magnification ×20) Fluorescence was quantified using image J and values are mean +/- SD of three pictures for each condition(n=3). Statistical significance was assessed by One-way ANOVA followed by Tukey test *(*, p<0,05; ***, p<0.001).*

The effect of miR-126-3p over-expression was then studied at gene level. HUVEC cells were transfected 50nM of mimics and 3µl of lipofectamine (in 400µl of OPTI-MEM). After 6 hours of transfection of miR-126-3p or Ns miR, cells were treated 48 hours with

TGFβ2 and IL1β. To assess gene expression, RT-qPCR were performed and Ct values obtained for each gene and each treatment condition were normalised to the Ct values of an endogenous control Hprt1. Then, fold change was calculated using $2^{-\Delta\Delta CT}$ method. Fibronectin, a component of the extracellular matrix, was the first gene to be analyse. In untreated cells, no significant change in fibronectin expression was observed between the transfected cells and non-transfected cells. In treated cells transfected with NS miR, fibronectin was significantly increased compared to non-transfected untreated cells (p=0,018). The transfection of miR-126-3p in treated cells resulted in a reduction of fibronectin expression in comparison to treated cells (p=0,051 and p=0,016) (**Figure 5.9**). In conclusion, miR-126-3p over-expression seems to inhibit fibronectin expression in HUVEC undergoing EndMT.

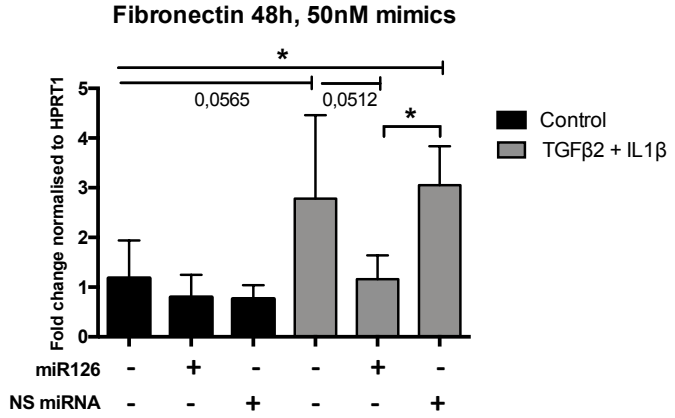


**Figure 5.10 Expression of fibronectin after miR-126-3p transfection in HUVEC undergoing EndMT**

HUVEC were transfected for 6 hours with 3μl of LF and 50nM of mimics.(n=6) Non-transfected cells were cultured in presence of lipofectamine for 6 hours. Transfections were performed with miR-126-3p and NsmiR followed by 48 hours of treatment with TGFβ2 and IL1β (10ng/mL). Total RNA was extracted, cDNA was synthesised by reverse transcription and a qRT-PCR was performed. Fibronectin expression was normalised to expression of the housekeeping gene Hprt1 and compared to the control. Errors bars are representative of standard deviations. All data is representative of three independent experiments and statistical significance was assessed by One-way ANOVA followed by Tukey test *(*, p <0.05).*

Effect of the over-expression of miR-126-3p was then assessed on the endothelial markers vWF, CD31 and on the mesenchymal marker αSMA . In chapter 3, vWF was found significantly down-regulated in TGFβ2 and IL1β treated cells. In **Figure 5.11**, differences in vWF expression were observed in non-transfected untreated cells. One independent experiment showed a high expression in the control cells (untreated and non-transfected). In transfected cells, no change of vWF expression was observed between the transfected cells and the non-transfected cells. This implies that miR-126-3p do not influence the expression of vWF.

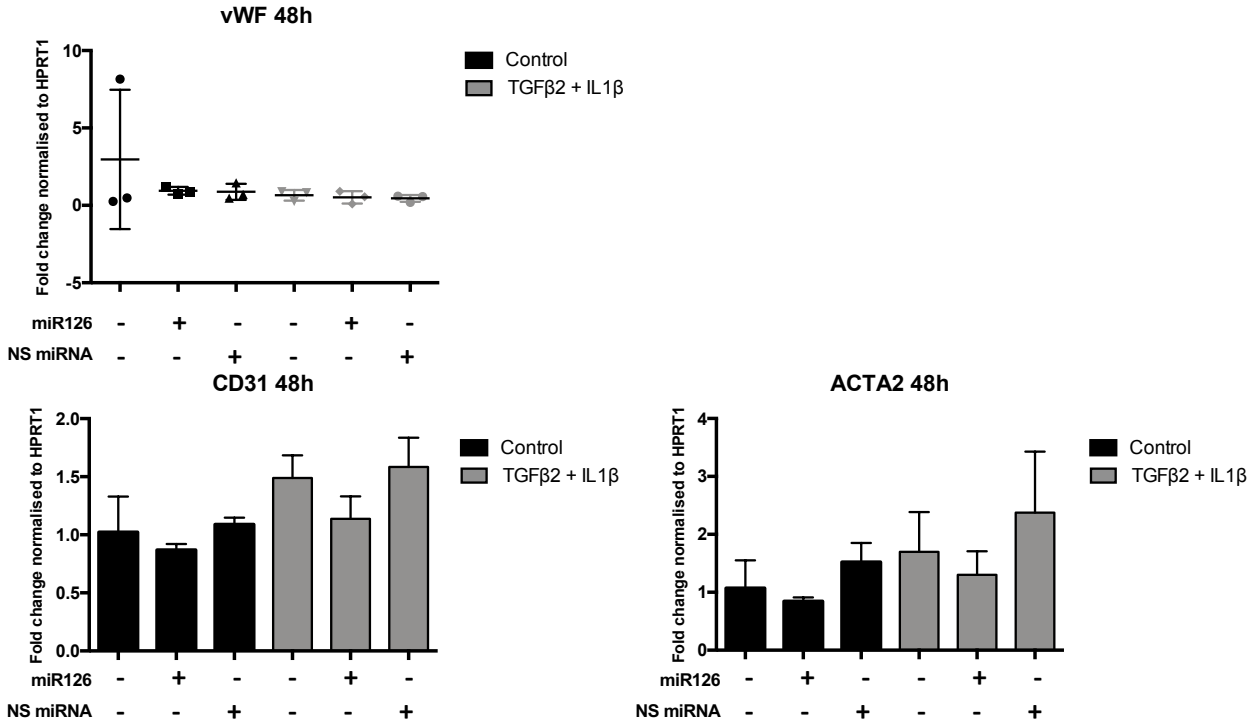


**Figure 5.11 Expression of endothelial and mesenchymal markers after miR-126-3p transfection in HUVEC undergoing EndMT**

Transfections were performed for 6 hours with 3μl of LF and 50nM of mimics. Non-transfected cells were cultured in presence of lipofectamine for 6 hours. Transfections were performed with miR-126-3p and NsmiR followed by 48 hours of treatment with TGFβ2 and IL1β (10ng/mL). Total RNA was extracted, cDNA was synthesised by reverse transcription and a qRT-PCR was performed. vWF (n=3) ,CD31 (n=2) and ACTA2 (n=3) expression were normalised to expression of the housekeeping gene Hprt1 and compared to the control. Errors bars are representative of standard deviations. Statistical significance was assessed by One-way ANOVA followed by Tukey test.

In **Figure 5.9**, the over-expression of miR-126-3p led to the restoration of CD31 protein level in HUVEC undergoing EndMT. Expression of CD31 was then studied at gene level in order to investigate the possible role of miR-126-3p. Interestingly, gene expression of CD31 was unchanged after treatment with TGFβ2 and IL1β. These results were correlated with results obtained in Chapter 3 where the treatment induced a decrease of CD31 at protein level but not at gene level. In addition, no change in CD31 gene expression was observed after transfection of miR-126-3p in treated cells. ACTA2 encodes for the protein αSMA and was found unchanged in TGFβ2 and IL1β treated cells in Chapter 3. In the same way than previous experiments, ACTA2 expression was found unchanged and no effect of miR-126-3p transfection was observed (**Figure 5.11**). Therefore, increased level of miR-126-3p do not seem to affect the expression of CD31 and αSMA at gene level.

In conclusion, miR-126-3p seems to partially prevent EndMT by reducing fibronectin expression at gene level and increasing CD31 expression at protein level in HUVEC undergoing EndMT. However, miR-126-3p do not influence the expression of vWF and αSMA.

### *5.4.2 Impact of miR-126-3p transfection on EndMT in HMEC1*

The primary endothelial cells are difficult to transfect and are more sensitive to the cytotoxicity of the transfection reagents. Evidence showed that variability in transfection efficiency can also be caused by the use of pooled multi-donor endothelial cells (Hunt *et al.*, 2010). Furthermore, highest transfection efficiency was observed in immortalised cell line (van Beijnum *et al.*, 2008), thus transfection of miR-126-3p were performed in HMEC1 cells. HMEC1 cells were transfected for 6 hours with 3µl of LF and 50nM of mimics. Non-transfected cells were cultured with lipofectamine. Post-transfection, cells were treated with TGFβ2 and IL1β for 24 or 48hours and fibronectin expression was examined by RT-qPCR. An endogenous control gene Hprt1 was quantified for normalisation and data were analysed with the delta delta Ct method ($2^{-\Delta\Delta CT}$ method). Each gene expression in treated cells was compared to the untreated cells.

Fibronectin expression tend to increase after 24 hours of TGFβ2/IL1β treatment and the transfection of miR-126-3p in treated cells tend to decrease fibronectin to the basal level. After 48 hours of treatment, fibronectin was found significantly up-regulated in treated cells transfected with NS miR and in non-transfected treated cells (p=0,076 and p=0,015 respectively). The transfection of miR-126-3p down-regulate fibronectin expression compared to the treated non transfected cells and the treated transfected with Ns miR cells (p=0,078 and p=0,015 respectively). Similar results were observed in primary cells (**Figure 5.10**). Thus, over-expression of miR-126-3p seems to reduce fibronectin expression to basal level in endothelial cells undergoing EndMT.

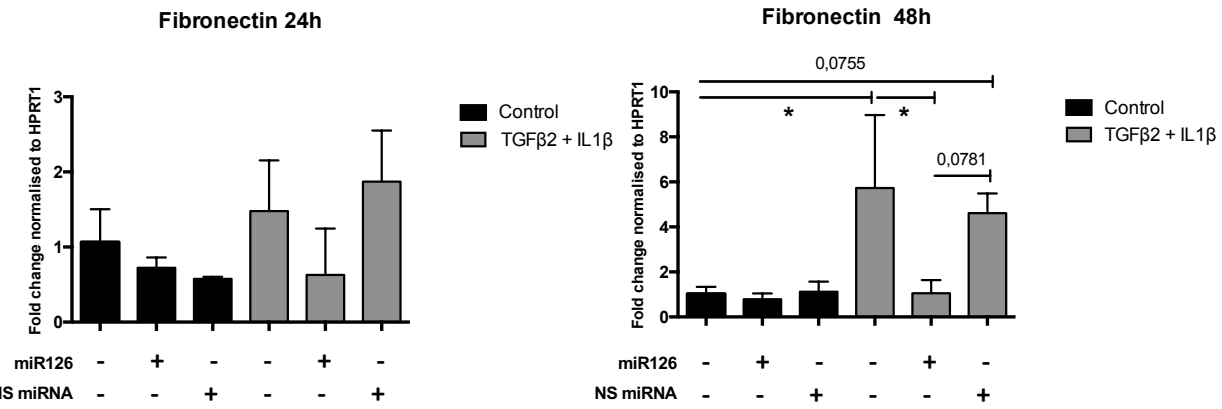


**Figure 5.12 Expression of fibronectin after miR-126-3p transfection in HMEC1 undergoing EndMT**

HMEC1 were transfected for 6 hours with 3µl of LF and 50nM of miR-126-3p mimics or Ns miR. Non-transfected cells were cultured in presence of lipofectamine for 6 hours . Post-transfection, cells were treated with TGFβ2 and IL1β(10ng/mL) for 24 or 48 hours (n=3 each). Total RNA was extracted, cDNA was synthesised by reverse transcription and a qRT-PCR was performed. Fibronectin expression was normalised to expression of the housekeeping gene Hprt1 and compared to the control. Errors bars are representative of standard deviations. All data is representative of three independent experiments and Statistical significance was assessed by One-way ANOVA followed by Tukey test *(*, p <0.05).*

In **Figure 5.11**, no change in vWF expression were observed post-transfection with miR-126-3p in HUVEC undergoing EndMT. vWF gene expression post-transfection was then assessed in HMEC1 cells by RT-qPCR. At 24 hours post- treatment, vWF expression tend to decrease whereas this trend was not observed in 48 hours treated cells. Similarly to the results obtained in HUVEC, no significant change of vWF was observed in cells treated 24 hours or 48 hours and transfected with miR-126-3p (**Figure 5.13**). Therefore, miR-126-3p does not impact on vWF factor expression in HUVEC undergoing EndMT.

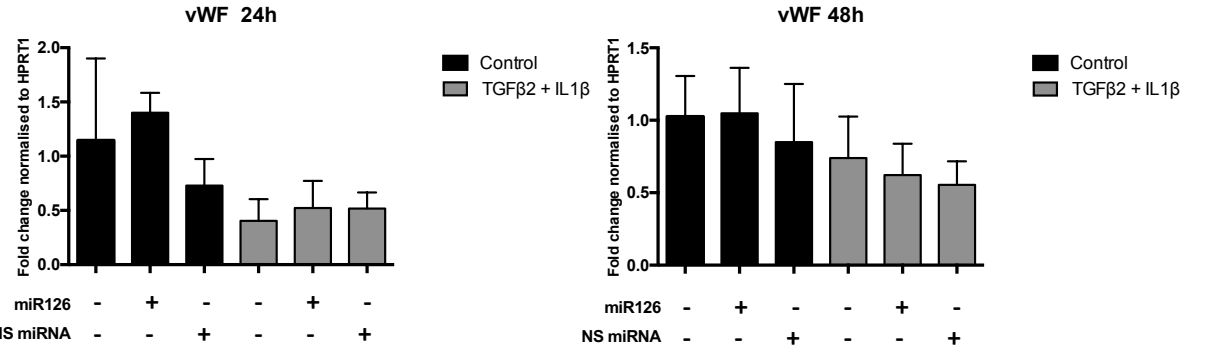


**Figure 5.13 Expression of vWF after miR-126-3p transfection in HMEC1 undergoing EndMT**

Six hours transfections were performed in HMEC1 cells with 3µl of LF and 50nM of miR-126-3p or Ns miR. LF was added for 6 hours to the non-transfected cells. Then, treatment with TGFβ2 and IL1β was incubated for 24 or 48 hours (n=3). Post-RNA extraction and reverse transcription, qRT-PCR was performed. vWF expression were normalised to expression of the housekeeping gene Hprt1 and compared to the control. Errors bars are representative of standard deviations. All data is representative of three independent experiments and statistical significance was assessed by One-way ANOVA followed by Tukey test.

### 5.4.3 Regulation of miR-126-3p targets expression

In Chapter 4, miR-126-3p direct targets were predicted using prediction target tools. From the list of predicted targets, two targets that could be involved in EndMT, were selected ADAM9 and SMURF2 respectively. In order to confirm the direct link between miR-126-3p and its predicted targets, transfection of miR-126-3p mimic was performed in HUVEC. In addition, cells were treated with TGFβ2 and IL1β to elucidate if ADAM9 and SMURF2 could be involved in EndMT. Six hours transfection were executed with 3μl of LF and 50nM of mimics followed by 48 hours of treatment. ADAM9 and SMURF2 were studied at gene expression level with RT-qPCR. In untreated and treated cells, ADAM9 tends to decrease post-transfection with miR-126-3p in comparison to the non-transfected cells. However, no change in expression was observed between the untreated cells and the treated cells implying that ADAM9 is not involved in the transdifferentiation. Regarding SMURF2 expression, no changes were observed between the treated and untreated cells but also between the transfected cells and non-transfected cells. This suggests that SMURF2 does not have a role in EndMT and is not directly targeted by miR-126-3p. In conclusion, the two targets selected do not seem implicated in the process of EndMT.

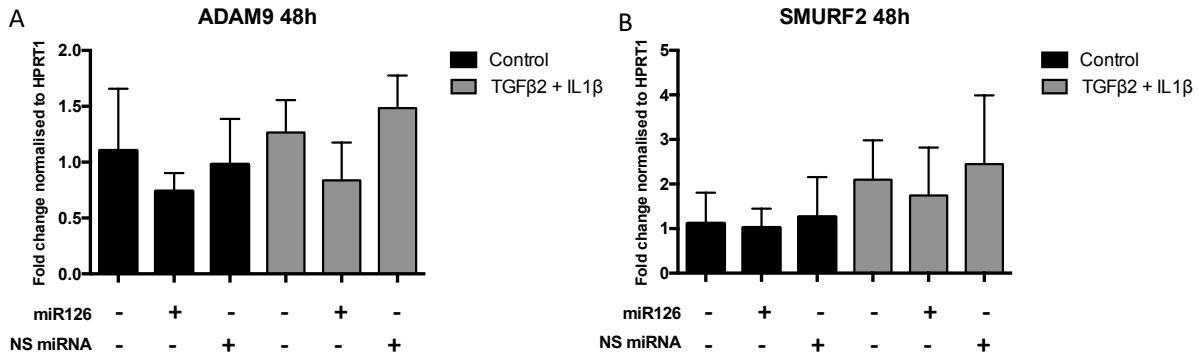


**Figure 5.14 Regulation of miR-126-3p targets in HUVEC undergoing EndMT**
HUVEC were transfected for 6 hours with 3μl of LF and 50nM of miR-126-3p or Ns miR. LF was added for 6 hours to the non-transfected cells. Cells were then treated with TGFβ2 and IL1β(10ng/mL). Post-RNA extraction and reverse transcription, qRT-PCR was performed. ADAM9 (n=4) and SMURF2 (n=3) expression were normalised to expression of the housekeeping gene Hprt1 and compared to the control. Errors bars are representative of standard deviations. All data is representative of three independent experiments and statistical significance was assessed by One-way ANOVA followed by Tukey test

### 5.4.4 Endothelial-to mesenchymal transition following myocardial infarction

In Chapter 3, *in vitro* model of EndMT was developed with TGFβ2 and IL1β treatment. Thus, expression level of TGFβ2 and IL1β was questioned in cardiac fibrosis. Mice underwent MI and were sacrificed 1, 3, 5 and 7 days later. Total RNA was obtained from Prof. Helen Arthur (Institute of Genetic Medicine, Newcastle University). TGFβ2 and IL1β were quantified in six MI hearts and two sham-operated hearts for each time point. TGFβ2 was consistently increased with a minimum of two fold change in hearts post-MI. IL1β expression was found highly up-regulated one day post-MI. No significant change of expression was observed at 3, 5 and 7 day's post-MI.(**Figure 5.15**) In conclusion, the increased expression of TGFβ2 and IL1β in cardiac fibrosis post-myocardial infarction might induces endothelial-to-mesenchymal transition *in vivo.*

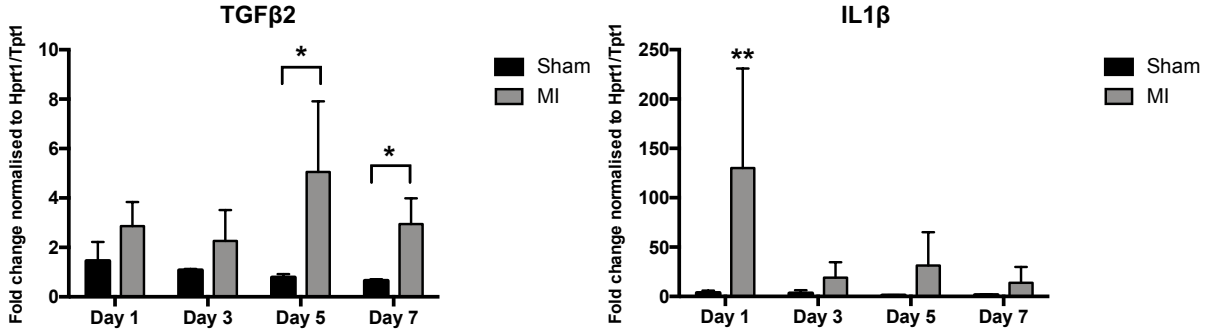


**Figure 5.15 TGFβ2 and Il1B expression in myocardial infarction mouse heart**
Mice underwent myocardial infarction were sacrificed at 1, 3, 5 and 7 days. Total RNA was extracted, cDNA was synthesised by reverse transcription and a qRT-PCR was performed. Hprt1 and Tpt1 expression were used as reference for normalisation. Data were normalised to two control mice and errors bars were representative of standard deviations. Fold change comparison was performed between mice post-MI (n=6) and sham operated mice (n=2) at 1, 3, 5, 7 days post-surgery. Statistical significance was calculated by multiple unpaired Student's *t* test *(*, p <0.05; **, p<0.01).*

.

Numerous studies have focused on the origin of fibroblast in the context of fibrosis and endothelial-to-mesenchymal transition is suggested as a potential source. However, some studies are contradicting one another and the contribution of EndMT to cardiac fibrosis remains elusive. Thus, the mouse line Cdh5-Cre-ERT2; Rosa26R-stop-YFP was studied for lineage tracing of endothelial cells using yellow fluorescent protein (YFP) expression to assess the occurrence of EndMT *in vivo*. This lineage tracing allows the expression of YFP only in cells with an endothelial origin. First , mice underwent myocardial infarction (MI) to generate fibrosis and were sacrificed 5 days post-MI. Sham-operated mice were considered as control. Sirius red staining was performed to assess fibrosis in mice heart post-MI. Sirius red stained the collagen in red and the healthy myocardium in green. One day post-MI, collagen expression was

very low and myocardium was mainly stained in green. Five days post-MI , collagen (red) was highly increased and a progressive loss of the myocardium was observed implying the presence of fibrosis (**Figure 5.16**).

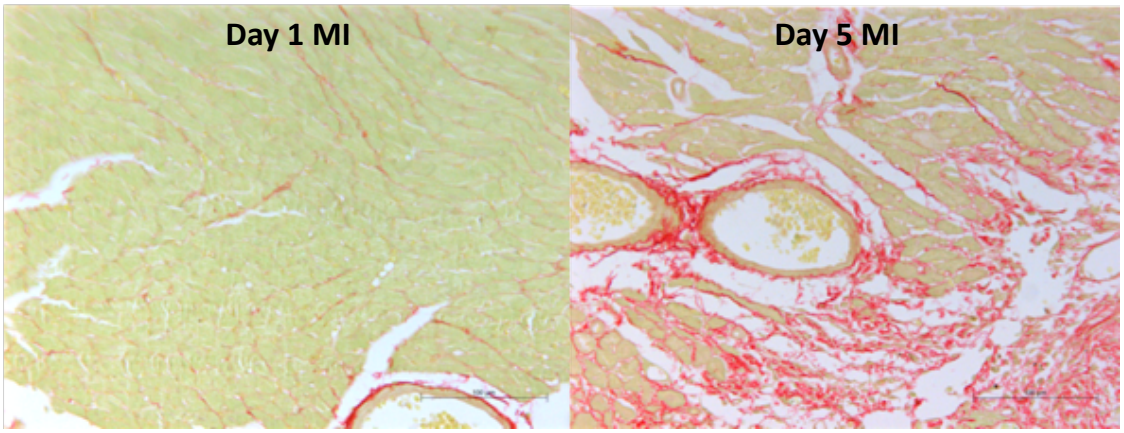


**Figure 5.16 Sirius red staining in mice heart post-MI**
Mice underwent MI and were sacrificed 1 or 5 days later. Sirius red staining was performed following standard procedure in mice heart post-myocardial infarction. Healthy myocardium is represented in green and collagen in red. These pictures were kindly provided by Professor Simi Ali (reference: Sarah Thompson's thesis) .

In order to validate the lineage tracing, double immunofluorescence for YFP and for the endothelial marker CD31 was performed. YFP was stained with an anti-GFP followed by a secondary antibody Alexa fluor 488 conjugate and CD31 was stained with an anti-CD31 followed by a secondary antibody. Both Cre positive and Cre negative were studied and sections were analysed in figure 5.14. In Cre negative mice, no green fluorescent protein (GFP) staining was observed in Sham-operated and MI heart. In Cre positive mice, YFP was found colocalised with CD31 staining both in sham-operated and MI heart implying that the lineage tracing of endothelial cells was accurate.

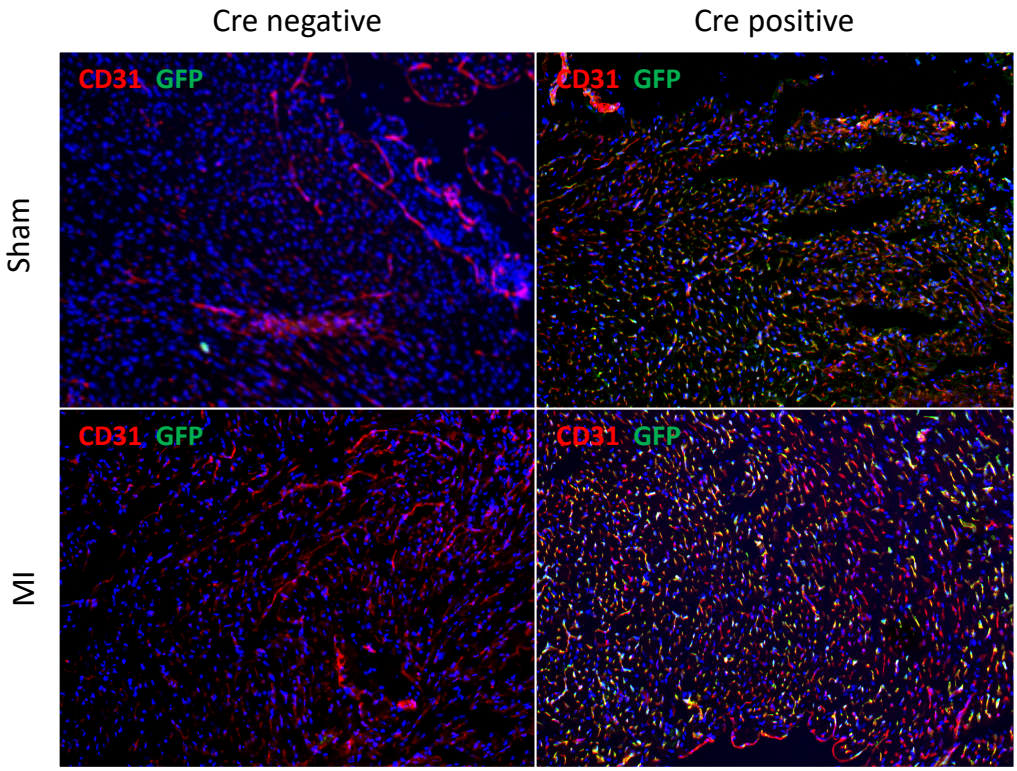


**Figure 5.17 Lineage tracing of endothelial cells in sham-operated and myocardial infarction heart**
Mice underwent MI and were sacrificed at 5 days post-MI. Double immunofluorescence for YFP and CD31 was performed in MI and sham operated heart. Endothelial cells expressing YFP was stained with anti-GFP and a secondary antibody Alexa fluor 488 conjugate( green) whereas CD31 was stained with an anti-CD31 and a secondary antibody Alexa fluor 594(red). Counterstaining was performed with DAPI. Pictures were taken with Zeiss axioimager II upright microscope (Original magnification ×10).

Double immunofluorescence was performed for GFP which represent the endothelial origin and for the mesenchymal marker αSMA in order to detect the presence of EndMT. In transverse sections of heart post-MI, images were taken in both MI and non-MI zones (A, B respectively) and can be seen in **Figure 5.18** and **5.19**. GFP positive vessels were seen in unaffected regions of the heart (B) as well as in the infarct border zone (A and white arrows head in C,D,E). Mesenchymal cells expressing αSMA were located in the infarct border zone. In the MI zone, several endothelial derived cells expressing GFP were also positive for αSMA expression(yellow arrow in C,D,E), suggestive of EndMT *in vivo*. In the non-MI zone, staining of αSMA and GFP were not colocalised.

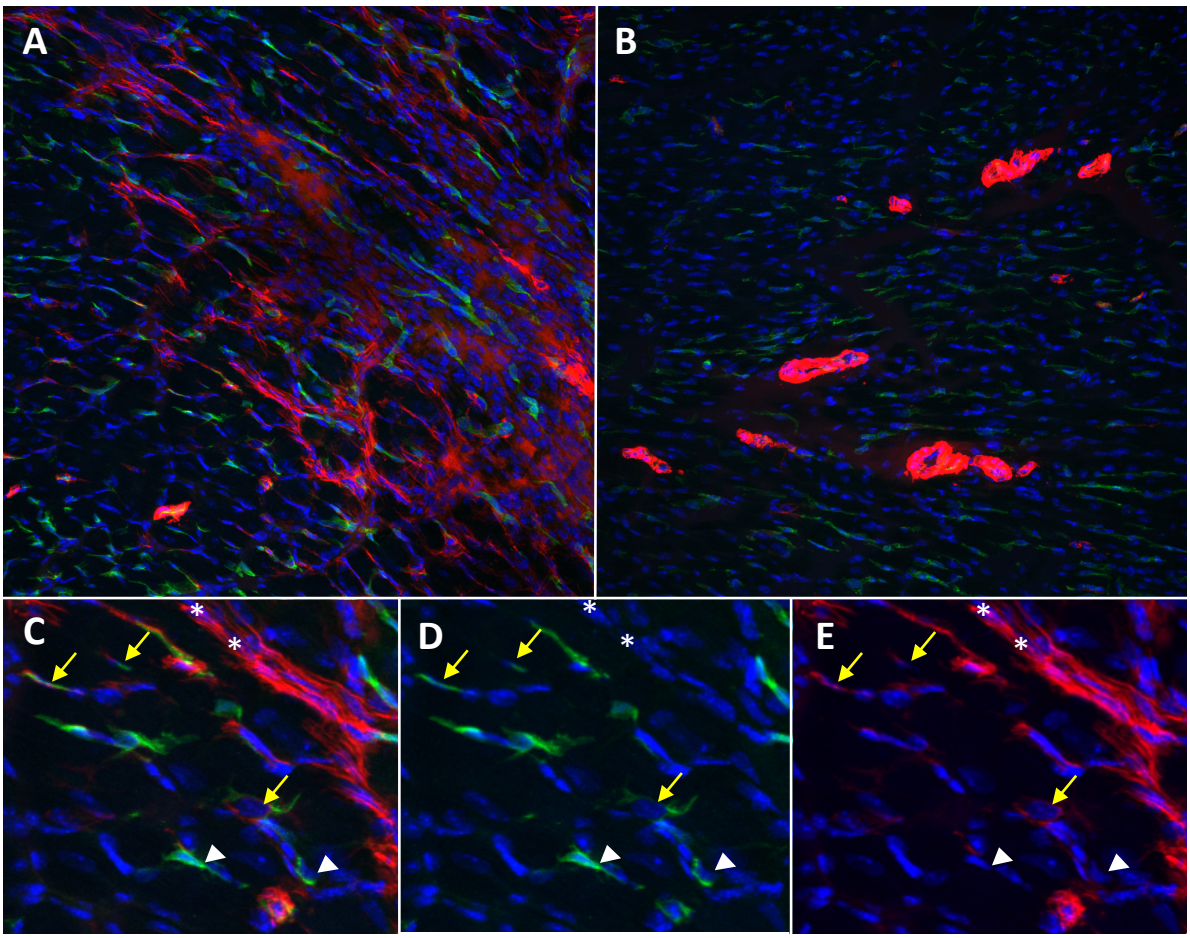


**Figure 5.18 Endothelial-to-mesenchymal transition in mice post-myocardial infarction.** Mice underwent MI and were sacrificed 5 days later. Immunofluorescence of transverse sections of mouse heart post-MI was performed. Endothelial cells expressing YFP were stained with anti-GFP and a secondary antibody Alexa fluor 488 conjugate (green). Mesenchymal cells were stained with αSMA Cy3 conjugate (red). Pictures were taken with confocal Nikon A1R invert in MI area(A) and non-MI zone(B) (Original magnification x20) (n=4). C,D,E represent an enlargement of picture A with merged and individual channels. Double positive cells to GFP and αSMA were indicated by the yellow arrow. Positive cells to GFP or αSMA were located by a white arrows head and a white stars respectively.

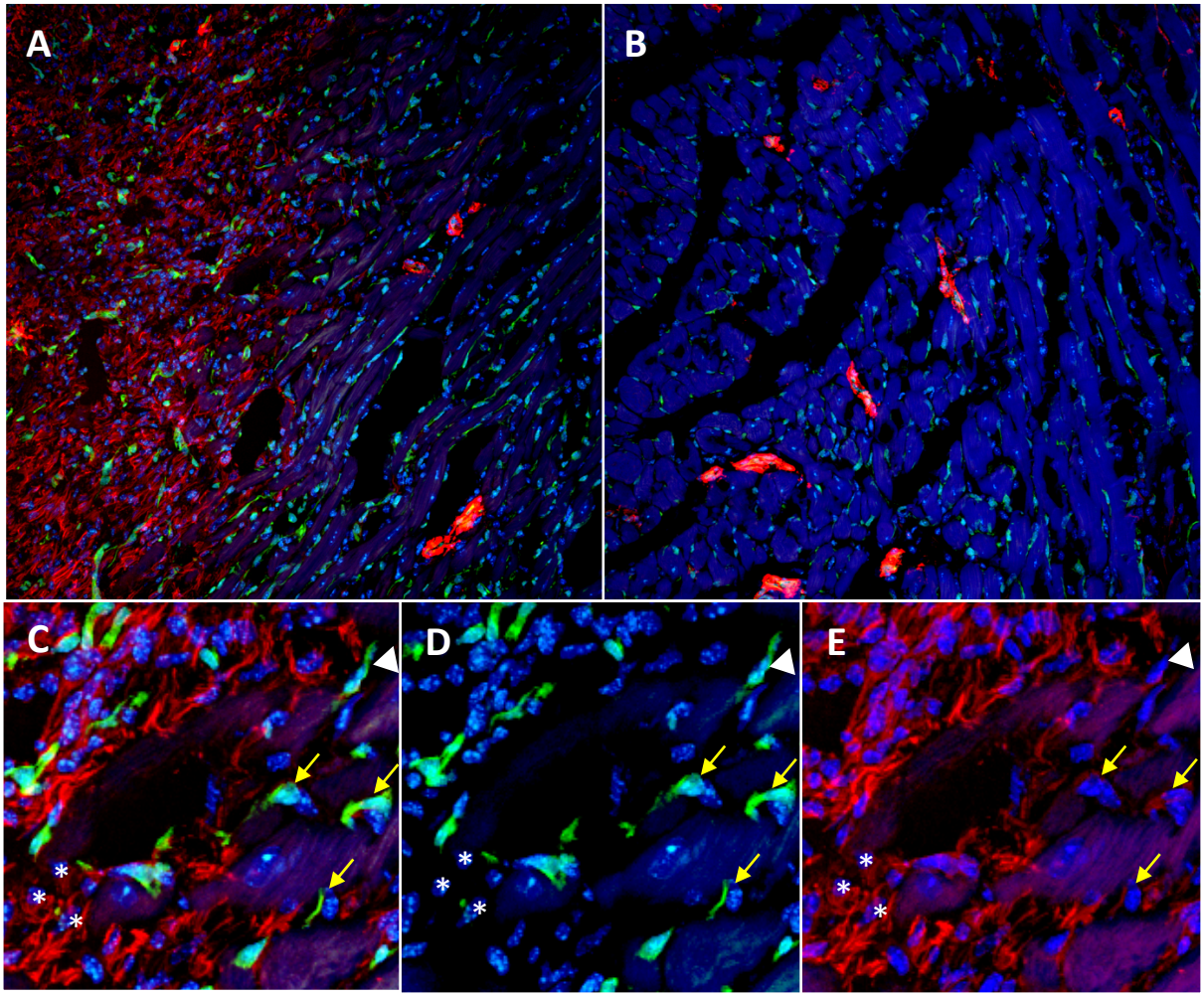


**Figure 5.19 Endothelial-to-mesenchymal transition in mice post-myocardial infarction.** Mice underwent MI and were sacrificed 5 days later. Immunofluorescence of transverse sections of mouse heart post-MI was performed. Endothelial cells expressing YFP were stained with anti-GFP and a secondary antibody Alexa fluor 488 conjugate (green). Mesenchymal cells were stained with αSMA Cy3 conjugate (red). Pictures were taken with confocal Nikon A1R invert in MI area(A) and non-MI zone(B) (Original magnification x20) (n=4). C,D,E represent an enlargement of picture A with merged and individual channels. Double positive cells to GFP and αSMA were indicated by the yellow arrow. Positive cells to GFP or αSMA were located by a white arrows head and a white stars respectively.

### *5.4.5 Localisation of miR-126-3p following myocardial infarction*

Previously in this chapter, miR-126-3p over-expression partially prevented the process of EndMT *in vitro*. In the figure 5.15, evidence showed the presence of EndMT *in vivo* in MI-induced cardiac fibrosis. Thus, localisation of miR-126-3p in cardiac fibrosis was questioned and investigated with the *in-situ* hybridisation technique. *In-situ* hybridisation is illustrated by the hybridisation of a probe complementary to the targeted RNA within the tissue. Probe signal is then amplified in order to visualise the miRNA localisation in a specific tissue. *In-situ* hybridisation for miR-126-3p was performed with a double-digoxigenin (DIG) labelled probe in frozen heart sections from

sham-operated and post-MI mice. After hybridisation step, probe was incubated with an anti-DIG antibody coupled with alkaline phosphatase (AP). Incubation of the hybridisation complex with an alkaline phosphatase substrate resulted in a blue precipitate indicating the localisation of miR-126-3p. Scramble hybridisation was performed to assess the background of the assay and to visualise non-specific staining.

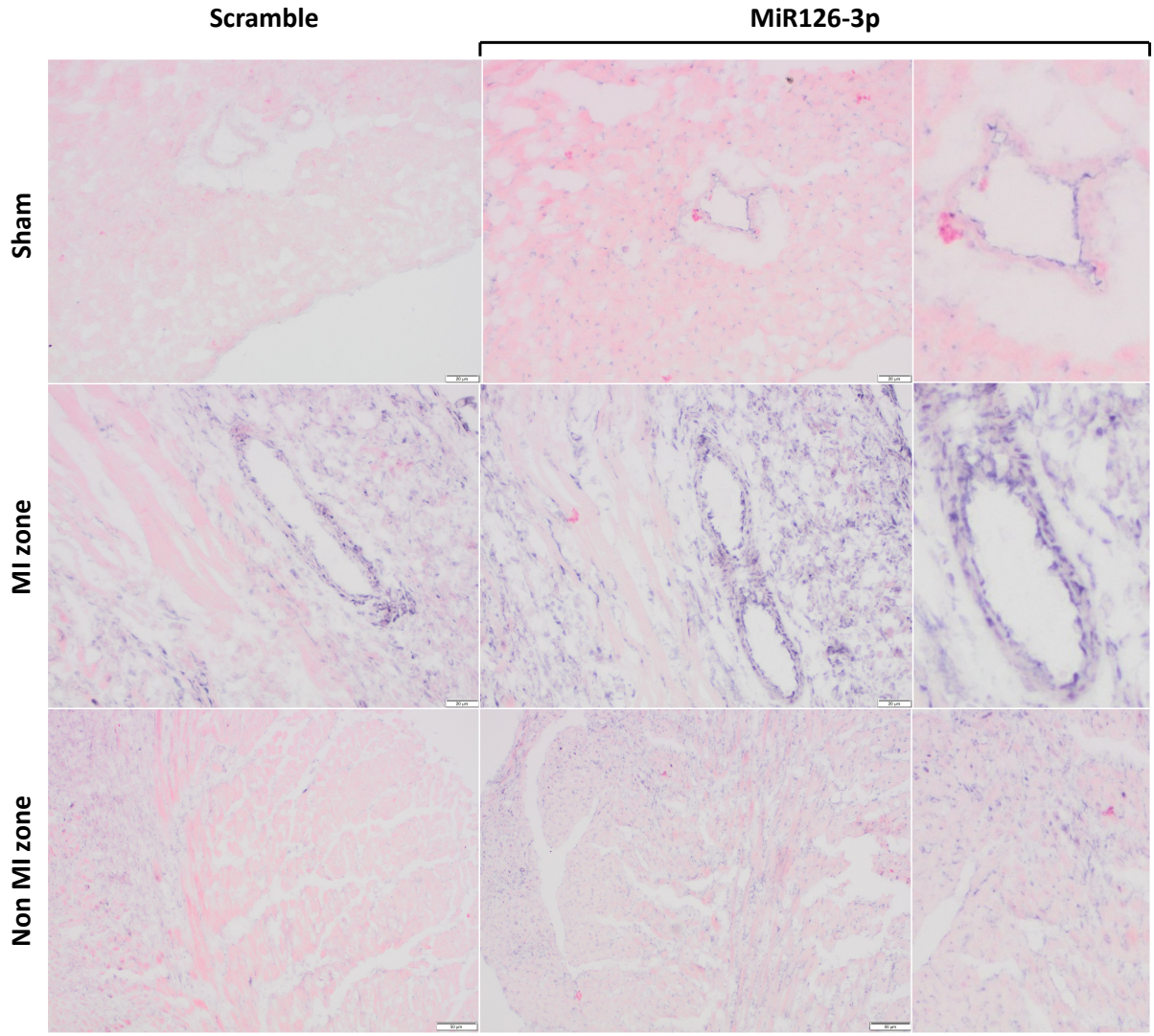


**Figure 5.20 *In-situ* hybridisation of miR-126-3p in mice post-myocardial infarction**
Mice underwent MI and were sacrificed 5 days later. *In- situ* hybridisation was performed in frozen sections of heart with 40 nM of miR-126-3p or scramble double-DIG labeled LNA probes. Hybridisation of the probe to the targeted miRNA was executed at 30 degree below the RNA melting temperature. Sections were incubated with anti-DIG coupled to AP. Substrate of AP was added and the presence of alkaline phosphatase converted the substrate into a blue precipitate. Counterstaining was performed with Nuclear Fast Red. Pictures were taken with Olympus microscope equipped with an SC50 camera in sham-operated(n=1) and MI heart(n=3) for both scramble and miR-126-3p hybridisation. For MI heart , two areas were distinguished the MI zone and the unaffected zone. (Original magnification x20)

In sham-operated heart, scramble hybridisation was clear and miR-126-3p hybridisation showed the presence of this miRNA mainly in endothelial cells. miR-126-3p was observed in the intima layer of the blood vessel and in the capillaries. In the

heart post-MI, miR-126-3p could not be localised as the signal for miR-126-3p could not be distinguished from the noise. Indeed, non-specific staining was observed in the scramble hybridisation and staining showed similar pattern as the one observed in miR-126-3p. In non-MI zone, miR-126-3p staining pattern was comparable to the one observed in sham-operated heart. Numerous optimisations including the increase of hybridisation temperature, the decrease of AP substrate development time or the decrease in probe concentration were performed to reduce the background staining in the fibrotic MI zone but were not successful (data not shown).

In conclusion, MiR-126-3p seems restricted to endothelial cells in healthy heart. Regarding the localisation of miR-126-3p in MI zone, the non-specific staining did not allow conclusions to be made.

### *5.4.6 Endothelial-to mesenchymal transition following unilateral ureteral obstruction*

In the context of kidney fibrosis, the contribution of EndMT was better defined. Lineage tracing of endothelial cells using a Tie2-Cre system revealed the presence of αSMA positive cells that are positive to the endothelial origin in the fibrotic kidney. The contribution of EndMT to the fibroblast population was estimated to 10% (LeBleu *et al.*, 2013b). In order to confirm the presence of EndMT in kidney fibrosis, the mouse line Cdh5-Cre-ERT2; Rosa26R-stop-YFP previously used to assess EndMT in cardiac fibrosis was studied in UUO mice model. Surgeries were performed by Ms Katie Cooke and part of the immunofluorescence staining was executed by Dr Emily Glover. Mice underwent unilateral ureteral obstruction on the left kidney and were sacrificed 5 days later. Both kidneys were collected as the right kidney was a direct control of the fibrotic left kidney. Sirius red staining was performed to assess the generation of fibrosis post-UUO. In the kidney post-UUO, increase of collagen deposition was observed suggesting the development of fibrosis (**Figure 5.21**).

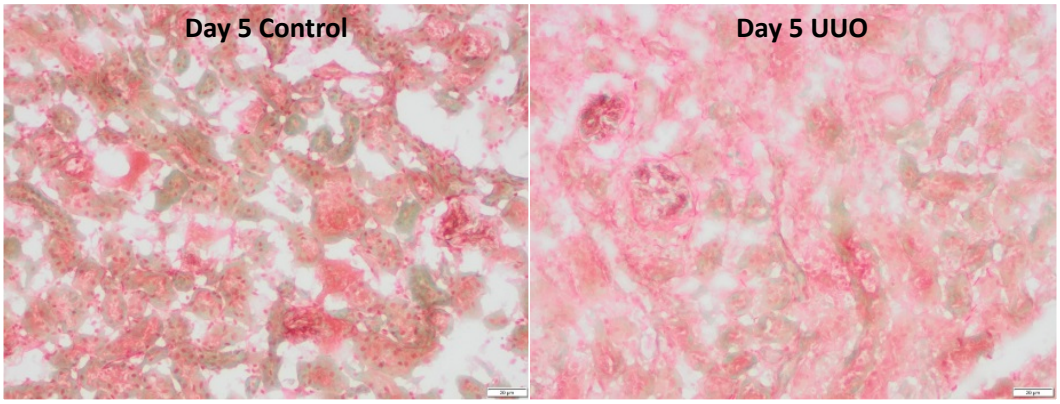


**Figure 5.21 Sirius red staining in mice healthy and fibrotic kidney**
Mice underwent left kidney UUO and were sacrificed 5 days later. Sirius red staining was performed following standard procedure in mice healthy and fibrotic kidney. Healthy kidney tissue is represented in green and collagen in red.

First, immunofluorescence for YFP was performed with an anti-GFP in frozen right control kidney sections of Cre-negative and Cre-positive mice. In Cre-positive mice, GFP staining was observed in glomeruli and capillaries meanwhile no GFP expression was observed in Cre-negative mice (**Figure 5.22**). This implies that Cre-positive mice allows the expression of GFP in endothelial cells.

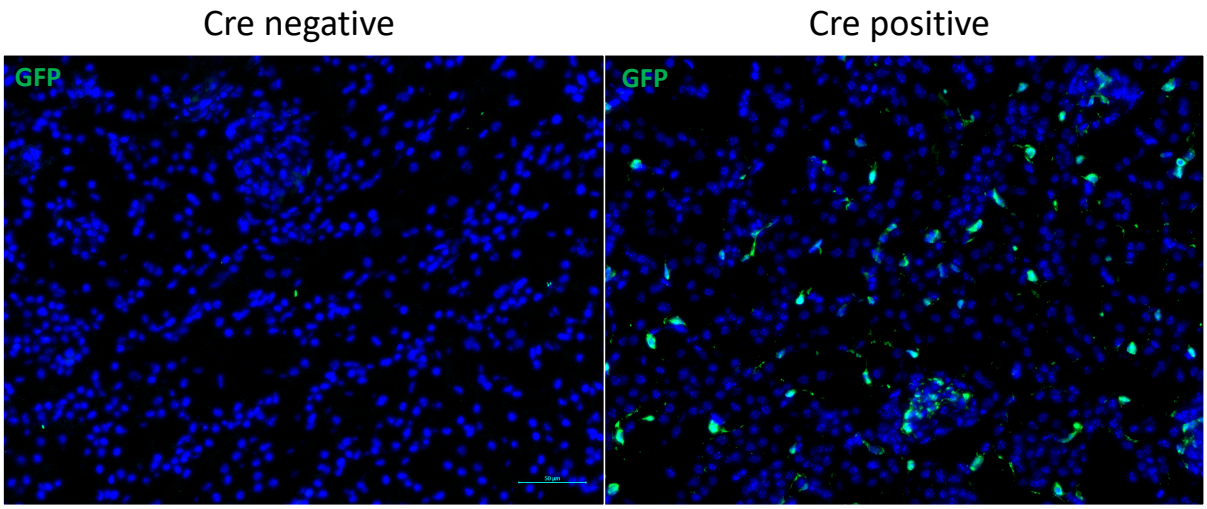


**Figure 5.22 Lineage tracing of endothelial cells in healthy kidney**
Healthy kidneys of Cre positive or Cre negative mice were stained for YFP lineage tracing. Endothelial cells expressing YFP was stained with anti-GFP and a secondary antibody Alexa fluor 488 conjugate( green) and DAPI was used for counterstaining. Pictures were taken with Zeiss axioimager II upright microscope (Original magnification ×20)(n=1).

To further validate the lineage tracing under the promoter of VE-cadherin, double immunofluorescence for GFP and for the endothelial marker CD31 was carried out in healthy right kidney and its associated fibrotic left kidney. In both right and left kidney, CD31 and GFP were colocalised in glomeruli. GFP staining also showed similar staining in the sections of right and left kidney that could correspond to the staining

within the capillaries. This was confirmed in the left kidney where the GFP staining was also positive to CD31 (**Figure 5.23**). Lineage tracing of the Cdh5-Cre-ERT2; Rosa26R-stop-YFP mouse model seems accurate and restricted to endothelial cells in kidneys despite the lack of correlation observed between GFP and CD31 in the right kidney.

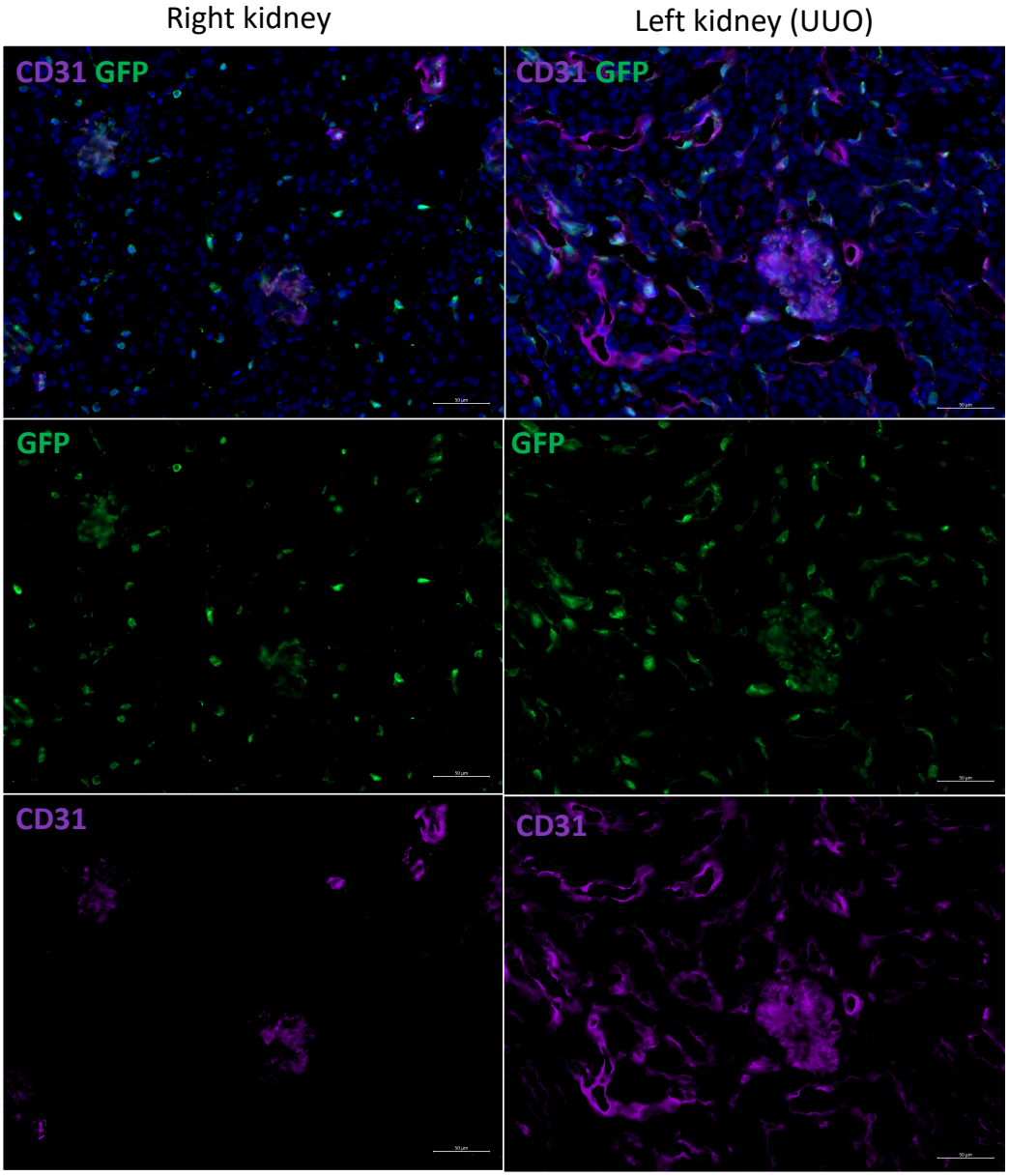


**Figure 5.23 Lineage tracing of endothelial cells in healthy and UUO kidneys**
Mice underwent left kidney UUO and were sacrificed 5 days later. Double immunofluorescence for YFP and CD31 was performed in healthy right kidney and fibrotic left kidney. Endothelial cells expressing YFP was stained with anti-GFP and a secondary antibody Alexa fluor 488 conjugate( green) whereas CD31 was stained with an anti-CD31 and a secondary antibody Alexa fluor 633 (purple). Counterstaining was performed with DAPI. Pictures were taken with Zeiss axioimager II upright microscope (Original magnification ×20)(n=1).

EndMT was then assessed in kidney fibrosis by double immunofluorescence. GFP staining allowed the identification of cells with an endothelial origin meanwhile αSMA staining showed the activated fibroblast population. In the healthy right kidney (B), YFP cells were observed in glomeruli, in capillaries and in the intima layer of blood vessel.

In addition, αSMA staining was found in vascular smooth muscle cells. In the fibrotic left kidney, αSMA was expressed by the VSMC and the myofibroblasts population. Excluding the blood vessel, colocalisation of the endothelial origin and αSMA was found in the fibrotic kidney (A, yellow arrows in C,D,E), suggestive of EndMT *in vivo*. In healthy kidney (B), staining of αSMA and GFP were not colocalised.(**Figure 5.24**)

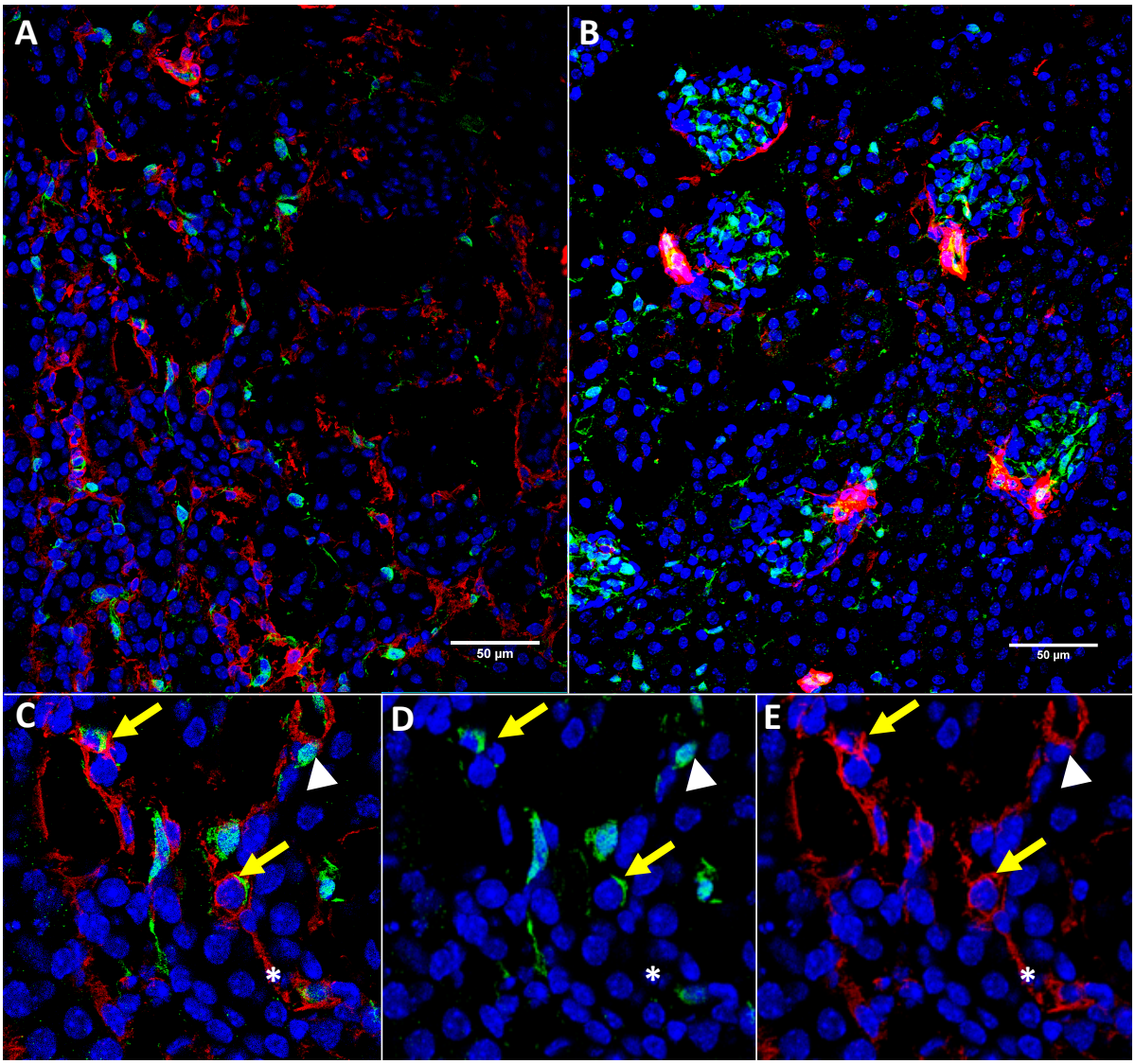


**Figure 5.24 Endothelial-to-mesenchymal transition in UUO mice.**
Mice underwent left kidney UUO and were sacrificed 5 days later. Immunofluorescence of transverse sections of left fibrotic kidney and its associated right kidney, was performed. Endothelial cells expressing YFP were stained with anti-GFP and a secondary antibody Alexa fluor 488 conjugate (green). Mesenchymal cells were stained with αSMA Cy3 conjugate (red). Pictures were taken with Leica SP8-STED confocal microscope in left kidney(A) and right kidney(B) (Original magnification x20) (n=4). C,D,E represent an enlargement of picture A with merged and individual channels. Double positive cells to GFP and αSMA were indicated by the yellow arrow. Positive cells to GFP or αSMA were annotated with white arrows head and white stars respectively.

### 5.4.7 Localisation of miR-126-3p following unilateral ureteral obstruction

In this chapter, localisation of miR-126-3p in normal heart was elucidated by *in-situ* hybridisation. Evidence showed that miR-126-3p was restricted to endothelial cells in healthy heart. To investigate the localisation of miR-126-3p in fibrotic kidney, same *in-situ* hybridisation protocol than **Figure 5.20** was applied on frozen healthy kidney sections and frozen fibrotic kidney sections from 5 days post-UUO mice. In order to visualise non-specific staining and define the background of the assay, scramble hybridisation was carried out in parallel of miR-126-3p hybridisation. Post-hybridisation, pictures were taken in structures expressing endothelial cells such as glomeruli (B,D) or blood vessels (A,B). In healthy kidney, scramble hybridisation was clear and miR-126-3p hybridisation showed the presence of this miRNA in the intima layer of the blood vessel (B) and in the glomeruli (D) (**Figure 5.25**).

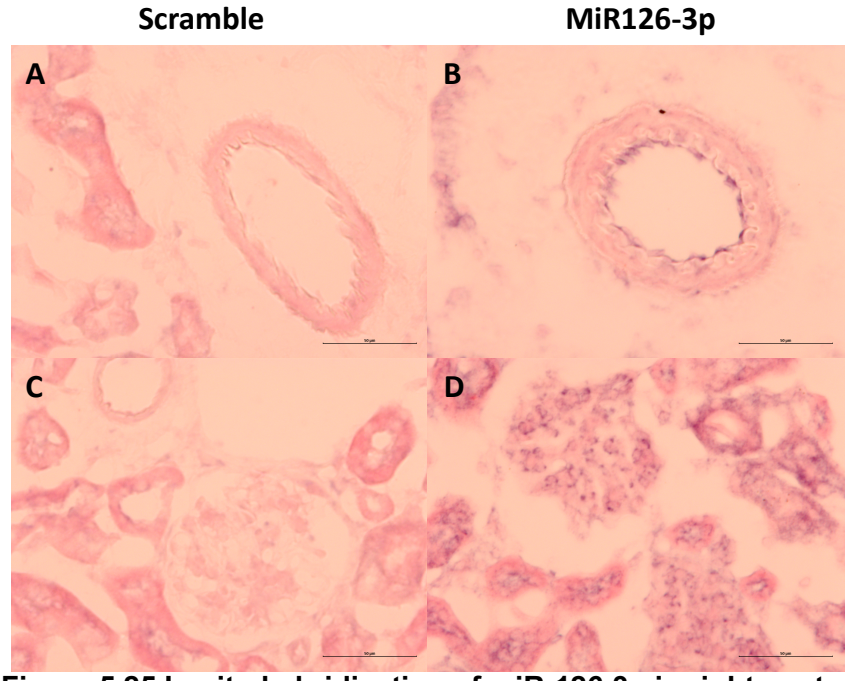


**Figure 5.25 In-situ hybridisation of miR-126-3p in right control kidney.**
*In situ*-hybridisation was performed in frozen sections of healthy right kidney with 40nM of miR-126-3p or scramble double-DIG labeled LNA probes. The probe was incubated at 30 degree below the RNA melting temperature for hybridisation. Then, anti-DIG coupled to alkaline phosphatase was added to the sections. Sections were incubated with a substrate of AP which is converted in blue precipitate in the presence of alkaline phosphatase. Nuclear Fast Red was used for counterstaining. Pictures were taken with Olympus microscope equipped with an SC50 camera in healthy right kidney for scramble or miR-126-3p hybridisation and were focused on specific structures of the kidney such as blood vessel (A,B) or glomeruli (C,D) (Original magnification x40).

In the fibrotic kidney post-UUO, miR-126-3p expression was similar to the expression in healthy kidney. MiR-126-3p was localised in the glomeruli and in blood vessel intima layer. Scramble hybridisation was clear and comparable to healthy kidney scramble

hybridisation. In conclusion, miR-126-3p seems restricted to endothelial cells in healthy and fibrotic kidneys.

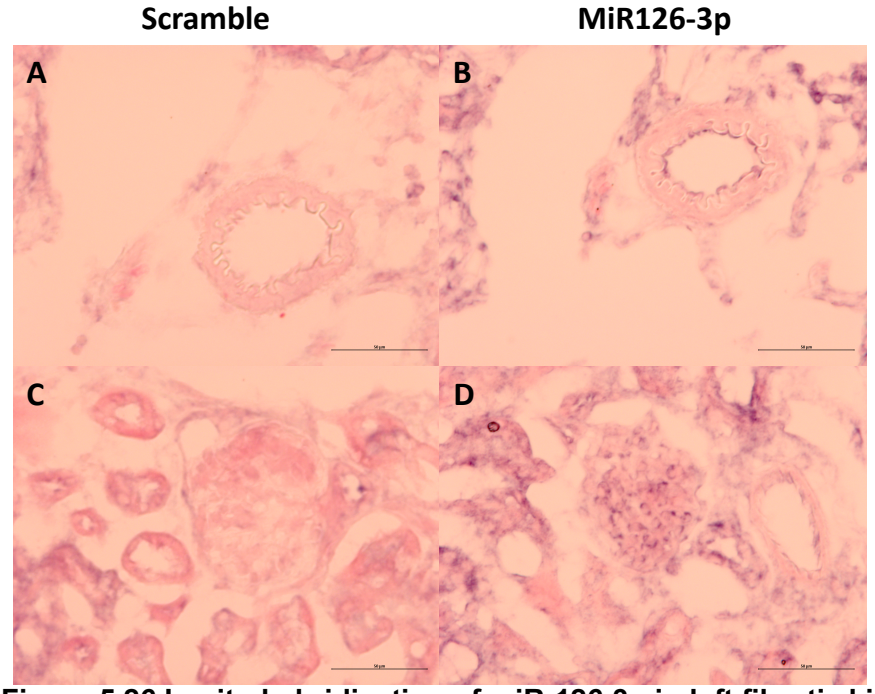


**Figure 5.26 In-situ hybridisation of miR-126-3p in left fibrotic kidney post-UUO**
Mice underwent left kidney UUO and were sacrificed 5 days later. *In situ*-hybridisation was performed in frozen sections of heart with 40nM of miR-126-3p or scramble double-DIG labeled LNA probes. Hybridisation of the probe to the targeted miRNA was executed at 30 degree below the RNA melting temperature. Sections were incubated with anti-DIG coupled to alkaline phosphatase. Substrate of alkaline phosphatase was added and the presence of alkaline phosphatase converted the substrate into a blue precipitate. Counterstaining was performed with Nuclear Fast Red. Pictures were taken with Olympus microscope equipped with an SC50 camera in healthy right kidney for scramble or miR-126-3p hybridisation and were focused on specific structures of the kidney such as blood vessels (A,B) or glomeruli (C,D) (Original magnification x40)

## 5.5 Discussion

Evidence showed that MiRNAs can regulate key biological processes including EndMT. Indeed, miR-21 was found markedly increased during EndMT in vitro and its inhibition was able to prevent EndMT both *in vitro* and *in vivo* in a model of cardiac fibrosis.(R. Kumarswamy *et al.*, 2012). In our study miR-126-3p was found down-regulated *in vitro* in cells undergoing EndMT and we aimed to investigate the role of miR-126-3p in EndMT *in vitro* and in the context of fibrosis *in vivo*.

In HUVEC cells, miR-126-3p mimic were transfected with lipofectamine to increase miR-126-3p level in the cells. Optimisation of lipofectamine volume and concentration of mimics were performed with mimic transfection control with Dy547 (described in materiel and methods). From this optimisation, the condition with 1µl of lipofectamine RNAimax and 11nM of mimics was selected for a 18 hours transfection. Surprisingly, immunofluorescence for CD31 of cells cultured with lipofectamine for 18 hours showed a clear decrease of CD31 expression compared to untreated cells. As lipofectamine can be cytotoxic to the cells, conditions for optimisation were replaced by 0,5µl of lipofectamine and 30nM of mimics. In addition, transfection time was reduced to 6 hours. With this new condition, CD31 expression in cells transfected with miR-126-3p or NsMiR was comparable to the expression in untreated cells and untreated cells cultured with lipofectamine.

Transfection in primary endothelial cells was suggested more difficult than transfection in endothelial cell line. In the study of Hunt et al, transfection in HUVEC with lipofectamine 2000 showed a decrease in cell viability of 10% after 24 hours of transfection and only 19% of cells were positive for the transfection (Hunt *et al.*, 2010). In our study, most of the cells were dead 24 hours post-transfection with lipofectamine RNAimax. Optimisation with mimic transfection control with Dy547 showed that mimic were successfully transfected after 18 hours of transfection and 18 hours transfection of miR-126-3p mimics showed a high increase in miR-126-3p level. However, CD31 expression was markedly decreased in cells cultured 18 hours in presence of lipofectamine , thus lipofectamine volume and transfection time point were reduced. Another study showed that DNA transfection into HUVEC rapidly induces the degradation of the exogenous DNA (Colombo *et al.*, 2001).This suggests that a low transfection efficiency and a rapid degradation of the exogenous miRNA could reduce

the effect of the miRNA on the cells. In our study, no effect on EndMT was seen with 30nM miR-126-3p transfection unlike the 50nM mimics transfection.

Thereafter, six hours transfection of miR-126-3p or NsmiR in HUVEC cells was followed by 48 hours of treatment with TGFβ2 and IL1β in order to assess the role of miR-126-3p in EndMT. With 30nM of mimics, no effect of miR-126-3p on CD31 was observed in treated cells. Mimic concentration was increased to 50nM and 100nM. Both 50nM and 100nM of miR-126-3p seemed to modulate the expression of CD31 in treated cells. In fact, CD31 was found significantly decreased in HUVEC post-treatment and the transfection of miR-126-3p was able to restore the level of CD31 expression at protein level. Interestingly, miR-126-3p over-expression did not modulate CD31 expression at gene level. At gene expression level, fibronectin was found significantly increased in treated cells and miR-126-3p over-expression significantly reduced its expression. However, the transfection of miR-126-3p did not affect the gene expression of vWF and αSMA. In chapter 3, CD31 and αSMA gene expression was found unchanged Post-treatment with TGFβ2 and IL1β. These results were correlated to the results obtained from the transfection experiments. As previously discussed, Maleszewska et al demonstrated that αSMA was significantly up-regulated at gene expression level after 7 days of treatment with TGFβ2 and IL1β. This can explain the unchanged expression of αSMA post-treatment and post-transfection.

Transfection of miR-126-3p in HMEC1 cells showed the same results as the transfection performed in HUVEC. Over-expression of miR-126-3p reduced fibronectin expression and did not affect vWF expression.

Interestingly, van Beijnum et al published a study where transfection was compared between HMEC1 and HUVEC. The transfection of a plasmid with a GFP reporter showed a transfection efficiency around 40% in the endothelial cells line meanwhile transfection in HUVEC only gave a limited change in fluorescence (van Beijnum *et al.*, 2008). In this chapter, HMEC1 were transfected under the same conditions used for HUVEC's transfection and final results were similar in both cell type.

Our study is the first to show a potential role of miR-126-3p in EndMT. In HUVEC, few miRNAs were described as regulator of EndMT. Indeed, miR-21 was found up-regulated in HUVEC undergoing EndMT and the use of miR-21 antagomir led to a restoration of VE cadherin and the reduction of FSP1 both at protein level. In addition, miR21 antagomir was studied at gene level. Increase in CD31 expression and

decrease of MMP2 and MMP9 expression meanwhile eNOS expression was unchanged(R. Kumarswamy *et al.*, 2012). Interestingly, Xu et al demonstrated the role of miR-126a-5p in endothelial cells undergoing EndMT under hypoxic conditions. Pulmonary microvascular endothelial cells exposed to hypoxia showed an increase of miR-126a-5p expression concomitantly with the increase of mesenchymal markers and the decrease of endothelial markers. Inhibition of miR-126-5p in hypoxic cells reduced the process of EndMT (Xu *et al.*, 2017). This shows that miRNAs that arise from two different strand of the same precursor can have an opposite role in biological processes. Furthermore, these results confirm that modulation of the expression of one miRNA can partially prevent or trigger EndMT. In our study, the transfection of miR-126-3p had an impact on CD31 and fibronectin expression but did not influence the expression of vWF.

Predicted target of miR-126-3p were studied in our EndMT *in vitro* system. In fact, neither ADAM9 nor SMURF2 were found up-regulated post-treatment with TGFβ2 and IL1β. Transfection of miR-126-3p tend to increase ADAM9 expression but did not modulate SMURF2 expression. This result suggests that ADAM9 and SMURF2 are not implicated in the process of EndMT. ADAM9 was described previously as a target of miR-126-3p in hepatocellular carcinoma cells and was validated as a direct target in prostate cancer(Xiang *et al.*, 2017; Hua *et al.*, 2018). In our study, cells transfected with miR-126-3p induced a non-significant decrease of ADAM9 expression but more experiments will be required to confirm this trend. SMURF2 is not described as validated target and might be part of the false positive prediction of the prediction target tools.

There are contradictory results about the involvement of EndMT in cardiac fibrosis and therefore we aimed to examine whether EndMT was present in cardiac fibrosis in vivo. The mouse model Cdh5-Cre-ERT2; Rosa26R-stop-YFP allows the lineage tracing of endothelial cells by inducing the expression of YFP in cells with an endothelial origin. In addition, mice underwent myocardial infarction in order to generate cardiac fibrosis. First, the accuracy of the lineage tracing under the promoter of VE-cadherin was verified by double immunofluorescence for YFP with an anti-GFP antibody and an endothelial marker CD31. In Cre negative mice, no GFP staining was observed meanwhile in Cre positive mice, GFP staining was colocalised with CD31 expression in both sham-operated and post-MI mice. To investigate the presence of EndMT,

αSMA marker was selected to represent the population of myofibroblasts. Alpha SMA is also expressed by vascular smooth muscle cells localised in the media layer of the blood vessels, thus EndMT was not assessed in blood vessels. Double immunofluorescence for YFP and αSMA was performed in sham-operated and post-MI heart. In MI heart, two zones were distinguished, the unaffected zone (non-MI zone) and the MI zone. No colocalisation was observed in non-MI zone and sham-operated hearts as αSMA was mainly expressed by the vascular smooth muscle cell . However in MI zone, myofibroblast population was detected and some αSMA positive cells were also positive for GFP implying the presence of EndMT.

Similar experiment with the same mouse model Cdh5-Cre-ERT2; Rosa26R-stop-YFP was performed to observe the occurrence of EndMT in the context of kidney fibrosis. Mice underwent UUO on the left kidney and the right kidney was used as control. Cre negative mice did not show any GFP staining and Cre positive mice revealed GFP staining colocalised with CD31 staining. Lineage tracing was assessed in both kidneys with the double staining GFP and CD31. Unlike the lineage tracing in heart, lineage tracing of endothelial cells in kidneys was very variable from one animal to another. CD31 and GFP were found colocalised in all kidneys, thus the lineage was accurate. However, the amount of YFP positive cells was markedly decreased in some kidneys( data not shown). To assess EndMT, only kidneys with normal level of GFP staining were used. Double immunofluorescence was performed with αSMA and GFP in both kidneys. In the healthly kidney, no colocalisation of GFP and αSMA was observed. However, colocalisation was observed in the left fibrotic kidney where cells positive for αSMA were also positive to an endothelial origin suggesting the occurrence of EndMT. In the study of Zeisberg et al, lineage tracing under the promoter of Tie1 (Tie1-Cre), revealed that 75% of alpha SMA positive cells were also positive for endothelial origin in mice heart post-aortic banding. However, a study demonstrated that immune cells could also express reporter by Tie1, thus the first study was invalidated (Gustafsson *et al.*, 2001). A second study using a Cre-Lox system under the promoter of VE-cadherin/Cdh5 assessed the contribution of EndMT in cardiac fibrosis study and concluded that no significant contribution of endothelial cells to the fibroblast population was observed. Interestingly, fibroblast identification was based on Col1A1 expression which did not overlap with FSP1 (0%) and αSMA (7%) mesenchymal markers. This suggests that only a part of fibroblast population was studied. (Moore-Morris, Guimarães-Camboa, Banerjee, Alexander C. Zambon, *et al.*, 2014). Using the model Cdh5-Cre-ERT2; Rosa26R-stop-YFP, cells in MI heart were found positive to

αSMA and to an endothelial origin suggesting the presence of EndMT in cardiac fibrosis .

Zeisberg et al demonstrated the implication of EndMT in renal fibrosis in three different mice models: (STZ)-induced diabetic nephropathy, UUO and COL4A3 KO. In UUO mice, EndMT was detected one week after ureter ligation by the co-expression of CD31 and FSP1.This co-expression was also observed in 22 weeks COL4A3 KO mice and in 6 months STZ induced diabetic nephropathy mice (Zeisberg *et al.*, 2008). In early development of interstitial kidney fibrosis, lineage tracing using Tie2-cre recombinase (Kisanuki *et al.*, 2001) identified a population of alpha SMA positive cells with an endothelial origin (Li *et al.*, 2009). Tie2-cre recombinase was also studied in UUO model where approximatively 10% of mesenchymal cells on site were positive for endothelial origin (LeBleu *et al.*, 2013b). These results suggest that EndMT contributes to the pool of myofibroblast both in cardiac and kidney fibrosis.

In order to link EndMT to miR-126-3p *in vivo*, *in-situ* hybridisation was performed to localise miR-126-3p within healthy and fibrotic tissue. Hybridisation with a scramble miRNA was used as a control. In healthy heart and kidney, scramble hybridisation was clear and miR-126-3p was mainly localised in the endothelial cells. In heart post-MI, scramble miRNA showed non-specific staining in the extracellular matrix and similar staining was observed for miR-126-3p. Therefore, conclusion could not be made regarding the localisation of miR-126-3p in the MI zone. In the unaffected area, miR-126-3p staining was comparable to the staining in the healthy heart. In the fibrotic kidney, miR-126-3p was localised in the glomeruli and in the intima layer of the blood vessel , thus mainly in endothelial cells. This suggests that miR-126-3p is localised in endothelial cells in both cardiac and renal tissue. In the study of Kriegel et al, in-situ hybridisation for miR-382 was optimised in kidney post-UUO and demonstrated that miR-382 was down-regulated in the fibrotic kidney. They described that non-specific staining can be caused by a dried tissue and that tissue section should always be covered by liquid (Kriegel and Liang, 2013). In our project, sections were not covered with coverslip during hybridisation and might have dried out during this step. However, only the MI-zone was affected with non-specific staining, thus non-specific staining was not caused by drying. Interestingly, Sigma-aldrich company described that a non-specific staining can be caused by the presence of intracellular lipid droplet. Indeed, heart tissue can contain these droplets which can catch some of the color precipitate

on cryosections. This issue can be prevented by the delipidization of the sections with chloroform and will need to be address in the future experiments.

# Chapter 6. General discussion

Fibrosis is described as a pathologic tissue repair due to an accumulation of extracellular matrix secreted by the myofibroblast population. In fibrotic disease , studies are focused on myofibroblast origin and have revealed that non-proliferating myofibroblasts could be derived from other cell types. This specifically includes the process of endothelial-to-mesenchymal transition (EndMT). Studies of EndMT *in-vivo* using lineage tracing of endothelial cells reported that 27% to 35% and 10% of myofibroblasts involved in cardiac fibrosis and kidney fibrosis respectively were endothelial in origin. Over the last decade, miRNAs have increasingly been described as key regulators in biological processes through repression or degradation of targeted mRNA. Their profile and potential role remains mainly undescribed in EndMT, although MiRNAs have been more widely studied in the related process of epithelial-to-mesenchymal transition (EMT). We hypothesized that miRNA could play a role in EndMT and might prevent the progressive development of fibrosis.

## 6.1 In vitro model of EndMT

Our first aim was to develop a model of EndMT *in vitro* based on a treatment with TGFβ2 and IL1β. Treatment with TGFβ2 and IL1β was applied to HMEC1 cell line and to the primary endothelial cells HUVEC. EndMT was assessed at gene and protein level by the decrease of endothelial markers and the increase of mesenchymal markers.

At gene expression level, HMEC1 showed significant increase of fibronectin and decrease of vWF 48 hours post-treatment with TGFβ2 and IL1β. In addition, up-regulation of fibronectin at protein level was observed 6 days post-treatment.

HUVEC were treated with TGFβ2 and IL1β and results in the down-regulation of vWF and VE cadherin 48 hours post-treatment whereas fibronectin was found significantly increased in the first 24 hours. Unexpectedly, αSMA expression, the marker for activated fibroblast, was unchanged. To investigate EndMT in HUVEC at protein level, cells were treated for 6 days and fibronectin was found significantly increased and endothelial markers such as VE- cadherin and CD31 were significantly decreased.

In both cell type, the treatment induced an increase of fibronectin expression at protein and gene level meanwhile vWF gene expression was decreased. Additionally, HUVEC post-treatment showed a decrease in level of VE-cadherin at gene and protein level.

Numerous models of EndMT have been generated in HUVEC with the induction of oxidative stress, treatment with TGFβ2 alone or combined with IL1β (R Kumarswamy *et al.*, 2012; Maleszewska *et al.*, 2013; Montorfano *et al.*, 2014). Maleszewska et al demonstrated that the combination of TGFβ2 and IL1β led to a synergistic induction of EndMT in HUVEC. Thus, TGFβ2 alone can induce EndMT but requires a daily renewal or a longer treatment to observe the decrease of endothelial markers and the increase of mesenchymal markers. Our results at gene expression level were similar to this study. Indeed, Maleszewska et al showed that vWF was significantly down-regulated 3 days post-treatment and fibronectin significantly up-regulated 24 hours post-treatment. In correlation, with our results, the treatment did not induce an increase of alpha SMA before the day 7. (Maleszewska *et al.*, 2013).

In HUVEC, the transcription factors Snail and Slug were found significantly up-regulated 72 hours post treatment which was in correlation to previous observations. In TGFβ1-induced EndMT model both Snail and Slug were up-regulated post-treatment in HUVEC. (Cooley *et al.*, 2014). Increased expression of Snail was also observed human coronary endothelial cells undergoing hypoxic conditions (Xu *et al.*, 2015). Furthermore, in endothelial cells treated with TGFβ2 or TGFβ1, silencing of Snail prevented EndMT (Medici *et al.*, 2011) .

Based on the TGFβ2 and IL1β treatment, EndMT model was successfully established in HMEC1 and HUVEC. HMEC-1 cells were a suitable model for EndMT research as it allows less variability for data acquisition and were positive to most endothelial markers. However, treatment with TGFβ2 and IL1β was able to modulate the protein expression of VE-cadherin and CD31 in HUVEC, whereas, these marker could not be assessed in HMEC1. Indeed, CD31 and VE-cadherin immunofluorescence did not show any staining. Therefore, the use of primary endothelial cells seemed most appropriate to establish a model of EndMT *in vitro*.

## 6.2 MiRNA profile in EndMT model

After establishing a model of EndMT *in vitro* with TGFβ2 and IL1β treatment, miRNAs profile was investigated in our model. In HUVEC 24 hours post-treatment, miR21-5p and miR195-5p were found significantly up-regulated. The increased expression of this two miRNA has been previously described in the context of the EndMT and was concordant with our data. Indeed. MiR-21-5p and miR-195-5p were found up-regulated in TGFβ2-induced EndMT in mouse cardiac endothelial cells. In addition, two studies

described the increase in miR21-5p expression in HUVEC undergoing EndMT with TGFβ treatment (R. Kumarswamy *et al.*, 2012; Guo *et al.*, 2015).

Thereafter, miRNAs profile was assessed with the nCounter miRNA assay from Nanostring technologies. Total RNA extracted from untreated HUVEC and HUVEC undergoing EndMT with different time of TGFβ2/ IL1β treatment were assayed in duplicate in the nCounter plate. Up to 800 miRNAs were quantified without amplification in each sample. Differential miRNA expression was observed between the untreated and treated cells. Some miRNAs were found up-regulated and some others were down-regulated in EndMT. Two miRNAs were selected as potential regulator of EndMT according to their abundance, the fold change expression and the significance of the expression changes: miR-126-3p and miR-146a-5p.

MiR-126-3p was found down-regulated with a 2,9 fold decrease in nCounter assay in HUVEC 24 hours post-treatment. This results was confirmed by RT-qPCR where miR-126-3p was significantly decreased with a 2,4 fold decrease 24 hours post-treatment. ($P<0,0001$). As to miR-146a-5p, its expression in HUVEC 24 hours post-treatment was up-regulated with 31-fold increase from the nCounter assay and 59-fold increase from RT-qPCR data.

Interestingly, miR-126-3p has been described in the literature as endothelial specificand participates in the regulation of angiogenesis and vascular integrity. In vitro, over-expression of miR-126-3p in human saphenous vein endothelial cells results in increased migration and proliferation by the silencing of the validated target SPRED1 and PiK3R2 (Qu *et al.*, 2017). Additionally, knockdown of miR-126-3p in zebrafish lead to vascular leakage and hemorrhaging (Fish *et al.*, 2008; Wang *et al.*, 2008). The down-regulation of miR-126-3p in endothelial cells undergoing a transdifferentiation and losing progressively their endothelial features implies that miR-126-3p might have a role in the regulation of endothelial-to-mesenchymal transition.

## 6.3 Role of miR-126-3p in EndMT

As miR-126-3p expression was significantly downregulated in cells undergoing EndMT, we aimed to investigate the role of miR-126-3p in EndMT *in vitro* and in the context of fibrosis *in vivo*.

Over-expression of miR-126-3p in EndMT was studied by mimic transfection with lipofectamine in HUVEC cells undergoing EndMT. The transfection in primary endothelial cells is known to be difficult as Primary cells are more sensitive to the

cytotoxicity of transfection reagent and can rapidly degrade exogenous nucleic acids. Hunt et al showed a low transfection efficiency with lipofectamine 2000 in HUVEC and decrease in cell viability to 10% after 24 hours of transfection (Hunt *et al.*, 2010). In addition, there was rapid degradation of the exogenous DNA following HUVEC transfection (Colombo *et al.*, 2001). In our study, transfection in HUVEC was optimised and HUVEC were transfected for 6 hours with 50nM of mimics and 0,5µl of lipofectamine RNaimax.

Following transfection of miR-126-3p or NsmiR, HUVEC cells were treated for 48 hours with TGFβ2 and IL1β in order to assess the role of miR-126-3p in EndMT. At protein level, CD31 was found significantly down-regulated in HUVEC undergoing EndMT and miR-126-3p transfection restored CD31 expression. Nevertheless, miR-126-3p over-expression did not modulate CD31 expression at gene level. Post-treatment, fibronectin was significantly up-regulated and miR-126-3p transfection resulted in a decrease of fibronectin expression. However, over-expression of miR-126-3p did not affect gene expression of vWF and αSMA.

Our study is the first to show a partial role of miR-126-3p in EndMT. In the study of Kumarswamy et al, partial prevention of EndMT was also observed with the transfection of miR-21-5p antagomir. Indeed, miR-21-5p was up-regulated in TGFβ2-induced EndMT, and its inhibition results in the restoration of VE cadherin and the reduction of FSP1 protein. Furthermore, effect of miR-21 antagomir was studied at gene level and result in restoration of CD31 expression meanwhile eNOS expression was unchanged.(R. Kumarswamy *et al.*, 2012) These results suggests that miRNA are able to partially prevent or trigger EndMT. In our project, miR-126-3p transfection did modulate CD31 and fibronectin expression but did not affect vWF expression. These results could contribute to a new therapeutic strategy in EndMT-induced fibrosis.

Before studying miRNA in EndMT *in vivo*, the transition was assessed in the context of fibrosis. Lineage tracing of endothelial cells was performed with the mouse model Cdh5-Cre-ERT2; Rosa26R-stop-YFP which allows the expression of YFP in in cells with an endothelial origin. To investigate EndMT in cardiac fibrosis, mice underwent myocardial infarction-induced fibrosis. The presence of EndMT was assessed in sham operated and MI heart by double immunofluorescence of αSMA a marker of activated fibroblast and YFP. Expression of αSMA is also observed by vascular smooth muscle cells localised in the medial layer of the blood vessels, thus blood vessels were excluded of EndMT study. MI heart was divided in two zones : the unaffected zone

(non-MI zone) and the MI zone. No colocalisation was observed in non-MI zone and sham-operated hearts meanwhile in the MI zone, αSMA positive cells were also positive for GFP implying the presence of EndMT.

Similar experiments were conducted with the same mouse model Cdh5-Cre-ERT2; Rosa26R-stop-YFP to assess the occurrence of EndMT kidney fibrosis. Mice underwent UUO on the left kidney and the right kidney was used as control. Double immunofluorescence was performed with αSMA and GFP in both kidneys. In the healthly kidney, no colocalisation of GFP and αSMA was observed. In the left fibrotic kidney colocalisation of αSMA with an endothelial origin was observed. This implies the occurrence of EndMT in both cardiac and kidney fibrosis.

Studies on EndMT in cardiac fibrosis are controversial.. On one hand, EndMT was observed in heart post-aortic banding with a lineage tracing of endothelial cells under the promoter of Tie1. On the other hand, lineage tracing under the promoter of VE-cadherin/Cdh5 did not observe the contribution of EndMT in cardiac fibrosis (Moore-Morris, Guimarães-Camboa, Banerjee, Alexander C. Zambon, *et al.*, 2014). Assessment of EndMT in cardiac fibrosis was therefore required prior to the examining the role of miRNA in the process.

In the context of kidney fibrosis, three different mice models STZ-induced diabetic nephropathy, UUO and COL4A3 KO showed the occurrence of EndMT (Zeisberg *et al.*, 2008). These results were confirmed with the lineage tracing of endothelial cells under the Tie2 promoter. Indeed, approximatively 10% of αSMA positive cells were also positive for endothelial origin.(LeBleu *et al.*, 2013b). In concordance with literature, our results showed the contribution of EndMT to the myofibroblast population both in cardiac and kidney fibrosis.

Localisation of miR-126-3p in EndMT *in vivo*, was then performed with *in-situ* hybridisation of miR-126-3p within healthy and fibrotic tissue. Scramble miRNA hybridisation served as a control. In healthy heart and kidney, no background was observed and miR-126-3p seemed mainly localised in endothelial cells. In heart post-MI, scramble miRNA showed non-specific staining in the extracellular matrix in the MI zone and similar staining pattern was visualised for miR-126-3p. Optimisation was carried out but conclusion could not be made regarding the localisation of miR-126-3p in the MI zone. In the fibrotic kidney, miR-126-3p was found localised in the glomeruli and in the intima layer of the blood vessel, thus mainly in endothelial cells. This suggests that miR-126-3p is localised in endothelial cells in both cardiac and renal

tissue. Interestingly, Sigma-aldrich Company advertised that non-specific staining could be caused by the presence of intracellular lipid droplet which can catch some of the color precipitate on cryosections. This might explain our difficulties to remove non-specific staining within the MI zone of heart sections. Future experiments might require the delipidisation of the sections with chloroform in order to reduce background staining observed in heart post-MI sections.

In conclusion, miR-126-3p might have a translational significance as increasing level of miR-126-3p in endothelial cells partially prevented EndMT. The contribution of EndMT to the fibroblast population in fibrotic disease might be reduced by overexpression of miR-126-3p, and therefore slow down the progression of fibrosis. In addition, miR-126-3p was exclusively localised in endothelial cells in heart and kidney which make this miRNA an attractive target for future therapy. Results from this study are summarised in **Figure 6.1**.

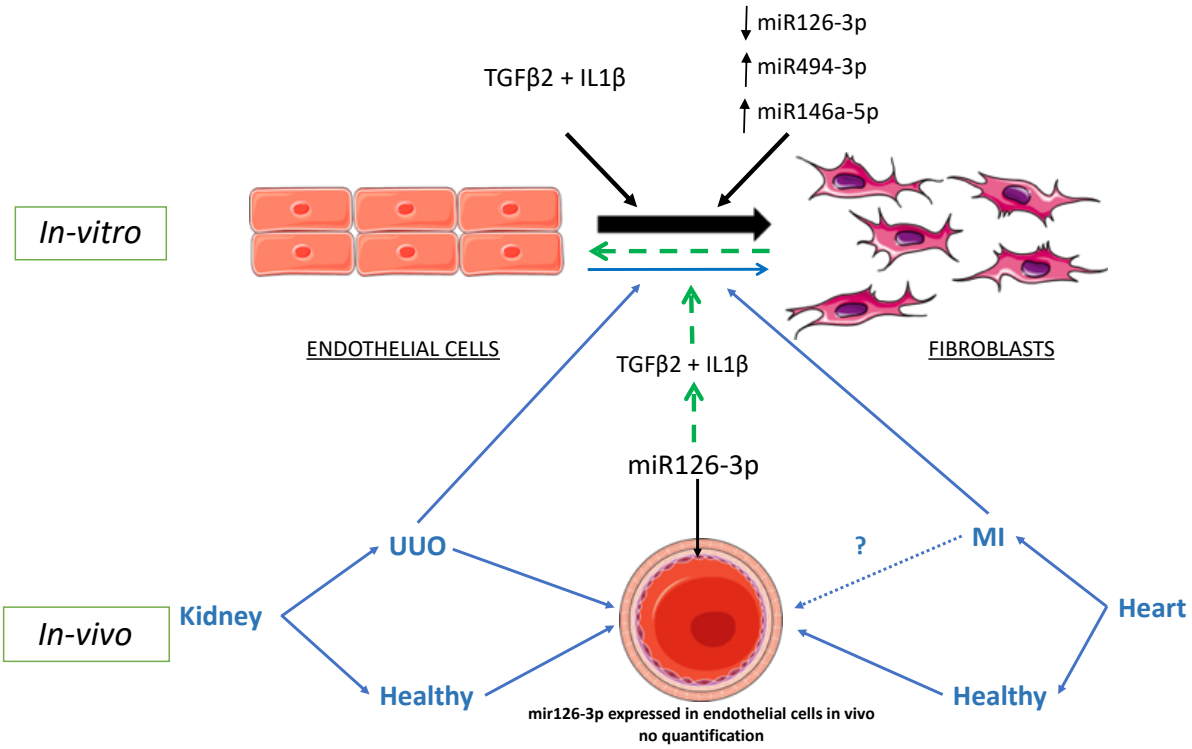


**Figure 6.1 Summary of the study**

## 6.4 Study limitations and future directions

Limitations regarding individual experiments were discussed in each chapter. One of the limitations of the study was the use of pooled donor primary endothelial cells.

Pooled donor endothelial cells are more representative of the inter-patient variability. However, evidence showed that the transfection efficiency in these cells may vary according to the batch of cells. Transfection in immortalized endothelial cells might be more reproducible but our study was based on transdifferention of endothelial cells to mesenchymal cells and this requires a cell type bearing all the endothelial features. Therefore, HUVEC was the most relevant cell type despite the inter-patient variability.

Another limitation concerned the mechanism of miRNA target recognition. MiRNA do not require full complementary with its target to modulate target expression. In addition miRNAs can regulate numerous mRNA that can be predicted in online prediction target tools. Each prediction target tool has developed its own algorithm which results in different prediction, targeted and multiple false positive prediction. Furthermore, studying the mechanism of a miRNA can be affected by false predictions and targeting miRNA involved in EndMT for therapy could have an impact on the numerous signalling pathway targeted by miR-126-3p.

The main limitation of this study was the translation of EndMT *in vitro* to human studies. Assessing EndMT in human tissue sample is not as accurate as lineage tracing in animal model. However, few studies have provided evidence on the occurrence of EndMT in fibrosis in human. In chronic kidney dysfunction, colocalisation of endothelial and mesenchymal markers was observed in fibrotic tissue suggesting the presence of EndMT (Wang *et al.*, 2017). To date, no study has investigated the link of miRNA to the process of EndMT in humans. This work would require the isolation of endothelial cells expressing mesenchymal markers in order to quantify the miRNA but this is difficult due to small amount of tissue. Thus, the study of miRNA in EndMT in human fibrotic disease can be problematic

This study investigated the expression and the role of miRNAs in EndMT. From the miRNAs profile in cells undergoing EndMT, miR-126-3p was found significantly down-regulated. Its over-expression resulted in a partial inhibition of the EndMT process. To study miR-126-3p in the context of EndMT *in vivo*, the transition was assessed in both renal and cardiac fibrosis. MiR-126-3p was localised and seemed restricted to endothelial cells. However, direct link between miR-126-3p and EndMT was not assessed.

To address this, following experiments could be performed:

- As miR-126-3p is mainly expressed in endothelial cells, total RNA including small RNAs could be extracted from fibrotic and healthy tissue and expression of miR-126-3p could be compared by RT-qPCR

- Endothelial cells undergoing EndMT in fibrotic tissue could be isolated by laser capture and miRNA profile and changes in phenotype could be directly assessed *in vivo*

- MiR-126-3p localization could be investigated in human healthy and fibrotic tissue. As miR-126-3p seems restricted to endothelial cells, expression of this miRNA could be directly linked to the expression in endothelial cells.

- MiR21-5p was found up-regulated in EndMT and its inhibition with antagomir partially prevented EndMT. Transfection of miR-126-3p mimics and miR21-5p inhibitors could have a synergistic effect in preventing EndMT and might be able to fully reverse the process.

# Appendix A

**QIAGEN Manchester** secondment October'2014-January'2015
Prerequisite for the Marie Curie-Innovative Doctoral Programme was the industrial experience acquired during PhD.

### Background

In polymerisation chain reaction (PCR), positive and negative controls are necessary to ensure that the reaction runs well. The main role of positive control (PC) is to make sure that primers detect and amplify their specific sequence.
At QIAGEN Manchester Ltd, long oligonucleotides are used as positive control in most kits. Plasmids appear to be another solution which could present some advantages.

Plasmids are circular DNA molecules, separated from the chromosomal DNA, which can replicate independently within a suitable host due to the presence of an origin of replication(ORI). Artificial plasmids are commonly used as vector for sequence of interest in conjunction with gene of resistance to antibiotics. The presence of genes of resistance associated to a growth medium containing the specific antibiotics ensures the conservation of the plasmid in the bacteria; Bacteria without plasmid (and then without the sequence of interest) will not form colonies. Colonies can be selected and the plasmids are extracted and can be used as a positive control.
Plasmids as PC could present some advantages:

- If restricted to the amplified sequence of the sequence of interest, a multitude of sequence could be inserted in a single plasmid.
- This reduces the complexity of PC mix when multiplexing.
- This increase the accuracy when plasmid is used as standard for quantification.

Long term cost effective: once the sequences for positive control are cloned into the plasmid, it could be amplified easily by bacteria culture amplification.

### Aim

The main objective of this study is to compare the use of plasmid with the use of long oligonucleotides as positive control in PCR

## Project plan

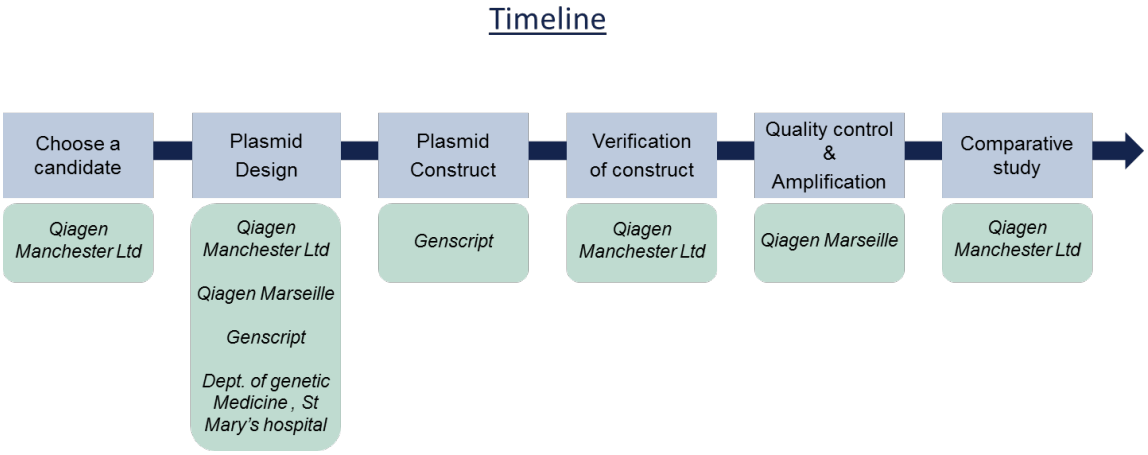


**Figure 1: Timeline of project**

## Suppliers and contributors

Several suppliers and contributors have been involved in this project. Each supplier and each contributor had specific requirements.

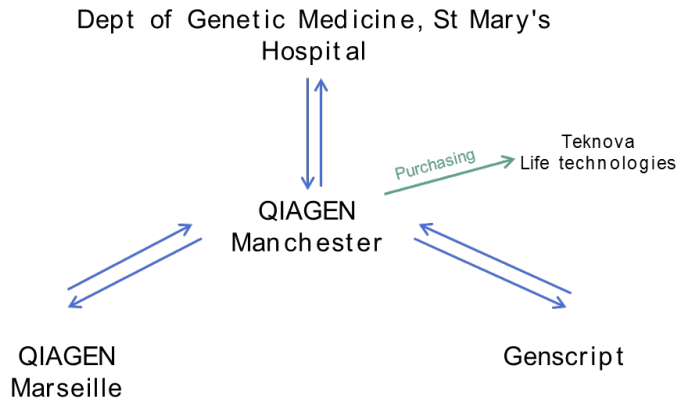


**Figure 2: Suppliers and contributors involved in the project**

Qiagen Marseille was participating to the project for quality control and inserts amplification within plasmid. They recommend the use of the vector PcrIITOPO as the quality control protocol was previously used with this vector.

Genscript was recommended by Qiagen Marseille for the cloning. They asked for providing 5ug of the plasmid PcrIITOPO.

The Department of Genetics of St Mary's Hospital was involved in the project for the amplification of plasmid without insert.

Materials were purchased from Life technologies and Teknova.

## Selection of the positive control

Plasmid is a molecule of DNA. Therefore, the first criterion was to target a kit for DNA detection in which plasmid could be used as positive control.

The second criterion was to ensure the specificity of primers. Primers of a specific sequence 1 should not amplify a specific sequence 2 due to the presence of all sequences on the same plasmid.

The choice was oriented to FGFR3 kit. This kit targets DNA related to fibroblast-growth factor 3 and their five mutations.

The kit contains reaction mix to detect mutations and a control of FGFR3 (a bit more context).

- Control
- Mutation R248C
- Mutation S249C
- Mutation G372C
- Mutation Y375C
- Mutation K652E

The Positive Control consists in 6 sequences of nearly 150 to 200 nucleotides (see Appendix 1). This kit was a suitable candidate for this project due to the number of sequences present in the positive control. Manufacture of one plasmid would have been beneficial compared to the manufacturing of six long oligonucleotides. Furthermore, a report of cross amplification was already performed and conclude that one pair of primers amplifies only one sequence.

**Design of plasmid**

Further to meeting with QIAGEN Marseille, vector PcrIITOPO was selected to facilitate the quality control process and theplasmid amplification.

PcrIITOPO is a vector from Life technologies. It contains two selective marker ampicillin and kanamycin, several restriction sites and some promoters.Particularity of this vector is the linearised stage of the vector due to the presence of topoisomerase at each 5’ extremity. Topoisomerase I cleave phosphodiester after 5’CCCTT and bound to the phosphate in 3’. The phosphotyrosyl bound could be attacked by a hydroxyl and released the topoisomerase.(Figure 2)

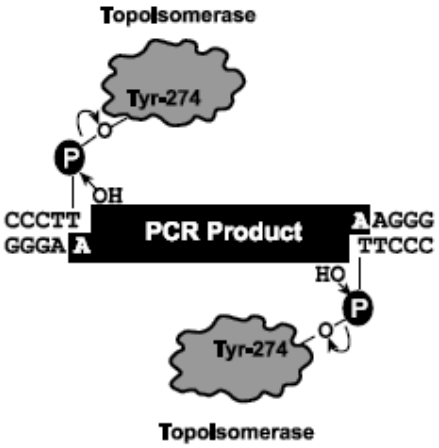


**Figure 3: Mechanism of vector PcrIITOPO**

However, as the PcrIITOPO plasmid is property of LifeTechnologies, the company manufacturing the insert is not allowed to insert directly sequences in PcrIITOPO. A first plasmid will be necessary to insert sequences of interest and then sequences could be inserting in PCRIITOPO. The first vector is usually a vector PuC.

To design the plasmid, restriction enzymes contained in insert were checked in order to avoid using restriction enzyme which will cut the sequence as well as the plasmid.

The map of PcrIITOPO in Figure 20 highlights the main restriction sites on the plasmid.

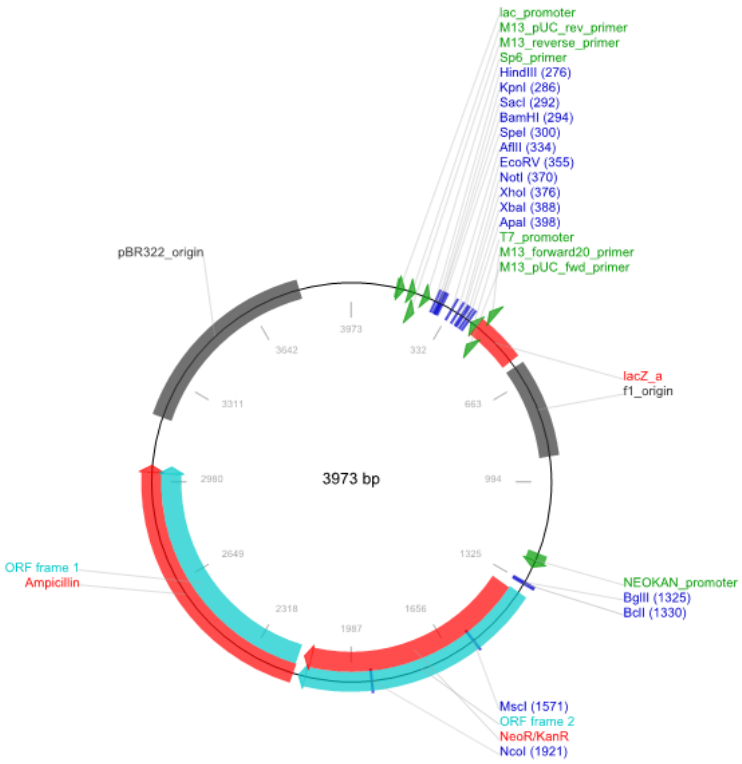


**Figure 4: Map of the vector PcrIITOPO**

Regarding the sequences, maximum size of amplicons was verified to avoid amplification of non-specific sequences.

Indeed, if the maximum size of one amplicon is equivalent to the length of two sequences of interest, one pair of primers would be able to amplify two sequences. In this case, an alien sequence (sequence that cannot be amplified)was introduced between sequences of interest. In our project, alien sequences were not necessary.

To complete the design, enzyme for linearisation was required. Two linearisation enzyme were already used by QIAGEN Marseille: *BamH1* and *Spe1* and were not selected for the insertion of our sequence. Sequence was designed with *NotI* and *XbaI* linearization enzyme.


**Figure 5: Sequence of Interest**

**Quote for Genscript**

Quote was submitted to Genscript. and asked in return 5ug of PcrIITOPO. Kits with PcrIITOPO plasmid (Life technologies) contains only 100ng to 500ng of linear plasmid, thus amplification of the empty plasmid was necessary.

**Amplification of PcrIITOPO without insert**

With the help of the department of genetic medicine in St Mary's hospital, ligation and amplification of the plasmid were performed. The amplification consisted in a transformation of the plasmid into bacteria, bacteria culture and extraction of the plasmids. A transformation was carried out chemically and transformed cells were spread onto plate. Few colonies were grown up; Blue colonies were picked for analysis. DNA was extracted and digest by *EcoRI* was performed to check the size of the plasmid.(Figure 6)


Figure 6: Digestion  by EcoRI of plasmid without insert

After four months internship, ligation and amplification of the PcrIITOPO plasmid failed. The manufactured plasmid from Genscript was ordered without custom cloning (without transfer into PcrIITOPO). In future plasmid design, the sequence used for quality control could be integrated in the insert.

Qiagen Marseille manufacture and quality control were transferred to Hilden facilities.

# Appendix B

**Almac secondment** June 2016
Prerequisite for the Marie Curie-Innovative Doctoral Programme is the industrial experience acquired during PhD.

TGFβ2 was suggested as an inducer of endothelial–to-mesenchymal transition and its signalling remains poorly studied. TGFβ2 can bind to the same receptors as TGFβ1, but with a lower affinity. However, TGFβ2 has a higher affinity for TβRIII also called Betaglycan. Betaglycan cannot transduce signalling but acts as an anchor to help the binding to TβRII. Evidence suggest that TGFβ2 could to bind to ALK5, a receptor implicated in tehe development of fibrosis through its interaction with TGFβ1. In the same receptor family, ALK2 has been shown to be involved in EndMT. In fact, knock-out of ALK2 lead to decreased EndMT in heart development.
In order to study the signalling pathway of TGFβ2 in EndMT, synthesis of two peptides was performed in Almac.

## Peptide 1

**Soluble part of betaglycan.**
P144 : TSLDASIIWAMMQN **14 AA**

***Final product : Unlabelled peptide and labelled peptide with TAMRA***

## Peptide 2

**TGFβ2 active peptide**

CLRPLYIDFKRDLGWKWIHEPKGYNANFCAGA **32 AA** {Ogawa, 1994 #2341}

Active form

CLRPLYIDFKRDLGWKWIHEPKGYNANFCAGA

CLRPLYIDFKRDLGWKWIHEPKGYNANFCAGA

***Final Product: dimer labelled with FAM***

**Figure 1: Sequence of peptides synthesised in Almac**

Peptide 1 represent a soluble part of betaglycan receptor labelled with carboxytetramethylrhodamine (TAMRA). Peptide 2 is a mimic of biologically active TGFβ2 once dimerised.

From the pool of monomer for peptide 2, several dimers could be formed. Dimerisation with a disulphide bond between Cys1 and Cys29 forms the most active dimer. One of the monomer will be labelled with N-(5-Fluoresceinyl) maleimide (FAM).

**Soluble part of Betaglycan**

The soluble part of Betaglycan was synthesised by Solide Phase Peptide Synthesis on ABI 431 synthesizer. After synthesis, the resin was split in half and one portion of the resin was cleaved. Peptides were analysed with a mass spectrophotometer Bruker and HPLC water Alliance. Peptides gave a peak for the predicted correct mass of 1578 Da and an additional peak of a truncated peptide of 1204 Da on the mass spectrophotometer. HPLC gave one major peak at 55% of acetonitrile/ water gradient. Purification was performed by Gilson HPLC and fraction were collected manually. The fractions were analysed by mass spectrophotometer and HPLC. The fraction containing the peptide gave one major peak by HPLC, and the correct mass on mass spectrophotometer. The fraction was lyophilised and gave 4mg of pure product.

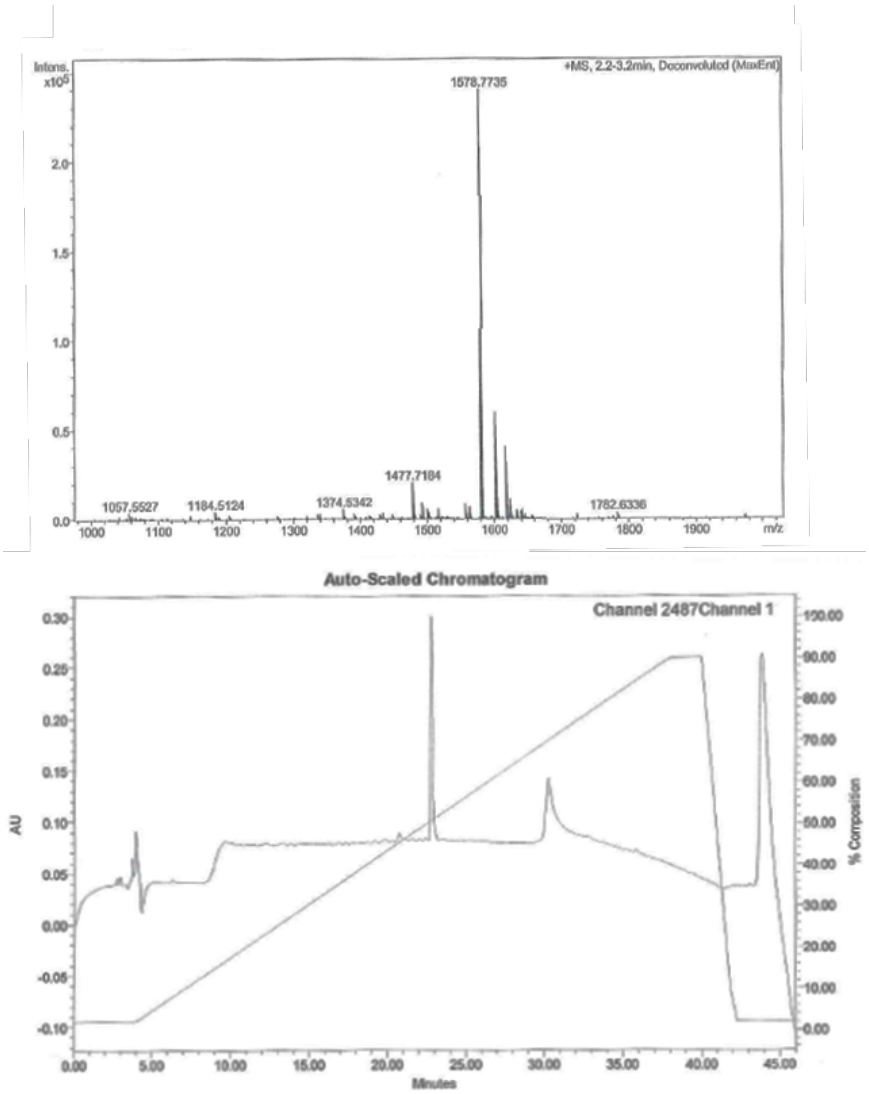


**Figure 2: Purified unlabelled peptide of soluble part of Betaglycan**

The compound gave a peak with a correct mass of 1578 Da on mass spectrophotometer and gave one major peak on HPLC. A peak at 35 minutes is an impurity due to the column and not due to the purified fraction

Half of the resin was cleaved and labelled with TAMRA. The same protocol was used for purification. The purified fraction gave a correct mass at 1991 Da but the fraction was not lyophilised. The quality of the purified fraction was lost and a second purification was performed. The second purification gave too low quantity of material and more experiments were required.

## Active TGFβ2

Active TGFB2 peptide is a specific dimer with a disulphide bond between cysteine1 and cysteine29. A strategy of dimerization was elaborated. Two monomers have been synthesized individually and were synthesized with a tert-butyloxycarbonyl group(Boc-

) protection on the first cysteine. Without such protection, dimerization could occur with a disulphide bond between Cysteine1-Cysteine1 or Cysteine29-Cysteine29. The protective Boc group needs a special strategy to be removed. The strategy was to add NPYS protection on free cysteine of the first monomer and fluorescein on the free cysteine of the second monomer. Following this, Boc- was removed from the monomer 2 containing fluorescein. The next step would involve mixing monomer 1 and 2 at pH 7.4, to allow the dimerization. Finally deprotection will remove Boc from monomer 1.

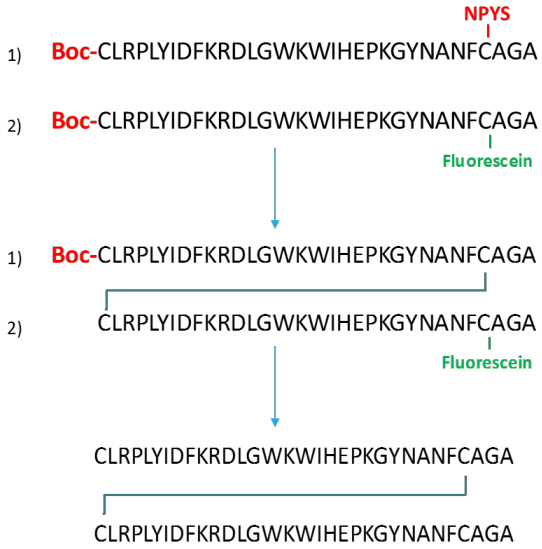


Figure 3: Strategy for dimerization of TGFβ2 peptide

First monomer was synthesized on ABI 431 and mass spectrophotometer analysis revealed several truncates and the correct mass of 3793 Da. HPLC showed three peaks.

A protective group NPYS was added to the cleavage mixture in order to bind and protect the free cysteine. Monomer with NPYS was purified but collected fractions did not give the right mass of 3943 Da.

Synthesis of the monomer has been improved in order to reduce the number of truncates. A second monomer was synthesized and mass spectrophotometry gave the correct mass and several truncates. HPLC revealed four peaks. The resin was cleaved and peptide was purified. The purified peptide was labelled with fluorescein. Fluorescein binding was monitored by mass spectrophotometer and the mixture was purified. Compound was not found after purification and more experiments were required

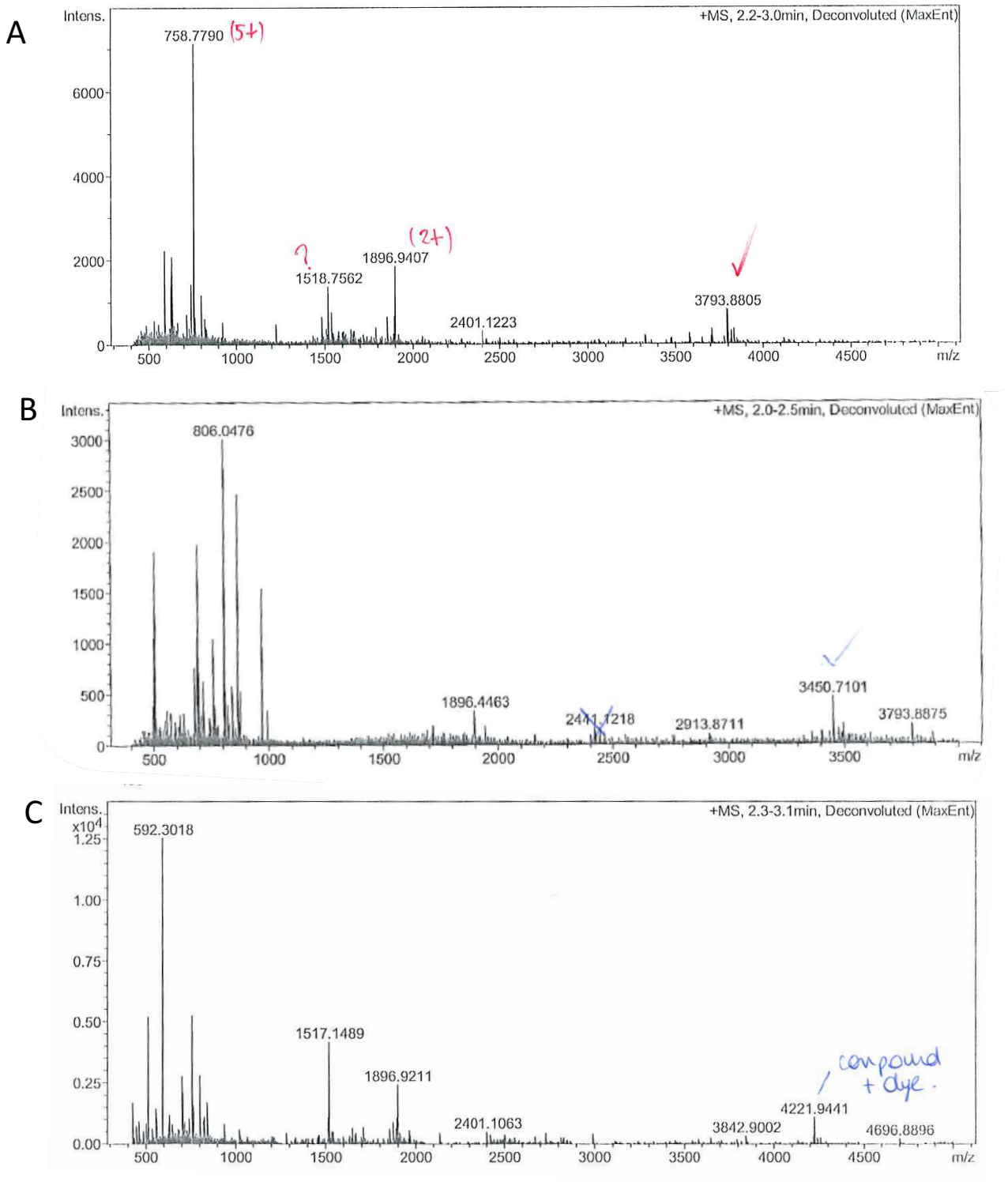


Figure 4: Monomers of of TGFβ2 peptide
(A)Analysis by mass spectrophotometer of monomer 1. Data showed 2 truncates and the compound. (B) Analysis by mass spectrophotometer of monomer 2. Data revealed 3 truncates and the compound. (C) Labelling of monomer 2 with fluorescein. A peak with low abundance gave the correct mass of 4221 Da.

# Appendix C

**Conferences:**

- 33rd Ernst Klenk Symposium in Molecular Medicine : Tissue regeneration, wound healing
  and fibrosis, 2017, Cologne
  *N. Jordan, E. Singh, R. E. Redgrave, B. Innes, D. Hall, H. M. Arthur, C. Ward, S. Ali*
  ***Preventing endothelial-to-mesenchymal transition by enhancing miR-126-3p expression***

- Gordon Research Conference Tissue repair and regeneration, 2017, New London, USA
  *N. Jordan, N. Townshend, R. E. Redgrave, H. M. Arthur, C. Ward, S. Ali*
  ***Preventing endothelial-to-mesenchymal transition by enhancing miR-126-3p expression***

- British microcirculation society annual meeting 2016, Newcastle
  *N. Jordan, N. Ellis, E. Singh, B. Innes, R. E. Redgrave, H. M. Arthur, C. Ward, S. Ali*
  ***Identification of MiRNAs signature in endothelial-to-mesenchymal transition***

- North East postgraduate conference 2016, Newcastle
  **Open lab book workshop "*MiRNAs: From extraction to amplification*"**

**Publication:**

- Glover K.E., **Jordan N.**, Ali S. & Sheerin S. (2018) **Regulation of endothelial–to-mesenchymal transition by microRNAs in chronic allograft dysfunction.** (in press)Transplantation.

**Awards:**

1. BSI Travel Award 2017 (£1000)
2. Newcastle University Travel Award 2017 (£400)
3. Travel Support from Lab reagent companies 2016 (£150)

**Professional memberships :**

- Student member of the British society for immunology (BSI), UK.
- Student member of the British microcirculation society (BMI), UK

# References


Abe, R., Donnelly, S. C., Peng, T., Bucala, R. and Metz, C. N. (2001) 'Peripheral blood fibrocytes: differentiation pathway and migration to wound sites.', *Journal of immunology (Baltimore, Md. : 1950)*, 166(12), pp. 7556–62.

Agarwal, V., Bell, G. W., Nam, J.-W. and Bartel, D. P. (2015) 'Predicting effective microRNA target sites in mammalian mRNAs', *eLife*, 4.

Aisagbonhi, O., Rai, M., Ryzhov, S., Atria, N., Feoktistov, I. and Hatzopoulos, A. K. (2011) 'Experimental myocardial infarction triggers canonical Wnt signalling and endothelial-to-mesenchymal transition.', *Disease models & mechanisms*, 4(4), pp. 469–83.

Ali, S. R., Ranjbarvaziri, S., Talkhabi, M., Zhao, P., Subat, A., Hojjat, A., Kamran, P., Muller, A. M. S., Volz, K. S., Tang, Z., Red-Horse, K. and Ardehali, R. (2014) 'Developmental Heterogeneity of Cardiac Fibroblasts Does Not Predict Pathological Proliferation and Activation', *Circulation Research*, 115(7), pp. 625–635.

van Amerongen, M., Bou-Gharios, G., Popa, E., van Ark, J., Petersen, A., van Dam, G., van Luyn, M. and Harmsen, M. (2008) 'Bone marrow-derived myofibroblasts contribute functionally to scar formation after myocardial infarction', *The Journal of Pathology*, 214(3), pp. 377–386.

Arciniegas, E., Sutton, A. B., Allen, T. D. and Schor, A. M. (1992) 'Transforming growth factor beta 1 promotes the differentiation of endothelial cells into smooth muscle-like cells in vitro.', *Journal of cell science*, 103 ( Pt 2, pp. 521–9.

Aurora, A. B., Mahmoud, A. I., Luo, X., Johnson, B. A., van Rooij, E., Matsuzaki, S., Humphries, K. M., Hill, J. A., Bassel-Duby, R., Sadek, H. A. and Olson, E. N. (2012) 'MicroRNA-214 protects the mouse heart from ischemic injury by controlling $Ca^{2+}$ overload and cell death.', *The Journal of clinical investigation*, 122(4), pp. 1222–32.

Azhar, M., Runyan, R. B., Gard, C., Sanford, L. P., Miller, M. L., Andringa, A., Pawlowski, S., Rajan, S. and Doetschman, T. (2009) 'Ligand-specific function of transforming growth factor beta in epithelial-mesenchymal transition in heart development', *Dev Dyn*, 238(2), pp. 431–442.

Bartel, D. P. (2004) 'MicroRNAs: genomics, biogenesis, mechanism, and function', *Cell*, 116(2), pp. 281–297.

Bartel, D. P. (2009) 'MicroRNAs: target recognition and regulatory functions.', *Cell*, 136(2), pp. 215–33.

van Beijnum, J. R., van der Linden, E. and Griffioen, A. W. (2008) 'Angiogenic profiling and

comparison of immortalized endothelial cells for functional genomics', *Experimental Cell Research*, 314(2), pp. 264–272.

Bernardo, B. C., Gao, X.-M., Winbanks, C. E., Boey, E. J. H., Tham, Y. K., Kiriazis, H., Gregorevic, P., Obad, S., Kauppinen, S., Du, X.-J., Lin, R. C. Y. and McMullen, J. R. (2012) 'Therapeutic inhibition of the miR-34 family attenuates pathological cardiac remodeling and improves heart function.', *Proceedings of the National Academy of Sciences of the United States of America*, 109(43), pp. 17615–20.

Bernstein, E., Caudy, A. A., Hammond, S. M. and Hannon, G. J. (2001) 'Role for a bidentate ribonuclease in the initiation step of RNA interference.', *Nature*, 409(6818), pp. 363–366.

Bijkerk, R., de Bruin, R. G., van Solingen, C., Duijs, J. M. G. J., Kobayashi, K., van der Veer, E. P., ten Dijke, P., Rabelink, T. J., Goumans, M. J. and van Zonneveld, A. J. (2012) 'MicroRNA-155 functions as a negative regulator of RhoA signalling in TGF-β-induced endothelial to mesenchymal transition.', *MicroRNA (Shariqah, United Arab Emirates)*, 1(1), pp. 2–10.

Bohnsack, M. T., Czaplinski, K. and Gorlich, D. (2004) 'Exportin 5 is a RanGTP-dependent dsRNA-binding protein that mediates nuclear export of pre-miRNAs.', *RNA (New York, N.Y.)*, 10(2), pp. 185–91.

Borchert, G. M., Lanier, W. and Davidson, B. L. (2006) 'RNA polymerase III transcribes human microRNAs', *Nature Structural & Molecular Biology*, 13(12), pp. 1097–1101.

Bouchie, A. (2013) 'First microRNA mimic enters clinic', *Nature Biotechnology*, 31(7), pp. 577–577.

Boyer, A. S., Ayerinskas, I. I., Vincent, E. B., McKinney, L. A., Weeks, D. L. and Runyan, R. B. (1999) 'TGFβ2 and TGFβ3 Have Separate and Sequential Activities during Epithelial–Mesenchymal Cell Transformation in the Embryonic Heart', *Developmental Biology*, 208(2), pp. 530–545.

Braun, J. E., Huntzinger, E., Fauser, M. and Izaurralde, E. (2011) 'GW182 Proteins Directly Recruit Cytoplasmic Deadenylase Complexes to miRNA Targets', *Molecular Cell*, 44(1), pp. 120–133.

Braun, J. E., Truffault, V., Boland, A., Huntzinger, E., Chang, C.-T., Haas, G., Weichenrieder, O., Coles, M. and Izaurralde, E. (2012) 'A direct interaction between DCP1 and XRN1 couples mRNA decapping to 5′ exonucleolytic degradation', *Nature Structural & Molecular Biology*, 19(12), pp. 1324–1331.

Brilla, C. G. and Weber, K. T. (1992) 'Reactive and reparative myocardial fibrosis in arterial hypertension in the rat.', *Cardiovascular research*, 26(7), pp. 671–7.

Bucala, R., Spiegel, L. A., Chesney, J., Hogan, M. and Cerami, A. (1994) 'Circulating

fibrocytes define a new leukocyte subpopulation that mediates tissue repair.', *Molecular medicine (Cambridge, Mass.)*, 1(1), pp. 71–81.

CAI, X., Hagedorn, C. H. and Cullen, B. R. (2004) 'Human microRNAs are processed from capped, polyadenylated transcripts that can also function as mRNAs', *RNA*, 10(12), pp. 1957–1966.

Caley, M. P., Martins, V. L. C. and O'Toole, E. A. (2015) 'Metalloproteinases and Wound Healing.', *Advances in wound care*, 4(4), pp. 225–234.

Calin, G. A., Dumitru, C. D., Shimizu, M., Bichi, R., Zupo, S., Noch, E., Aldler, H., Rattan, S., Keating, M., Rai, K., Rassenti, L., Kipps, T., Negrini, M., Bullrich, F. and Croce, C. M. (2002) 'Frequent deletions and down-regulation of micro- RNA genes miR15 and miR16 at 13q14 in chronic lymphocytic leukemia.', *Proceedings of the National Academy of Sciences of the United States of America*, 99(24), pp. 15524–9.

Camarillo, C., Swerdel, M. and Hart, R. P. (2011) 'Comparison of microarray and quantitative real-time PCR methods for measuring MicroRNA levels in MSC cultures.', *Methods in molecular biology (Clifton, N.J.)*, 698, pp. 419–29.

Camenisch, T. D., Molin, D. G. M., Person, A., Runyan, R. B., Gittenberger-de Groot, A. C., McDonald, J. A. and Klewer, S. E. (2002) 'Temporal and distinct TGFbeta ligand requirements during mouse and avian endocardial cushion morphogenesis.', *Developmental biology*, 248(1), pp. 170–81.

Chakraborty, S., Zawieja, D. C., Davis, M. J. and Muthuchamy, M. (2015) 'MicroRNA signature of inflamed lymphatic endothelium and role of miR-9 in lymphangiogenesis and inflammation', *American Journal of Physiology-Cell Physiology*, 309(10), pp. C680–C692.

Chandhoke, A. S., Karve, K., Dadakhujaev, S., Netherton, S., Deng, L. and Bonni, S. (2016) 'The ubiquitin ligase SMURF2 suppresses TGFβ-induced epithelial-mesenchymal transition in a sumoylation-regulated manner.', *Cell death and differentiation*, 23(5), pp. 876–88.

Chaudhuri, V., Zhou, L. and Karasek, M. (2007) 'Inflammatory cytokines induce the transformation of human dermal microvascular endothelial cells into myofibroblasts: a potential role in skin fibrogenesis', *Journal of Cutaneous Pathology*, 34(2), pp. 146–153.

Chen, C., Ridzon, D. A., Broomer, A. J., Zhou, Z., Lee, D. H., Nguyen, J. T., Barbisin, M., Xu, N. L., Mahuvakar, V. R., Andersen, M. R., Lao, K. Q., Livak, K. J. and Guegler, K. J. (2005) 'Real-time quantification of microRNAs by stem-loop RT-PCR', *Nucleic Acids Research*, 33(20), pp. e179–e179.

Chen, P.-Y., Qin, L., Barnes, C., Charisse, K., Yi, T., Zhang, X., Ali, R., Medina, P. P., Yu, J., Slack, F. J., Anderson, D. G., Kotelianski, V., Wang, F., Tellides, G. and Simons, M. (2012) 'FGF Regulates TGF-β Signalling and Endothelial-to-Mesenchymal Transition via

Control of let-7 miRNA Expression', *Cell Reports*, 2(6), pp. 1684–1696.
Chen, Z., Lu, S., Xu, M., Liu, P., Ren, R. and Ma, W. (2017) 'Role of miR-24, Furin, and Transforming Growth Factor-β1 Signal Pathway in Fibrosis After Cardiac Infarction.', *Medical science monitor : international medical journal of experimental and clinical research*, 23, pp. 65–70.
Chendrimada, T. P., Gregory, R. I., Kumaraswamy, E., Norman, J., Cooch, N., Nishikura, K. and Shiekhattar, R. (2005) 'TRBP recruits the Dicer complex to Ago2 for microRNA processing and gene silencing', *Nature*, 436(7051), pp. 740–744.
Choi, S.-H., Hong, Z.-Y., Nam, J.-K., Lee, H.-J., Jang, J., Yoo, R. J., Lee, Y. J., Lee, C. Y., Kim, K. H., Park, S., Ji, Y. H., Lee, Y.-S., Cho, J. and Lee, Y.-J. (2015) 'A Hypoxia-Induced Vascular Endothelial-to-Mesenchymal Transition in Development of Radiation-Induced Pulmonary Fibrosis.', *Clinical cancer research : an official journal of the American Association for Cancer Research*, 21(16), pp. 3716–26.
Choi, S.-H., Hong, Z.-Y., Nam, J.-K., Lee, H.-J., Jang, J., Yoo, R. J., Lee, Y. J., Lee, C. Y., Kim, K. H., Park, S., Ji, Y. H., Lee, Y.-S., Cho, J. and Lee, Y.-J. (2015) 'A Hypoxia-Induced Vascular Endothelial-to-Mesenchymal Transition in Development of Radiation-Induced Pulmonary Fibrosis', *Clinical Cancer Research*, 21(16), pp. 3716–3726.
Colombo, M. G., Citti, L., Basta, G., De Caterina, R., Biagini, A. and Rainaldi, G. (2001) 'Differential ability of human endothelial cells to internalize and express exogenous DNA.', *Cardiovascular drugs and therapy*, 15(1), pp. 25–9.
Cooley, B. C., Nevado, J., Mellad, J., Yang, D., Hilaire, C. S., Negro, A., Fang, F., Chen, G., San, H., Walts, A. D., Schwartzbeck, R. L., Taylor, B., Lanzer, J. D., Wragg, A., Elagha, A., Beltran, L. E., Berry, C., Feil, R., Virmani, R., Ladich, E., Kovacic, J. C. and Boehm, M. (2014) 'TGF-β signalling mediates endothelial-to-mesenchymal transition (EndMT) during vein graft remodeling.', *Science translational medicine*, 6(227), p. 227ra34.
Correia, A. C. P., Moonen, J.-R. A. J., Brinker, M. G. L. and Krenning, G. (2016) 'FGF2 inhibits endothelial–mesenchymal transition through microRNA-20a-mediated repression of canonical TGF-β signalling', *Journal of Cell Science*, 129(3), pp. 569–579.
Covas, D. T., Panepucci, R. A., Fontes, A. M., Silva, W. A., Orellana, M. D., Freitas, M. C. C., Neder, L., Santos, A. R. D., Peres, L. C., Jamur, M. C. and Zago, M. A. (2008) 'Multipotent mesenchymal stromal cells obtained from diverse human tissues share functional properties and gene-expression profile with CD146+ perivascular cells and fibroblasts', *Experimental Hematology*, 36(5), pp. 642–654.
Darby, I., Skalli, O. and Gabbiani, G. (1990) 'Alpha-smooth muscle actin is transiently expressed by myofibroblasts during experimental wound healing.', *Laboratory investigation;*

*a journal of technical methods and pathology*, 63(1), pp. 21–9.

Denli, A. M., Tops, B. B. J., Plasterk, R. H. A., Ketting, R. F. and Hannon, G. J. (2004) 'Processing of primary microRNAs by the Microprocessor complex', *Nature*, 432(7014), pp. 231–235.

Dieci, G., Conti, A., Pagano, A. and Carnevali, D. (2013) 'Identification of RNA polymerase III-transcribed genes in eukaryotic genomes', *Biochimica et Biophysica Acta (BBA) - Gene Regulatory Mechanisms*, 1829(3–4), pp. 296–305.

Dweep, H., Sticht, C., Pandey, P. and Gretz, N. (2011) 'miRWalk – Database: Prediction of possible miRNA binding sites by "walking" the genes of three genomes', *Journal of Biomedical Informatics*, 44(5), pp. 839–847.

Federmann, M., Risti, B. and Hess, O. M. (1994) '[Left ventricular insufficiency: systolic versus diastolic dysfunction].', *Schweizerische medizinische Wochenschrift*, 124(26), pp. 1196–202.

Feng, B., Cao, Y., Chen, S., Chu, X., Chu, Y. and Chakrabarti, S. (2016a) 'miR-200b Mediates Endothelial-to-Mesenchymal Transition in Diabetic Cardiomyopathy.', *Diabetes*, 65(3), pp. 768–79.

Feng, B., Cao, Y., Chen, S., Chu, X., Chu, Y. and Chakrabarti, S. (2016b) 'miR-200b Mediates Endothelial-to-Mesenchymal Transition in Diabetic Cardiomyopathy', *Diabetes*, 65(3), pp. 768–779.

Feng, B. and Chakrabarti, S. (2012) 'miR-320 Regulates Glucose-Induced Gene Expression in Diabetes', *ISRN Endocrinology*, 2012, pp. 1–6.

Filipowicz, W., Bhattacharyya, S. N. and Sonenberg, N. (2008) 'Mechanisms of post-transcriptional regulation by microRNAs: are the answers in sight?', *Nature Reviews Genetics*, 9(2), pp. 102–114.

Fish, J. E., Santoro, M. M., Morton, S. U., Yu, S., Yeh, R.-F., Wythe, J. D., Ivey, K. N., Bruneau, B. G., Stainier, D. Y. R. and Srivastava, D. (2008) 'miR-126 Regulates Angiogenic Signalling and Vascular Integrity', *Developmental Cell*, 15(2), pp. 272–284.

Frangogiannis, N. G. (2008) 'The immune system and cardiac repair', *Pharmacological Research*, 58(2), pp. 88–111.

Frid, M. G., Kale, V. A. and Stenmark, K. R. (2002) 'Mature vascular endothelium can give rise to smooth muscle cells via endothelial-mesenchymal transdifferentiation: in vitro analysis.', *Circulation research*, 90(11), pp. 1189–96.

Gabbiani, G., Ryan, G. B. and Majne, G. (1971) 'Presence of modified fibroblasts in granulation tissue and their possible role in wound contraction.', *Experientia*, 27(5), pp. 549–50.

Garside, V. C., Chang, A. C., Karsan, A. and Hoodless, P. A. (2013) 'Co-ordinating Notch, BMP, and TGF-β signalling during heart valve development', *Cellular and Molecular Life Sciences*, 70(16), pp. 2899–2917.

Gebert, L. F. R., Rebhan, M. A. E., Crivelli, S. E. M., Denzler, R., Stoffel, M. and Hall, J. (2014) 'Miravirsen (SPC3649) can inhibit the biogenesis of miR-122', *Nucleic Acids Research*, 42(1), pp. 609–621.

Geng, H. and Guan, J. (2017) 'MiR-18a-5p inhibits endothelial–mesenchymal transition and cardiac fibrosis through the Notch2 pathway', *Biochemical and Biophysical Research Communications*, 491(2), pp. 329–336.

Gerdes, A. M. (2002) 'Cardiac myocyte remodeling in hypertrophy and progression to failure', *Journal of Cardiac Failure*, 8(6), pp. S264–S268.

Gersch, C., Dewald, O., Zoerlein, M., Michael, L. H., Entman, M. L. and Frangogiannis, N. G. (2002) 'Mast cells and macrophages in normal C57/BL/6 mice.', *Histochemistry and cell biology*, 118(1), pp. 41–9.

Ghosh, A. K., Nagpal, V., Covington, J. W., Michaels, M. A. and Vaughan, D. E. (2012) 'Molecular basis of cardiac endothelial-to-mesenchymal transition (EndMT): differential expression of microRNAs during EndMT', *Cell Signal*, 24(5), pp. 1031–1036.

Gittenberger-De Groot, A. C., Peeters, M.-P. F. M. V., Mentink, M. M. T., Gourdie, R. G. and Poelmann, R. E. (1998) 'Epicardium-Derived Cells Contribute a Novel Population to the Myocardial Wall and the Atrioventricular Cushions'.

Gomez, I. G., MacKenna, D. A., Johnson, B. G., Kaimal, V., Roach, A. M., Ren, S., Nakagawa, N., Xin, C., Newitt, R., Pandya, S., Xia, T.-H., Liu, X., Borza, D.-B., Grafals, M., Shankland, S. J., Himmelfarb, J., Portilla, D., Liu, S., Chau, B. N. and Duffield, J. S. (2015) 'Anti–microRNA-21 oligonucleotides prevent Alport nephropathy progression by stimulating metabolic pathways', *Journal of Clinical Investigation*, 125(1), pp. 141–156.

Goumans, M.-J., Valdimarsdottir, G., Itoh, S., Rosendahl, A., Sideras, P. and ten Dijke, P. (2002) 'Balancing the activation state of the endothelium via two distinct TGF-beta type I receptors.', *The EMBO journal*, 21(7), pp. 1743–53.

Grimson, A., Farh, K. K.-H., Johnston, W. K., Garrett-Engele, P., Lim, L. P. and Bartel, D. P. (2007) 'MicroRNA Targeting Specificity in Mammals: Determinants beyond Seed Pairing', *Molecular Cell*, 27(1), pp. 91–105.

Grishok, A., Pasquinelli, A. E., Conte, D., Li, N., Parrish, S., Ha, I., Baillie, D. L., Fire, A., Ruvkun, G. and Mello, C. C. (2001) 'Genes and mechanisms related to RNA interference regulate expression of the small temporal RNAs that control C. elegans developmental timing.', *Cell*, 106(1), pp. 23–34.

Guaiquil, V., Swendeman, S., Yoshida, T., Chavala, S., Campochiaro, P. A. and Blobel, C. P. (2009) 'ADAM9 is involved in pathological retinal neovascularization.', *Molecular and cellular biology*, 29(10), pp. 2694–703.

Guo, Y., Li, P., Bledsoe, G., Yang, Z.-R., Chao, L. and Chao, J. (2015) 'Kallistatin inhibits TGF-β-induced endothelial–mesenchymal transition by differential regulation of microRNA-21 and eNOS expression', *Experimental Cell Research*, 337(1), pp. 103–110.

Gustafsson, E., Brakebusch, C., Hietanen, K. and Fassler, R. (2001) 'Tie-1-directed expression of Cre recombinase in endothelial cells of embryoid bodies and transgenic mice', *Journal of Cell Science*, 114(4).

Ha, M. and Kim, V. N. (2014) 'Regulation of microRNA biogenesis', *Nature Reviews Molecular Cell Biology*, 15(8), pp. 509–524.

Hamada, S., Satoh, K., Fujibuchi, W., Hirota, M., Kanno, A., Unno, J., Masamune, A., Kikuta, K., Kume, K. and Shimosegawa, T. (2012) 'MiR-126 acts as a tumor suppressor in pancreatic cancer cells via the regulation of ADAM9.', *Molecular cancer research : MCR*, 10(1), pp. 3–10.

Han, J., Lee, Y., Yeom, K.-H., Nam, J.-W., Heo, I., Rhee, J.-K., Sohn, S. Y., Cho, Y., Zhang, B.-T. and Kim, V. N. (2006) 'Molecular Basis for the Recognition of Primary microRNAs by the Drosha-DGCR8 Complex', *Cell*, 125(5), pp. 887–901.

Hashimoto, N., Phan, S. H., Imaizumi, K., Matsuo, M., Nakashima, H., Kawabe, T., Shimokata, K. and Hasegawa, Y. (2010) 'Endothelial–Mesenchymal Transition in Bleomycin-Induced Pulmonary Fibrosis', *American Journal of Respiratory Cell and Molecular Biology*, 43(2), pp. 161–172.

He, M., Chen, Z., Martin, M., Zhang, J., Sangwung, P., Woo, B., Tremoulet, A. H., Shimizu, C., Jain, M. K., Burns, J. C. and Shyy, J. Y.-J. (2017) 'miR-483 Targeting of CTGF Suppresses Endothelial-to-Mesenchymal TransitionNovelty and Significance', *Circulation Research*, 120(2), pp. 354–365.

Hein, S., Arnon, E., Kostin, S., Schönburg, M., Elsässer, A., Polyakova, V., Bauer, E. P., Klövekorn, W.-P. and Schaper, J. (2003) 'Progression from compensated hypertrophy to failure in the pressure-overloaded human heart: structural deterioration and compensatory mechanisms.', *Circulation*, 107(7), pp. 984–91.

Herrera-Carrillo, E. and Berkhout, B. (2017) 'Dicer-independent processing of small RNA duplexes: mechanistic insights and applications', *Nucleic Acids Research*, 45(18), pp. 10369–10379.

Hinz, B., Celetta, G., Tomasek, J. J., Gabbiani, G. and Chaponnier, C. (2001) 'Alpha-smooth muscle actin expression upregulates fibroblast contractile activity', *Mol Biol Cell*, 12(9), pp.

2730–2741.
HIRAO, T., NANBA, D., TANAKA, M., ISHIGURO, H., KINUGASA, Y., DOKI, Y., YANO, M., MATSUURA, N., MONDEN, M. and HIGASHIYAMA, S. (2005) 'Overexpression of ADAM9 enhances growth factor-mediated recycling of E-cadherin in human colon cancer cell line HT29 cells', *Experimental Cell Research*, 312(3), pp. 331–9.
Hua, Y., Liang, C., Miao, C., Wang, S., Su, S., Shao, P., Liu, B., Bao, M., Zhu, J., Xu, A., Zhang, J., Li, J., Wang, Z., Liu, B., Bao, M., Bao, M., Zhu, J., Zhu, J., Xu, A., Xu, A., Zhang, J., Zhang, J., Li, J., Li, J., Wang, Z. and Wang, Z. (2018) 'MicroRNA-126 inhibits proliferation and metastasis in prostate cancer via regulation of ADAM9', *Oncology Letters*, 15(6), pp. 9051–9060.
Hullinger, T. G., Montgomery, R. L., Seto, A. G., Dickinson, B. A., Semus, H. M., Lynch, J. M., Dalby, C. M., Robinson, K., Stack, C., Latimer, P. A., Hare, J. M., Olson, E. N. and van Rooij, E. (2012) 'Inhibition of miR-15 Protects Against Cardiac Ischemic Injury', *Circulation Research*, 110(1), pp. 71–81.
Humphreys, B. D., Lin, S. L., Kobayashi, A., Hudson, T. E., Nowlin, B. T., Bonventre, J. V, Valerius, M. T., McMahon, A. P. and Duffield, J. S. (2010) 'Fate tracing reveals the pericyte and not epithelial origin of myofibroblasts in kidney fibrosis', *Am J Pathol*, 176(1), pp. 85–97.
Hunt, M. A., Currie, M. J., Robinson, B. A. and Dachs, G. U. (2010) 'Optimizing transfection of primary human umbilical vein endothelial cells using commercially available chemical transfection reagents.', *Journal of biomolecular techniques : JBT*, 21(2), pp. 66–72.
Huntzinger, E., Kuzuoğlu-Öztürk, D., Braun, J. E., Eulalio, A., Wohlbold, L. and Izaurralde, E. (2013) 'The interactions of GW182 proteins with PABP and deadenylases are required for both translational repression and degradation of miRNA targets', *Nucleic Acids Research*, 41(2), pp. 978–994.
Hutvágner, G., McLachlan, J., Pasquinelli, A. E., Bálint, E., Tuschl, T. and Zamore, P. D. (2001) 'A cellular function for the RNA-interference enzyme Dicer in the maturation of the let-7 small temporal RNA.', *Science (New York, N.Y.)*, 293(5531), pp. 834–8.
Inoue, Y. and Imamura, T. (2008) 'Regulation of TGF-β family signalling by E3 ubiquitin ligases', *Cancer Science*, 99(11), pp. 2107–2112.
Ishisaki, A., Hayashi, H., Li, A.-J. and Imamura, T. (2003) 'Human Umbilical Vein Endothelium-derived Cells Retain Potential to Differentiate into Smooth Muscle-like Cells', *Journal of Biological Chemistry*, 278(2), pp. 1303–1309.
Ivey, M. J. and Tallquist, M. D. (2016) 'Defining the Cardiac Fibroblast.', *Circulation journal : official journal of the Japanese Circulation Society*, 80(11), pp. 2269–2276.

Iwasaki, S., Kobayashi, M., Yoda, M., Sakaguchi, Y., Katsuma, S., Suzuki, T. and Tomari, Y. (2010) 'Hsc70/Hsp90 chaperone machinery mediates ATP-dependent RISC loading of small RNA duplexes.', *Molecular cell*, 39(2), pp. 292–9.

Jonas, S. and Izaurralde, E. (2015) 'Towards a molecular understanding of microRNA-mediated gene silencing', *Nature Reviews Genetics*, 16(7), pp. 421–433.

Kanasaki, K., Shi, S., Kanasaki, M., He, J., Nagai, T., Nakamura, Y., Ishigaki, Y., Kitada, M., Srivastava, S. P. and Koya, D. (2014) 'Linagliptin-Mediated DPP-4 Inhibition Ameliorates Kidney Fibrosis in Streptozotocin-Induced Diabetic Mice by Inhibiting Endothelial-to-Mesenchymal Transition in a Therapeutic Regimen', *Diabetes*, 63(6), pp. 2120–2131.

Kanisicak, O., Khalil, H., Ivey, M. J., Karch, J., Maliken, B. D., Correll, R. N., Brody, M. J., J. Lin, S.-C., Aronow, B. J., Tallquist, M. D. and Molkentin, J. D. (2016) 'Genetic lineage tracing defines myofibroblast origin and function in the injured heart', *Nature Communications*, 7, p. 12260.

Katz, A. M. and Rolett, E. L. (2016) 'Heart failure: when form fails to follow function', *European Heart Journal*, 37(5), pp. 449–454.

Kemp, C. D. and Conte, J. V. (2012) 'The pathophysiology of heart failure', *Cardiovascular Pathology*, 21(5), pp. 365–371.

Ketting, R. F., Fischer, S. E., Bernstein, E., Sijen, T., Hannon, G. J. and Plasterk, R. H. (2001) 'Dicer functions in RNA interference and in synthesis of small RNA involved in developmental timing in C. elegans', *Genes & Development*, 15(20), pp. 2654–2659.

Khouri, M. G., Peshock, R. M., Ayers, C. R., de Lemos, J. A. and Drazner, M. H. (2010) 'A 4-Tiered Classification of Left Ventricular Hypertrophy Based on Left Ventricular Geometry: The Dallas Heart Study', *Circulation: Cardiovascular Imaging*, 3(2), pp. 164–171.

Khvorova, A., Reynolds, A. and Jayasena, S. D. (2003) 'Functional siRNAs and miRNAs exhibit strand bias.', *Cell*, 115(2), pp. 209–16.

Kim, V. N., Han, J. and Siomi, M. C. (2009) 'Biogenesis of small RNAs in animals', *Nature Reviews Molecular Cell Biology*, 10(2), pp. 126–139.

Kisanuki, Y. Y., Hammer, R. E., Miyazaki, J., Williams, S. C., Richardson, J. A. and Yanagisawa, M. (2001) 'Tie2-Cre Transgenic Mice: A New Model for Endothelial Cell-Lineage Analysis in Vivo', *Developmental Biology*, 230(2), pp. 230–242.

Kokubo, H., Tomita-Miyagawa, S., Hamada, Y. and Saga, Y. (2007) 'Hesr1 and Hesr2 regulate atrioventricular boundary formation in the developing heart through the repression of Tbx2', *Development*, 134(4), pp. 747–755.

Kokudo, T., Suzuki, Y., Yoshimatsu, Y., Yamazaki, T., Watabe, T. and Miyazono, K. (2008) 'Snail is required for TGF -induced endothelial-mesenchymal transition of embryonic stem

cell-derived endothelial cells', *Journal of Cell Science*, 121(20), pp. 3317–3324.
Komamura, K. (2013) 'Similarities and Differences between the Pathogenesis and Pathophysiology of Diastolic and Systolic Heart Failure.', *Cardiology research and practice*, 2013, p. 824135.
Kong, P., Christia, P. and Frangogiannis, N. G. (2014) 'The pathogenesis of cardiac fibrosis', *Cellular and Molecular Life Sciences*, 71(4), pp. 549–574.
Konstam, M. A., Kramer, D. G., Patel, A. R., Maron, M. S. and Udelson, J. E. (2011) 'Left Ventricular Remodeling in Heart Failure', *JACC: Cardiovascular Imaging*, 4(1), pp. 98–108.
Korpal, M., Lee, E. S., Hu, G. and Kang, Y. (2008) 'The miR-200 family inhibits epithelial-mesenchymal transition and cancer cell migration by direct targeting of E-cadherin transcriptional repressors ZEB1 and ZEB2.', *The Journal of biological chemistry*, 283(22), pp. 14910–4.
Krenning, G., Moonen, J.-R. A. J., van Luyn, M. J. A. and Harmsen, M. C. (2008) 'Vascular smooth muscle cells for use in vascular tissue engineering obtained by endothelial-to-mesenchymal transdifferentiation (EnMT) on collagen matrices', *Biomaterials*, 29(27), pp. 3703–3711.
Krenning, G., Zeisberg, E. M. and Kalluri, R. (2010) 'The origin of fibroblasts and mechanism of cardiac fibrosis.', *Journal of cellular physiology*, 225(3), pp. 631–7.
Kriegel, A. J. and Liang, M. (2013) 'MicroRNA <em>In situ</em> Hybridization for Formalin Fixed Kidney Tissues', *Journal of Visualized Experiments*, (81).
Kryczka, J., Przygodzka, P., Bogusz, H. and Boncela, J. (2017) 'HMEC-1 adopt the mixed amoeboid-mesenchymal migration type during EndMT', *European Journal of Cell Biology*, 96(4), pp. 289–300.
Kumarswamy, R., Volkmann, I., Jazbutyte, V., Dangwal, S., Park, D.-H. and Thum, T. (2012) 'Transforming Growth Factor- -Induced Endothelial-to-Mesenchymal Transition Is Partly Mediated by MicroRNA-21', *Arteriosclerosis, Thrombosis, and Vascular Biology*, 32(2), pp. 361–369.
Kumarswamy, R., Volkmann, I., Jazbutyte, V., Dangwal, S., Park, D. H. and Thum, T. (2012) 'Transforming growth factor-beta-induced endothelial-to-mesenchymal transition is partly mediated by microRNA-21', *Arterioscler Thromb Vasc Biol*, 32(2), pp. 361–369.
Kwon, O.-S., Kim, K.-T., Lee, E., Kim, M., Choi, S.-H., Li, H., Fornace, A. J., Cho, J.-H., Lee, Y.-S., Lee, J.-S., Lee, Y.-J. and Cha, H.-J. (2016) 'Induction of MiR-21 by Stereotactic Body Radiotherapy Contributes to the Pulmonary Fibrotic Response', *PLOS ONE*. Edited by Y. Zhou, 11(5), p. e0154942.
Ladak, S. S., Ward, C. and Ali, S. (2016) 'The potential role of microRNAs in lung allograft

rejection.', *The Journal of heart and lung transplantation : the official publication of the International Society for Heart Transplantation*, 35(5), pp. 550–9.
Lagos-Quintana, M., Rauhut, R., Lendeckel, W. and Tuschl, T. (2001) 'Identification of novel genes coding for small expressed RNAs', *Science*, 294(5543), pp. 853–858.
Lagos-Quintana, M., Rauhut, R., Meyer, J., Borkhardt, A. and Tuschl, T. (2003) 'New microRNAs from mouse and human.', *RNA (New York, N.Y.)*, 9(2), pp. 175–9.
Lagos-Quintana, M., Rauhut, R., Yalcin, A., Meyer, J., Lendeckel, W. and Tuschl, T. (2002) 'Identification of tissue-specific microRNAs from mouse.', *Current biology : CB*, 12(9), pp. 735–9.
de Lange, F. J., Moorman, A. F. M., Anderson, R. H., Männer, J., Soufan, A. T., de Gier-de Vries, C., Schneider, M. D., Webb, S., van den Hoff, M. J. B. and Christoffels, V. M. (2004) 'Lineage and Morphogenetic Analysis of the Cardiac Valves', *Circulation Research*, 95(6), pp. 645–654.
Lau, N. C., Lim, L. P., Weinstein, E. G. and Bartel, D. P. (2001) 'An abundant class of tiny RNAs with probable regulatory roles in Caenorhabditis elegans', *Science*, 294(5543).
Lazzeroni, D., Rimoldi, O. and Camici, P. G. (2016) 'From Left Ventricular Hypertrophy to Dysfunction and Failure', *Circulation Journal*, 80(3), pp. 555–564.
LeBleu, V. S., Taduri, G., O'Connell, J., Teng, Y., Cooke, V. G., Woda, C., Sugimoto, H. and Kalluri, R. (2013a) 'Origin and function of myofibroblasts in kidney fibrosis', *Nat Med*, 19(8), pp. 1047–1053.
LeBleu, V. S., Taduri, G., O'Connell, J., Teng, Y., Cooke, V. G., Woda, C., Sugimoto, H. and Kalluri, R. (2013b) 'Origin and function of myofibroblasts in kidney fibrosis', *Nat Med*, 19(8), pp. 1047–1053.
Lee, R. C., Feinbaum, R. L. and Ambros, V. (1993) 'The C. elegans heterochronic gene lin-4 encodes small RNAs with antisense complementarity to lin-14', *Cell*, 75(5), pp. 843–854.
Lee, Y., Jeon, K., Lee, J.-T., Kim, S. and Kim, V. N. (2002) 'MicroRNA maturation: stepwise processing and subcellular localization.', *The EMBO journal*, 21(17), pp. 4663–70.
Lee, Y., Kim, M., Han, J., Yeom, K.-H., Lee, S., Baek, S. H. and Kim, V. N. (2004) 'MicroRNA genes are transcribed by RNA polymerase II.', *The EMBO journal*, 23(20), pp. 4051–60.
Lewis, B. P., Burge, C. B. and Bartel, D. P. (2005) 'Conserved Seed Pairing, Often Flanked by Adenosines, Indicates that Thousands of Human Genes are MicroRNA Targets', *Cell*, 120(1), pp. 15–20.
Lewis, B. P., Shih, I., Jones-Rhoades, M. W., Bartel, D. P. and Burge, C. B. (2003) 'Prediction of mammalian microRNA targets.', *Cell*, 115(7), pp. 787–98.

Li, J., Qu, X. and Bertram, J. F. (2009) 'Endothelial-myofibroblast transition contributes to the early development of diabetic renal interstitial fibrosis in streptozotocin-induced diabetic mice', *Am J Pathol*, 175(4), pp. 1380–1388.
Li, L., Kim, I.-K., Chiasson, V., Chatterjee, P. and Gupta, S. (2017) 'NF-κB mediated miR-130a modulation in lung microvascular cell remodeling: Implication in pulmonary hypertension', *Experimental Cell Research*, 359(1), pp. 235–242.
Li, Z. and Jimenez, S. A. (2011) 'Protein kinase Cδ and c-Abl kinase are required for transforming growth factor β induction of endothelial-mesenchymal transition in vitro.', *Arthritis and rheumatism*, 63(8), pp. 2473–83.
Ling, S. H. M., Qamra, R. and Song, H. (2011) 'Structural and functional insights into eukaryotic mRNA decapping', *Wiley Interdisciplinary Reviews: RNA*, 2(2), pp. 193–208.
Liu, H., Li, G., Zhao, W. and Hu, Y. (2016) 'Inhibition of MiR-92a May Protect Endothelial Cells After Acute Myocardial Infarction in Rats: Role of KLF2/4.', *Medical science monitor : international medical journal of experimental and clinical research*, 22, pp. 2451–62.
Liu, J., Valencia-Sanchez, M. A., Hannon, G. J. and Parker, R. (2005) 'MicroRNA-dependent localization of targeted mRNAs to mammalian P-bodies.', *Nature cell biology*, 7(7), pp. 719–23.
Liu, Z., Wang, J., Cheng, H., Ke, X., Sun, L., Zhang, Q. C. and Wang, H.-W. (2018) 'Cryo-EM Structure of Human Dicer and Its Complexes with a Pre-miRNA Substrate', *Cell*, 173(5), p. 1191–1203.e12.
Lo, W.-Y., Peng, C.-T. and Wang, H.-J. (2017) 'MicroRNA-146a-5p Mediates High Glucose-Induced Endothelial Inflammation via Targeting Interleukin-1 Receptor-Associated Kinase 1 Expression', *Frontiers in Physiology*, 8, p. 551.
Lopez-Castejon, G. and Brough, D. (2011) 'Understanding the mechanism of IL-1β secretion.', *Cytokine & growth factor reviews*, 22(4), pp. 189–95.
Lu, D., Yao, Q., Zhan, C., Le-Meng, Z., Liu, H., Cai, Y., Tu, C., Li, X., Zou, Y. and Zhang, S. (2017) 'MicroRNA-146a promote cell migration and invasion in human colorectal cancer via carboxypeptidase M/src-FAK pathway', *Oncotarget*, 8(14), pp. 22674–22684.
Luna-Zurita, L., Prados, B., Grego-Bessa, J., Luxán, G., del Monte, G., Benguría, A., Adams, R. H., Pérez-Pomares, J. M. and de la Pompa, J. L. (2010) 'Integration of a Notch-dependent mesenchymal gene program and Bmp2-driven cell invasiveness regulates murine cardiac valve formation', *Journal of Clinical Investigation*, 120(10), pp. 3493–3507.
Lund, E., Güttinger, S., Calado, A., Dahlberg, J. E. and Kutay, U. (2004) 'Nuclear Export of MicroRNA Precursors', *Science*, 303(5654), pp. 95–98.
Ma, L., Lu, M.-F., Schwartz, R. J. and Martin, J. F. (2005) 'Bmp2 is essential for cardiac

cushion epithelial-mesenchymal transition and myocardial patterning.', *Development (Cambridge, England)*, 132(24), pp. 5601–11.

MacEwan, D. J. (2002) 'TNF ligands and receptors--a matter of life and death.', *British journal of pharmacology*, 135(4), pp. 855–75.

MacGrogan, D., Luna-Zurita, L. and de la Pompa, J. L. (2011) 'Notch signalling in cardiac valve development and disease', *Birth Defects Research Part A: Clinical and Molecular Teratology*, 91(6), pp. 449–459.

Mackay, F., Loetscher, H., Stueber, D., Gehr, G. and Lesslauer, W. (no date) *Tumor Necrosis Factor c~ (TNF-c~)-induced Cell Adhesion to Human Endothelial Cells Is under Dominant Control of One TNT Receptor Type, TNF-R55*.

MacRae, I. J., Zhou, K., Li, F., Repic, A., Brooks, A. N., Cande, W. Z., Adams, P. D. and Doudna, J. A. (2006) 'Structural Basis for Double-Stranded RNA Processing by Dicer', *Science*, 311(5758), pp. 195–198.

Mahler, G. J., Farrar, E. J. and Butcher, J. T. (2013) 'Inflammatory cytokines promote mesenchymal transformation in embryonic and adult valve endothelial cells.', *Arteriosclerosis, thrombosis, and vascular biology*, 33(1), pp. 121–30.

Majno, G., Gabbiani, G., Hirschel, B. J., Ryan, G. B. and Statkov, P. R. (1971) 'Contraction of granulation tissue in vitro: similarity to smooth muscle.', *Science (New York, N.Y.)*, 173(3996), pp. 548–50.

Maleszewska, M., Moonen, J. R., Huijkman, N., van de Sluis, B., Krenning, G. and Harmsen, M. C. (2013) 'IL-1beta and TGFbeta2 synergistically induce endothelial to mesenchymal transition in an NFkappaB-dependent manner', *Immunobiology*, 218(4), pp. 443–454.

Markwald, R. R., Fitzharris, T. P. and Smith, W. N. (1975) 'Sturctural analysis of endocardial cytodifferentiation', *Dev Biol*, 42(1), pp. 160–180.

Massague, J. and Chen, Y. G. (2000) 'Controlling TGF-beta signalling', *Genes Dev*, 14(6), pp. 627–644.

Medici, D., Potenta, S. and Kalluri, R. (2011) 'Transforming growth factor-beta2 promotes Snail-mediated endothelial-mesenchymal transition through convergence of Smad-dependent and Smad-independent signalling', *Biochem J*, 437(3), pp. 515–520.

Meister, G., Landthaler, M., Patkaniowska, A., Dorsett, Y., Teng, G. and Tuschl, T. (2004) 'Human Argonaute2 Mediates RNA Cleavage Targeted by miRNAs and siRNAs', *Molecular Cell*, 15(2), pp. 185–197.

Mercado-Pimentel, M. E. and Runyan, R. B. (2007) 'Multiple transforming growth factor-beta isoforms and receptors function during epithelial-mesenchymal cell transformation in the embryonic heart', *Cells Tissues Organs*, 185(1–3), pp. 146–156.

Mihira, H., Suzuki, H. I., Akatsu, Y., Yoshimatsu, Y., Igarashi, T., Miyazono, K. and Watabe, T. (2012) 'TGF-β-induced mesenchymal transition of MS-1 endothelial cells requires Smad-dependent cooperative activation of Rho signals and MRTF-A', *The Journal of Biochemistry*, 151(2), pp. 145–156.

Montorfano, I., Becerra, A., Cerro, R., Echeverría, C., Sáez, E., Morales, M. G., Fernández, R., Cabello-Verrugio, C. and Simon, F. (2014) 'Oxidative stress mediates the conversion of endothelial cells into myofibroblasts via a TGF-β1 and TGF-β2-dependent pathway', *Laboratory Investigation*, 94(10), pp. 1068–1082.

Moore-Morris, T., Guimarães-Camboa, N., Banerjee, I., Zambon, A. C., Kisseleva, T., Velayoudon, A., Stallcup, W. B., Gu, Y., Dalton, N. D., Cedenilla, M., Gomez-Amaro, R., Zhou, B., Brenner, D. A., Peterson, K. L., Chen, J. and Evans, S. M. (2014) 'Resident fibroblast lineages mediate pressure overload-induced cardiac fibrosis.', *The Journal of clinical investigation*, 124(7), pp. 2921–34.

Moore-Morris, T., Guimarães-Camboa, N., Banerjee, I., Zambon, A. C., Kisseleva, T., Velayoudon, A., Stallcup, W. B., Gu, Y., Dalton, N. D., Cedenilla, M., Gomez-Amaro, R., Zhou, B., Brenner, D. A., Peterson, K. L., Chen, J. and Evans, S. M. (2014) 'Resident fibroblast lineages mediate pressure overload–induced cardiac fibrosis', *Journal of Clinical Investigation*, 124(7), pp. 2921–2934.

Morlando, M., Ballarino, M., Gromak, N., Pagano, F., Bozzoni, I. and Proudfoot, N. J. (2008) 'Primary microRNA transcripts are processed co-transcriptionally', *Nature Structural & Molecular Biology*, 15(9), pp. 902–909.

Nakajima, Y., Miyazono, K., Kato, M., Takase, M., Yamagishi, T. and Nakamura, H. (1997) 'Extracellular fibrillar structure of latent TGF beta binding protein-1: role in TGF beta-dependent endothelial-mesenchymal transformation during endocardial cushion tissue formation in mouse embryonic heart.', *The Journal of cell biology*, 136(1), pp. 193–204.

*nCounter® Technology | NanoString Technologies* (no date).

Nie, L., Lyros, O., Medda, R., Jovanovic, N., Schmidt, J. L., Otterson, M. F., Johnson, C. P., Behmaram, B., Shaker, R. and Rafiee, P. (2014) 'Endothelial-mesenchymal transition in normal human esophageal endothelial cells cocultured with esophageal adenocarcinoma cells: role of IL-1beta and TGF-beta2', *Am J Physiol Cell Physiol*, 307(9), pp. C859-77.

Nishihara, T., Zekri, L., Braun, J. E. and Izaurralde, E. (2013) 'miRISC recruits decapping factors to miRNA targets to enhance their degradation', *Nucleic Acids Research*, 41(18), pp. 8692–8705.

Norris, R. A., Borg, T. K., Butcher, J. T., Baudino, T. A., Banerjee, I. and Markwald, R. R. (2008) 'Neonatal and Adult Cardiovascular Pathophysiological Remodeling and Repair',

*Annals of the New York Academy of Sciences*, 1123(1), pp. 30–40.
Okada, C., Yamashita, E., Lee, S. J., Shibata, S., Katahira, J., Nakagawa, A., Yoneda, Y. and Tsukihara, T. (2009) 'A high-resolution structure of the pre-microRNA nuclear export machinery.', *Science (New York, N.Y.)*, 326(5957), pp. 1275–9.
Okamura, K., Hagen, J. W., Duan, H., Tyler, D. M. and Lai, E. C. (2007) 'The Mirtron Pathway Generates microRNA-Class Regulatory RNAs in Drosophila', *Cell*, 130(1), pp. 89–100.
Olena, A. F. and Patton, J. G. (2010) 'Genomic organization of microRNAs.', *Journal of cellular physiology*, 222(3), pp. 540–5.
Olivey, H. E., Mundell, N. A., Austin, A. F. and Barnett, J. V. (2006) 'Transforming growth factor-β stimulates epithelial–mesenchymal transformation in the proepicardium', *Developmental Dynamics*, 235(1), pp. 50–59.
Osterreicher, C. H., Penz-Osterreicher, M., Grivennikov, S. I., Guma, M., Koltsova, E. K., Datz, C., Sasik, R., Hardiman, G., Karin, M. and Brenner, D. A. (2011) 'Fibroblast-specific protein 1 identifies an inflammatory subpopulation of macrophages in the liver', *Proceedings of the National Academy of Sciences*, 108(1), pp. 308–313.
Ozsolak, F., Poling, L. L., Wang, Z., Liu, H., Liu, X. S., Roeder, R. G., Zhang, X., Song, J. S. and Fisher, D. E. (2008) 'Chromatin structure analyses identify miRNA promoters.', *Genes & development*, 22(22), pp. 3172–83.
Pan, Z., Sun, X., Ren, J., Li, X., Gao, X., Lu, C., Zhang, Y., Sun, H., Wang, Y., Wang, H., Wang, J., Xie, L., Lu, Y. and Yang, B. (2012) 'miR-1 exacerbates cardiac ischemia-reperfusion injury in mouse models.', *PloS one*, 7(11), p. e50515.
Paranya, G., Vineberg, S., Dvorin, E., Kaushal, S., Roth, S. J., Rabkin, E., Schoen, F. J. and Bischoff, J. (2001) 'Aortic valve endothelial cells undergo transforming growth factor-beta-mediated and non-transforming growth factor-beta-mediated transdifferentiation in vitro.', *The American journal of pathology*, 159(4), pp. 1335–43.
Paraskevopoulou, M. D., Georgakilas, G., Kostoulas, N., Vlachos, I. S., Vergoulis, T., Reczko, M., Filippidis, C., Dalamagas, T. and Hatzigeorgiou, A. G. (2013) 'DIANA-microT web server v5.0: service integration into miRNA functional analysis workflows.', *Nucleic acids research*, 41(Web Server issue), pp. W169-73.
Pearse, S. G. and Cowie, M. R. (2014) 'Heart failure: classification and pathophysiology', *Medicine*, 42(10), pp. 556–561.
Ponikowski, P., Voors, A. A., Anker, S. D., Bueno, H., Cleland, J. G. F., Coats, A. J. S., Falk, V., González-Juanatey, J. R., Harjola, V.-P., Jankowska, E. A., Jessup, M., Linde, C., Nihoyannopoulos, P., Parissis, J. T., Pieske, B., Riley, J. P., Rosano, G. M. C., Ruilope, L.

M., Ruschitzka, F., Rutten, F. H. and van der Meer, P. (2016) ‘2016 ESC Guidelines for the diagnosis and treatment of acute and chronic heart failure’, *European Journal of Heart Failure*, 18(8), pp. 891–975.

Potts, J. D. and Runyan, R. B. (1989) ‘Epithelial-mesenchymal cell transformation in the embryonic heart can be mediated, in part, by transforming growth factor beta’, *Dev Biol*, 134(2), pp. 392–401.

Qian, L., Laake, L. W. Van, Huang, Y., Liu, S., Wendland, M. F. and Srivastava, D. (2011) ‘miR-24 inhibits apoptosis and represses Bim in mouse cardiomyocytes’, *Journal of Experimental Medicine*, 208(3), pp. 549–560.

Qiao, L., Nishimura, T., Shi, L., Sessions, D., Thrasher, A., Trudell, J. R., Berry, G. J., Pearl, R. G. and Kao, P. N. (2014) ‘Endothelial Fate Mapping in Mice With Pulmonary Hypertension’, *Circulation*, 129(6), pp. 692–703.

Qu, Q., Bing, W., Meng, X., Xi, J., Bai, X., Liu, Q., Guo, Y., Zhao, X. and Bi, Y. (2017) ‘Upregulation of miR-126-3p promotes human saphenous vein endothelial cell proliferation <i>in vitro</i> and prevents vein graft neointimal formation <i>ex vivo</i> and <i>in vivo</i>’;, *Oncotarget*, 8(63), pp. 106790–106806.

Ranchoux, B., Antigny, F., Rucker-Martin, C., Hautefort, A., Pechoux, C., Bogaard, H. J., Dorfmuller, P., Remy, S., Lecerf, F., Plante, S., Chat, S., Fadel, E., Houssaini, A., Anegon, I., Adnot, S., Simonneau, G., Humbert, M., Cohen-Kaminsky, S. and Perros, F. (2015) ‘Endothelial-to-Mesenchymal Transition in Pulmonary Hypertension’, *Circulation*, 131(11), pp. 1006–1018.

Reinhart, B. J., Slack, F. J., Basson, M., Pasquinelli, A. E., Bettinger, J. C., Rougvie, A. E., Horvitz, H. R. and Ruvkun, G. (2000) ‘The 21-nucleotide let-7 RNA regulates developmental timing in Caenorhabditis elegans’, *Nature*, 403(6772), pp. 901–906.

Ren, X.-P., Wu, J., Wang, X., Sartor, M. A., Qian, J., Jones, K., Nicolaou, P., Pritchard, T. J. and Fan, G.-C. (2009) ‘MicroRNA-320 Is Involved in the Regulation of Cardiac Ischemia/Reperfusion Injury by Targeting Heat-Shock Protein 20’, *Circulation*, 119(17), pp. 2357–2366.

Rieder, F., Kessler, S. P., West, G. A., Bhilocha, S., de la Motte, C., Sadler, T. M., Gopalan, B., Stylianou, E. and Fiocchi, C. (2011) ‘Inflammation-induced endothelial-to-mesenchymal transition: a novel mechanism of intestinal fibrosis’, *Am J Pathol*, 179(5), pp. 2660–2673.

Ro, S., Park, C., Young, D., Sanders, K. M. and Yan, W. (2007) ‘Tissue-dependent paired expression of miRNAs’, *Nucleic Acids Research*, 35(17), pp. 5944–5953.

Rodriguez, A., Griffiths-Jones, S., Ashurst, J. L. and Bradley, A. (2004) ‘Identification of mammalian microRNA host genes and transcription units.’, *Genome research*, 14(10A), pp.

1902–10.
Rodriguez, A., Griffiths-Jones, S., Ashurst, J. L. and Bradley, A. (2004) 'Identification of Mammalian microRNA Host Genes and Transcription Units', *Genome Research*, 14(10a), pp. 1902–1910.
Ruby, J. G., Jan, C. H. and Bartel, D. P. (2007) 'Intronic microRNA precursors that bypass Drosha processing', *Nature*, 448(7149), pp. 83–86.
Runyan, R. B. and Markwald, R. R. (1983) 'Invasion of mesenchyme into three-dimensional collagen gels: A regional and temporal analysis of interaction in embryonic heart tissue', *Developmental Biology*, 95(1), pp. 108–114.
Rutenberg, J. B., Fischer, A., Jia, H., Gessler, M., Zhong, T. P. and Mercola, M. (2006) 'Developmental patterning of the cardiac atrioventricular canal by Notch and Hairy-related transcription factors', *Development*, 133(21), pp. 4381–4390.
Sarmiento, D., Montorfano, I., Cerda, O., Cáceres, M., Becerra, A., Cabello-Verrugio, C., Elorza, A. A., Riedel, C., Tapia, P., Velásquez, L. A., Varela, D. and Simon, F. (2015) 'Increases in reactive oxygen species enhance vascular endothelial cell migration through a mechanism dependent on the transient receptor potential melastatin 4 ion channel', *Microvascular Research*, 98, pp. 187–196.
Sasaki, T., Shiohama, A., Minoshima, S. and Shimizu, N. (2003) 'Identification of eight members of the Argonaute family in the human genome☆', *Genomics*, 82(3), pp. 323–330.
Schieber, M. and Chandel, N. S. (2014) 'ROS function in redox signalling and oxidative stress.', *Current biology : CB*, 24(10), pp. R453-62.
Schirone, L., Forte, M., Palmerio, S., Yee, D., Nocella, C., Angelini, F., Pagano, F., Schiavon, S., Bordin, A., Carrizzo, A., Vecchione, C., Valenti, V., Chimenti, I., De Falco, E., Sciarretta, S. and Frati, G. (2017) 'A Review of the Molecular Mechanisms Underlying the Development and Progression of Cardiac Remodeling', *Oxidative Medicine and Cellular Longevity*, 2017, pp. 1–16.
Schmierer, B. and Hill, C. S. (2007) 'TGFbeta-SMAD signal transduction: molecular specificity and functional flexibility', *Nat Rev Mol Cell Biol*, 8(12), pp. 970–982.
Segura, A. M., Frazier, O. H. and Buja, L. M. (2014) 'Fibrosis and heart failure', *Heart Failure Reviews*, 19(2), pp. 173–185.
Sehgal, S. and Drazner, M. H. (2007) 'Left ventricular geometry: does shape matter?', *American heart journal*, 153(2), pp. 153–5.
Serini, G., Bochaton-Piallat, M. L., Ropraz, P., Geinoz, A., Borsi, L., Zardi, L. and Gabbiani, G. (1998) 'The fibronectin domain ED-A is crucial for myofibroblastic phenotype induction by transforming growth factor-beta1', *J Cell Biol*, 142(3), pp. 873–881.

Singer, I. I. (1979) ‘The fibronexus: a transmembrane association of fibronectin-containing fibers and bundles of 5 nm microfilaments in hamster and human fibroblasts.’, *Cell*, 16(3), pp. 675–85.
Singer, I. I., Kawka, D. W., Kazazis, D. M. and Clark, R. A. (1984) ‘In vivo co-distribution of fibronectin and actin fibers in granulation tissue: immunofluorescence and electron microscope studies of the fibronexus at the myofibroblast surface.’, *The Journal of cell biology*, 98(6), pp. 2091–106.
Song, C.-L., Liu, B., Diao, H.-Y., Shi, Y.-F., Zhang, J.-C., Li, Y.-X., Liu, N., Yu, Y.-P., Wang, G., Wang, J.-P. and Li, Q. (2016) ‘Down-regulation of microRNA-320 suppresses cardiomyocyte apoptosis and protects against myocardial ischemia and reperfusion injury by targeting IGF-1.’, *Oncotarget*, 7(26), pp. 39740–39757.
Souders, C. A., Bowers, S. L. K. and Baudino, T. A. (2009) ‘Cardiac Fibroblast: The Renaissance Cell’, *Circulation Research*, 105(12), pp. 1164–1176.
Srivastava, S. P., Koya, D. and Kanasaki, K. (2013) ‘MicroRNAs in kidney fibrosis and diabetic nephropathy: roles on EMT and EndMT’, *Biomed Res Int*, 2013, p. 125469.
Standart, N. and Jackson, R. J. (2007) ‘MicroRNAs repress translation of m7Gppp-capped target mRNAs in vitro by inhibiting initiation and promoting deadenylation’, *Genes & Development*, 21(16), pp. 1975–1982.
Stark, A., Brennecke, J., Russell, R. B. and Cohen, S. M. (2003) ‘Identification of Drosophila MicroRNA Targets’, *PLoS Biology*. Edited by Ronald H. A. Plasterk, 1(3), p. e60.
Sugi, Y., Yamamura, H., Okagawa, H. and Markwald, R. R. (2004) ‘Bone morphogenetic protein-2 can mediate myocardial regulation of atrioventricular cushion mesenchymal cell formation in mice’, *Dev Biol*, 269(2), pp. 505–518.
Sun, Y., Li, Y., Wang, H., Li, H., Liu, S., Chen, J. and Ying, H. (2017) ‘miR-146a-5p acts as a negative regulator of TGF-β signalling in skeletal muscle after acute contusion’, *Acta Biochimica et Biophysica Sinica*, 49(7), pp. 628–634.
Sundberg, C., Ivarsson, M., Gerdin, B. and Rubin, K. (1996) ‘Pericytes as collagen-producing cells in excessive dermal scarring.’, *Laboratory investigation; a journal of technical methods and pathology*, 74(2), pp. 452–66.
Suzuki, H. I., Katsura, A., Yasuda, T., Ueno, T., Mano, H., Sugimoto, K. and Miyazono, K. (2015) ‘Small-RNA asymmetry is directly driven by mammalian Argonautes’, *Nature Structural & Molecular Biology*, 22(7), pp. 512–521.
Svobodova, E., Kubikova, J. and Svoboda, P. (2016) ‘Production of small RNAs by mammalian Dicer.’, *Pflugers Archiv : European journal of physiology*, 468(6), pp. 1089–102.
Tam, W. (2001) ‘Identification and characterization of human BIC, a gene on chromosome 21

that encodes a noncoding RNA.', *Gene*, 274(1–2), pp. 157–67.
Thum, T., Gross, C., Fiedler, J., Fischer, T., Kissler, S., Bussen, M., Galuppo, P., Just, S., Rottbauer, W., Frantz, S., Castoldi, M., Soutschek, J., Koteliansky, V., Rosenwald, A., Basson, M. A., Licht, J. D., Pena, J. T. R., Rouhanifard, S. H., Muckenthaler, M. U., Tuschl, T., Martin, G. R., Bauersachs, J. and Engelhardt, S. (2008) 'MicroRNA-21 contributes to myocardial disease by stimulating MAP kinase signalling in fibroblasts', *Nature*, 456(7224), pp. 980–984.
Timmerman, L. A., Grego-Bessa, J., Raya, A., Bertrán, E., Pérez-Pomares, J. M., Díez, J., Aranda, S., Palomo, S., McCormick, F., Izpisúa-Belmonte, J. C. and de la Pompa, J. L. (2004) 'Notch promotes epithelial-mesenchymal transition during cardiac development and oncogenic transformation', *Genes & Development*, 18(1), pp. 99–115.
Tomasek, J. J., Gabbiani, G., Hinz, B., Chaponnier, C. and Brown, R. A. (2002) 'Myofibroblasts and mechano-regulation of connective tissue remodelling', *Nat Rev Mol Cell Biol*, 3(5), pp. 349–363.
Tritschler, F., Huntzinger, E. and Izaurralde, E. (2010) 'Role of GW182 proteins and PABPC1 in the miRNA pathway: a sense of déjà vu', *Nature Reviews Molecular Cell Biology*, 11(5), pp. 379–384.
Turner, N. A. (2014) 'Effects of interleukin-1 on cardiac fibroblast function: Relevance to post-myocardial infarction remodelling', *Vascular Pharmacology*, 60(1), pp. 1–7.
Unverferth, D. V., Baker, P. B., Swift, S. E., Chaffee, R., Fetters, J. K., Uretsky, B. F., Thompson, M. E. and Leier, C. V. (1986) 'Extent of myocardial fibrosis and cellular hypertrophy in dilated cardiomyopathy', *The American Journal of Cardiology*, 57(10), pp. 816–820.
Valencia-Sanchez, M. A., Liu, J., Hannon, G. J. and Parker, R. (2006) 'Control of translation and mRNA degradation by miRNAs and siRNAs', *Genes & Development*, 20(5), pp. 515–524.
Wang, C., Zhang, W., Zhang, L., Chen, X., Liu, F., Zhang, J., Guan, S., Sun, Y., Chen, P., Wang, D., Un Nesa, E., Cheng, Y. and Yousef, G. M. (2016) 'miR-146a-5p mediates epithelial–mesenchymal transition of oesophageal squamous cell carcinoma via targeting Notch2', *British Journal of Cancer*, 115(12), pp. 1548–1554.
Wang, J.-X., Jiao, J.-Q., Li, Q., Long, B., Wang, K., Liu, J.-P., Li, Y.-R. and Li, P.-F. (2011) 'miR-499 regulates mitochondrial dynamics by targeting calcineurin and dynamin-related protein-1', *Nature Medicine*, 17(1), pp. 71–78.
Wang, J., Sridurongrit, S., Dudas, M., Thomas, P., Nagy, A., Schneider, M. D., Epstein, J. A. and Kaartinen, V. (2005) 'Atrioventricular cushion transformation is mediated by ALK2 in

the developing mouse heart', *Dev Biol*, 286(1), pp. 299–310.
Wang, K., Liu, F., Liu, C.-Y., An, T., Zhang, J., Zhou, L.-Y., Wang, M., Dong, Y.-H., Li, N., Gao, J.-N., Zhao, Y.-F. and Li, P.-F. (2016) 'The long noncoding RNA NRF regulates programmed necrosis and myocardial injury during ischemia and reperfusion by targeting miR-873.', *Cell death and differentiation*, 23(8), pp. 1394–405.
Wang, K., Long, B., Li, N., Li, L., Liu, C.-Y., Dong, Y.-H., Gao, J.-N., Zhou, L.-Y., Wang, C.-Q. and Li, P.-F. (2016) 'MicroRNA-2861 regulates programmed necrosis in cardiomyocyte by impairing adenine nucleotide translocase 1 expression', *Free Radical Biology and Medicine*, 91, pp. 58–67.
Wang, S., Aurora, A. B., Johnson, B. A., Qi, X., McAnally, J., Hill, J. A., Richardson, J. A., Bassel-Duby, R. and Olson, E. N. (2008) 'The endothelial-specific microRNA miR-126 governs vascular integrity and angiogenesis.', *Developmental cell*, 15(2), pp. 261–71.
Wang, Z., Han, Z., Tao, J., Wang, J., Liu, X., Zhou, W., Xu, Z., Zhao, C., Wang, Z., Tan, R. and Gu, M. (2017) 'Role of endothelial-to-mesenchymal transition induced by TGF-β1 in transplant kidney interstitial fibrosis.', *Journal of cellular and molecular medicine*, 21(10), pp. 2359–2369.
Weber, K. T. (1989) 'Cardiac interstitium in health and disease: the fibrillar collagen network.', *Journal of the American College of Cardiology*, 13(7), pp. 1637–52.
Westholm, J. O. and Lai, E. C. (2011) 'Mirtrons: microRNA biogenesis via splicing', *Biochimie*, 93(11), pp. 1897–1904.
Widyantoro, B., Emoto, N., Nakayama, K., Anggrahini, D. W., Adiarto, S., Iwasa, N., Yagi, K., Miyagawa, K., Rikitake, Y., Suzuki, T., Kisanuki, Y. Y., Yanagisawa, M. and Hirata, K. -i. (2010) 'Endothelial Cell-Derived Endothelin-1 Promotes Cardiac Fibrosis in Diabetic Hearts Through Stimulation of Endothelial-to-Mesenchymal Transition', *Circulation*, 121(22), pp. 2407–2418.
Witkos, T. M., Koscianska, E. and Krzyzosiak, W. J. (2011) 'Practical Aspects of microRNA Target Prediction.', *Current molecular medicine*, 11(2), pp. 93–109.
Xiang, L., Ou, H., Liu, X., Chen, Z., Li, X., Huang, Y. and Yang, D. (2017) 'Loss of tumor suppressor miR-126 contributes to the development of hepatitis B virus–related hepatocellular carcinoma metastasis through the upregulation of ADAM9', *Tumor Biology*, 39(6), p. 101042831770912.
Xu, X., Tan, X., Hulshoff, M. S., Wilhelmi, T., Zeisberg, M. and Zeisberg, E. M. (2016) 'Hypoxia-induced endothelial-mesenchymal transition is associated with RASAL1 promoter hypermethylation in human coronary endothelial cells', *FEBS Letters*, 590(8), pp. 1222–1233.
Xu, X., Tan, X., Tampe, B., Sanchez, E., Zeisberg, M. and Zeisberg, E. M. (2015) 'Snail Is a

Direct Target of Hypoxia-inducible Factor 1α (HIF1α) in Hypoxia-induced Endothelial to Mesenchymal Transition of Human Coronary Endothelial Cells.', *The Journal of biological chemistry*, 290(27), pp. 16653–64.

Xu, Y., He, Q., Shen, Z., Shu, X., Wang, C., Zhu, J., Shi, L. and Du, L. (2017) 'MiR-126a-5p is involved in the hypoxia-induced endothelial-to-mesenchymal transition of neonatal pulmonary hypertension', *Hypertension Research*, 40(6), pp. 552–561.

Yang, X., Qin, Y., Shao, S., Yu, Y., Zhang, C., Dong, H., Lv, G. and Dong, S. (2016) 'MicroRNA-214 Inhibits Left Ventricular Remodeling in an Acute Myocardial Infarction Rat Model by Suppressing Cellular Apoptosis via the Phosphatase and Tensin Homolog (PTEN)', *International Heart Journal*, 57(2), pp. 247–250.

Yekta, S., Shih, I.-H. and Bartel, D. P. (2004) 'MicroRNA-Directed Cleavage of HOXB8 mRNA', *Science*, 304(5670), pp. 594–596.

Yoda, M., Kawamata, T., Paroo, Z., Ye, X., Iwasaki, S., Liu, Q. and Tomari, Y. (2010) 'ATP-dependent human RISC assembly pathways.', *Nature structural & molecular biology*, 17(1), pp. 17–23.

Zeisberg, E. M. and Kalluri, R. (2010) 'Origins of cardiac fibroblasts', *Circ Res*, 107(11), pp. 1304–1312.

Zeisberg, E. M., Potenta, S. E., Sugimoto, H., Zeisberg, M. and Kalluri, R. (2008) 'Fibroblasts in kidney fibrosis emerge via endothelial-to-mesenchymal transition', *J Am Soc Nephrol*, 19(12), pp. 2282–2287.

Zeisberg, E. M., Tarnavski, O., Zeisberg, M., Dorfman, A. L., McMullen, J. R., Gustafsson, E., Chandraker, A., Yuan, X., Pu, W. T., Roberts, A. B., Neilson, E. G., Sayegh, M. H., Izumo, S. and Kalluri, R. (2007) 'Endothelial-to-mesenchymal transition contributes to cardiac fibrosis', *Nat Med*, 13(8), pp. 952–961.

Zekri, L., Huntzinger, E., Heimstadt, S. and Izaurralde, E. (2009) 'The Silencing Domain of GW182 Interacts with PABPC1 To Promote Translational Repression and Degradation of MicroRNA Targets and Is Required for Target Release', *Molecular and Cellular Biology*, 29(23), pp. 6220–6231.

Zhang, H., Hu, J. and Liu, L. (2017) 'MiR-200a modulates TGF-β1-induced endothelial-to-mesenchymal shift via suppression of GRB2 in HAECs', *Biomedicine & Pharmacotherapy*, 95, pp. 215–222.

Zhang, J., Zhang, Z., Zhang, D. Y., Zhu, J., Zhang, T. and Wang, C. (2013) 'microRNA 126 Inhibits the Transition of Endothelial Progenitor Cells to Mesenchymal Cells via the PIK3R2-PI3K/Akt Signalling Pathway', *PLoS ONE*. Edited by A. Navarro, 8(12), p. e83294.

Zhou, C., Jiang, C.-Q., Zong, Z., Lin, J.-C. and Lao, L.-F. (2017) 'miR-146a promotes growth

of osteosarcoma cells by targeting ZNRF3/GSK-3β/β-catenin signalling pathway', *Oncotarget*, 8(43), pp. 74276–74286.